National Library of Canada
Bibliothèque nationale du Canada

Canadian Theses Service
Service des thèses canadiennes

Ottawa, Canada
K1A 0N4

NOTICE

The quality of this microform is heavily dependent upon the quality of the original thesis submitted for microfilming. Every effort has been made to ensure the highest quality of reproduction possible.

If pages are missing, contact the university which granted the degree.

Some pages may have indistinct print especially if the original pages were typed with a poor typewriter ribbon or if the university sent us an inferior photocopy.

Previously copyrighted materials (journal articles, published tests, etc.) are not filmed.

Reproduction in full or in part of this microform is governed by the Canadian Copyright Act, R.S.C. 1970, c. C-30.

AVIS

La qualité de cette microforme dépend grandement de la qualité de la thèse soumise au microfilmage. Nous avons tout fait pour assurer une qualité supérieure de reproduction.

S'il manque des pages, veuillez communiquer avec l'université qui a conféré le grade.

La qualité d'impression de certaines pages peut laisser à désirer, surtout si les pages originales ont été dactylographiées à l'aide d'un ruban usé ou si l'université nous a fait parvenir une photocopie de qualité inférieure.

Les documents qui font déjà l'objet d'un droit d'auteur (articles de revue, tests publiés, etc.) ne sont pas microfilmés.

La reproduction, même partielle, de cette microforme est soumise à la Loi canadienne sur le droit d'auteur, SRC 1970, c. C-30.

NL-339 (r. 88/04)

Canada

THE UNIVERSITY OF ALBERTA

ANALYSIS OF REINFORCED CONCRETE PANELS LOADED AXIALLY AND LATERALLY

by

© BRUNO MASSICOTTE

A THESIS

SUBMITTED TO THE FACULTY OF GRADUATE STUDIES AND RESEARCH

IN PARTIAL FULFILMENT OF THE REQUIREMENTS FOR THE DEGREE

OF DOCTOR OF PHILOSOPHY

DEPARTMENT OF CIVIL ENGINEERING

EDMONTON, ALBERTA

FALL, 1988

Permission has been granted to the National Library of Canada to microfilm this thesis and to lend or sell copies of the film.

The author (copyright owner) has reserved other publication rights, and neither the thesis nor extensive extracts from it may be printed or otherwise reproduced without his/her written permission.

L'autorisation a été accordée à la Bibliothèque nationale du Canada de microfilmer cette thèse et de prêter ou de vendre des exemplaires du film.

L'auteur (titulaire du droit d'auteur) se réserve les autres droits de publication; ni la thèse ni de longs extraits de celle-ci ne doivent être imprimés ou autrement reproduits sans son autorisation écrite.

ISBN 0-315-45689-2

THE UNIVERSITY OF ALBERTA

RELEASE FORM

NAME OF AUTHOR: BRUNO MASSICOTTE

TITLE OF THESIS: ANALYSIS OF REINFORCED CONCRETE PANELS LOADED AXIALLY AND LATERALLY

DEGREE: DOCTOR OF PHILOSOPHY

YEAR THIS DEGREE GRANTED FALL 1988

Permission is hereby granted to THE UNIVERSITY OF ALBERTA LIBRARY to reproduce single copies of this thesis and to lend or sell such copies for private, scholarly or scientific research purposes only.

The author reserves other publication rights, and neither the thesis nor extensive extracts from it may be printed or otherwise reproduced without the author's written permission.

(signed) B. Massicotte

PERMANENT ADDRESS

124, rue de l'Hôpital

Lorettéville, Québec

G2B 3E8

Date : July 5, 1988

THE UNIVERSITY OF ALBERTA

FACULTY OF GRADUATE STUDIES AND RESEARCH

The undersigned certify that they have read, and recommend to the Faculty of Graduate Studies and Research for acceptance, a thesis entitled ANALYSIS OF REINFORCED CONCRETE PANELS LOADED AXIALLY AND LATERALLY submitted by B. MASSICOTTE in partial fulfilment of the requirements for the degree of DOCTOR OF PHILOSOPHY .

Dr. J.G. MacGregor (Supervisor)

Dr. A.E. Elwi

Dr. D.W. Murray

Dr. S.H. Simmonds

Dr. A. Craggs

Dr. D. Mitchell (External Examiner)

Date : July 5, 1988

To

Hélène

Gabriel
Pierre

ABSTRACT

Reinforced concrete panels supported on four edges and subjected simultaneously to inplane and lateral loads are encountered commonly in civil engineering structures. In many cases one of the two load types can be neglected or the coupling effect of the two loadings is not significant and their effects can be treated separately. However, in some applications, such as bridge decks, offshore structures, etc, inplane and transverse loads must be considered simultaneously to adequately predict the response and the ultimate carrying capacity of such elements. A research program involving experiments and numerical modelling has been undertaken at the University of Alberta to study the behavior of reinforced concrete panels loaded axially and transversely. In the present study, the modelling of reinforced concrete panels with the finite element method is described.

The development of an incremental hypoelastic plane stress material model for reinforced concrete and its implementation in a 3D degenerated plate shell element are described. The material model for concrete allows for strain softening after cracking and crushing and includes fixed and rotating crack models. A rational tension stiffening relationship is introduced, in which the post cracking stress strain response is described in terms of the reinforcement ratios and the angle of the crack to the reinforcement.

The finite element model predictions are compared to the results of various experimental investigations: reinforced concrete members loaded axially in tension, prestressed concrete wall segments loaded in biaxial tension, reinforced concrete panels subjected to shear and combined shear and biaxial

compression, and finally, reinforced concrete plates loaded axially and transversely.

The finite element model is also used to carry out a parametric study on reinforced concrete panels subjected to inplane and lateral loads, in which the geometry of the panels, their boundary conditions and the type of loading are varied.

RESUME

Les panneaux en béton armé supportés sur les quatre côtés et soumis simultanément à des charges dans leur plan et latérales se rencontrent communément dans les structures de Génie civil. Dans plusieurs cas un des deux types de charge peut être négligé ou l'effect du couplage des deux chargements est négligeable et leurs effets peuvent être traités séparément. Cependant, dans certaines applications, comme les dalles de ponts, les structures *offshore*, etc, les charges dans le plan et latérales doivent être considérées simultanément afin de pouvoir prédir adéquatement le comportement et la capacité ultime de tels éléments. Un programme de recherche incluant des essais expérimentaux et de la modélisation numérique a été entrepris à l'Université de l'Alberta pour étudier le comportement de panneaux en béton armé chargés dans leur plan et latérallement. La présente étude décrit la modélisation de panneaux en béton armé par la méthode des élément finis.

Le développement d'un modèle incremental hypoélastique en contraintes planes pour le béton armé et de son implantation dans un élément de coque dégénéré 3D sont décrits. Le radoucissement des contraintes dans le béton après la fissuration et l'écrasement sont inclus dans le modèle ainsi que des fissures à orientation fixe ou variable. Un modèle rationel décrivant le raidissement en tension après la fissuration, où la relation contrainte-déformation est décrite en fonction du pourcentage d'armature et de l'orientation des fissures par rapport à l'armature, a été développé.

Les prédictions du modèle par éléments finis sont comparées à divers résultats expérimentaux : des pièces en béton armé chargées axiallement, des

segments de murs en béton précontraint soumis à des charges biaxialles en tension, des panneaux en béton armé soumis à du cisaillement et à du cisaillement combiné à des charges de compression biaxialles, et finallement, des plaques en béton armé chargées dans leur plan et latérallement.

Le modèle par éléments finis est également utilisé pour réaliser une étude paramétrique sur le comportement des panneaux en béton armé soumis à des charges axialles dans leur plan et latérales, dans laquelle la géométrie des panneaux, les conditions de retenues et le type de chargement sont variés.

ACKNOWLEDGEMENTS

The author wishes to express his deep appreciation and gratitude to Professors James G. MacGregor and Alaa E. Elwi for their supervision and guidance. The author thanks Mrs Louise Dumont for the typing of the manuscript .

The author would like to acknowledge the following organizations for their financial support: the National Sciences and Engineering Research Council of Canada, the Alberta Heritage Fund and the University of Alberta Faculty of Graduate Studies and Research .

The author deeply appreciates the support and patience of his wife throughout the course of this study.

TABLE OF CONTENTS

Chapter		Page
List of Tables		xiv
List of Figures		xvi
List of Symbols		xxiii
1.	Introduction	1
	1.1 Problem statement	1
	1.2 Research scope	2
	1.2.1 Existing experimental results and analytical solutions	3
	1.2.2 Existing finite element models for plates	4
	1.2.3 Objectives of the research	5
	1.3 The finite element program	7
	1.3.1 NISA	7
	1.3.2 The plate-shell element	8
	1.3.3 Solution strategies	10
	1.3.4 Tracing the stress path in a load step	11
	1.4 Organization of the Thesis	12
2.	Modelling of reinforced concrete members in tension	21
	2.1 Scope	21
	2.2 Plain concrete members in tension	24
	2.2.1 Cracking energy	24
	2.2.2 Observation from experiments	25

2.2.3 Proposed stress-strain curve in tension 27
2.3 Reinforced concrete members in tension 29
2.3.1 Qualitative description of tension stiffening 29
2.3.2 CEB model for tension stiffening 30
2.3.3 Proposed approach for tension stiffening 32
2.3.4 Stabilized cracking condition 34
2.3.5 Postcracking conditions 38
2.3.6 Crack not orthogonal to reinforcement 40
2.3.7 Effective reinforcement ratio 43
2.4 Comparison with experimental results 43
2.4.1 Direct tension tests 44
2.4.2 Bending test 45
2.4.3 Shear panels 45
2.5 Design equations 47

3. Reinforced concrete model 91
3.1 Scope 91
3.2 Constitutive relationships 92
3.2.1 Incremental formulation 92
3.2.2 Stress-strain relationships 94
3.2.3 Biaxial failure envelope 95
3.2.4 Poisson's ratio 97
3.2.5 Uniaxial stress-strain curve 98
3.2.6 Shear modulus 103
3.2.7 Comparison with experimental results 103
3.3 Postfailure modelling 104
3.3.1 Tensile failure 104

3.3.2 Multiple cracks 106
3.3.3 Compression failure 107
3.4 Material properties 109
3.5 Implementation in the plate-shell element 112
3.6 Plate problems 113

4. Validation of the finite element model 128
4.1 Orthotropically reinforced concrete panels 128
4.1.1 Experimental program 128
4.1.2 Modelling with NISA 129
4.2 Prestressed concrete wall segments 135
4.2.1 Experimental investigation 135
4.2.2 Modelling with NISA 136
4.3 Reinforced concrete panels loaded axiallu and transversely . . 137
4.3.1 Experimental program 137
4.3.2 Modelling with NISA 140
4.3.3 Analysis of the model results 143
4.3.4 Summary 145

5. Behavior of reinforced concrete panels 187
5.1 Solutions available 187
5.2 Parametric study 188
5.3 Results of the parametric study 190
5.3.1 Load type and boundary conditions 190
5.3.2 Magnitude of the inplane load 191
5.3.3 Reinforcement ratio ρ_x and ρ_y 192
5.3.4 Panel slenderness 193

5.3.5 Loading sequence 196
5.4 Summary of the parametric study 197

6. Summary, conclusions and recommendations 215
6.1 Summary 215
6.2 Conclusions 216
6.3 Recommendations for future study 217

References 219

Appendix A Parametric description of notched tension specimens . . 228
A.1 Parametric description 228
A.2 Observation from experimental investigation 231

Appendix B Modelling of reinforced concrete panels subjected to axial load and lateral loading 236
B.1 Finite element modelling 236
B.2 Test set up effects 239
B.2.1 Overhanging strip and discrete supports 239
B.2.2 Inplane load application 240
B.2.3 Corner support 241
B.3 Summary 242

LIST OF TABLES

Table		Page
2.1	E_c to E_1 ratios	49
2.2	Evaluation of factor K in Equation 2.3	49
2.3	Coordinates for the adopted strain softening curve in Fig. 2.7	50
2.4	Data used to evaluate f_{STcr} and ε_{STcr} in the example	50
2.5	Values of f_{STcr} and ε_{STcr} for axially loaded prisms with properties given in Table 2.4	51
2.6	Values of f_{STy} and ε_{STy} for axially loaded prisms with properties given in Table 2.4	52
2.7	Data for tension and bending tests	53
2.8	Data for shear panels	54
2.9	Parameters in the tension stiffening model	54
2.10	Results obtained for the shear panels	55
4.1	Data of the Vecchio and Collins (1982) test series	147
4.2	Failure characteristics of the Vecchio and Collins (1982) test series	148
4.3	Concrete properties for prestressed wall segments MacGregor *et al* (1979)	149
4.4	Nominal dimensions of Aghayere and MacGregor (1988) test series	149
4.5	Reinforcement area in Aghayere and MacGregor (1988) test series	150
4.6	Actual specimen thicknesses and reinforcement positions in	

	Aghayere and MacGregor (1988)test series	150
4.7	Concrete properties in Aghayere and MacGregor (1988) test series	151
4.8	Test results in Aghayere and MacGregor (1988) test series	151
4.9	Concrete properties used in analyzing Aghayere and MacGregor (1988) test series A and B	152
4.10	Comparison of the finite element predictions to the test results . .	153
5.1	Panel specifications in the parametric study	196
5.2	Loading and boundary conditions used in the parametric study . .	200
5.3	Results of the parametric study	201
5.4	Bending moments at the center of the panels analyzed in the parametric study	203
A.1	Parameters assumed for the example	233
A.2	Parameters measured in Gopalaratnam and Shah (1985)	233
A.3	Specimen response in the example	234

LIST OF FIGURES

Figure		Page
1.1	Bridge	14
1.2	Offshore structure	14
1.3	Barges	15
1.4	Precast panels	16
1.5	Plate dimensions, coordinates and loading	17
1.6	3D degenarated plate-shell element	
	(a) Bicubic element	18
	(b) Displacement of a point	18
1.7	Layers in the plate-shell element	
	(a) Layers over the element thickness	19
	(b) Reinforcement layer	19
1.8	Constant Arc-Length Method	20
2.1	Complete stress-strain curve for concrete	56
2.2	Tension softening in concrete	57
2.3	Tension stiffening	
	(a) Reinforced concrete member	58
	(b) Concrete contribution	58
2.4	Tension specimen response	
	(a) Tension specimen	59
	(b) Stress - Elongation	59
	(c) Stress - Strain	59
2.5	Plain concrete member in tension	

(a) Member in Tension 60
(b) Actual Strain Distribution 60
(c) Simplified Strain Distribution 60
2.6 Test specimens
(a) Notched beam 61
(b) Splitting test 61
(c) Tension specimens 61
2.7 Adopted tension softening curve 62
2.8 Notched tension specimen
(a) Notched tension specimen 63
(b) Stress - Strain Curves 63
2.9 Reinforced concrete member in tension
(a) Cracked member 64
(b) Free Body Diagram 64
2.10 Tension stiffening effect 65
2.11 Stress distribution in a cracked member
(a) Cracked member 66
(b) Steel stress 66
(c) Concrete stress 66
2.12 CEB model 67
2.13 Assumed strain distribution
(a) At cracking 68
(b) After cracking 68
2.14 Phases in the tension stiffening model
(a) Concrete member 69
(b) Concrete contribution 69

2.15 Tension stiffening curve

(a) Reinforcement ratio of 2.5% 70

(b) Reinforcement ratio of 1.5% 71

(c) Reinforcement ratio of 0.75% 72

2.16 Tension stiffening response for different ρ values 73

2.17 Reinforcement non orthogonal to the crack

(a) Relative orientations 74

(b) Forces at the crack 74

2.18 Effective concrete embedment area 75

2.19 Comparison of model and Rostásy *et al* (1976) tension test V1 . . . 76

2.20 Comparison of model and Rostásy *et al* (1976) tension test V2 . . . 77

2.21 Comparison of model and Rostásy *et al* (1976) tension test V3 . . . 78

2.22 Comparison of model and Rostásy *et al* (1976) tension test V4 . . . 79

2.23 Comparison of model and Rostásy *et al* (1976) tension test V5 . . . 80

2.24 Comparison of model and Rizkalla *et al* (1983) tension test #2 . . . 81

2.25 Comparison of model and Rostásy *et al* (1976) flexure test H1 . . . 82

2.26 Comparison of model and Vecchio and Collins (1982) panel PV3 . 83

2.27 Comparison of model and Vecchio and Collins (1982) panel PV4 . 84

2.28 Comparison of model and Vecchio and Collins (1982) panel PV6 . 85

2.29 Comparison of model and Vecchio and Collins (1982) panel PV16 . 86

2.30 Comparison of model and Vecchio and Collins (1982) panel PV23 . 87

2.31 Vecchio and Collins (1982) shear panel after cracking 88

2.32 Vecchio *et al* (1982) and Collins *et al* (1987)
tension stiffening curves 89

2.33 Proposed tension stiffening curves for design 90

3.1 Coordinate system 115

3.2 Uniaxial stress-strain curve

(a) Normal stress-strain curve 116

(b) Steep stress-strain curve 116

3.3 Biaxial failure envelope

(a) Failure envelope 117

(b) Tension - compression 117

3.4 Interpolation function for the uniaxial ultimate strains 118

3.5 Reference stress-strain curve 119

3.6 Equivalent uniaxial strain

(a) Proportional loading 120

(b) Nonproportional loading 121

3.7 Comparison of model and Kupfer *et al* (1969) in tension-compression 122

3.8 Comparison of model and Kupfer *et al* (1969) in compression, ratio = -1.0/0.0 123

3.9 Comparison of model and Kupfer *et al* (1969) in compression, ratio = -1.0/-0.52 124

3.10 Comparison of model and Kupfer *et al* (1969) in compression, ratio = -1.0/-1.0 125

3.11 Postcracking stress-strain curve 126

3.12 Postcrushing stress-strain curve 127

4.1 Comparison of model and Vecchio and Collins (1982) test PV3

(a) Longitudinal strain 154

(b) Shear strain 155

4.2 Comparison of model and Vecchio and Collins (1982) test PV4

(a) Longitudinal strain 156

(b) Shear strain 157
4.3 Comparison of model and Vecchio and Collins (1982) test PV27
(a) Longitudinal strain 158
(b) Shear Strain 159
4.4 Comparison of model and Vecchio and Collins (1982) test PV19
(a) Longitudinal strain 160
(b) Transverse strain 161
(c) Shear strain 162
4.5 Comparison of model and Vecchio and Collins (1982)
test PV25, longitudinal and shear strains, Test PV25 163
4.6 Comparison of model and Vecchio and Collins (1982) test PV29
(a) Longitudinal strain 164
(b) Transverse strain 165
(c) Shear strain 166
4.7 Comparison of model and MacGregor *et al* (1979) wall segment #1 167
4.8 Comparison of model and MacGregor *et al* (1979) wall segment #3 168
4.9 Aghayere and MacGregor (1988) test set up
(a) Geometry and reinforcement of the A series 169
(b) Loading apparatus 170
(c) Corner support 171
4.10 Reinforcing steel tension coupon 172
4.11 Modelling of Aghayere and MacGregor (1988) A and B series . . . 173
4.12 Mesh used for Aghayere and MacGregor (1988) square specimens . 174
4.13 Mesh used for Aghayere and MacGregor (1988) rectangular
specimens 175
4.14 Central deflection in Aghayere and MacGregor (1988)

specimen A3 176
4.15 Central deflection Aghayere and MacGregor (1988) specimens A1 and A2 177
4.16 Central deflection Aghayere and MacGregor (1988) specimens B1 and B2 178
4.17 Principal bending moments in Aghayere and MacGregor (1988) specimen A2 179
4.18 Concrete damage in Aghayere and MacGregor (1988) specimen A2 at peak load 180
4.19 Concrete damage in Aghayere and MacGregor (1988) specimen A2 at peak load 181
4.20 Concrete damage in Aghayere and MacGregor (1988) specimen A2 before collapse 182
4.21 Reinforcement transverse strains in Aghayere and MacGregor (1988) specimen A2 183
4.22 Membrane forces in Aghayere and MacGregor (1988) specimen B1 before collapse 184
4.23 Reinforcement membrane forces in Aghayere and MacGregor (1988) specimen B1 before collapse 185
4.24 Principal bending moments in Aghayere and MacGregor (1988) specimen B1 before collapse 186
5.1 Response of the first six panels of the PS1 series, b/a = 1.0 204
5.2 Response of the first six panels of the PS2 series, b/a = 2.0 205
5.3 Effect of the inplane load magnitude for the PS1 series 206
5.4 Effect of the inplane load magnitude for the PS2 series 207
5.5 Effect of the reinforcement ratios in the two directions for

	the square panels	208
5.6	Effect of the reinforcement ratios in the two directions for the rectangular panels	209
5.7	Effect of the inplane load in slender panels, a/h = 40.0 , b/a = 1.0 .	210
5.8	Effect of the inplane load for stocky panels, a/h = 20.0 , b/a = 1.0 .	211
5.9	Effect of the slenderness on the failure load	212
5.10	Effect of the slenderness on the ultimate capacity	213
5.11	Effect of the loading sequence, a/h = 30.0 , a/b = 1.0.	214
A.1	Results for the example	235
B.1	Effect of the number of elements and the number of layers	244
B.2	Effect of the solution strategies	245
B.3	Effect of the cracking model	246
B.4	Effect of the supports	247
B.5	Effects of the edge rotation	248
B.6	Effect of the edge rotation for specimen A1	249
B.7	Effect of the edge rotation for specimen B1.	250
B.8	Effect of inplane load eccentricity for specimen B1.	251
B.9	Effect of the corner supports for specimen A2	252
B.10	Effect of the corner supports for specimen B1	253
B.11	Effect of the corner supports for specimen B2	254

LIST OF SYMBOLS

Scalars

a	Panel width in the direction of the x axis
A_c	Area of concrete
A_{cef}	Effective embedment area of concrete
A_s	Area of steel
b	Tension specimen width at reference section; panel length in the direction of the y axis
b_o	Tension specimen width
c_a	Depth of the notch in notched tension specimens
d	Distance from the extreme compression fiber to the centroid of tension steel
d_a	Maximum aggregate size
dw	Incremental work; incremental crack width
$d\varepsilon$	Incremental strain
$d\sigma$	Incremental stress
e	Inplane load eccentricity
E	Current tangent modulus
E_c	Initial concrete Young's modulus

E_{cm}	Average concrete Young's modulus
E_i , E_j	Current tangent modulus at load steps i and j
E_s	Reinforcement Young's modulus
E_{sec}	Secant modulus
E_1 , E_2	Tangent modulus on the concrete softening branch
E_{1m} , E_{2m}	Tangent modulus on the average softening branch
f'_c	Compressive strength of concrete
f''_c	Reduced compressive strength of concrete
f_{cr}	Cracking stress in concrete
f_s	Steel stress
f_{scr}	Steel stress at cracking
f_{SO}	Concrete stress due to tension softening
f_{ST}	Concrete stress due to tension stiffening
f_{STcr}	Tension softening stress in concrete at cracking
f_{STy}	Tension softening stress in concrete at yielding
f'_t	Uniaxial tensile strength of concrete
f_y , f_{yi}	Yield stresses
f_{yeq}	Equivalent yield stress
G_{cr}	Cracked shear modulus
G_f	Fracture energy per unit area
G_{ip}	Inplane shear modulus

G_{tr}	Transverse shear modulus
G_o	Initial shear modulus
G_{min}	Minimum shear modulus
h	Specimen thickness; plate thickness
h_s	Thickness of a reinforcement layer
I_m	Inplane load magnitude
I_{mb}	Inplane load magnitude at balance failure
K_θ	Rotational spring stiffness
K_1 , K_2	Factors defined in Eqs. 3.21 and 3.22 respectively
l_1	Length of region I in CEB model
l_2	Length of region II in CEB model
L_o	Gauge length in tension specimen
m_{ACI}	Resisting bending moment evaluate using the ACI stress block
m_x	Bending moment caused by stresses oriented in the x direction
m_y	Bending moment caused by stresses oriented in the y direction
m_y^*	Bending moment in the y direction without the P-Δ effects
M_o	Bending moment along specimen edges
n	Ratio of E_s to E_c
n_r	Number of bars crossing a crack
N_y	Membrane force caused by stresses oriented in the y direction
p_u	Inplane load at failure per unit length

P , P_u	Total inplane load, total inplane load at failure
q_u	Lateral load per unit area at failure
Q_u	Total lateral load at failure
r	Radius of the half cylinder used to apply the inplane load to the specimen
r - s - t	Element coordinate system
R_ε	Ratio of ε to ε_{cu}
S_m	Average crack spacing
T	Tensile force on a member
T_c	Tensile force carried by concrete
T_{cr}	Tensile force at cracking
T_s	Tensile force carried by steel
u , v , w	Nodal displacements of the middle plane in the the plate-shell element
w	Crack width
w_c	Width of fracture process zone
w_o	Maximum crack width at the end of tension softening
W_f	Cracking energy density
α	Principal stress ratio
α , β	Nodal rotations of the middle plane in the the plate-shell element
α_{ct}	Stress ratio at which failure mode changes from tensile to compressive in the tension-compression region

β_1 , β_2	Tension stiffening factors related to bond properties
δ	Elongation in a tension specimen
δ_{uncr}	Elongation before cracking
δ_1 , δ_2	Elongation after cracking
Δ_{max}	Deflection at the center of a panel at maximum load level
Δ_u , Δ_{ult}	Ultimate deflection at the center of a panel
ΔS	Arc length
$\Delta\theta$, $\Delta\theta_i$	Angle between a crack and reinforcement
ε_A , ε_B	Principal strains
ε_c	Strain in concrete
ε_{cm}	Average strain in concrete
ε_{cmax}	Maximum strain on the compression softening branch
ε_{co}	Strain in concrete at f'_c (positive)
ε_{cr}	Strain in concrete at cracking
ε_{cu}	Ultimate uniaxial strain in concrete at σ_{cu} (negative)
ε_{c1} , ε_{c2}	Strain in concrete in regions I and II
ε_f	Strain at focal point for unloading from compression softening
ε_{ieq} , ε_{jeq}	Equivalent uniaxial strains
ε_m	Average strain on a member
ε_{max}	Maximum strain of the tension softening curve
ε_r	Strain in a rebar

ε_r , ε_s , ε_t,	Axial strains in the r-s-t coordinate system
ε_s	Strain in steel
ε_{sm}	Average strain in steel
ε_{s1} , ε_{s2}	Strain in steel in regions I and II
ε_{ST}	Tension stiffening strain
ε_{STcr}	Tension stiffening strain at cracking
ε_{STy}	Tension stiffening strain at yielding
ε_y , ε_{yi}	Yield strains
ε_{yeq}	Equivalent yield strain
ε_μ	Strain at change of slope on the tension softening branch
ε^*	Pseudo ultimate strain
ϕ	Reinforcement bar diameter
ϕ_i	Participation factor
γ_{rs} , γ_{rt} , γ_{st}	Shear strains in the r-s-t coordinate system
γ_u	Ultimate shear strain
λ , λ_m	Load factors
μ	Stress ratio at the change of slope on the concrete tension softening branch
ν_o , ν	Initial and current Poisson's ratios
θ_e	Rotation of the edge of a panel
ρ , ρ_i	Reinforcement ratio
ρ_{eff}	Effective reinforcement ratio

ρ_{effx} , ρ_{effy}	Effective reinforcement ratio in two orthogonal directions
ρ_{eq}	Equivalent reinforcement ratio
ρ_l , ρ_t	Longitudinal and transverse reinforcement ratios
ρ_1 , ρ_2	Reinforcement ratios in directions 1 and 2
ρ_{lim}	Reinforcement ratio at $\varepsilon_{c2} = \varepsilon_{max}$
ρ_{stbl}	Reinforcement ratio for stable cracking
ρ_x , ρ_y	Reinforcement ratios in directions x and y
ρ_{yld}	Reinforcement ratio at $\varepsilon_{c2} = \varepsilon_y$
σ	Stress
σ_A , σ_B	Principal stresses, $\sigma_A \geq \sigma_B$
σ_{Ai} , σ_{Aj}	Maximum principal stresses at steps i and j
σ_{Bi} , σ_{Bj}	Minimum principal stresses at steps i and j
σ_{cmax}	Stress corresponding to ε_{cmax}
σ_{cu}	Ultimate concrete compressive strength in biaxial state of stresses
σ_f	Stress at focal point for unloading from compression softening
σ_o	Stress outside crack region
σ_r , σ_s , σ_t,	Axial stresses in the r-s-t coordinate system
τ_{rs} , τ_{rt} , τ_{st}	Shear stresses in the r-s-t coordinate system
τ_u	Ultimate shear stresses
ξ	Shear reduction coefficient
ψ_d , ψ_L , ψ_{Lo}	Geometrical parameters defined in Eqs. A.3 to A.5

ψ_1, ψ_2	Material parameters defined in Eqs. A.6 and A.7
ζ	Distribution coefficient
ζ_{cr}	Distribution coefficient at cracking
ζ_y	Distribution coefficient at yielding.
1 - 2	Material coordinate system

Vectors and Matrices

$\mathbf{C}_i$	Constitutive matrix at the end of load step i
$\mathbf{C}_m$	Constitutive matrix in the material coordinate system
$\mathbf{C}_{rs}$	Constitutive matrix in r-s-t coordinate system
$\mathbf{C}_{12}$	Constitutive matrix in the element coordinate system
$\mathbf{P}_m$	Load vector at load step m
$\mathbf{P}_1$	Basic load vector
$\mathbf{P}_2$	Constant load vector
$\mathbf{R}$	Rotation matrix
$\Delta\varepsilon$	Strain increment vector
$\Delta\varepsilon_{ij}$	Strain increment vector between steps i and j
$\Delta\sigma$	Stress increment vector
$\Delta\sigma_{ij}$	Stress increment vector between steps i and j
ε	Current strain vector

ε_o	Initial strain vector
σ_i , σ_j	Stress vectors steps i and j

CHAPTER I

INTRODUCTION

1.1 Problem statement

Reinforced concrete or prestressed concrete panels supported on four edges and loaded axially and transversely are found commonly in Civil Engineering Structures. In many cases one of the two load types is small with respect to the other and can be neglected. Frequently, when the slenderness of the structural element is not critical, the two load types can be treated separately. However, there are some situations such as bridge decks, offshore structures, barge hulls, precast panels, etc. (Figs. 1.1 to 1.4) where the two loading types have to be taken into account simultaneously. Transverse loads can be hydrostatic pressures, point loads or uniform pressures whereas inplane loads are usually uniformly distributed along panel edges, and can be either uniaxial or biaxial.

The sequence of application of combined inplane and lateral loads varies. However two extreme cases can be identified; the inplane load may be applied first and kept constant followed by a variable lateral load or, inversely, the lateral load may be applied first and maintained constant followed by a variable inplane load. In between the two extreme cases, any load application sequence can be imagined. For example, a bridge deck (Fig. 1.1) is subjected to an inplane load at midspan due to dead load effects. While this load is maintained, rheological effects (creep, shrinkage) must be taken into account. When a truck travels

across the bridge, the inplane load builds up progressively, without any significant lateral load, until a truck wheel passes over the region considered, thus applying a lateral load.

The interaction between the two load types is a function of the relative importance of the these loads and the panel response to their combination. The types of failure can also vary, being either by instability for slender panels with large axial loads, or by material failure, which would be expected in stocky panels or in panels with high lateral load.

Modelling such structural elements requires experimental study and analytical models to understand the behavior of panels subjected to various combinations of inplane and lateral loads and to assess the failure mechanism and the ultimate carrying capacity. A review of experimental work and numerical models is presented in the following sections, together with the research objectives.

1.2 Research scope

A research program has been initiated at the University of Alberta where both experimental and numerical approaches are being used to investigate the problem. The work presented herein forms the numerical aspect of the research program. The experimental work was reported by Aghayere and MacGregor (1988). Other experimental studies with varying degrees of generality have been carried out (Swartz *et al*, 1974; Kordina *et al*, 1973, 1979, 1982). A summary of available experimental investigations is briefly presented below, followed by a survey of finite element studies on reinforced concrete panels.

1.2.1 Existing experimental results and analytical solutions

Swartz *et al* (1974) tested slender rectangular panels with an aspect ratio b/a equal to 2.0, simply supported along the boundaries and subjected to an inplane compressive load applied along the short side. Based on these tests, they proposed a design method to evaluate the carrying capacity of slender panels under inplane compression without eccentricity or any lateral loads.

Kordina *et al* (1973; 1979; 1982) tested simply supported square reinforced concrete panels where the axial load was applied eccentrically along two opposite edges. In these tests, axial loads and bending moments were applied simultaneously. In that investigation, with no truly lateral loads applied to the panels, the maximum primary bending moments, without the second order effects included, occur along the edges where the loads are applied and the moment at the center of the plate is only one quarter of the edge moment.

Various analytical solutions for panels subjected to both inplane and transverse loads have been derived for metallic materials such as steel and aluminium, mainly for the aeronautics or ship industries (Conway, 1949). Some of these analytical solutions can be applied to reinforced concrete plates, with some modifications.

In 1986, an experimental program was initiated at the University of Alberta by Aghayere and MacGregor to investigate slender reinforced concrete plates subjected to inplane and transverse loads. These tests provided a first insight into the behavior of such components. Of the nine panels tested, eight had combined loading and one was loaded laterally only. All panels were simply supported along the boundary. Based on this test series, an analytical model and a

simple design procedure were proposed. This test series will be examined more closely later in this study.

1.2.2 Existing finite element models for reinforced concrete plates

The analysis of reinforced concrete structures by the finite element method was initiated two decades ago by Ngo and Scordelis (1967) for beams. A few years later, Jofriet and McNeice (1971) and Bell and Elms (1971) were among the first people to apply nonlinear finite element techniques to reinforced concrete slabs. A global stiffness method was used where an overall moment-curvature relation, reflecting the various stages of material behavior, was assumed.

However, it was recognized rapidly that layered plate elements, where the layers are used to perform an integration over the plate thickness, would represent more adequately the plate stiffness. This approach, now widely accepted was used by Hand *et al* (1973) and Scanlon and Murray (1974) who also proposed one of the first tension softening models for post cracking modelling of concrete.

Time dependant effects such as creep and shrinkage have been incorporated in various models by Scanlon and Murray (1974), and by Kabir (1976). The analysis of reinforced concrete shells, with coupling of membrane and bending actions, was introduced by Lin and Scordelis (1975). Van Greunen (1979), adding to the work by Lin and Scordelis (1975) and Kabir (1976), analyzed the effects of prestressing and time dependent phenomena using a triangular plate-shell element.

In the studies presented above, some use a hypoelastic description of concrete whereas, in other studies, plasticity based concrete models are adopted. Currently, the following characteristics describe the typical approach used to model plate and shell type structures :

1. plate-shell elements with the ability to model the coupling between inplane and bending effects are used (equilibrium in the deformed configuration);
2. the concrete is divided into layers over the element thickness and plane stress conditions are assumed in each layer;
3. reinforcing steel is modelled using additional layers with unidirectional properties only;
4. hypoelastic material models are commonly used;
5. punching shear failure, due to the effects of shear stresses in the transverse direction (through the plate thickness) , is not accounted for.

These aspects summarize briefly the state-of-the-art in the modelling of plate and shell structures made of reinforced or prestressed concrete. The research undertaken in the present study incorporates the latest developments in all the aspects mentioned above.

1.2.3 Objectives of the research

The ultimate objective of the research carried out at the University of Alberta on rectangular reinforced concrete panels loaded axially and transversely is to provide a better understanding of the behavior, and hence realistic design rules. The present work focuses on the prediction of panel

response using the finite element method. The combination of experimental work (Aghayere and MacGregor, 1988) and finite element analysis approaches an ideal situation.

Once the validity of a finite element model is established by comparison to the experimental results, it becomes a powerful research tool which can be used to study aspects related to the behavior of panels. It can also be used to extend the range of the experimental results. In some cases, it can be part of a design process for uncommon structures. With today's developments in microcomputer technology, the finite element method is becoming a more common design tool. Depending on the type of element used and its versatility, it should be possible to extend the type of problem to various structural elements other than plates. This, however, falls outside of the objectives of this study. The prediction of the response of panels is the aspect on which all the attention will be focussed. The scope of this work is limited to panels subjected to uniaxial inplane load in compression and uniformly distributed lateral loads. Also, only panels supported along four edges are considered.

To fulfil this main goal, two ingredients are required: first, the type of plate element used must have the capability of handling large deflections and second order effects, and secondly, the material model must describe adequately the reinforced concrete behavior in plane stress conditions. The element used and the features available in the finite element computer program selected to carry out this study are presented in the following section. The material model is introduced in a subsequent chapter.

1.3 The finite element program

As mentioned in the previous section, the prediction of the behavior of reinforced concrete panels, subjected to any type of loads, requires a valid concrete material model and a suitable reinforcement representation in the context of reinforced concrete plates. Then such a material model must be embedded in a suitable plate bending finite element.

The type of finite element selected for the analysis reported in this study is the plate-shell element implemented in program NISA (Stegmüller *et al*, 1983) which was initially developed at the Institut für Baustatik at Stuttgart University in Germany and modified later at the University of Alberta. The description of the finite element model is presented under the four following aspects: the program NISA, the plate-shell element, the solution strategies adopted to follow a nonlinear response and the technique adopted to follow the stress path in each load step.

1.3.1 NISA

NISA (Stegmüller, 1983) is a nonlinear incremental finite element structural analysis program, written in Fortran 77. This program has various types of finite elements: truss, spring (boundary and coupling), beam, thin walled open section beam with warping, two dimensional element and the three dimensional degenerated plate-shell element developed by Ramm (1976) and used in this study. It is basically a nonlinear finite element program for large strain and large displacement problems, where material nonlinearities can be represented and where geometric nonlinearities are allowed using either the Total or the Updated Lagrangian formulations (Bathe, 1982). The program also

includes a capability for continuous eigenvalue analysis of the deformed structure.

1.3.2 The plate-shell element

Among several elements available in NISA, the 3D degenerated plate-shell element (Fig. 1.6a) is one of the main assets of the program. Degenerated 3D plate shell elements, initially introduced by Ahmad *et al* (1968), extended the analysis of shells into the range of thick shells, not possible before with elements based on the Kirchhoff assumptions where shear strains are assumed negligible. Improvements to these elements were proposed by Pawsey and Clough (1971) with the concept of selective reduced integration for thin shells. Ramm (1977) extended the domain of application of 3D degenerated plate-shell elements into large deformations and removed the problem encountered by early users related to the shear locking phenomenon. Ramm concluded that the shear locking problem with this type of element was probably caused more by computer inaccuracy than by the element formulation itself.

This plate-shell element has five degrees-of-freedom per node, three displacements (u, v, w) and two rotations (α, β) as shown in Fig. 1.6a . The displacement of any point in the element is defined as a function of the midplane displacements and rotations. Independent interpolation functions are used for each of these degrees-of-freedom which allow for shear deformations and membrane forces as illustrated in Fig. 1.6b .

This element can be used for shells with 9 or 16 nodes per element and, in the case of plates, with 4 nodes or more (Fig. 1.6b). In this study, the 16 node bicubic element is adopted. Stegmüller *et al* (1983) suggest that although

elements with a smaller number of nodes should give good results, the rate of convergence may be a problem in some cases. However the 16 node element is reliable and can be used with confidence. A full 4 x 4 Gaussian integration rule over the element plane is adopted. Over the thickness, corresponding to each of the integration points in the r-s plane of the element, the element is divided into layers in which plane stress conditions are assumed (Fig. 1.7a). The strains are evaluated from the interpolation functions at each integration point through the thickness and are used in the constitutive relationships to form the stiffness matrix and to evaluate the stress conditions at each layer. In NISA a Simpson's type integration is performed over the thickness.

In the case of reinforced concrete, the element is assumed to be made of concrete which is divided in layers over the thickness whereas the reinforcing steel or prestressing tendons are represented by additional layers with uniform thickness located at a constant relative depth inside the element (Fig. 1.7b). Eight different reinforcement layers can be specified, each having only unidirectional properties. The reinforcement layers can be located anywhere in the thickness of the concrete element. The program was modified at the University of Alberta to include initial strains or temperature strains for concrete and reinforcement layers in the analysis before loads are applied. In the case of initial strains for concrete, an orientation in the r-s plane of the element can be selected. For the reinforcement, initial strains allow modelling of prestressing tendons with the limitation that over a given element the layer remains at the same position relative to the two faces of the element.

1.3.3 Solution Strategies

Solution strategies can be divided in two levels: first, the solution techniques, which determine the type of approach used to bring the analysis to a converged and adequate solution, and secondly, the iteration techniques, which are related to the type of stiffness matrix used during the iteration process. In the solution technique category one can mention methods such as the load control method, the constant arc-length method, the Quasi-Newton methods (e.g. the BFGS method), etc. A survey of those methods is presented by Crisfield (1982). The iteration techniques are limited to the standard or modified Newton Raphson methods and both are used in any of the solution techniques mentioned before. With the standard Newton Raphson technique, the stiffness matrix is updated at every iteration whereas, with the modified Newton Raphson, the stiffness matrix at the beginning of the load step is used throughout the iteration process. This second approach is usually more economical in terms of computer time but requires more iterations to obtain convergence.

Program NISA allows access to a load control method or a modified constant arc-length method (CALM) introduced by Ramm (1980). Both approaches can be used with either the standard or the modified Newton Raphson techniques. The CALM is an important feature of NISA. This technique allows one to trace a problem response near limit points and on unloading paths which cannot be obtained with load control methods. Basically with the CALM the solution is forced to follow a plane perpendicular to the original arc ΔS as illustrated in Fig. 1.8 . The load control method would be at point 2' at the end of the second iteration whereas the CALM forces the solution to reach point 2 ,

located along the line normal to the initial tangent at m . The load vector $\mathbf{P_m}$ applied to the system at load step m is defined as

$$\mathbf{P_m} = \lambda_m \mathbf{P_1} \tag{1.1}$$

in which $\mathbf{P_1}$ is a basic load vector and λ_m is an indeterminate scalar called the load factor. The technique evaluates λ at each iteration to get closer to the converged solution. More details on this powerful technique are presented in the original paper by Ramm (1980). The CALM technique usually implies a proportional loading history. Program NISA, however, allows an additional constant load vector $\mathbf{P_2}$ to cover certain nonproportional loading problems. In this case Eq. 1.1 becomes

$$\mathbf{P_m} = \lambda_m \mathbf{P_1} + \mathbf{P_2} \tag{1.2}$$

The vector $\mathbf{P_2}$ is not affected by the value of λ and is added directly to the total load vector $\mathbf{P_m}$. This feature is useful in problems where a load remains constant, eg. the inplane load in axially and transversely loaded panels (discussed in section 1.1), while the second set of loads, eg. lateral loads in these panels, are varied by the load factor λ_m . The CALM, with an additional constant load when needed, has been used throughout this study.

1.3.4 Tracing the stress path in a load step

One important modification made at the University of Alberta in the solution strategy is the definition used for the initial strain field ε_o at each iteration. The initial strain field is used to evaluate the incremental strain $\Delta\varepsilon$, which is used in the constitutive relations to evaluate the change in stress field, as

$$\Delta\varepsilon = \varepsilon - \varepsilon_o \tag{1.3}$$

in which ε is the current strain field. Initially, in NISA , ε_0 was kept constant during the iteration process in a given load step, equal to the strain field at the last converged load step. Referring to Fig. 1.8, ε_0 is the strain field corresponding to point m whereas the current strain field is that which exists at points 1, 2, etc. This approach means that the closer one gets to the converged solution, the larger the incremental strain $\Delta\varepsilon$ one has to use in the constitutive relationship. Thus tracing the strain history within a load step becomes less accurate unless the computational effort is proportionally increased. At the same time the strain history is no longer compatible with the current tangent stiffness matrix. It appeared rapidly in the first tests performed with the program that such method could lead to erroneous solutions. The technique adopted in NISA now updates the strain field ε_0 at every iteration which results in faster convergence and noticeable reduction in the computation time. Also the finite element response, in terms of prediction of test results, becomes more reliable.

1.4 Organization of the Thesis

In addition to this chapter, five more chapters and two appendices form this thesis.

In Chapter 2 , the behavior of plain concrete members and reinforced concrete members subjected to uniaxial tension are described. A method of describing the tension stiffening phenomenon is proposed and compared to experimental results.

In Chapter 3 , the constitutive relationships for concrete adopted in this study are presented. The post cracking and the post crushing responses are

described. The fixed and rotating crack models available with the model are described.

In Chapter 4 , the results of validation tests, involving several series of reinforced concrete and prestressed concrete panels, are presented to verify the reliability of the finite element program and the material model introduced in Chapter 3 .

In Chapter 5 , a parametric study on the behavior of reinforced concrete panels loaded axially and transversely is initiated in which the geometry of the panels , the boundary conditions and the type of loading are varied.

In Chapter 6 , a summary of the research and the conclusions that can be drawn are discussed. Recommendations for future work are also presented.

In Appendix A, a parametric description of a notched tension specimen for plain concrete is derived.

Finally, in Appendix B, the modelling of reinforced concrete plates loaded laterally and transversely with the finite element method is examined.

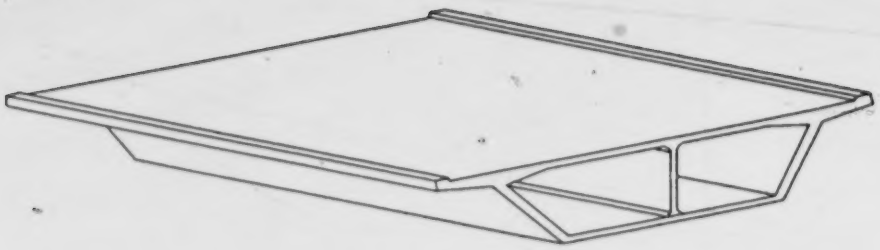

Figure 1.1 - Bridge

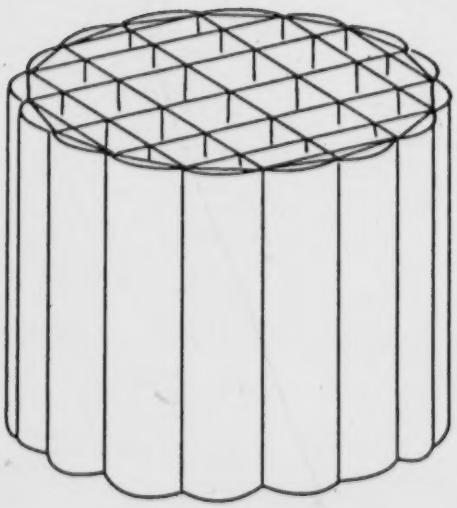

Figure 1.2 - Offshore structure

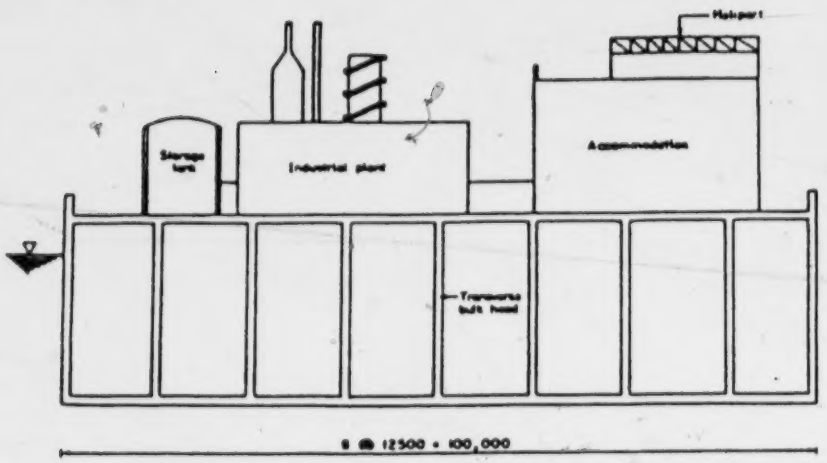

LONGITUDINAL SECTION OF FLOATING PLANT

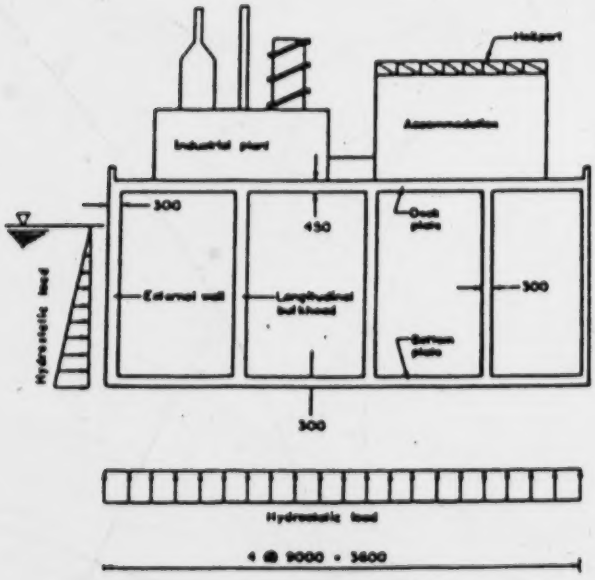

CROSS-SECTION OF FLOATING PLANT

Figure 1.3 - Barges

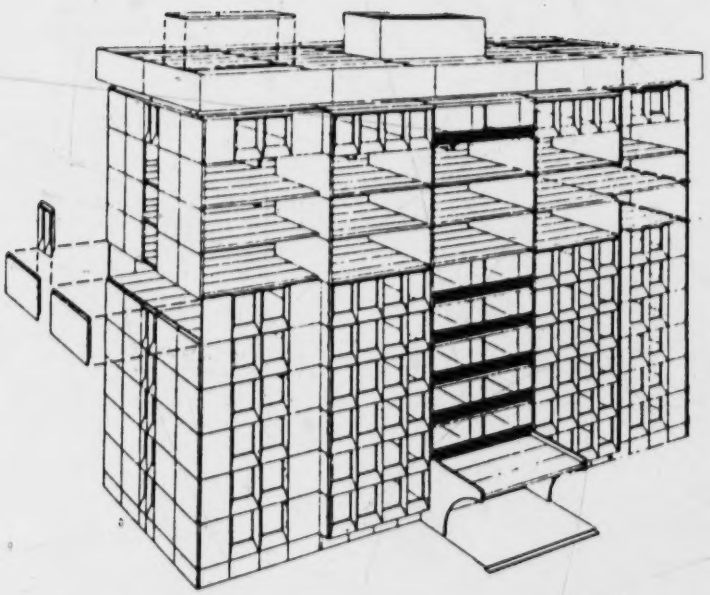

Figure 1.4 - Precast panels

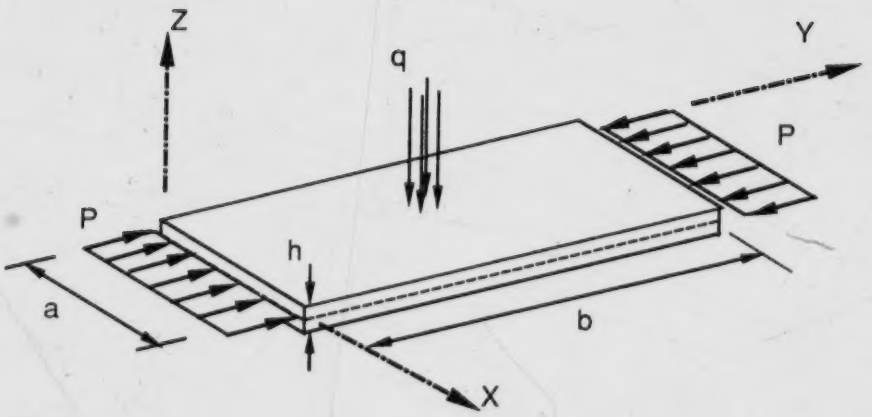

Figure 1.5 - Plate dimensions, coordinates and loading

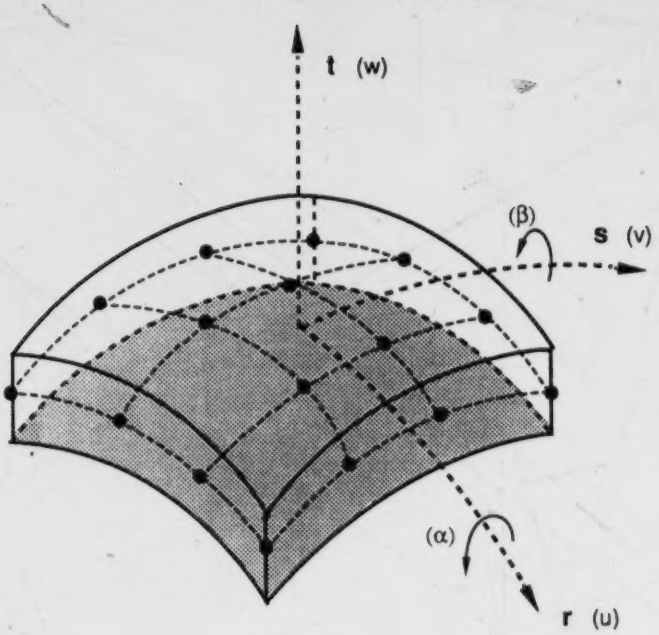

a) Bicubic element

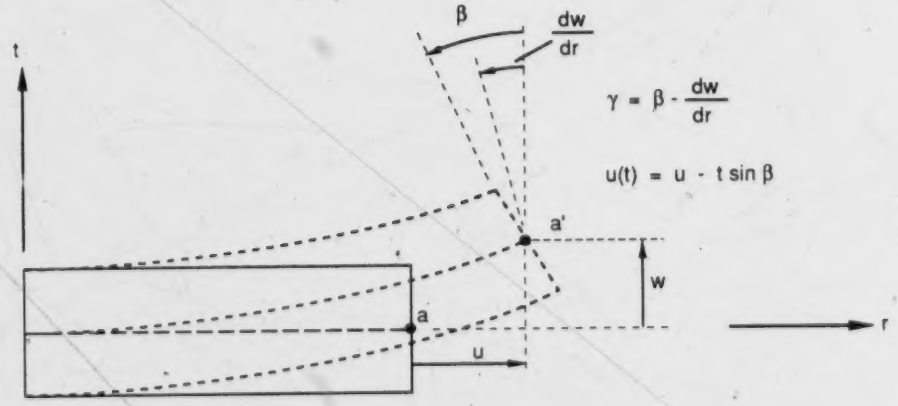

b) Displacement of a point

Figure 1.6 - 3D degenerated plate-shell element

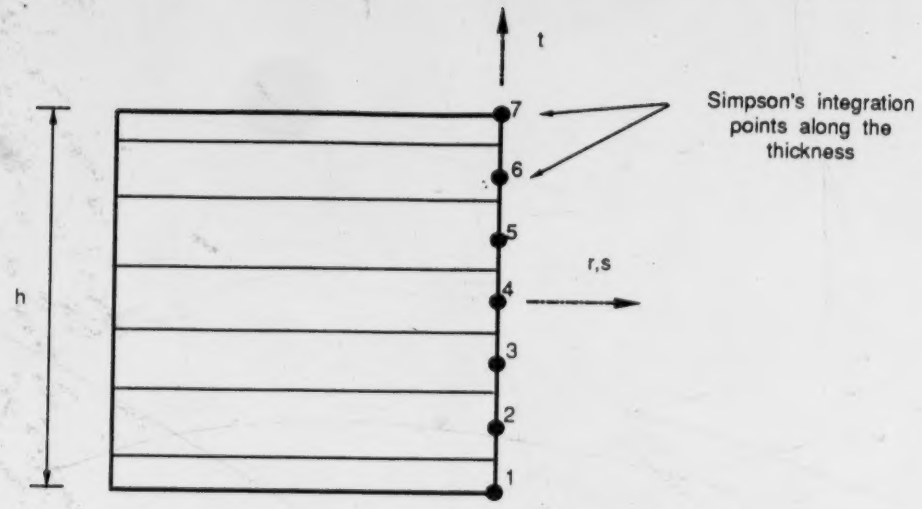

a) Layers over the element thickness

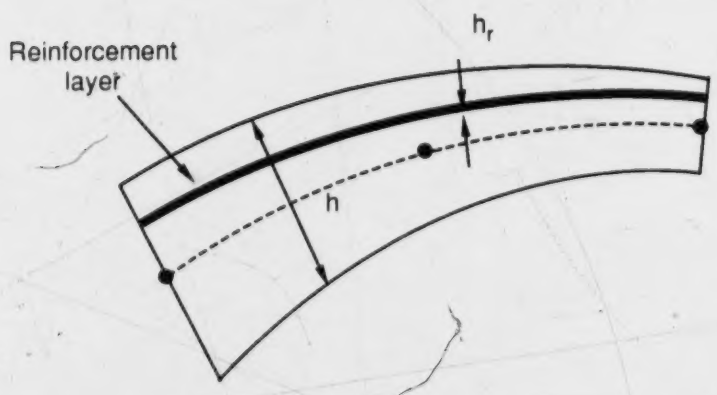

b) Reinforcement layer

Figure 1.7 - Layers in the plate-shell element

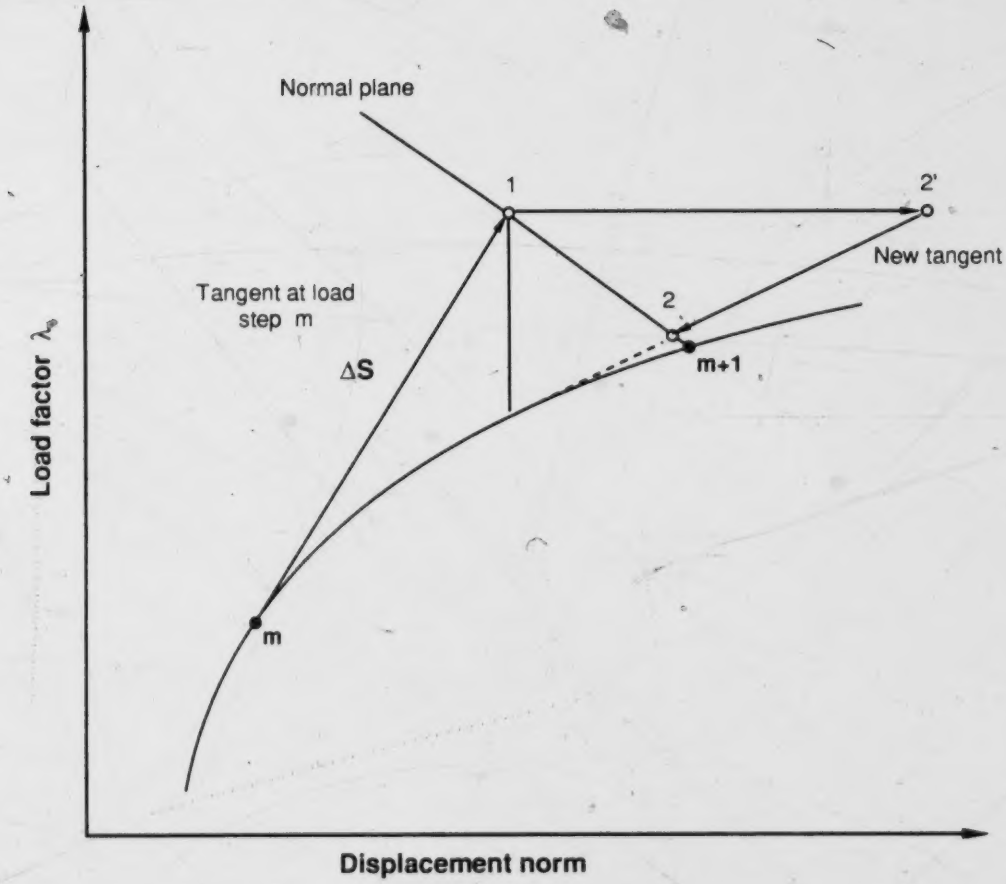

Figure 1.8 - Constant Arc-Length Method

CHAPTER II

MODELLING OF REINFORCED CONCRETE MEMBERS IN TENSION

2.1 Scope

The behavior of reinforced concrete members in tension is currently an important research topic. There are several reasons for this. Among them is the fact that tensile behavior in concrete has been neglected until recently because it usually does not significantly affect member ultimate strength. However the effect of tensile stresses in concrete must be taken into account when the load deflection characteristics of a member are needed, whether this member primarily carries tensile forces or combined tensile and compressive stresses as in flexural problems. Thus in the modelling of a reinforced concrete member with the finite element method, the effects of tension softening and tension stiffening become important and a realistic model should be used in the analysis.

The terminology used to define the postcracking behavior of reinforced concrete members is sometimes confusing. Various terms are used to define the same phenomenon, and a single expression may be used to define different phenomena. To avoid any confusion, the terms strain softening, tension softening and tension stiffening used in this study are defined as follows.

Strain softening refers to any material response where the rate of change of incremental work $dw = d\sigma \cdot d\varepsilon$ is negative. This applies to concrete in the

postcracking or postcrushing response as illustrated in Fig. 2.1. The tension softening phenomenon is associated with the crack process zone development observed in plain concrete members after the tensile strength has been reached (Fig. 2.2).

On the other hand, the tension stiffening effect is a complex phenomenon encountered in reinforced or prestressed concrete members. In this case, concrete progressively releases the stresses present at cracking and transfers the corresponding forces to the surrounding reinforcement by virtue of the bond properties at the concrete-reinforcement interface. As shown in Fig. 2.3a, the tension stiffening effect is measured by the ability of concrete to retain a part of the tensile force after cracking. However the portion of the tensile force carried by concrete after cracking exhibits , when isolated, what has been defined earlier as a strain softening behavior, as illustrated in Fig. 2.3b.

In the literature published on tension softening and tension stiffening, especially when a finite element approach is considered, emphasis is mainly placed on crack growth and localized effects (e.g. Bazant and Oh, 1983). In the case of reinforced concrete, bond properties at the concrete-reinforcement interface, shear force and bond slip have been investigated in detail, at a small scale (e.g. Gerstle *et al*, 1982). This type of research is important and provides insight into the mechanics of phenomena such as crack growth, bond slip, etc. However this approach is not yet applicable to full scale problems like bridges, offshore structures, shear walls, etc in which a global response is needed.

Several global alternatives to include the tension stiffening effect exist in the literature, e.g. the European Model Code approach (CEB, 1978 and 1985),

which deals with uniaxial tension and bending problems, and the Collins and Mitchell (1987) method which deals with uniaxial tension only but can be applied in bending cases. As illustrated in a recent report by the ACI Committee 224 (1986), there exist various approaches in the modelling of the global postcracking behavior of reinforced concrete members in finite element applications. The user is usually faced with the selection of a postcracking stress-strain curve for concrete and has to adjust the shape of the strain softening curve in tension from one problem to another. Schnobrich (1985) pointed out that no consensus exists on the value that should be assigned to the maximum strain of the stress-strain curve in tension but suggests that, to be conservative, the yield strain of the reinforcement should be used as an upper bound. He also indicated that the inclusion of a realistic tension stiffening model is very important when analyzing lightly reinforced sections.

In the work presented in this study the global behavior of reinforced concrete structures is considered and the approach used to describe the tension stiffening phenomenon accounts for the average effects of many localized phenomena on the overall member behavior.

This chapter is divided into four sections. First, the behavior of plain concrete members is analyzed, followed by a new approach to define the tension stiffening behavior of reinforced concrete members. The concepts of effective concrete area and effective reinforcement ratios used with the proposed model are discussed. Finally, the response of the model is compared to experimental results from the literature.

2.2 Plain concrete members in tension

In the last few years a significant research effort has been devoted to the understanding of plain concrete behavior in tension. Some aspects of this subject are described in this section , particularly the energy dissipated in a crack. A simple relationship is proposed to evaluate the cracking energy based on several experimental results. Finally, a stress-strain curve for plain concrete in tension is presented.

2.2.1 Cracking energy

The cracking energy per unit of area G_f, also called the fracture energy, can be defined as the energy dissipated in the opening of a crack. For a plain concrete specimen in direct tension (Fig. 2.4a), the expression for G_f can be written as

$$G_f = \int_0^{w_o} \sigma \, dw \qquad (2.1)$$

in which σ is the average stress over the considered area , w is the crack width in the fracture process zone and w_o is the crack width when σ reaches zero at the end of the tension softening branch. The cracking energy is then equal to the area under a stress-elongation curve, illustrated by the shaded area in Fig. 2.4b where the elongation δ is measured over the gage length L_o. As stated by Hillerborg (1985), G_f can be considered as a material property, independent of the specimen dimensions and the gage length L_o used to measure the elongation, as long as L_o is larger than the width of the fracture process zone, w_c . For this reason using different gage lengths L_o changes the shape of the stress-elongation curve but not the crack width w and hence G_f remains unaffected. The width

of the fracture process zone, w_c, is a simplifying assumption used to define an average crack strain, ε_m. This is illustrated in Fig. 2.5c. The expression for G_f can be rearranged and expressed as a function of a stress-strain law, more common in the description of engineering materials. Thus W_f is defined as the strain energy density (or work per unit of volume) dissipated by cracking expressed as

$$W_f = \frac{G_f}{w_c} = \int_0^{\varepsilon_{max}} \sigma \, d\varepsilon \qquad (2.2)$$

W_f represents the area under a stress-strain curve for concrete in tension. Hillerborg (1985) pointed out that unlike metallic materials, the energy absorbed by plain concrete members in tension is mainly associated with the descending branch. Also damage consists mainly of cracks perpendicular to the principal tensile stress and the σ-w curve (Fig. 2.4b) is not dependent on stresses in other directions. Additionally the independence of σ-w curves with respect to specimen shapes allows one to use G_f for any type of structure. This also permits measuring G_f from various schemes. The most commonly used are illustrated on Fig. 2.6. In the next two sections, some relationships relating the tensile strength f'_t to G_f and W_f are derived based on available experimental results.

2.2.2 Observation from experiments

To derive a stress-strain curve for concrete in direct tension, the values of at least two parameters are needed, as far as Eq. 2.1 is concerned: G_f and w_c. Experimental investigations usually provide G_f but w_c must be assumed. Once these parameters are known, W_f can be evaluated and subsequently the stress-

strain curve, W_f being equal to the area underneath a complete stress-strain curve with the ascending and descending branches.

An examination of experimental results for concrete in direct tension shows clearly that the ascending branch is almost linear while the descending branch is nonlinear, with a very steep slope just after cracking which decreases progressively as the strain increases. Various types of softening branches after cracking have been proposed: linear, bilinear, exponential, etc. Among all those, the bilinear one, similar to Fig. 2.7, is probably the most desirable, because it is simple and represents well the actual shape of the softening branch. Hillerborg (1985) compared bilinear tension softening curves to different experimental results and noted good agreement between the assumed and measured curves. He also observed that the change of slope in the softening region usually occurs at a stress level of about one third of the cracking stress. However, by adopting a bilinear tension softening curve, two more slopes are needed to define completely the behavior of concrete in direct tension.

The stress-strain curve adopted herein is illustrated in Fig. 2.7. It is entirely defined by the tensile strength, f'_t, the initial modulus, E_c, the descending branch moduli, E_1 and E_2, and the stress ratio at the change in slope, μ. The evaluation of these parameters is possible only by examining test results.

A well documented test series on the behavior of plain concrete prisms in direct tension has been published by Gopalaratnam and Shah (1985). A parametric description of prisms, such as those tested by Gopalaratnam and Shah (Fig. 2.8a), is presented in Appendix A. One of their tests was reported in sufficient detail to allow the following parameters to be evaluated:

- $E_c / E_1 = -5.86$;
- $E_c / E_2 = -49$;
- $w_c = 0.7$ in $= 2\, d_a$;

in which d_a is the maximum aggregate size. These values indicate the order of magnitude of the various terms.

Bazant and Oh (1983) analyzed several test results from various researchers performed on different types of test set up. They concluded that the ratio of w_c to d_a ranges from 1.5 to 4.0 for various types of concrete and they suggest that w_c equal to $3\, d_a$ would generally be a good assumption. They also proposed a relationship relating E_1 to E_c, based on best fit on several experimental results. Ratios of E_c to E_1, evaluated using their equation, are presented in Table 2.1 for tensile strengths varying from 1 to 4 MPa.

2.2.3 Proposed stress-strain curve in tension

Based on experimental observations mentioned in the previous sections, a trilinear stress-strain curve is adopted, with a linear ascending branch and a bilinear softening branch for concrete after cracking. The change of slope in the descending branch occurs at one third of f'_t, as proposed by Hillerborg. The value for w_c proposed by Bazant and Oh where w_c is equal to three times the aggregate size d_a is also adopted. Based on the analysis presented in Appendix A, the ratio of E_c to E_1 is taken as a constant value equal to - 6.0 . This value corresponds to a tensile strength of 2.5 MPa if the Bazant and Oh equation is used (see Table 2.1). For the evaluation of the cracking energy, it appears from Gopalaratnam and Shah (1985) and also from Bazant and Oh (1983) that G_f (or

W_f) is a function of f'_t ; the higher f'_t , the higher G_f . The type of relationship adopted in this study is

$$G_f = K\ w_c\ \frac{f'^2_t}{E_c} \tag{2.3}$$

Calculated values for K , based on available experimental results, are presented in Table 2.2 . In most cases not all the information required to evaluate K was available and some parameters had to be calculated or measured on figures. Based on an average value for K of 5.26 , it is reasonable to use a rounded off value of 5 as an estimate of K. This means that W_f is given by the following equation:

$$W_f = 5\ \frac{f'^2_t}{E_c} = 5\ f'_t \varepsilon_{cr} \tag{2.4}$$

Hence the total area under the stress-strain curve in tension is equal to ten times the area under the ascending branch. With W_f given by Eq. 2.4, the ratio of E_c to E_2 is equal to - 33.0 . The stress-strain curve for plain concrete in tension adopted in this study is shown in Fig. 2.7 . The parameters defining the curve are summarized in Table 2.3 .

The value adopted for w_c and used to evaluate W_f from G_f corresponds to measurements on concrete specimens. To model the response of plain concrete specimens with the finite element method, where a smeared crack approach is used , w_c must be taken equal to the spacing of the integrations points , but , if a very fine mesh is used, w_c should not be taken less than $3d_a$. However, no finite element mesh should be finer than $3d_a$.

2.3 Reinforced concrete members in tension

In the last section , the behavior of plain concrete members in tension was discussed while, in this section, the behavior of reinforced concrete members is examined. The term used to define the concrete contribution of the tensile behavior of reinforced concrete members after cracking is the tension stiffening effect.

In this section, the tension stiffening phenomenon is described qualitatively and the CEB model is summarized. A new approach to consider the tension stiffening effect is then introduced and the various stages of the cracking process are described using this new model. The effect of cracks at an angle to the reinforcement is also taken into account. Finally, the results of a limited parametric study using the proposed approach are presented.

2.3.1 Qualitative description of tension stiffening

The tension stiffening phenomenon can be defined as the increase in stiffness in a reinforced concrete member due to the interaction between concrete and reinforcement, as illustrated in Fig. 2.3. The reason for such behavior can be explained as follows. As a member cracks (Fig 2.9a), concrete between the cracks tends to move back to its original (unstressed) position. This is restrained by the reinforcement, thus developing some tensile stresses in concrete (Fig. 2.9b).

The ability to restrain the concrete is a function of the existing bond between reinforcement and concrete. With perfect bond, no slip occurs between concrete and reinforcement, while with poor bond, relative displacement can occur. Also, not all concrete develops (or maintains) some tensile stresses but

rather only a portion of the concrete area, called the effective area A_{cef} . More explanations and relationships on the effective area are presented in section 2.3.7 .

Typical load-deformation curves are illustrated in Fig. 2.10 (adapted from CEB, 1985). It can be seen that tension stiffening decays as the load increases beyond the cracking load and that good bond properties increase the stiffening effect. Also, tension stiffening is more significant for low reinforcement ratios than for higher ones, as illustrated by the values of T_c in Fig. 2.10. This was also shown experimentally by Rao (1966) in case of beams.

Figure 2.11 shows qualitatively how the stress in concrete and reinforcement varies between the cracks. It is assumed that some tensile stresses may exist at the crack itself due to the tension softening effect described in the previous section. As illustrated, the average stress in the steel is the same for good or poor bond, only local stresses differ.

2.3.2 CEB model for tension stiffening

In the model for tension stiffening described by CEB (1985), the tensile stress in the concrete at the cracks is assumed to be zero and the member is divided into two regions: region I, uncracked, and region II, fully cracked (Fig. 2.12). In region I, both the concrete and steel behave as if the concrete had an infinite tensile strength while in region II the reinforcing steel carries all the tensile force on the member after cracking. The relative length of the two regions, determined by a distribution coefficient ζ , was derived in case of beams by Rao (1966), and is defined for reinforced concrete members in uniaxial tension as

$$\zeta = 1 - \beta_1 \beta_2 \left(\frac{f_{scr}}{f_s}\right)^2 \qquad (2.5)$$

where

$\beta_1 = 1.0$ for high bond bars ;

$\beta_1 = 0.5$ for smooth (plain) bars ;

and

$\beta_2 = 1.0$ for first loading;

$\beta_2 = 0.5$ for long term or cyclic loading.

Reinforcement stresses f_{scr} and f_s are those existing in region II at cracking and after cracking respectively, assuming no stress in the concrete for both cases. The average strains in the steel over the length S_m are expressed as

$$\varepsilon_{sm} = (1 - \zeta)\, \varepsilon_{s1} + \zeta \varepsilon_{s2} \qquad (2.6)$$

in which ε_{s1} and ε_{s2} , corresponding to the reinforcement strains in regions I and II respectively, are given by the following equation:

$$\varepsilon_{s1} = \frac{T}{E_c A_c + E_s A_s} \qquad (2.7)$$

$$\varepsilon_{s2} = \frac{T}{E_s A_s} \qquad (2.8)$$

This method can be used in design to evaluate the average behavior of a member for a given axial load T. A similar approach is presented by CEB (1985) for bending where the actual curvature of a section is expressed as a weighted average of the curvatures in region I and in region II.

2.3.3 Proposed approach for tension stiffening

The CEB model described in section 2.3.2 was derived for use in design and is applied, for example, in crack width calculations. However this model does not represent completely the actual behavior of concrete and, in its present form, cannot be included in a finite element environment. The CEB model for tension stiffening is used to evaluate the average strain (or curvature) in a member for a given load level. In the case of finite element analysis, the strain is known from the displacement field while the average stress carried by concrete is needed.

Since the CEB model describes adequately the tension stiffening phenomenon, the proposed approach keeps the essence of the CEB method and incorporates new features like tension softening at cracks. Also the equations are derived in terms of a stress-strain law based on equilibrium. The assumptions for the model can be summarized into six points:

1) The CEB model regions I and II are used to determine the average strain in the member (ε_{ST}) and the relative weight of each region is described by the distribution coefficient ζ defined in Eq. 2.5 . The average stress in the member is found from equilibrium conditions. For an average crack spacing S_m , the lengths l_1 and l_2 , of regions I and II , are defined

$$l_1 = (1 - \zeta)\, S_m \qquad (2.9)$$

$$l_2 = \zeta\, S_m \qquad (2.10)$$

2) In region II, governed by cracking, tension softening is assumed to take place over the entire length of the region based on the stress-strain law

defined in Fig. 2.7 and in Table 2.3 . The concrete stress in region II is referred to as f_{SO}, since it follows the softening law of concrete.

3) At cracking, perfect bond between concrete and reinforcement is assumed. The strain in region I is then equal to ε_{cr}, for both concrete and steel. In region II , the strain is governed by the strain softening response of concrete after cracking ε_{c2} and is the same for the reinforcement (Fig. 2.13a).

4) After cracking the average strain in the reinforcement ε_{sm} between two cracks is equal to the average strain in concrete ε_{cm} over the same region but locally the steel and concrete strains do not coincide, allowing for bond slip through the factors β_1 and β_2. This is expressed in the following equation:

$$\varepsilon_{sm} = \frac{1}{S_m} \int_0^{S_m} \varepsilon_s \, dx = \varepsilon_{cm} = \frac{1}{S_m} \int_0^{S_m} \varepsilon_c \, dx \qquad (2.11)$$

5) The member reaches its maximum carrying capacity when yielding occurs in the cracked region. No strain hardening is taken into account in the reinforcement.

6) The effective reinforcement ratio, ρ_{eff} , as defined by CEB (1978), is adopted in this model. In the equations derived in this section , the term ρ is used for simplicity but it must be interpreted as ρ_{eff} which must be used in all cases.

In this model it must be realized that the stresses used in region I after cracking do not correspond to actual values since concrete is allowed to strain

beyond f'_t ($\varepsilon_{c1} > \varepsilon_{cr}$) as in the CEB model where this region is assumed uncracked at stress levels greater than f'_t. However this assumption is used only to evaluate the average strain on the member ε_{ST} and not the stress f_{ST} which is evaluated from actual equilibrium conditions.

In all these assumptions, the introduction of a progressive release of stresses in the cracked region, due to the tension softening behavior of concrete, allows one to define more precisely the various stages involved in the tension stiffening phenomenon. The introduction of tension softening in region II affects the ratio of f_{scr} to f_s used in Eq. 2.5 . Since stresses in the concrete are allowed at the crack, f_{scr} in this model is smaller than it would be with the CEB model, hence affecting the distribution coefficient ζ .

The two main phases describing tension stiffening , the cracking condition and the postcracking conditions, can now be described. The relationships derived in the next two sections are based on equilibrium of forces between the cracked and the uncracked regions. The subscript ST is used hereafter to describe stress and strain coordinates on the tension stiffening curve for concrete.

2.3.4 Stabilized cracking condition

The stabilized cracking condition prevails just after cracking when the axial load on the member at cracking T_{cr} , is kept constant and stresses redistribute between concrete and reinforcement. This stage occurs during the formation of primary cracks. After a crack has just formed, the stress in the concrete in region II decreases at a rate equal to $-E_c / 6$, as stated in the second assumption, while steel at the same location is stressed at a rate E_s . If ρ is the reinforcement ratio, and

n is the modular ratio, equal to the ratio of E_s to E_c, the stabilized cracking condition is found as

- the change in load carried by the concrete in region II for an increment of strain $\Delta\varepsilon$ is:

$$\Delta T_c = - \frac{A_c E_c}{6} \Delta\varepsilon$$

- the change in load carried by the steel in region II for the same strain increment $\Delta\varepsilon$ is :

$$\Delta T_s = A_s E_s \Delta\varepsilon$$

- from the equilibrium condition $\Delta T_c + \Delta T_s = 0$, one can define the minimum reinforcement ratio required to maintain constant strain at the crack when the load T_{cr} is applied to the member :

$$\rho_{stbl} = \frac{1}{6n} \qquad (2.12)$$

For ρ greater than or equal to ρ_{stbl}, the strain in region II will remain equal to ε_{cr} at a load T_{cr}. In a stroke controlled test, the load on the member will stay constant for a given displacement. This could be interpreted also as the minimum area of steel needed for a test set up to measure accurately the tension softening branch in a plain concrete tension test (section 2.2), based on the assumption that concrete unloads at the crack at a rate $- E_c / 6$.

For ρ smaller than ρ_{stbl}, cracking is not stable and the crack opens until steel has picked up the tensile force released by concrete. In doing so the strain will increase beyond ε_μ (see Fig. 2.7). Hence concrete in region II will follow the tension softening branch along the second segment of the strain softening

curve and can continue past the maximum strain of that curve, ε_{max} , if the amount of reinforcement is not sufficient to stabilize the opening of the crack. From equilibrium, when the strain in concrete is between ε_{μ} and ε_{max} , the conditions at cracking are:

- force in the reinforced concrete member just before cracking:

$$T_{cr} = A_c f_t + A_s E_s \varepsilon_{cr}$$

- force at the cracked section after crack opening is stabilized :

$$T_{cr} = A_c \left(\frac{16}{33} f_t - \frac{E_c}{33} \varepsilon_{c2} \right) + A_s E_s \varepsilon_{c2}$$

- equating these two equations gives:

$$\varepsilon_{c2} = \varepsilon_{cr} \frac{(17 + 33\, n\rho)}{(33\, n\rho - 1)} \qquad (2.13)$$

Since ε_{c2} expressed by the tension softening law is limited to $16\, \varepsilon_{cr}$, the limit value for ρ corresponding to a value of ε_{c2} equal to ε_{max} would be:

$$\rho_{lim} = \frac{1}{15n} \qquad (2.14)$$

For a reinforcement ratio smaller than ρ_{lim} , tension softening does not contribute at cracking and all forces carried by concrete in region II before cracking are transferred to the reinforcement, resulting in the following strain, assuming no slip at cracking:

$$\varepsilon_{c2} = \varepsilon_{cr} \left(1 + \frac{1}{n\rho}\right) \qquad (2.15)$$

This value of ε_{c2} is limited by yielding of reinforcement at the crack when cracking occurs which defines ρ_{yld} by isolating ρ in Eq. 2.15 with ε_{c2} set to ε_y:

$$\rho_{yld} = \frac{\varepsilon_{cr}}{n\,(\varepsilon_y - \varepsilon_{cr})} \qquad (2.16)$$

The average strain and stress for the member at cracking are defined by:

$$\varepsilon_{STcr} = (1 - \zeta_{cr})\,\varepsilon_{cr} + \zeta_{cr}\,\varepsilon_{c2} \geq \varepsilon_{cr} \qquad (2.17)$$

$$f_{STcr} = (1 - \zeta_{cr})\,f'_t + \zeta_{cr} f_{SO} \geq f_{SO} \qquad (2.18)$$

in which ζ from Eq. 2.5 becomes:

$$\zeta_{cr} = 1 - \beta_1\beta_2 \geq \frac{w_c}{S_m} \qquad (2.19)$$

The point defined by ε_{STcr} and f_{STcr} on the stress-strain curve for concrete with the tension stiffening effect included corresponds to the average conditions prevailing in a reinforced concrete member at a load T_{cr}. The distribution factor ζ_{cr} should be larger than the ratio of the width of the fracture zone (w_c) to the crack spacing (S_m), as expressed in Eq. 2.19, the length of region II being at least equal to w_c .

To illustrate the effect of ρ and ζ on the variation of f_{STcr} and ε_{STcr}, an example is presented in which the various parameters derived in this section are evaluated in the case of an axially loaded and axially reinforced prism. The properties of the member selected and the values of parameters in the example are given in Table 2.4 . The reinforcement ratios ρ_{stbl} , ρ_{lim} and ρ_{yld} were evaluated using Eqs. 2.12, 2.14 and 2.16 respectively. Three reinforcement ratios and three values for the $\beta_1\beta_2$ product were selected. Results of the example are given in Table 2.5 . As expected, for ρ larger than ρ_{stbl} , ε_{STcr} and f_{STcr} are equal to ε_{cr} and f'_t respectively. With a reinforcement ratio between ρ_{stbl} and ρ_{lim}, there are some stresses at the crack and the strain ε_{STcr}

increases when $\beta_1\beta_2$ decreases while f_{STcr} decreases with $\beta_1\beta_2$. For ρ smaller than ρ_{lim}, the behavior is similar to the previous case except no stress remains at the crack.

2.3.5 Postcracking conditions

The state of the member after cracking can be established from equilibrium in the same manner as for conditions at cracking. However, due to the nonlinear nature of the relationships involved, there is no closed form solution. For this reason, two conditions related to the reinforcement are examined: yielding in region II and average yielding of the member. In the first case the following relationships are obtained:

- the force at the crack (region II) with all concrete stresses released is:

$$T = A_s E_s \varepsilon_y$$

- the force in the member in region I :

$$T = A_c E_c \varepsilon_{c1} + A_s E_s \varepsilon_{s1}$$

- the average strain on the member when yielding occurs in region II is:

$$\varepsilon_{STy} = (1 - \zeta_y)\, \varepsilon_{s1} + \zeta_y \varepsilon_y$$

- using the basic assumption that in region I $\varepsilon_c = \varepsilon_s$, one obtains:

$$\varepsilon_{STy} = \frac{(n\rho + \zeta_y)}{1 + n\rho}\, \varepsilon_y \qquad (2.20)$$

in which

$$\zeta_y = 1 - \beta_1\beta_2 \left(\frac{f_{sxr}}{f_y}\right)^2 \qquad (2.21)$$

The corresponding stress in the concrete is found from the equilibrium of the forces in region II and the average force on the member:

- at the crack:

$$T = A_s E_s \varepsilon_y$$

- force on the member from average strain:

$$T = A_c f_{STy} + A_s E_s \varepsilon_{STy}$$

- which leads to:

$$f_{STy} = n \rho E_c (\varepsilon_y - \varepsilon_{STy}) \qquad (2.22)$$

When steel yields at the crack, the member has reached its ultimate tensile strength and the strain value increases until average yielding at the reinforcement is attained. When the average strain in the member reaches ε_y, the stiffening effect of the concrete ends as illustrated in Fig. 2.14 a . The three points defining the phases on the tension stiffening curve are illustrated in Fig. 2.14b .

To illustrate which stress and strain values are associated with those points, the examples presented in section 2.3.4 are used again and results are given in Table 2.6 . These results show clearly that tension stiffening is proportionally more important for lower reinforcement ratios and that better bond quality ($\beta_1\beta_2$ closer to 1.0) increases the stiffening effect.

The equations derived in this section and in the previous section, provide the coordinates of three points (Fig. 4.14b): the cracking condition (ε_{STcr} , f_{STcr}), yielding at the crack (ε_{STy} , f_{STy}) and overall yielding (ε_y , 0). The tension

stiffening response between these points is assumed linear, except between the cracking point and yielding at the crack conditions.

It was mentioned earlier that the response is nonlinear in this portion of the curve. For simplicity, a second order relationship is adopted which is expressed as

$$f_{ST} = f_{STy} + (f_{STcr} - f_{STy}) \left[1 - \frac{(\varepsilon_m - \varepsilon_{STcr})}{(\varepsilon_{STy} - \varepsilon_{STcr})} \right]^2 \qquad (2.23)$$

where ε_m is the average strain at which the concrete stress f_{ST} is evaluated. The CEB equation for tension stiffening, Eq. 2.5, also is a second order relationship.

Using this equation the complete concrete stress-strain curves for the example presented in this section and the previous section are illustrated in Figs. 2.15a, 2.15b and 2.15c for ρ values of 2.5 %, 1.5 % and 0.75 % respectively. In Fig. 2.16, stress-strain curves are shown for the three reinforcement ratios for $\beta_1\beta_2$ equal to 0.9 . As it can be seen on this figure, tension stiffening stresses for high ρ values are very close to the strain softening curve. Hence, when reinforcement ratios are larger than or equal to ρ_{stbl}, the strain softening law can be used as a good approximation for the tension stiffening contribution of concrete. This rule is adopted in this study.

2.3.6 Crack not orthogonal to reinforcement

Frequently, cracks in a reinforced concrete member do not form in an orthogonal orientation with respect to the reinforcement. For one crack crossing one rebar (Fig. 2.17a) and assuming that only the strain perpendicular to the crack is non zero, the strain in the rebar (ε_r) is expressed as

$$\varepsilon_r = \varepsilon_m \cos^2 \Delta\theta \tag{2.24}$$

in which ε_m is the average strain in the direction normal to the crack and $\Delta\theta$ is the angle between the reinforcement orientation (θ_r) and the normal to the crack (θ_{cr}). The component of the rebar force in the direction normal to the crack becomes

$$T_s = A_s E_s \varepsilon_m \cos^3 \Delta\theta \tag{2.25}$$

Based on Fig. 2.17b, the force normal to the crack T_{cr} can be expressed as

$$T_{cr} = A_c f_{ST} (1 + n \rho \cos^4 \Delta\theta) \tag{2.26}$$

with

$$A_c = A_c^* \cos \Delta\theta$$

$$A_s = \rho A_c$$

From Eq. 2.26, the equivalent reinforcement ratio ρ_{eq}, can be defined as

$$\rho_{eq} = \rho \cos^4 \Delta\theta \tag{2.27}$$

This value indicates the amount of steel required in the direction normal to the crack to produce the same effect as the actual reinforcement. When yielding occurs in the rebar, the equivalent yielding strain normal to the crack, ε_{yeq}, is given by:

$$\varepsilon_{yeq} = \frac{\varepsilon_y}{\cos^2 \Delta\theta} \tag{2.28}$$

Eqs. 2.27 and 2.29 were derived for one rebar. More general relationships for more than one rebar can be given by the following equations, in which n_r is the number of bars crossing a crack:

$$\rho_{eq} = \sum_{i=1}^{n_r} \rho_i \cos^4 \Delta\theta_i \tag{2.29}$$

$$\varepsilon_{yeq} = \sum_{i=1}^{n_r} \frac{\phi_i \varepsilon_{yi}}{\cos^2 \Delta\theta_i} \tag{2.30}$$

$$f_{yeq} = \sum_{i=1}^{n_r} \frac{\phi_i f_{y_i}}{\cos^2 \Delta\theta_i} \tag{2.31}$$

where ϕ_i is a participation factor defined as

$$\phi_i = \frac{\rho_i}{\rho_{eq}} \cos^4 \Delta\theta_i \tag{2.32}$$

To avoid numerical problems, a limit must be placed on $\Delta\theta$, since bars almost parallel to a crack do not contribute significantly to the tension stiffening behavior. For example, one can use an absolute limit such as 10 degrees.

In this model, only the strain in the direction of the normal to the crack is used to derive the relationships. However this simplification should not affect the model significantly in a tension-compression case since the strain in the direction of the compression stress is significantly smaller the the tensile strain. In biaxial tension, for cracks at angle to the reinforcement, the actual strain in the reinforcement could be larger than what is assumed in this model. A more complete model which considers the actual strain field was presented by Link *et al* (1988).

2.3.7 Effective reinforcement ratio

As mentioned before, not all the concrete in a given section is affected by the presence of the reinforcement and maintains some tensile stresses after cracking. In this study the CEB Model Code (1978) concepts of effective concrete embedment zone and effective reinforcement ratio are adopted.

The effective concrete embedment zone in the vicinity of a reinforcing bar after cracking is called A_{cef} and is defined as the area of concrete of width and height equal to 15 times the bar diameter ($15\,\phi$), centered on this bar. This area is however truncated by the geometrical limits of the member and does not overlap with effective concrete area of other bars. Figure 2.18 illustrates the limits used to define the effective concrete area for some applications.

From the definition of A_{cef} , the effective reinforcement ratio is expressed as

$$\rho_{eff} = \frac{A_s}{A_{cef}} \tag{2.33}$$

in which A_s is the rebar area. Since ρ_{eff} is always larger or equal than ρ , the tension stiffening effect would be reduced. For all occurrences of ρ in the equations presented in this chapter, the effective reinforcement ratio must be used if ρ_{eff} is less than ρ . Not doing so can lead to unconservative results.

2.4 Comparison with experimental results

Member behavior expressed by the tension stiffening model introduced in the previous section must be compared to experimental results. Three types of tests will be used to verify the model: direct tension tests and flexural tests, where

cracks form perpendicularly to reinforcement, and shear panels, where the reinforcement is at an angle with respect to the cracks.

2.4.1 Direct tension tests

Rostásy *et al* (1976) performed a series of direct tension tests on 6 meter long reinforced concrete members with 300 mm x 500 mm cross sections. The five tests reported are called V1 to V5 . The specimen properties are given in Table 2.7. For each of these tests, a comparison is made in terms of stress quantities defined as

$$f_{test} = \frac{T}{A_c} \tag{2.34}$$

$$f_{STtest} = \frac{T - A_s E_s \varepsilon_{ST}}{A_c} \tag{2.35}$$

$$f_{model} = \frac{A_c f_{STmodel} + A_s E_s \varepsilon_{ST}}{A_c} \tag{2.36}$$

$$f_{steel} = \frac{A_s E_s \varepsilon_{ST}}{A_c} \tag{2.37}$$

in which $f_{STmodel}$ is evaluated using the equations of section 2.3 .

Results of the comparison are shown on Figs. 2.19 to 2.23, corresponding to tests V1 to V5 respectively. In all five cases experimental values and the model agree well.

Rizkalla *et al* (1983) carried out a series of tests on rectangular panels loaded uniaxially. The specimen chosen is referred to as #2 in the paper and was 762 mm (30 in.) long, 305 mm (12 in.) wide and 178 mm (7 in.) thick. The reinforcement ratio in the loaded direction was equal to 1.47% with no reinforcement in the transverse direction. Data used in the model are given in

Table 2.7. Comparisons of the model predictions and experimental results are presented in Fig. 2.24, showing excellent agreement.

In these axial tension tests, reinforcement ratios were below ρ_{stbl} except for Rizkalla's test and Rostásy's test V4 where ρ values were larger than ρ_{stbl}. It should be mentioned that β_1 and β_2 (Eq. 2.5) were taken equal to one in all cases since deformed bars were used and no cyclic loads were applied to these specimens. Also a constant value for w_c / S_m^* equal to 0.1 was used and effective reinforcement ratios were evaluated following the rules presented in section 2.3.7.

2.4.2 Bending test

Rostásy *et al* (1976) also tested a specimen subjected to uniform moment, without axial load. This specimen had the same cross sectional dimensions as the uniaxial tension series, with a 4 meter clear span between supports. The test was modelled using the proposed approach and comparison with test results are illustrated in Fig. 2.25 . The properties used for the analysis are given in Table 2.7. The agreement between experimental and analytical behavior is satisfactory.

2.4.3 Shear panels

Several square reinforced concrete panels were tested by Vecchio and Collins (1982) at the University of Toronto, many of them in pure shear. Five panels were selected, namely panels PV3, PV4, PV6, PV16 and PV23. These panels were loaded in pure shear except for panel PV23 which was loaded in combined shear and biaxial compression. All these panels had the same reinforcement ratio in orthogonal directions and the actual reinforcement ratios in the panels are equal to the equivalent reinforcement ratios defined in Eq. 2.33 . Material properties for these panels are given in Table 2.8, parameter values used

with the model are shown in Table 2.9 and points along the tension stiffening curve for concrete are presented in Table 2.10 .

A comparison between the tension stiffening curves derived from the experimental results and the model is presented in Fig. 2.26 to Fig. 2.30 for tests PV3 to PV23 respectively. The accuracy in this case is not as good as for the direct tension tests. This discrepancy is caused by several factors as explained hereafter. First, the type of test itself contributes the major portion of the differences. In direct tension tests, cracks forming at one point propagate through the entire cross section (Fig. 2.11), while in the case of the shear panels, the cracks were not continuous, as illustrated in Fig. 2.31. Hence, the assumption that cracks are completely open when reinforcement yields and that only the reinforcement carries the load, gives a lower value for f_{ST} which is conservative. This assumption is reasonable in most cases. However, in Vecchio *et al* (1982) test series, the yield stress (thus the yield strain) was small, often around 250 MPa in the cases where the agreement between the model and the test results is poor.

Another reason is the scale at which the experimental results are compared to the model prediction. Figures 2.26 to 2.30 show the stresses due to the total load minus these for the steel, calculated from the average strain measurements over the panel area. These strains varied considerably from one point to another, depending on the gage length used to measure them and the location on the panels. The steel stresses derived from these strain measurements were used to compute the portion of the load carried by concrete. Since the tensile force carried by concrete after cracking is relatively small when compared to the global forces involved, a small error in the evaluation of the forces in the

reinforcement magnifies the errors. As it will be seen in Chapter 4 , the global response of these panels, when modelled with the finite element analysis using the model introduced in this chapter for tension stiffening, agrees much more closely with experimental measurements.

2.5 Design Equations

Relationships derived in sections 2.2 and 2.3 allow one to understand the average behavior of tension stiffening. These equations can easily be coded in a finite element program for example. However, their application in a design situation is not appropriate and simplified relationships should be derived. Collins and Mitchell (1987) and Vecchio and Collins (1986) proposed similar equations for postcracking behavior of concrete in tension. The Collins and Mitchell equation is suitable for direct tension and is expressed as

$$f_{ST} = \frac{f_{cr}}{1 + \sqrt{500\,\varepsilon_{ST}}} \qquad (2.38)$$

In the case of Vecchio and Collins equation, the term 500 is replaced by 200 . This appears to be because it was derived based on experimental results on shear panels where the equivalent reinforcement ratio , as defined in Eq. 2.27, is usually smaller than in direct tension tests, giving higher tension stiffening stresses. Both equations are shown in Fig. 2.32 .

Since Eq. 2.38 is simple and can represent correctly the tension stiffening behavior, it is reasonable to keep it. The term inside the square root (200 or 500) should be redefined and a maximum limit for f_{ST} should be established. The proposed design equations are derived assuming that ε_y is equal to about 0.002 and n was taken equal to 8. The expression for f_{ST} is

$$f_{ST} = \frac{f_{cr}}{1 + (1000\ \rho - 5)\sqrt{20\ \varepsilon_{ST}}} \qquad (2.39)$$

for

$$\rho \geq 0.005$$

with

$$f_{ST} \leq 200 \frac{(\varepsilon_y - \varepsilon_{ST})}{\varepsilon_y} \rho f_{cr} \leq f_{cr} \qquad (2.40)$$

These two relationships are illustrated in Fig. 2.33 for ρ values of 1.0 % 1.5 % and 2 % where ε_y was taken equal to 0.002 . These can be compared to the theoretical curves presented in Fig. 2.16 . For cracks at angle to the reinforcement, ρ_{eq} and ε_{yeq} , obtained with Eqs. 2.27 and 2.28, should be utilized. The effective reinforcement ratio ρ_{eff} (Eq. 2.33) must be used to stay on the conservative side.

Table 2.1 - E_c to E_1 ratios

f'_t (MPa)	f'_t (psi)	E_c / E_1 [1]
1.0	145	2.89
1.5	218	3.93
2.0	290	4.96
2.5	363	6.00
3.0	435	7.03
3.5	508	8.09
4.0	580	9.11

(1) Evaluated using Eq. 27 in Bazant and Oh (1983)

Table 2.2 - Evaluation of factor K in Eq. 2.3

Reference	K_{min}	K_{max}	K_{ave}	Number of tests
Gopalaratnam and Shah (1985)	4.20	6.21	5.08	12
Hillerborg (1985)	4.21	8.27	7.37	4
Guo and Zhang (1986)	5.48	12.35	8.64	6
Bazant and Oh (1983) [1]	2.15	5.04	3.43	20
Yankelevsky and Reinhardt (1987)	—	—	6.24	10

Global average : K = 5.26

(1) From tests reported by the authors

Table 2.3 - Coordinates for the adopted strain softening curve in Fig. 2.7

Parameter	Value
E_1	$-E_c/6$
E_2	$-E_c/33$
μ	1/3
ε_μ	$5\,\varepsilon_{cr}$
ε_{max}	$16\,\varepsilon_{cr}$
ε_{cr}	f'_t/E_c

Table 2.4 - Data used to evaluate f_{STcr} and ε_{STcr} in the example

Parameter	Value
A_c	10000 mm^2
E_c	25000 MPa
f'_t	2.5 MPa
ε_{cr}	100 $\mu\varepsilon$
E_s	200000 MPa
f_y	400 MPa
ρ_{stbl}	2.08 %
ρ_{lim}	0.83 %
ρ_{yld}	0.66 %

Table 2.5 - Values of f_{STcr} and ε_{STcr} for axially loaded prisms with properties given in Table 2.4

A_s (mm^2)	ρ (%)	$\beta_1\beta_2$	T_{cr} (kN)	ε_{c2} ($\mu\varepsilon$)	f_{scr} (MPa)	f_{SO} (MPa)	f_{STcr} (MPa)	ε_{STcr} ($\mu\varepsilon$)
Case 1 - ρ greater than ρ_{stbl}								
250	2.50	—(1)	30.0	100	20	2.50	2.50	100
Case 2 - ρ between ρ_{stbl} and ρ_{lim}								
150	1.50	0.90	28.0	708	142	0.54	2.30	161
150	1.50	0.50	28.0	708	142	0.54	1.52	404
150	1.50	0.25	28.0	708	142	0.54	1.03	556
Case 3 - ρ less than ρ_{lim}								
75	0.75	0.90	26.5	1767	353	0	2.25	277
75	0.75	0.50	26.5	1767	353	0	1.25	934
75	0.75	0.25	26.5	1767	353	0	0.63	1350

(1) Values are identical for any $\beta_1\beta_2$ values

Table 2.6 - Values of f_{STy} and ε_{STy} for axially loaded prisms with properties given in Table 2.4

A_s (mm^2)	ρ (%)	$\beta_1\beta_2$	ζ_y	ε_{STy} ($\mu\varepsilon$)	f_{STy} (MPa)
Case 1 - ρ greater than ρ_{stbl}					
250	2.50	0.90	0.998	1996	0.02
250	2.50	0.50	0.999	1998	0.01
250	2.50	0.25	0.999	1999	0.01
Case 2 - ρ between ρ_{stbl} and ρ_{lim}					
150	1.50	0.90	0.887	1797	0.62
150	1.50	0.50	0.934	1887	0.35
150	1.50	0.25	0.968	1944	0.17
Case 3 - ρ less than ρ_{lim}					
75	0.75	0.90	0.299	677	2.00
75	0.75	0.50	0.611	1265	1.11
75	0.75	0.25	0.805	1634	0.56

Table 2.7 - Data[1] for tension and bending tests

Test	f'_t (MPa)	E_c (MPa)	f_y (MPa)	ρ (%)	ρ_{eff}[5] (%)
V1[2]	1.04	10350	599	0.375	0.735
V2[2]	0.84	8350	534	0.333	0.559
V3[2]	1.15	9230	599	0.666	1.120
V4[2]	1.21	9650	534	0.999	1.676
V5[2]	1.43	11420	599	0.375	0.735
H1[3]	1.10	10020	527	0.165	0.60
#2[4]	2.35	12500	455	1.47	1.47

(1) Values as reported in the references
(2) Rostásy *et al* (1976), axial tension tests
(3) Rostásy *et al* (1976), bending test
(4) Rizkalla *et al* (1983), axial tension test
(5) Evaluated from Eq. 2.33; deformed bars were used in all tests

Table 2.8 - Data[1] for shear panels

Test	f'_c (MPa)	f_{cr} (MPa)	E_c (MPa)	ρ (%)	f_y (MPa)
PV3	26.6	1.67	24020	0.483	662
PV4	26.6	1.93	24020	1.056	242
PV6	29.8	1.28	25020	1.785	266
PV16	21.7	0.94	22370	0.740	255
PV23	20.5	2.32	21930	1.785	518

(1) Values as reported in the reference

Table 2.9 - Parameters in the tension stiffening model

Test	ρ_{eq} (%)	ε_{yeq} ($\mu\varepsilon$)	ρ_{stbl} (%)	ρ_{lim} (%)	ρ_{yld} (%)
PV3	0.242	6620	2.00	0.80	0.13
PV4	0.528	2420	2.00	0.80	0.41
PV6	0.893	2660	2.09	0.83	0.25
PV16	0.370	2550	1.86	0.75	0.19
PV23	0.893	5180	1.82	0.73	0.23

Table 2.10 - Results obtained for the shear panels

Test	ε_{cr} ($\mu\varepsilon$)	ε_{c2} ($\mu\varepsilon$)	ε_{STcr} ($\mu\varepsilon$)	f_{STcr} (MPa)	ε_{STy} ($\mu\varepsilon$)	f_{STy} (MPa)
PV3	70	3544	417	1.50	4760	0.90
PV4	80	1900	262	1.74	958	0.71
PV6	51	728	119	1.16	2412	0.45
PV16	42	1312	169	0.85	1897	0.49
PV23	106	1237	219	2.19	4701	0.86

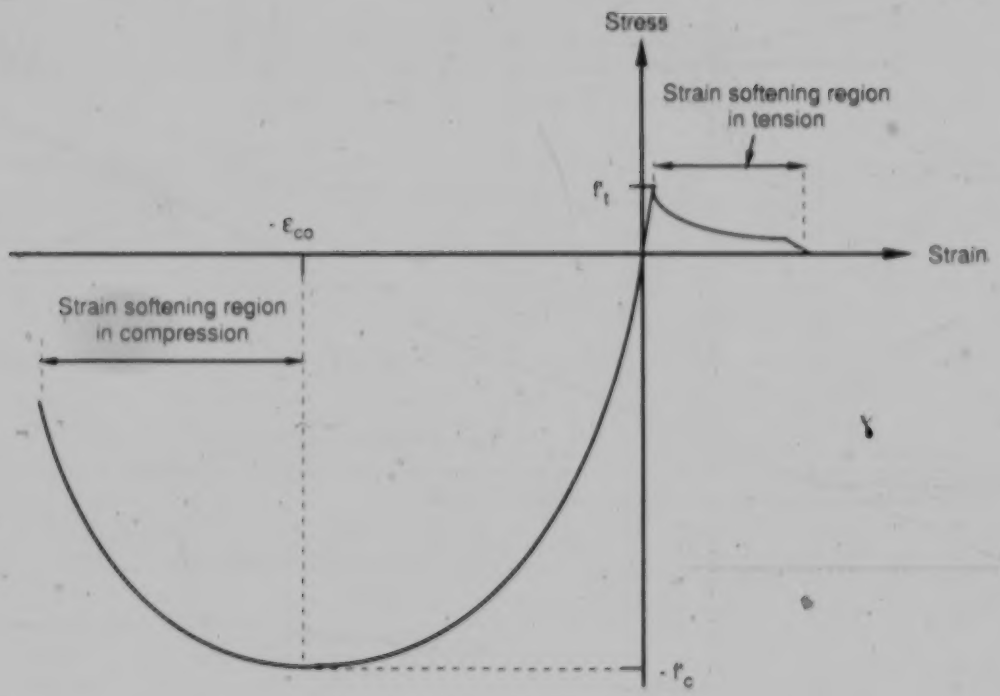

Figure 2.1 - Complete stress-strain curve for concrete

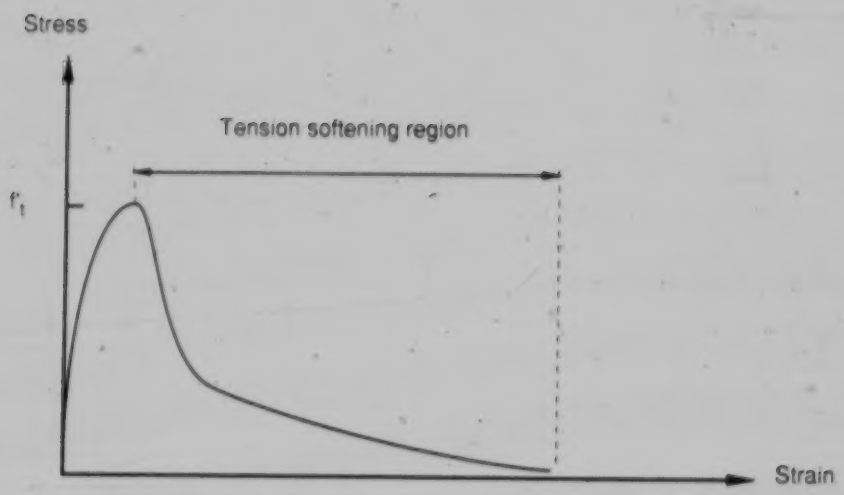

Figure 2.2 - Tension softening in concrete

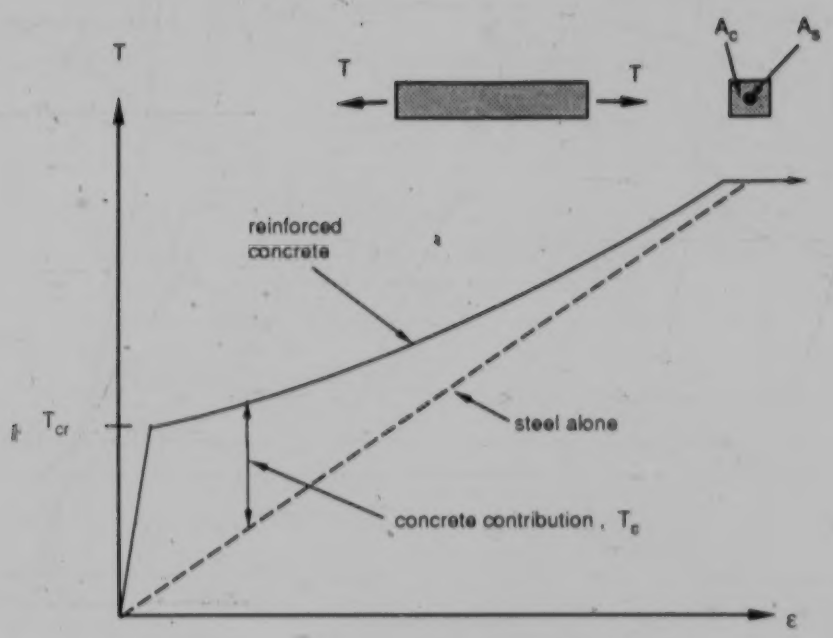

a) Reinforced concrete member

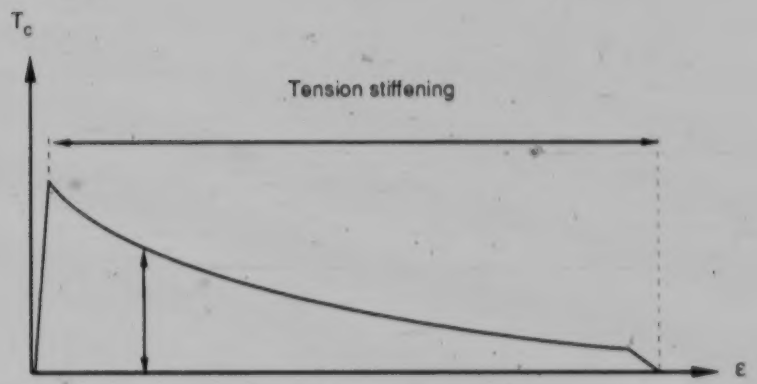

b) Concrete contribution

Figure 2.3 - Tension stiffening

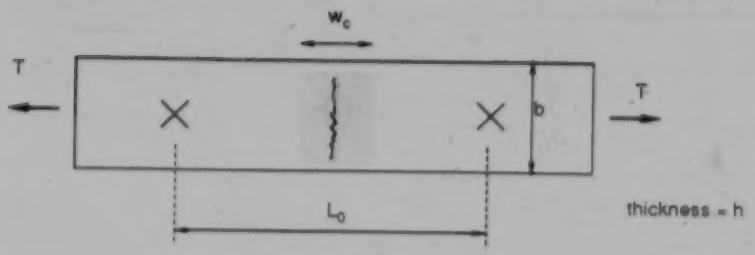

a) Tension Specimen

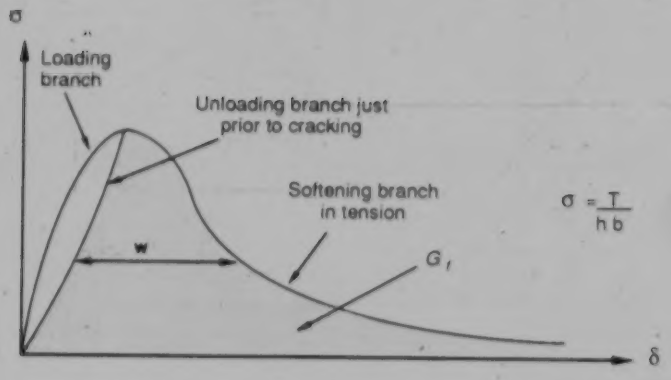

b) Stress - Elongation

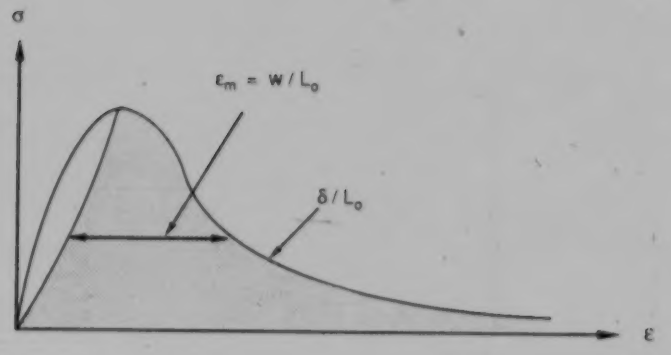

c) Stress - Strain

Figure 2.4 - Tension specimen response

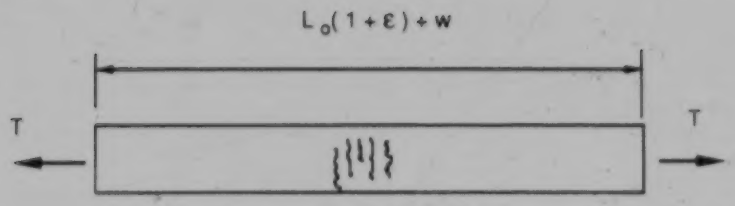

a) Member in Tension

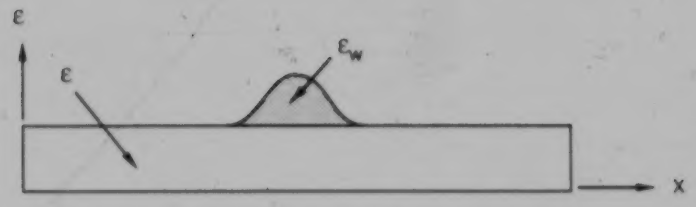

b) Actual Strain Distribution

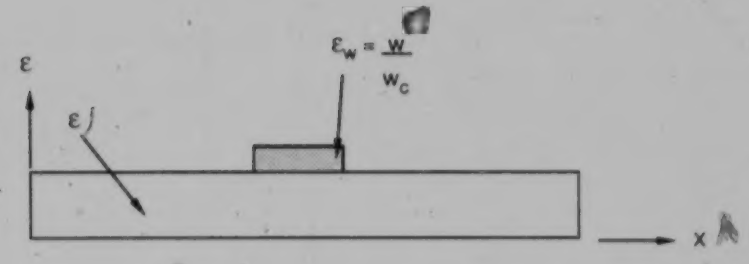

c) Simplified Strain Distribution

Figure 2.5 - Plain concrete member in tension

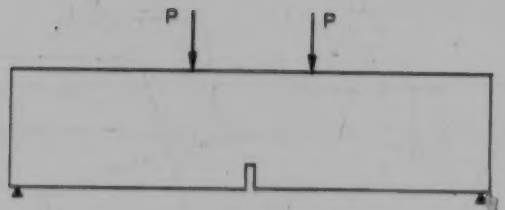

a) Notched beam

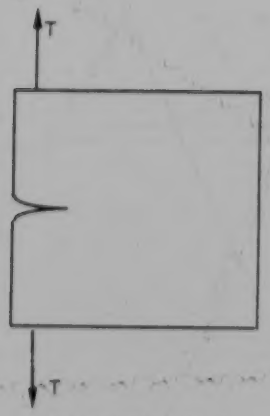

b) Splitting test

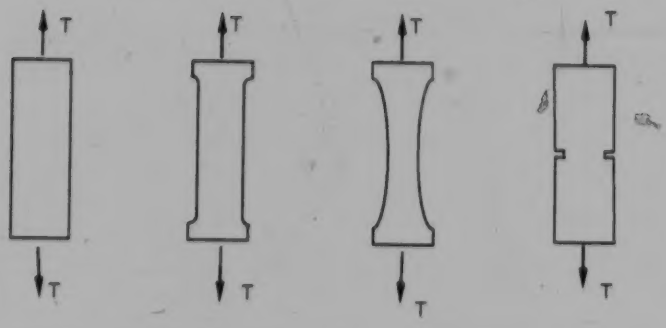

c) Tension specimens

Figure 2.6 - Test specimens

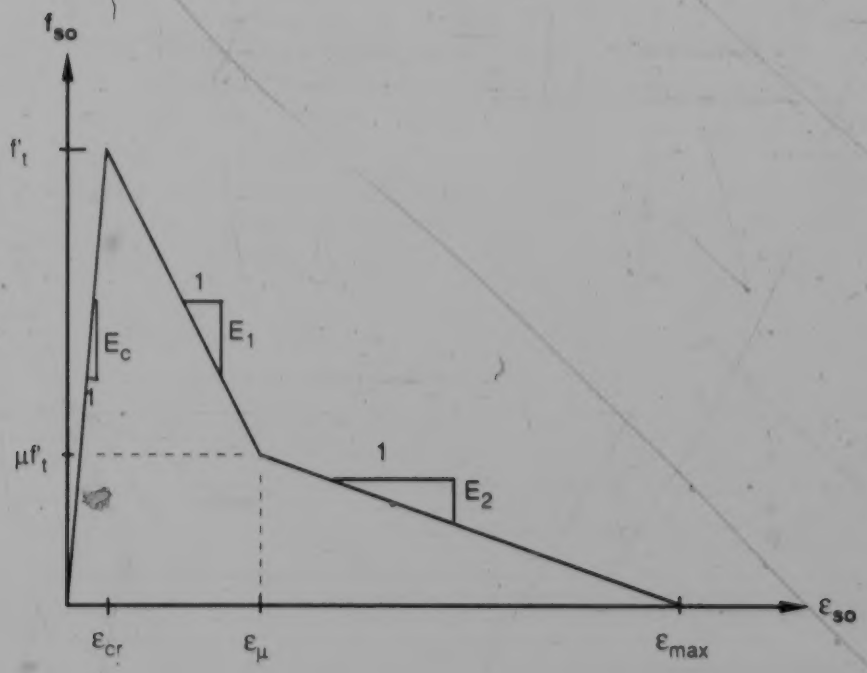

Figure 2.7 - Adopted tension softening curve

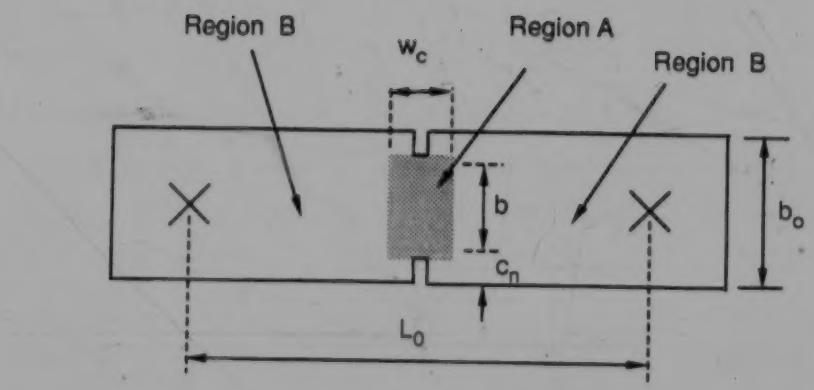

a) Notched Tension Specimen

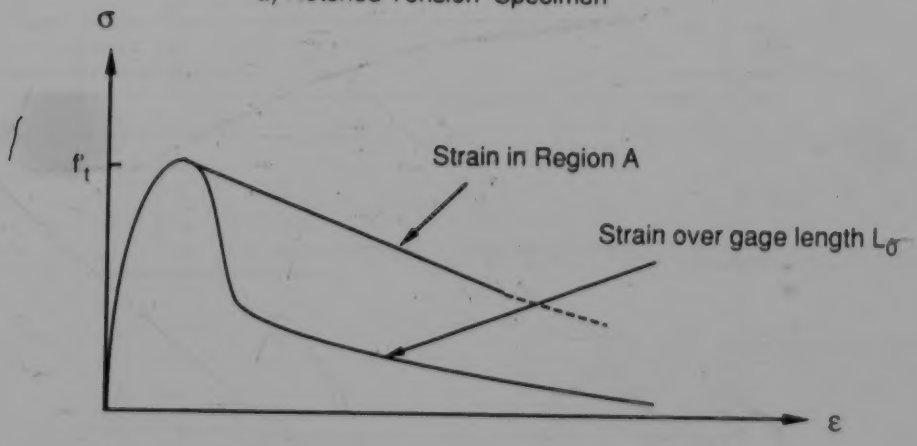

b) Stress - Strain Curves

Figure 2.8 - Notched tension specimen

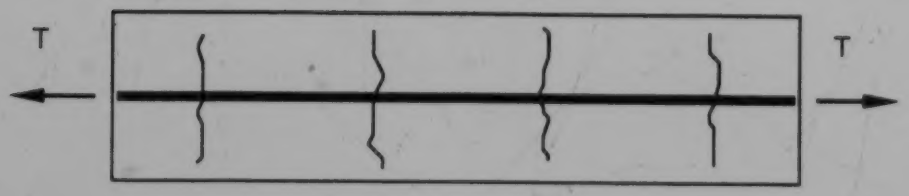

a) Cracked Member

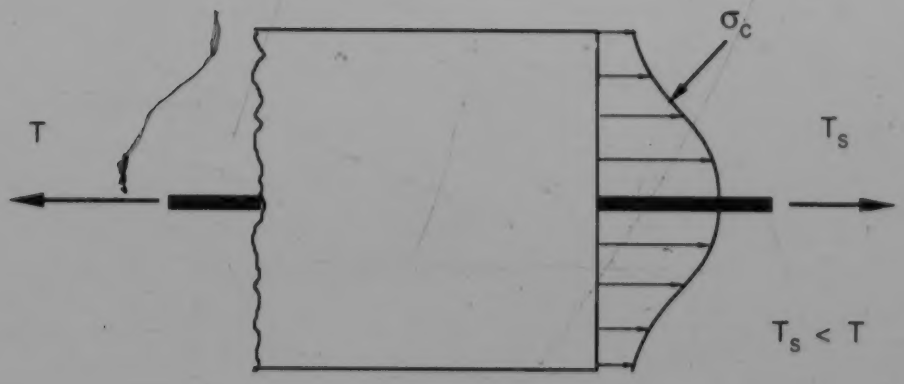

At a crack Between two cracks

b) Free Body Diagram

Figure 2.9 - Reinforced concrete member in tension

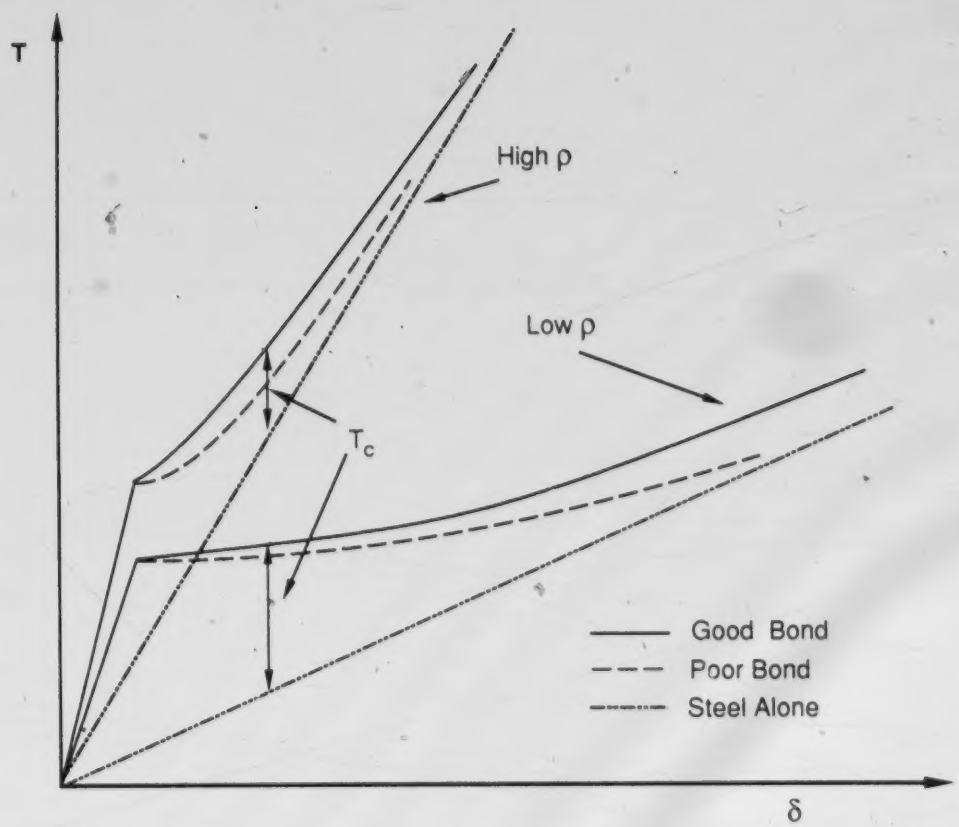

Figure 2.10 - Tension stiffening effect

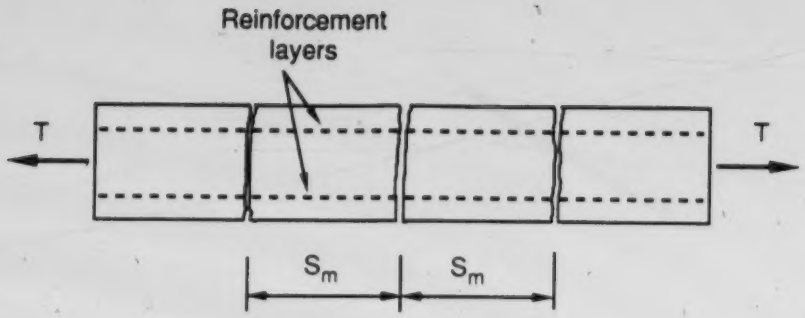

a) Cracked Member

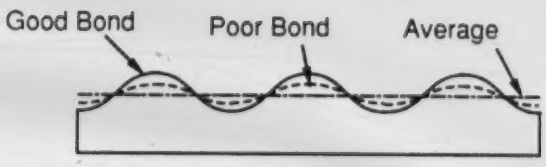

b) Steel Stress

c) Concrete Stress

Figure 2.11 - Stress distribution in a cracked member

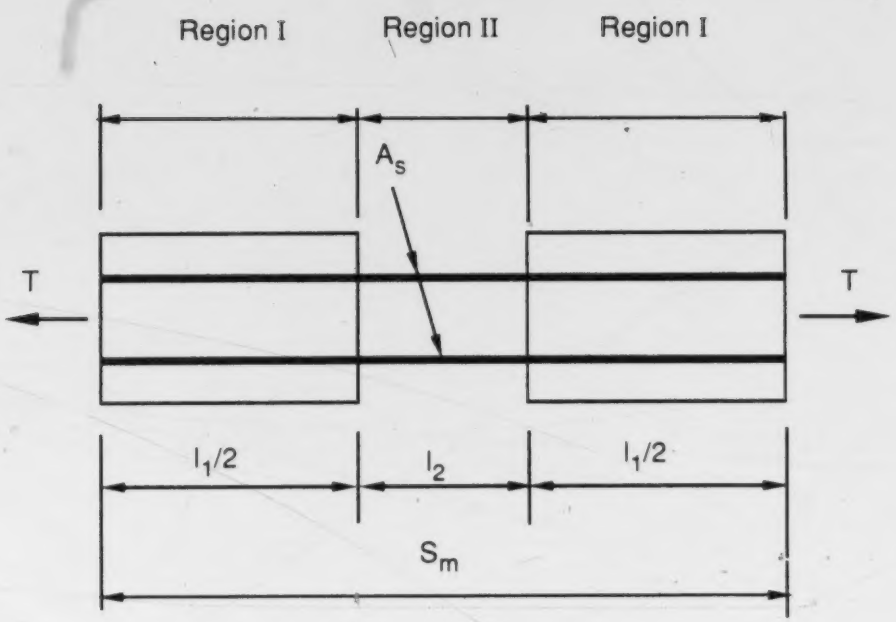

Figure 2.12 - CEB model

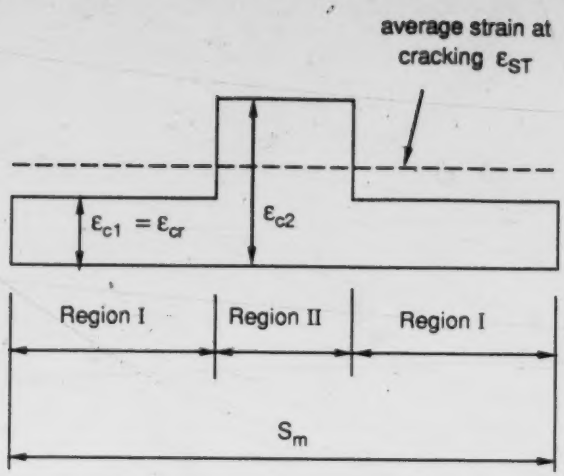

a) At Cracking

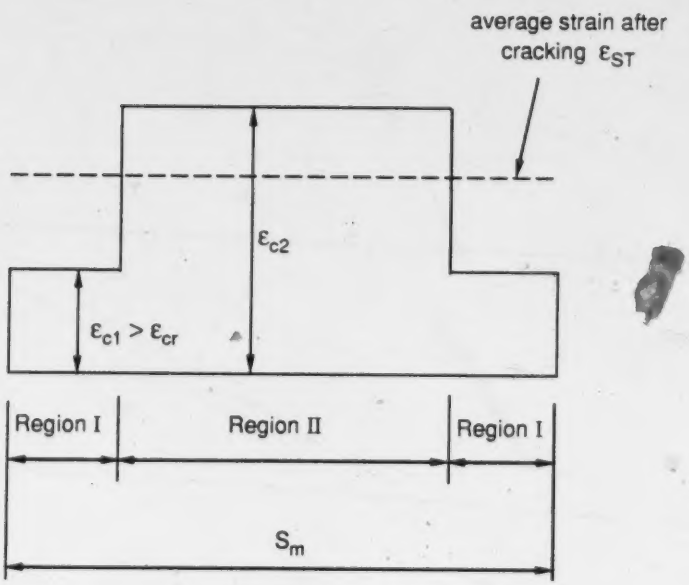

b) After Cracking

Figure 2.13 - Assumed strain distribution

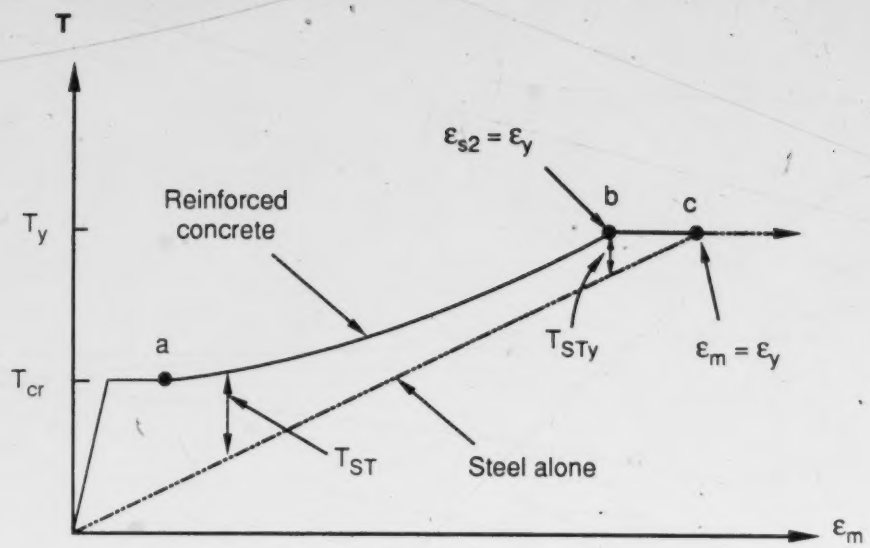

a) Concrete member

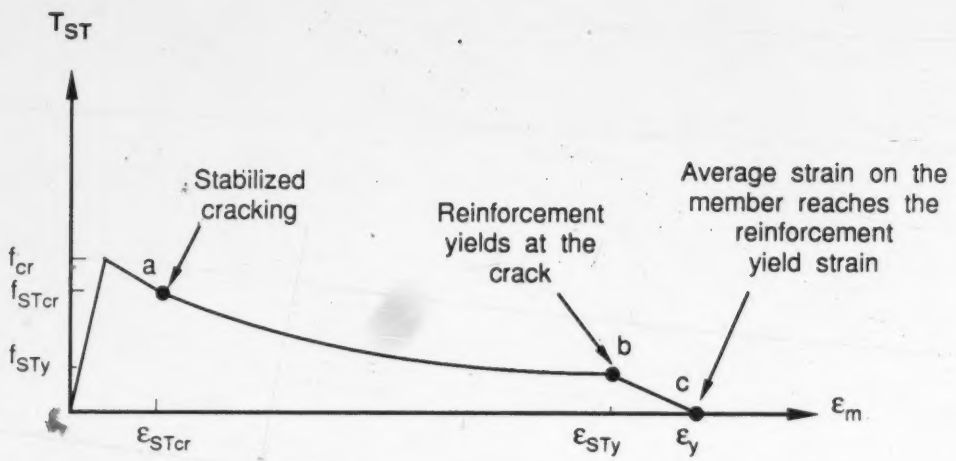

b) Concrete contribution

Figure 2.14 - Phases in the tension stiffening model

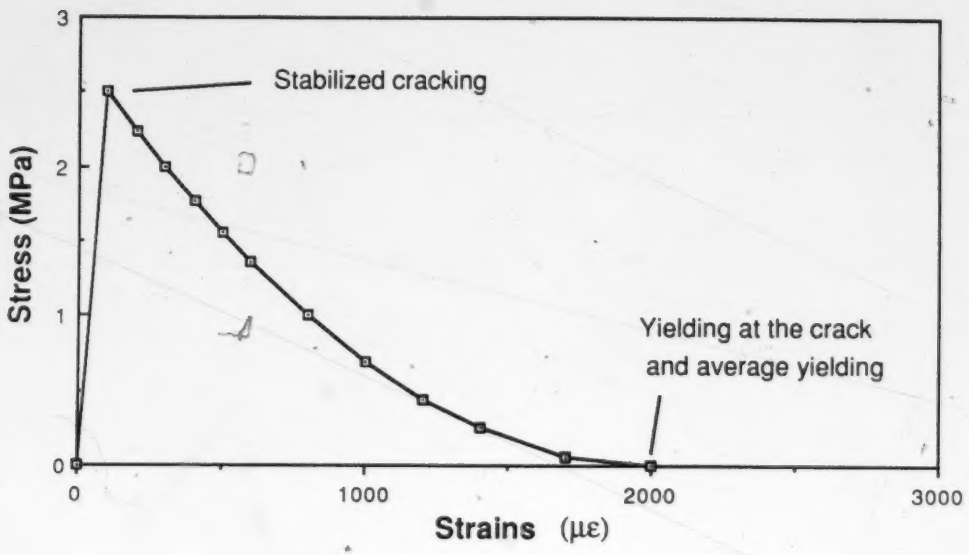

a) Reinforcement ratio of 2.5%

Figure 2.15 - Tension stiffening curve

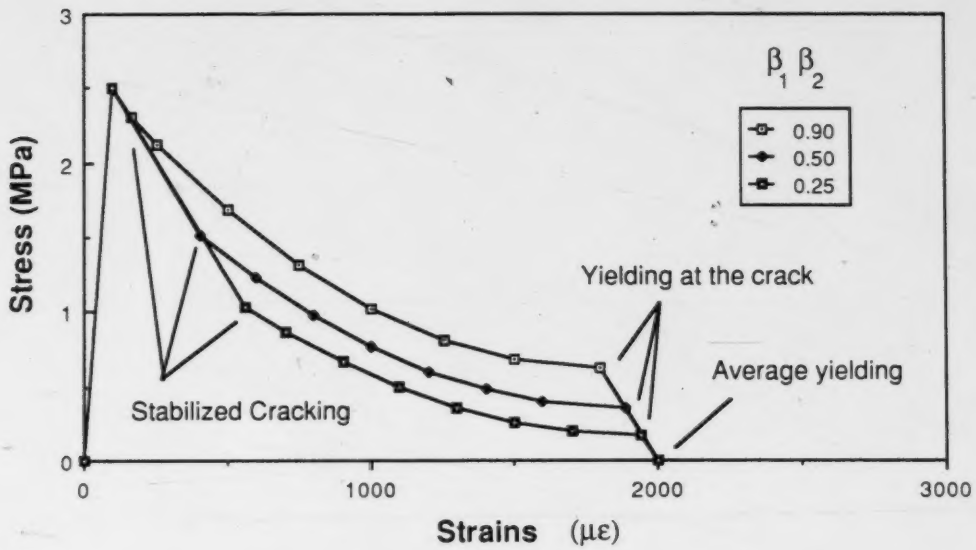

b) Reinforcement ratio of 1.5%

Figure 2.15 (continued)- Tension stiffening curve

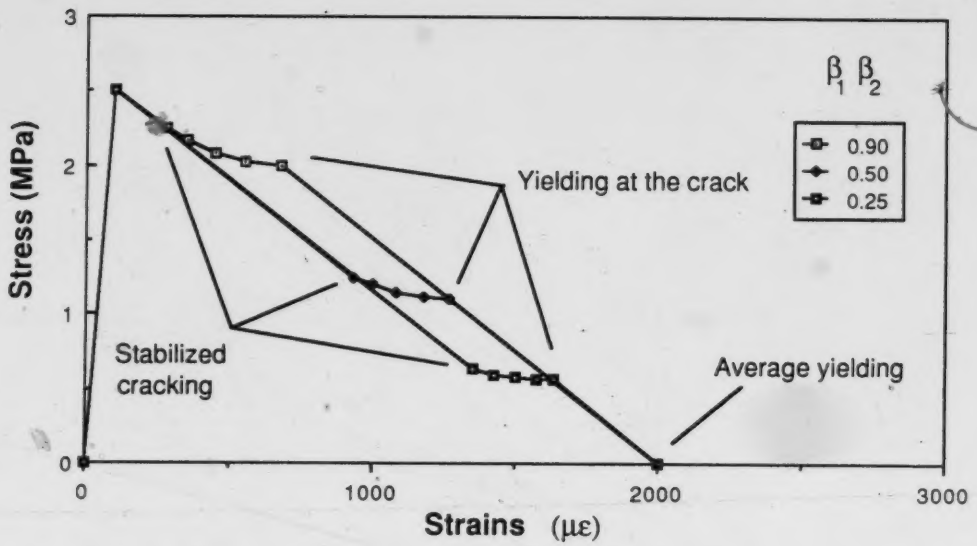

c) Reinforcement ratio of 0.75%

Figure 2.15 (continued) - Tension stiffening curve

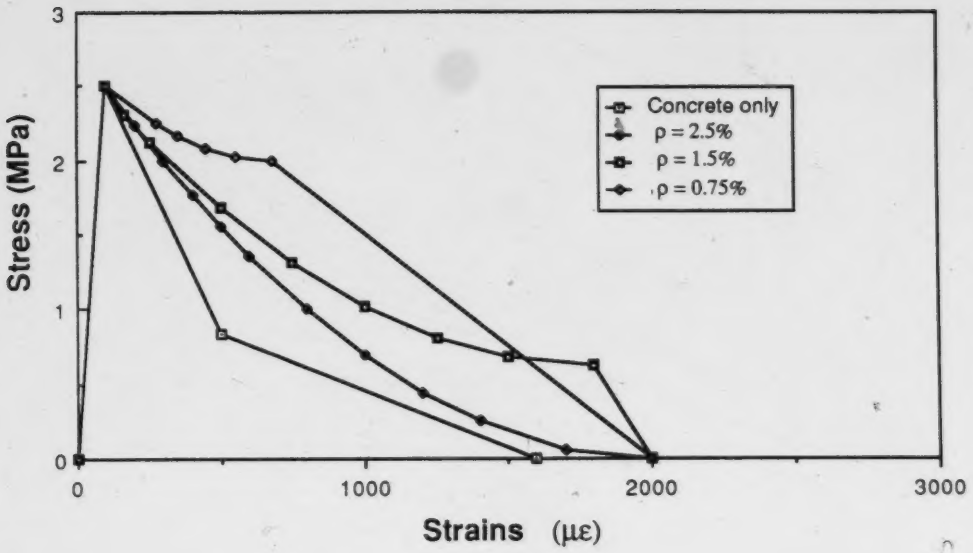

Figure 2.16 - Tension stiffening response for different ρ values

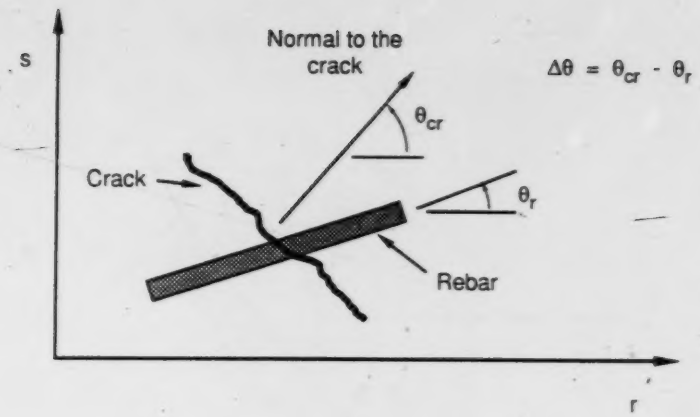

a) Relative orientations

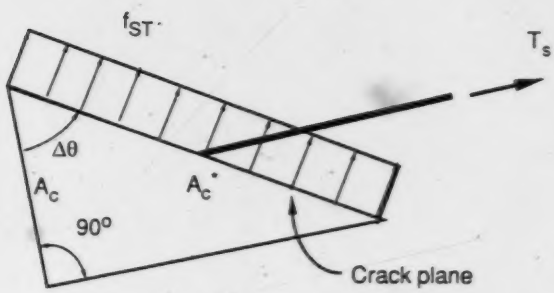

b) Forces at the crack

Figure 2.17 - Reinforcement non orthogonal to the crack

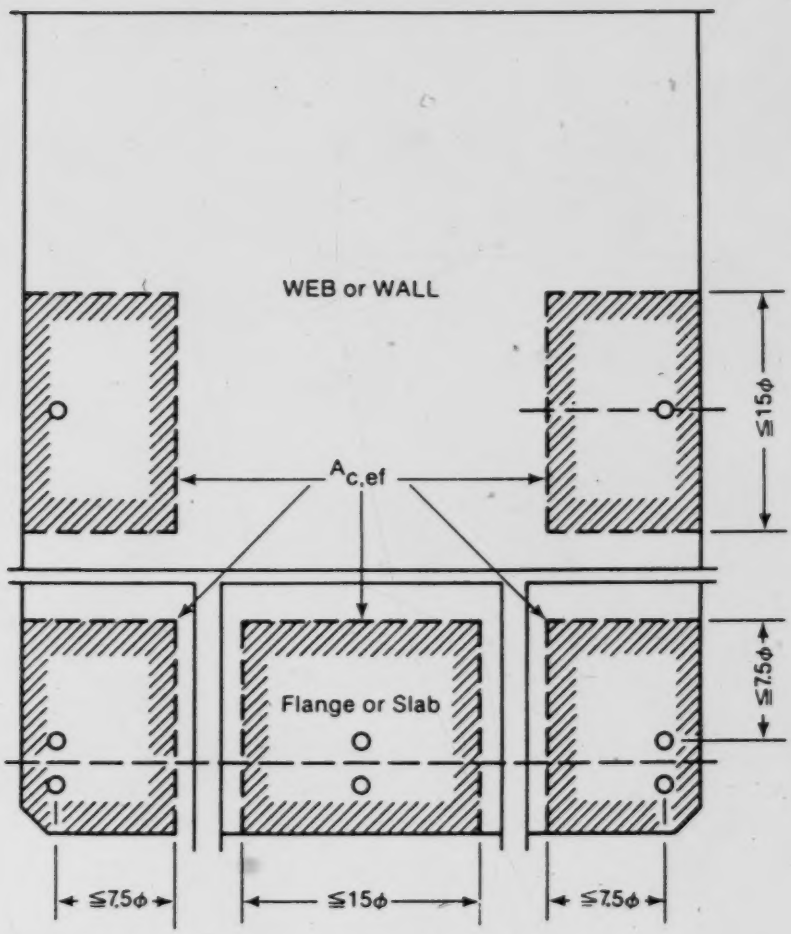

Figure 2.18 - Effective concrete embedment area

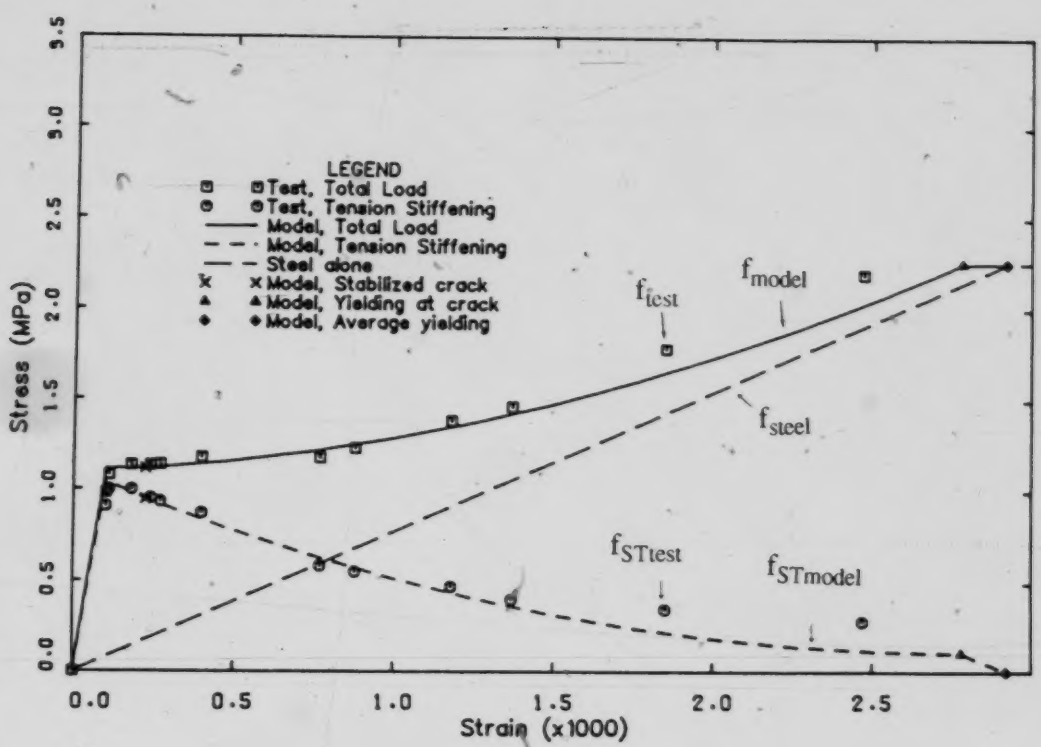

Figure 2.19 - Comparison of model and Rostásy *et al* (1976) tension test V1

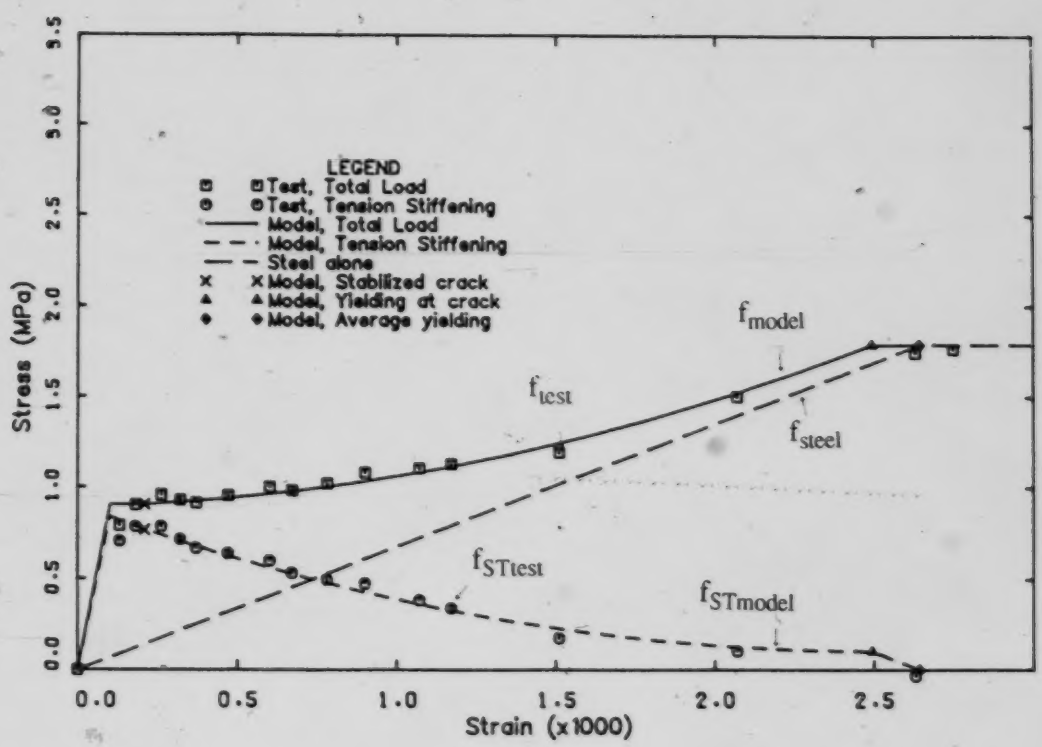

Figure 2.20 - Comparison of model and Rostásy *et al* (1976) tension test V2

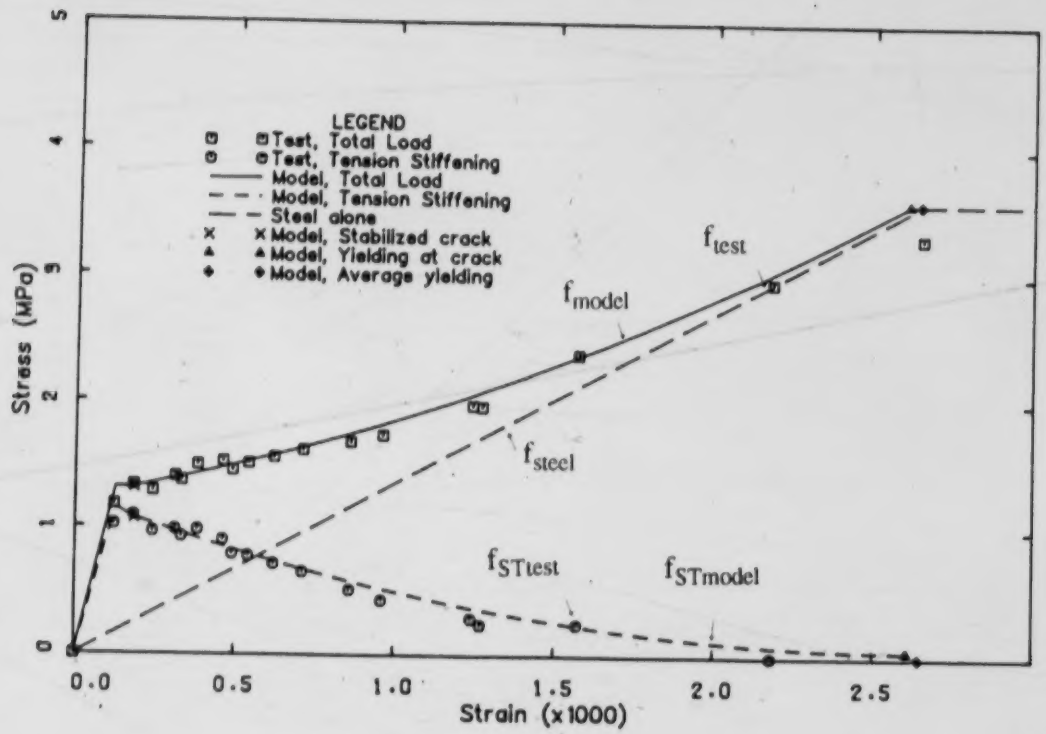

Figure 2.21 - Comparison of model and Rostásy *et al* (1976) tension test V3

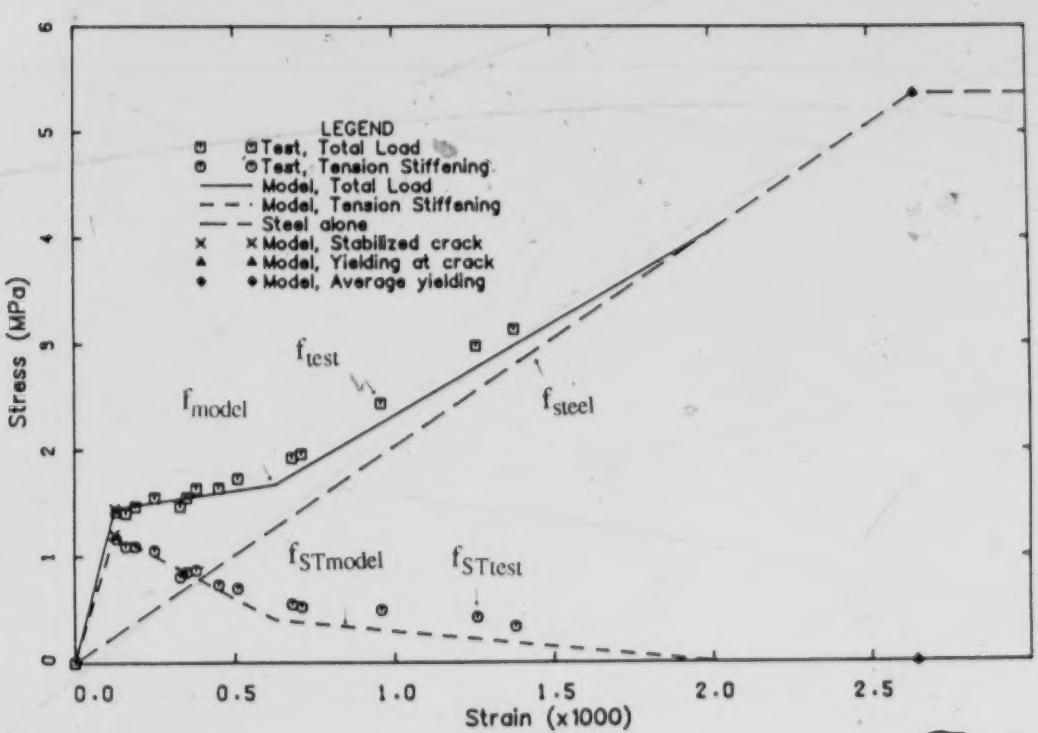

Figure 2.22 - Comparison of model and Rostásy *et al* (1976) tension test V4

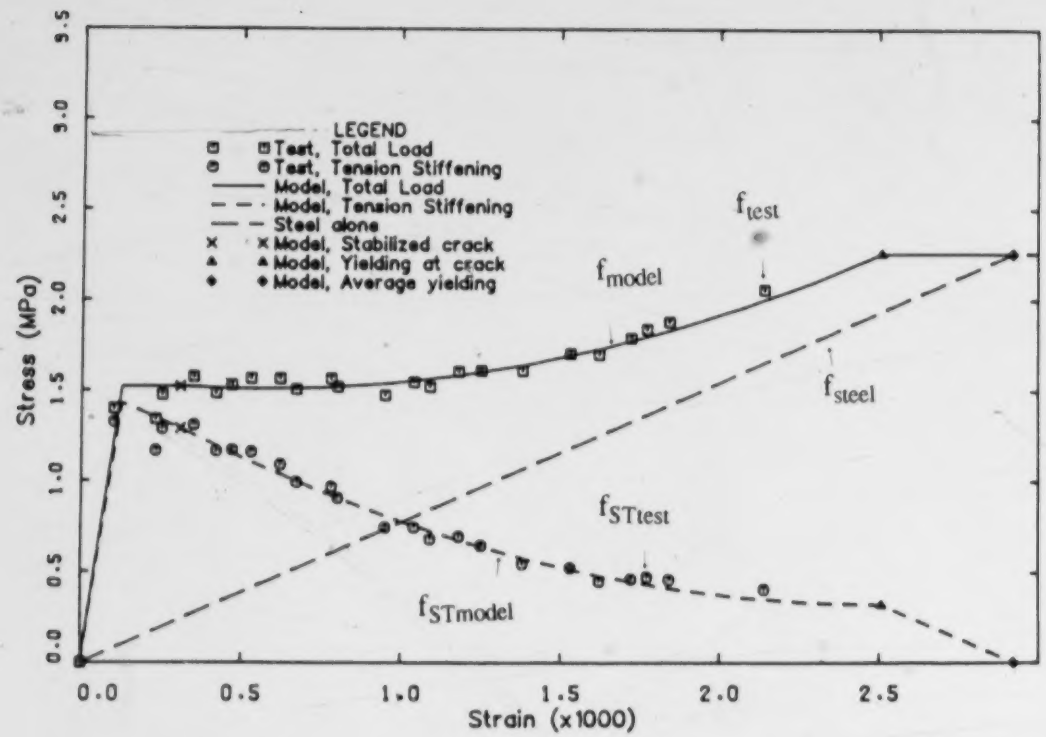

Figure 2.23 - Comparison of model and Rostásy *et al* (1976) tension test V5

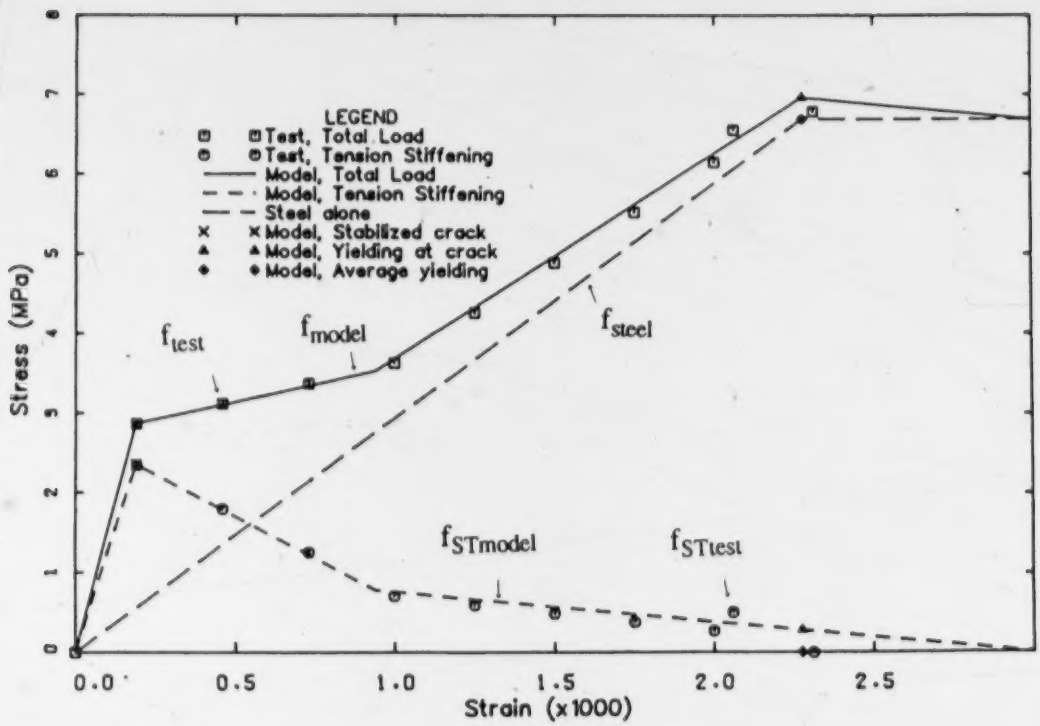

Figure 2.24 - Comparison of model and Rizkalla *et al* (1983) tension test #2

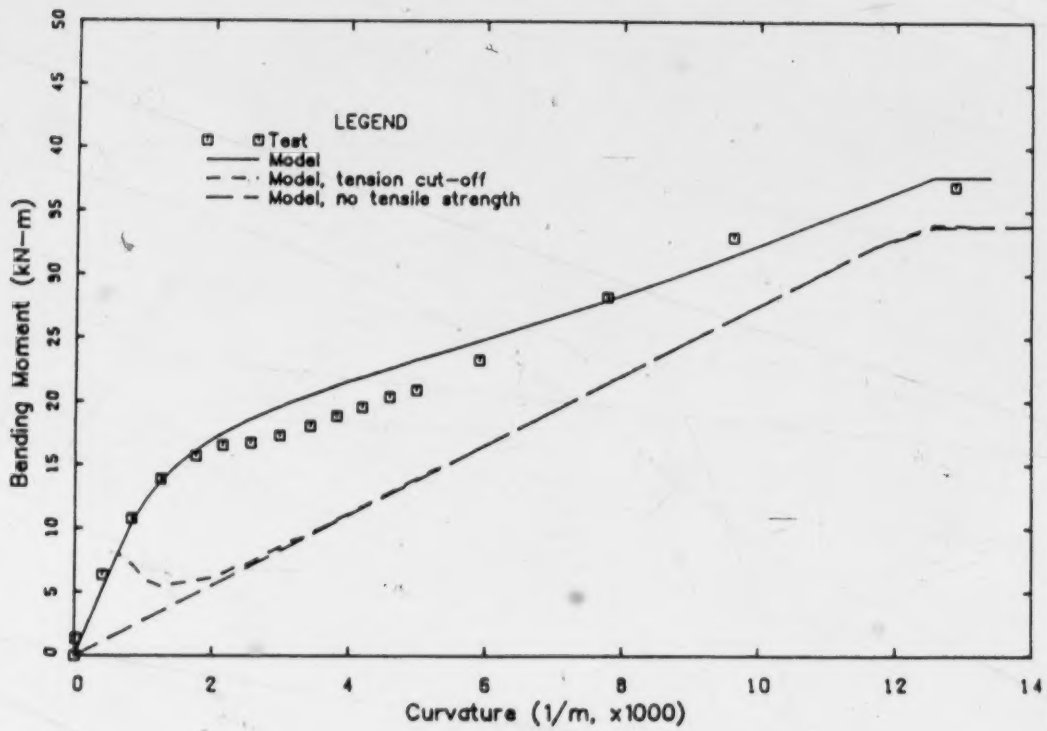

Figure 2.25 - Comparison of model and Rostásy *et al* (1976) flexure test H1

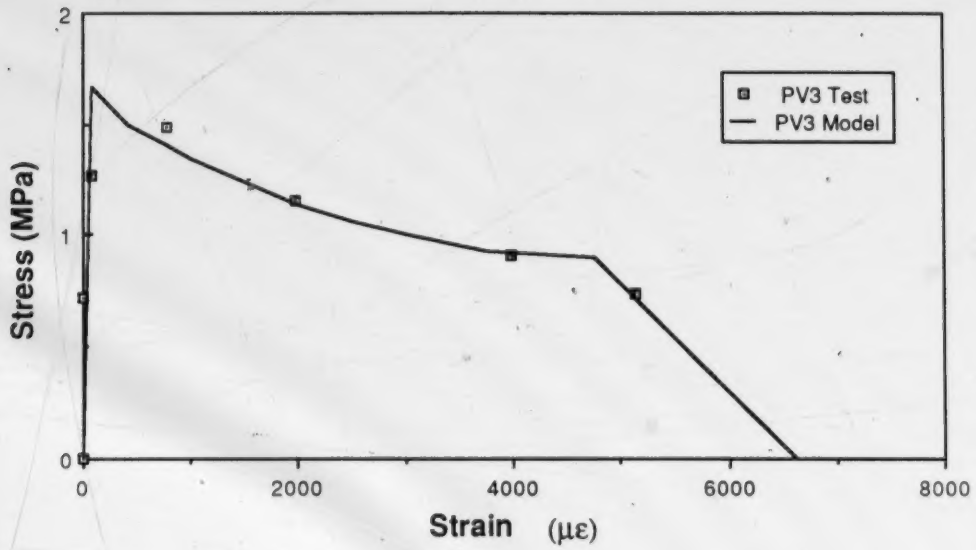

Figure 2.26 - Comparison of model and Vecchio and Collins (1982) panel PV3

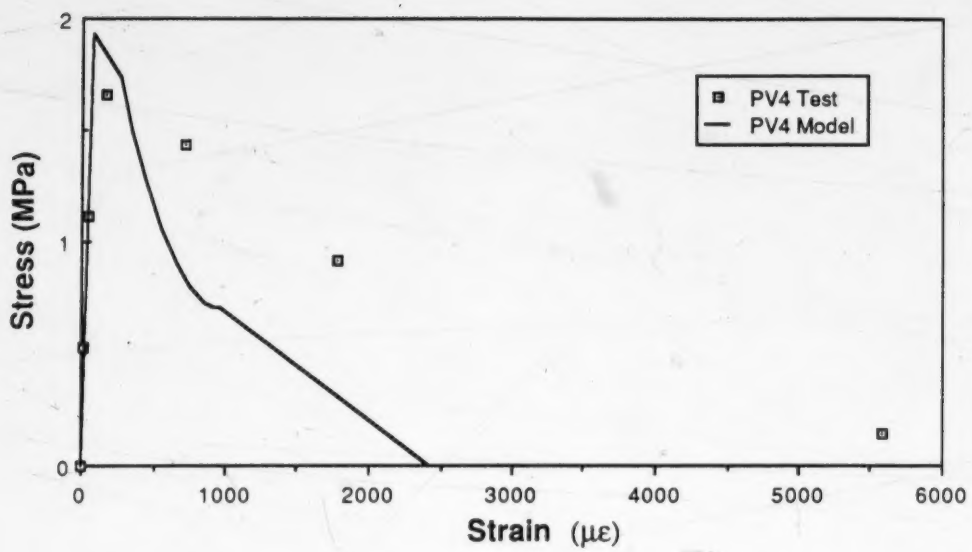

Figure 2.27 - Comparison of model and Vecchio and Collins (1982) panel PV4

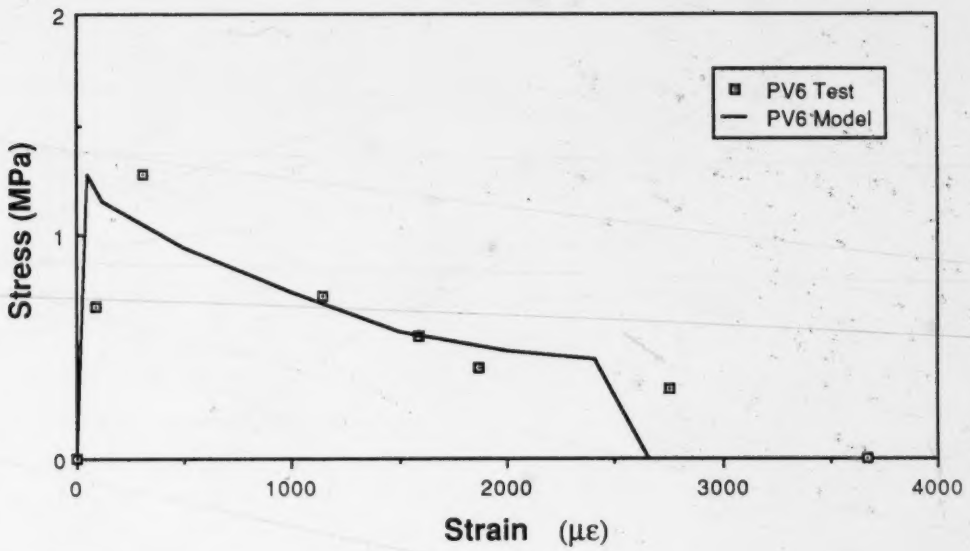

Figure 2.28 - Comparison of model and Vecchio and Collins (1982) panel PV6

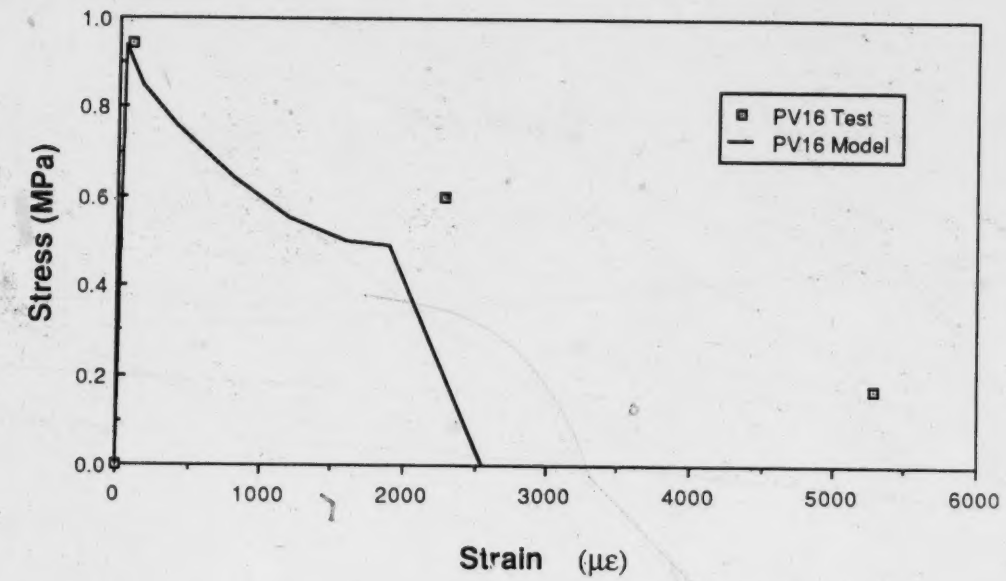

Figure 2.29 - Comparison of model and Vecchio and Collins (1982) panel PV16

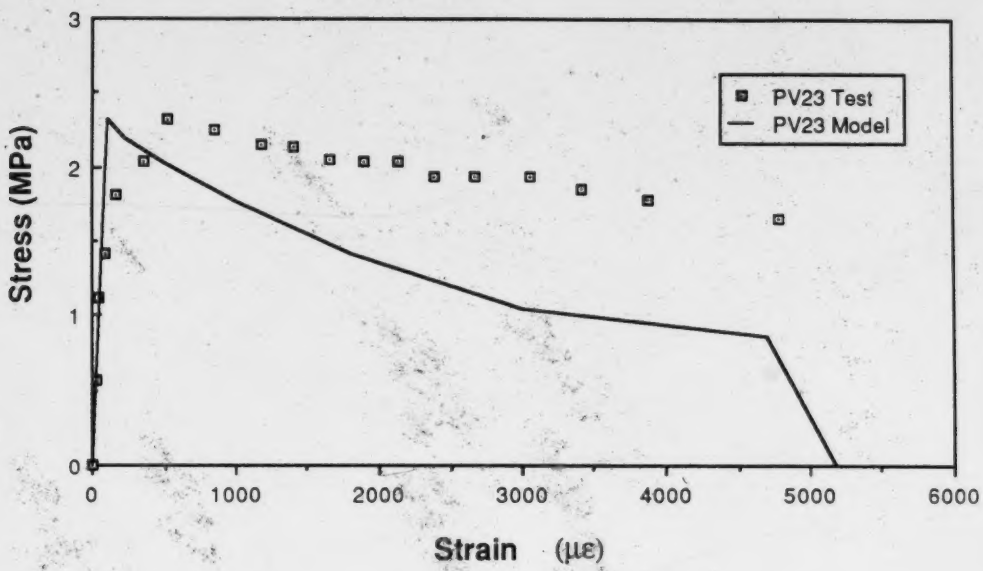

Figure 2.30 - Comparison of model and Vecchio and Collins (1982) panel PV23

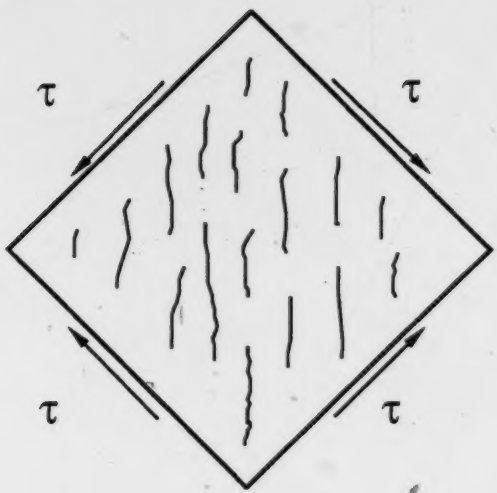

Figure 2.31 - Vecchio and Collins (1982) shear panel after cracking

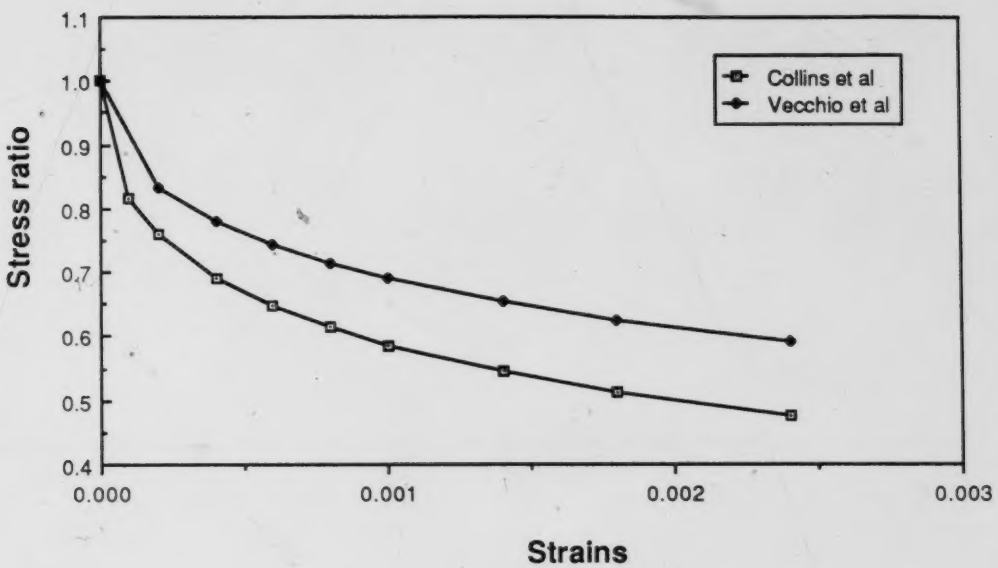

Figure 2.32 - Vecchio *et al* (1982) and Collins *et al* (1987) tension stiffening curves

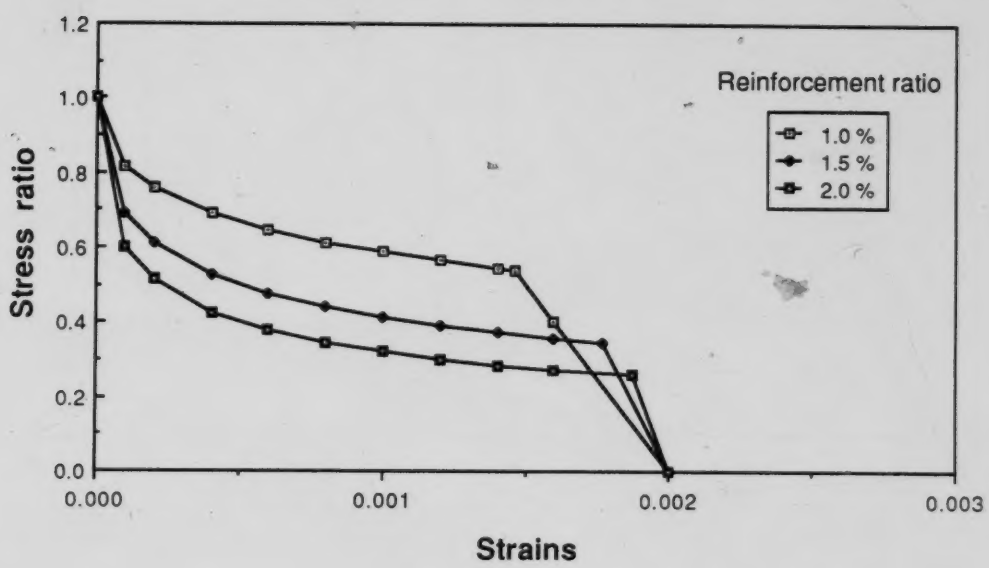

Figure 2.33 - Proposed tension stiffening curves for design

CHAPTER III

REINFORCED CONCRETE MODEL

3.1 Scope

The reinforced concrete model for planar structures described in this chapter has been developed intending that it should be simple, inexpensive (in terms of computer time) and accurate in its description of concrete behavior. As pointed out by Bahlis and Mirza (1987), a good compromise between simplicity and accuracy is achieved with incremental hypoelastic models. Several models published in the literature fall into that category, with the most widely used being the Darwin and Pecknold (1977) concrete model. Several adaptations of this model have been used by many authors such as Elwi and Murray (1979), Van Greunen (1979), Ramm and Kompfner (1984), etc. In the model proposed here, some of the characteristics of the Darwin and Pecknold model are kept.

Typical characteristics and assumptions on which the proposed model is based are summarized as

1. It is an hypoelastic incremental model.
2. It can be used in any plane stress situation and is adapted for thin plate-shell type structures.
3. Concrete is assumed isotropic up to either cracking or crushing.
4. After cracking concrete is treated as an orthotropic material.

5. Two cracks may form at one point in different directions.

6. After either crushing or cracking, stresses undergo strain softening and the tangent modulus is set to zero in the direction associated with failure.

7. When crushing occurs at one point failure is assumed in all directions.

8. In any stress condition, concrete can unload (before and after cracking or crushing) and the model is suitable for cyclic loading.

The proposed concrete model is presented , followed by a description of the postfailure conditions. The evaluation of the material properties used with the model is described and finally a discussion on modelling reinforced concrete plates and shells is presented. Throughout this chapter, algebraic values are used for the stresses in concrete and the associated strains. Thus tensile stresses are positive and compression stresses are negative.

3.2 Constitutive relationships

In this section the relationships used to define the material behavior until either cracking or crushing occurs are presented. The incremental formulation and the stress-strain relationships adopted are introduced. The biaxial failure envelope is defined and the relationship used for Poisson's ratio is presented. Finally, the equivalent uniaxial strain concept adopted for nonproportional loading is derived, followed by a comparison of the model response with respect to experimental results.

3.2.1 Incremental formulation

The incremental formulation is defined as follows:

$$\Delta\sigma = C_{rs}\,\Delta\varepsilon \tag{3.1}$$

in which the stress increment $\Delta\sigma$ is defined as

$$\Delta\sigma = < \Delta\sigma_r \; \Delta\sigma_s \; \Delta\sigma_t \; \Delta\tau_{rs} \; \Delta\tau_{rt} \; \Delta\tau_{st} > \tag{3.2}$$

where r , s and t are the element local axes as shown in Fig. 3.1 . The stress increment $\Delta\sigma_t$ is always equal to zero, based on the plane stress formulation for plate type elements. The strain increment $\Delta\varepsilon$ is expressed as

$$\Delta\varepsilon = < \Delta\varepsilon_r \; \Delta\varepsilon_s \; \Delta\varepsilon_t \; \Delta\gamma_{rs} \; \Delta\gamma_{rt} \; \Delta\gamma_{st} > \tag{3.3}$$

The constitutive matrix C_{rs} is referred to the element local axes r-s-t as

$$C_{rs} = R^T C_{12}\, R \tag{3.4}$$

in which C_{12} is defined in the frame of reference of the principal axes of orthotropy as

$$C_{12} = \frac{1}{1-\nu^2} \begin{bmatrix} E_1 & E_{12} & 0 & 0 & 0 & 0 \\ E_{12} & E_2 & 0 & 0 & 0 & 0 \\ 0 & 0 & 0 & 0 & 0 & 0 \\ 0 & 0 & 0 & (1-\nu^2)G_{ip} & 0 & 0 \\ 0 & 0 & 0 & 0 & (1-\nu^2)\xi G_{tr} & 0 \\ 0 & 0 & 0 & 0 & 0 & (1-\nu^2)\xi G_{tr} \end{bmatrix} \tag{3.5}$$

Moduli E_1 , E_2 , E_{12} , G_{ip} , and G_{tr} , and the Poisson's ratio ν will be defined later. The coefficient ξ , taken as 5/6 , corrects the shear stress resultants to their actual values to account for the parabolic shear stress distribution across the thickness. It is noted that the plane stress constitutive

relationships adopted for this model include also shear terms, encountered in plate and shell problems and associated with the third coordinate axis t . However, the principal axes of orthotropy 1 and 2 are confined to the plane r-s of the element. The transformation matrix **R** is thus defined as

$$\mathbf{R} = \begin{bmatrix} c^2 & s^2 & 0 & cs & 0 & 0 \\ s^2 & c^2 & 0 & -cs & 0 & 0 \\ 0 & 0 & 0 & 0 & 0 & 0 \\ -2cs & 2cs & 0 & c^2-s^2 & 0 & 0 \\ 0 & 0 & 0 & 0 & 1 & 0 \\ 0 & 0 & 0 & 0 & 0 & 1 \end{bmatrix} \tag{3.6}$$

in which

$$c = \cos \theta$$

$$s = \sin \theta$$

3.2.2 Prefailure stress-strain relationships

The uniaxial stress-strain curve for compression proposed by Saenz (1964) is adopted in this study. If σ_{cu} is the ultimate strength and ε_{cu} the associated strain (both negative) the stress-strain relationship is expressed as

$$\sigma = \frac{E_c \varepsilon}{1 + \left(\frac{E_c}{E_{sec}} - 2\right) R_\varepsilon + R_\varepsilon^2} \tag{3.7}$$

with

$$E_{sec} = \frac{\sigma_{cu}}{\varepsilon_{cu}} \tag{3.8}$$

$$R_\varepsilon = \frac{\varepsilon}{\varepsilon_{cu}} \tag{3.9}$$

and in which E_c is the initial tangent modulus. Equation 3.7 describes the stress-strain relationship of concrete up to the peak stress. The post peak relationship, or the strain softening branch beyond ε_{cu}, will be described later in this chapter. The type of curve described by Eq. 3.7 is illustrated in Fig. 3.2a . The tangent modulus E is given by

$$E = \frac{E_c \left(1 - R_\varepsilon^2 \right)}{\left[1 + \left(\frac{E_c}{E_{sec}} - 2 \right) R_\varepsilon + R_\varepsilon^2 \right]^2} \qquad (3.10)$$

The Saenz equation describes adequately usual concrete stress-strain curves. However this equation is valid only for ratios of E_c to E_{sec} larger than or equal to 2.0 . It is common however to have steeper stress-strain curves for high strength concrete (ACI Committee 363, 1984). To overcome that situation one can define the following pseudo ultimate strain:

$$\varepsilon^* = \frac{\varepsilon_{cu}}{\sqrt{\frac{E_c \, \varepsilon_{cu}}{f'_c}} - 1} \qquad (3.11)$$

This strain is obtained by isolating ε in Eq. 3.7 for a ratio of E_c to E_{sec} equal to 2.0 . The pseudo stress-strain curve obtained this way is illustrated on Fig. 3.2b and only the solid line portion of the curve is valid. Equations 3.7 to 3.10 can be used with ε_{cu} replaced by ε^* .

3.2.3 Biaxial failure envelope

In a plane stress situation, the biaxial stress failure envelope is defined in three regions in the principal stress coordinate system: biaxial tension, biaxial compression and tension-compression.

In the biaxial tension region, it is usually assumed that concrete cracks at f'_t, for any stress ratio. Some researchers (Tasuji *et al* , 1978) have noticed a slight increase in the tensile strength when the two principal tensile stresses are equal whereas other people (Kupfer *et al*, 1969) have observed the opposite. In both cases the difference with f'_t is not significant enough to necessitate a more accurate failure envelope and this value is used for any stress ratio (Fig. 3.3a).

In a biaxial compression state of stress, it is commonly accepted that the failure envelope is a function of the stress ratio and the Kupfer and Gerstle (1973) description is adopted in this study, being one of the most popular criteria. With principal stresses σ_A and σ_B , where $\sigma_A \geq \sigma_B$, the Kupfer and Gerstle relationship is expressed as

$$\sigma_{cu} = - \frac{1 + 3.65\ \alpha}{(1 + \alpha)^2} f_c \qquad (3.12)$$

with

$$\alpha = \frac{\sigma_A}{\sigma_B} \leq 1.0 \qquad (3.13)$$

in which σ_{cu} is the ultimate compressive strength (negative) . The negative sign in Eq. 3.12 is necessary because f'_c is the uniaxial compressive strength which is positive. The failure envelope is illustrated in Fig. 3.3a .

In the case of tension-compression, a bilinear failure envelope is adopted, as shown in Fig. 3.3b, similar to the envelope proposed by Balakrishnan and Murray (1986). The limit of $0.5\ f'_t$ for the tensile strength at point c and the intersection point of the two straight lines located at $-0.85\ f'_c$ (point b on Fig. 3.3b), were chosen on the basis of a fit of Kupfer *et al* (1969) data in that region. The value of α corresponding to point b is defined as

$$\alpha_{ct} = - \frac{23\ f'_t}{34\ f'_c} \qquad (3.14)$$

This ratio of σ_A to σ_B defines the transition point between tensile failure and compression failure. For a value of α larger than α_{ct} (algebraically), the failure will be by crushing of concrete at a strength determined by the limit value of σ_B on the failure envelope between points a - b. For α values smaller than α_{ct} , tensile failure will take place at a stress level determined by the failure envelope between points b - d. In that case, the compressive strength σ_{cu} is kept constant to $-0.85\ f'_c$.

3.2.4 Poisson's ratio

In tension and at low compressive stresses, Poisson's ratio (ν) remains unchanged. However, when the compressive stress in an uniaxial test is above approximately $0.75\ f'_c$, Poisson's ratio increases. This increase of ν near the ultimate strength is due to micro cracking which propagates through the mortar at a stress level of approximately $0.75\ f'_c$, called the critical stress (Hsu *et al* , 1963 ; Sturman *et al*, 1965). This phenomenon however is more important for uniaxial compression cases ($\alpha = 0$) than it is for biaxial compression stress conditions ($\alpha > 0$) due to the confinement effect of the second stress on the concrete expansion, as far as the Poisson's ratio between these two directions is concerned. For α equal to unity ($\sigma_A = \sigma_B$) Poisson's ratio remains equal to its initial value up to failure.

Elwi and Murray (1979) proposed a third order polynomial equation describing ν in terms of the ratio of the uniaxial strain to the strain at failure. This relationship was based on a fit of Kupfer *et al* (1969) results. However the value obtained for ν is a function of the number of experimental points used to

evaluate ν from the measured (or published) data. For smaller strain intervals, ν increases while if fewer points are used (larger intervals), ν diminishes. Theoretically, ν must be limited to 0.5 .

Based on those considerations, and for simplicity, the following relationship for the Poisson's ratio in a biaxial stress state is adopted:

$$\nu = \nu_o + (0.5 - \nu_o) \left(\frac{\sigma_B}{\sigma_{cu}}\right)^5 (1 - \alpha) \qquad (3.15)$$

in which ν_o is the initial Poisson's ratio selected by the user, σ_B is the minimum principal stress and σ_{cu} is the ultimate strength determined by the failure envelope for the current value of the ratio σ_A to σ_B . The factor $(1 - \alpha)$ is equal to 1.0 in a uniaxial state of stress, and reduces progressively to zero for equal stresses σ_A and σ_B. It takes into account the confinement effect produced by σ_A on σ_B.

3.2.5 Uniaxial stress-strain curve

So far the constitutive relationships, the stress-strain law, the biaxial failure envelope and the Poisson's ratio used in this model have been defined. In this section the stress-strain curves used in the model are introduced. As mentioned earlier, concrete is assumed isotropic until ultimate stress levels in tension or compression are reached. Two basic rules are followed in all situations:

- the stress-strain curve assumed in the evaluation of the tangent modulus is the one associated with the smallest (algebraically) principal stress, σ_B ;

- in case of nonproportional loading, only the stress-strain curve associated with the current load step prevails.

These two assumptions follow the Darwin and Pecknold (1977) and the Ramm and Kompfner (1984) models, with the exception that only one stress-strain curve is used instead of two, as in the original Darwin and Pecknold equivalent uniaxial strain model. In the first assumption the direction corresponding to the absolute maximum compressive stress (σ_B) is assumed to govern the concrete behavior since it is causing most of the deficiencies in concrete, giving rise to its nonlinear behavior.

In the biaxial compression state of stress, three stress-strain curves derived from Kupfer *et al* (1969) experimental results are used, associated with stress ratios α of 0.0, 0.52 and 1.0 . In all cases the uniaxial strength σ_{cu} is evaluated from the failure envelope defined in Eq. 3.12. The associated strain ε_{cu} is interpolated linearly between ε_{cu} values for α of 0.0 , 0.52 and 1.0 , equal $-\varepsilon_{co}$, $-1.65\ \varepsilon_{co}$ and $-1.5\ \varepsilon_{co}$ respectively, as illustrated in Fig. 3.4 . The three curves associated with values for α of 0.0 , 0.52 and 1.0 are shown in Fig. 3.5 .

In biaxial tension, E_c is used for any stress ratio until f'_t is reached. In tension-compression, σ_{cu} is found from the failure envelope. For α smaller than α_{ct} , σ_{cu} is kept constant at $-0.85\ f'_c$. The ultimate strain related to σ_{cu} is given by following linear rule:

$$\varepsilon_{cu} = \frac{\sigma_{cu}}{f'_c}\ \varepsilon_{\infty} \qquad (3.16)$$

For all cases, once the stress-strain curve has been determined, the tangent modulus at the current stress level is evaluated using Eq. 3.10. In case of unloading, the initial tangent modulus E_c is used. Hence moduli E_1, E_2 and E_{12}, in the constitutive matrix (Eq. 3.5) are all set equal to the current tangent modulus E.

Up to this point in this chapter, the selection of the uniaxial stress-strain curves as a function of the stress ratio α has been discussed. The method adopted to follow the current stress-strain curve is described hereafter. At the beginning of a load step, the constitutive matrix (Eqs. 3.4 and 3.5) is evaluated as a function of the stress conditions prevailing at this point, called the step i. This is used to evaluate the stress increment (Eq. 3.1) based on the strain increment (Eq. 3.3). If the total strain increment is used to evaluate the stress increment, the resulting stress vector does not represent the actual situation with a nonlinear stress-strain curve (Fig. 3.6a). To trace more closely the actual curve, the initial strain increment is subdivided in smaller increments, called subincrements. This procedure allows the solution to follow the nonlinear response of the material but forces it to iterate several times into the material model, which is time consuming. To eliminate this iterative process, one can use the concept of the equivalent uniaxial strain and use only one subincrement. The procedure adopted in the model uses an equivalent uniaxial strain approach, different from the equivalent uniaxial strain method proposed by Darwin and Pecknold (1977) or by Elwi and Murray (1979). The concept used herein is similar to the approach introduced by Ramm and Kompfner (1984).

Assuming that $\Delta\sigma_{ij}$ and $\Delta\varepsilon_{ij}$ (not in tensor notation) are the incremental (or subincremental) change between steps i and j, one has the following relationships:

$$\Delta\sigma_{ij} = C_i \Delta\varepsilon_{ij} \tag{3.17}$$

in which C_i is evaluated using the tangent modulus E_i corresponding to the stress level σ_{Bi} on the stress-strain curve associated with the iteration i (Fig. 3.6a). The stress field at iteration j is evaluated by

$$\sigma_j = \sigma_i + \Delta\sigma_{ij} \tag{3.18}$$

Let the principal stresses of states σ_i and σ_j be σ_{Ai}, $\sigma_{Bi} \leq \sigma_{Ai}$ and σ_{Aj}, $\sigma_{Bj} \leq \sigma_{Aj}$. If the ratio of the two principal stresses at load step i is the same as at step j, one would remain on the same stress-strain curve. As mentioned previously, the uniaxial stress-strain curve associated with σ_B governs the behavior. However, at the beginning of the load step the stress level is known but not the corresponding uniaxial strain. Since the stress-strain curve defined by Eq. 3.7 is a second order relationship, one can find the root associated with the stress σ_{Bi} at step i, called ε_{ieq}, defined as

$$\varepsilon_{ieq} = R_\varepsilon \varepsilon_{cu} \tag{3.19}$$

in which R_ε describes the root of Eq. 3.7 equal to

$$R_\varepsilon = \frac{- K_2 - \sqrt{K_2^2 - 4 K_1^2}}{2K_1} \tag{3.20}$$

where

$$K_1 = \frac{\sigma_{Bi}}{\varepsilon_{cu}} \tag{3.21}$$

$$K_2 = \frac{\sigma_{Bi}}{\varepsilon_{cu}} \left(\frac{E_c}{E_{sec}} - 2 \right) - E_c \qquad (3.22)$$

The constitutive matrix at load step i leads to a principal stress in direction B called the "initial σ_{Bj} " in Fig. 3.6a . The increment of stress in direction B, equal to the difference between σ_{Bj} and σ_{Bi} , divided by the tangent modulus at load step i , produces the equivalent increment of uniaxial strain $\Delta\varepsilon_{eq}$. Since ε_{ieq} is known, the equivalent uniaxial strain at step j , ε_{jeq} , is evaluated as

$$\varepsilon_{jeq} = \varepsilon_{ieq} + \frac{\sigma_{Bj} - \sigma_{Bi}}{E_i} \qquad (3.23)$$

Finally a new stress value for σ_{Bj} corresponding to ε_{jeq} on the stress-strain curve at step j is obtained from Eq. 3.7 , as illustrated in Fig. 3.6a where it is called the " new σ_{Bj} " .

In the case of nonproportional loading, the stress-strain curve obtained from the ratio of the principal stresses at load step i is different than the curve at load step j. In the concrete model, the stress-strain curve corresponding to the current stress ratio is used as the uniaxial stress-strain curve. In Fig. 3.6b , the uniaxial stress-strain curves associated with steps i and j are illustrated. The procedure in this case is the same as described previously except that the modulus E_i used in Eq. 3.23 must be replaced by E_j .

This procedure reduces the number of subincrements within each load step and only one subincrement can be used if the change of stress-strain curve is smooth. Another reason resides in the fact that the magnitude of the first estimate for σ_{Bi} is usually too large which may cause premature failure when a stress envelope is used (Fig. 3.3). This procedure can also indicate a material failure at

stress σ_{Bi} if this stress on the step j curve is beyond the strength for this curve when shifting from curve i to curve j in two subsequent steps.

3.2.6 Shear modulus

In Eq. 3.5, two shear moduli appear in the equation: G_{ip} and G_{tr} , the inplane shear modulus for plane stress and the transverse shear modulus for plate-shell elements respectively. Before failure these two shear moduli are equal and expressed by

$$G_{ip} = G_{tr} = \frac{E}{2(1+\nu)} \tag{3.24}$$

The tangent modulus E and the Poisson's ratio ν are those evaluated from Eqs. 3.10 and 3.15 respectively.

3.2.7 Comparison with experimental results

Stress-strain curves obtained with the relationships presented above were compared to Kupfer *et al* (1969) experimental results for tension-compression and biaxial compression states of stresses. For a meaningful comparison, one must follow the stress strain-curve by feeding the material model with strain increments $\Delta\varepsilon_{ij}$. If a given constant stress ratio α is needed, the strain increment must be adjusted until the stress ratio resulting from the stress-strain relationships corresponds to the needed ratio. In the current case, a Newton-Raphson procedure, working outside a finite element environment, is adopted: one strain increment (e.g. $\Delta\varepsilon_A$) and a stress ratio α are given as input data to a small computer program acting as a front end to the material model subroutines. The iteration proceeds over the second strain increment. This approach is helpful not only to compare the model to experimental results, but also to look

closely at the model response under various conditions on which one has a better control than if the model is used directly from a finite element program.

Results of the comparison for four different tension-compression stress ratios are presented in Fig. 3.7 . For the biaxial compression state of stress, results for three stress ratios are illustrated in Figs. 3.8 to 3.10 for α values of 0.0 , 0.52 and 1.0 respectively. In all cases the model response compares satisfactorily with experimental results.

3.3 Postfailure modelling

Concrete fails either in tension or in compression when the stresses reach the failure envelope. The post ultimate behavior differs whether it is tensile or compressive failure. Both cases are treated separately hereafter.

3.3.1 Tensile failure

In the case of tensile failure, only material properties associated with the direction normal to the crack are affected and the tangent modulus in this direction is set to zero to for the stiffness matrix (Eq. 3.5) but the stress normal to the crack is released progressively. However the tangent modulus in the direction parallel to the crack remains unaffected and concrete is then treated as an orthotropic material. Poisson's ratio is also set to zero after cracking.

The postcracking stress-strain law adopted herein includes the tension stiffening relationships introduced in section 2.3 . An example of such a curve is illustrated in Fig. 3.11 . Here again the equivalent uniaxial strains are used and ε_{cr} is defined as the ratio of f_{cr} to E_c .

Unloading from the strain softening branch follows the secant path between the last point on the tension softening curve and the origin; reloading follows the same path, which has been used by Rots *et al* (1987). Poisson's ratio is set back to its current value (Eq. 3.15) only when the principal strain becomes negative and the crack is assumed to be closed at this stage. When concrete is on the unloading path, the tangent modulus is set equal to the slope of the unloading branch but the concrete remains orthotropic. The stress rebound in the other direction is equal to $\nu_o \Delta\sigma$ where $\Delta\sigma$ is the stress reduction at the crack along the tension softening curve.

The shear modulus after cracking G_{cr} is reduced progressively as a function of the stress reduction at the crack. The postcracking shear modulus is expressed as follows, assuming concrete is cracked in direction A only:

$$G_{cr} = \frac{E_B}{4} \left(\frac{f_{ST}}{f_{cr}} + 1 \right) \geq G_{min} = 0.1\, G_o \tag{3.25}$$

with

$$G_o = \frac{E_c}{2(1+\nu_o)} \tag{3.26}$$

in which f_{ST} is the average tensile stress carried by concrete after cracking , f_{cr} is the cracking stress, both in direction A, and E_B is the tangent modulus in the direction parallel to the crack. If two cracks are open, G_{cr} is then equal to G_{min} which has a shear retention factor of 0.1 . The maximum value for G_{cr} in Eq. 3.25 is limited to G_o. When the average stress normal to the crack reaches zero at the end of the tension stiffening curve, the crack is assumed completely open and G_{cr} is reduced to G_{min}.

In the tension-compression region, the compressive strength σ_{cu} in the direction parallel to the crack is kept constant at $-0.85\ f'_c$ until the crack becomes completely open at which point the compressive strength is reduced to $-0.6\ f'_c$. A crack is assumed completely open in the model when the strain in the direction of the normal to the crack reaches the end of the tension stiffening curve. Starting at this this point, cracks are assumed wide. At the same time the ultimate strain ε_{cu} is increased to $-1.5\varepsilon_{co}$. The rationale behind those modifications lies in the fact that the compressive strength reduces when cracks parallel to the compressive stress become wider. The value of $-0.6\ f'_c$ is used commonly in similar situations for the compressive strength of struts in truss models. The increase of the strain ε_{cu} is justified by the general softening of the concrete response when several cracks parallel to the compressive stress direction open. The value of $1.5\ \varepsilon_{co}$ was chosen based on good agreement with experimental results. This phenomenon was observed in the Vecchio and Collins (1982) test series, and also mentioned by Collins and Mitchell (1987).

3.3.2 Multiple cracks

In this model only two cracks can form at a point. However the orientation of these cracks follow different rules and in this study four cracking models are adopted, divided in two categories: fixed crack models and rotating crack models.

For fixed crack models, two approaches are used. In the first case cracks at a point are orthogonal and the crack orientation is determined by the orientation of the first crack, the second crack forming perpendicular to the first one. This is the fixed orthogonal crack model. In the second fixed crack model, the second crack forms in the direction of the principal stress, as long as the

angle between the two cracks is larger than 45 degrees. This is the fixed non orthogonal crack model and this is essentially the type of cracking model present in the initial concrete model of NISA (Kompfner , 1983).

In the rotating crack models, cracks are assumed orthogonal and oriented in the direction of either the principal stresses or the principal strains, which give a stress rotating crack model and a strain rotating crack model respectively. Usually rotating crack models represent more adequately the actual concrete behavior (Milford and Schnobrich, 1984).

3.3.3 Compression failure

Unlike tensile failure where only the properties perpendicular to the crack change, when a compression failure occurs in one direction , all concrete at this point is assumed crushed and the tangent moduli and the Poisson's ratio are set to zero in the evaluation of the stiffness matrix (Eq. 3.5) while the shear modulus is reduced to G_{min} given by Eq. 3.25 . If both directions were in compression before crushing, both undergo strain softening. The ultimate stresses in each direction are σ_{cu} in direction B and $\alpha\sigma_{cu}$ in direction A (see Fig. 3.3a). The normal strains in each direction define the beginning of the strain softening curves. This gives two independent stress-strain curves, one in each direction A and B. The assumed strain softening curve in compression in either direction is illustrated in Fig. 3.12 . When compression failure occurs in a tension-compression state of stress, only concrete stressed in compression before the failure occurred undergoes strain softening which is always direction B in the model. The stress normal to direction A is set equal to zero.

The slope of the strain softening branch in compression is a function of the amount of confinement: the higher the confinement, the softer the curve. In this study only unconfined concrete is assumed. It is also commonly observed that high strength concrete, which has a steep ascending branch, also has a steeper softening branch than lower strength concrete with soft ascending and softening branches, as illustrated by the ACI Committee 363 (1984). Based on this observation, the slope of the softening branch is adjusted as a function of the steepness of the ascending branch. If the coordinates of point "a " in Fig. 3.12 are σ_{cu} and ε_{cu} (both negative quantities), the coordinates of point "b" are obtained based on the ratio of E_c to E_{sec} of the uniaxial curve as

$$\varepsilon_{cmax} = 2 \frac{E_c}{E_{sec}} \varepsilon_{cu} \geq 5\varepsilon_{cu} \tag{3.27}$$

$$\sigma_{cmax} = 0.2 \frac{E_c}{E_{sec}} \sigma_{cu} \geq 0.75\sigma_{cu} \tag{3.28}$$

with

$$E_{sec} = \frac{\sigma_{cu}}{\varepsilon_{cu}} \tag{3.29}$$

Hence for a ratio of E_c to E_{sec} equal to 1.0 , ε_{cmax} would be twice as big as ε_{cu} and σ_{cmax} one fifth of σ_{cu} , while for a ratio of E_c to E_{sec} equal to 2.0 , ε_{cmax} and σ_{cmax} would be equal to $4\,\varepsilon_{cu}$ and $0.4\,\sigma_{cu}$ respectively.

In the model, unloading from the softening branch is allowed. Several types of unloading paths are proposed in the literature: Darwin and Pecknold (1974), Yankelevsky and Reinhardt (1987), among others. The complexity in these models comes from the modelling of hystereses produced in cyclic loadings. In the present case, unloading and reloading are assumed to take place

along the same path which is defined in function of a focal point of coordinates σ_f and ε_f, where σ_{cu} ans ε_{cu} are negatives:

$$\sigma_f = -0.1\,\sigma_{cu} \tag{3.30}$$

$$\varepsilon_f = \varepsilon_{cu} - 1.1\,\frac{\sigma_{cu}}{E_c} \tag{3.31}$$

Some unloading paths are illustrated in Fig. 3.12 . This simplified model in compression correctly simulates concrete behavior without the energy absorption feature provided by hysteresis.

3.4 Material properties

In sophisticated concrete models, several material properties are needed. For the current model, one needs E_c, f'_c, f'_t, ν_o, ε_{co}, ρ_{eff}, w_c and S_m. Normally for concrete, only f'_c is known. The other variables are rarely measured in practice and their values must be evaluated. Relationships are presented hereafter to estimate these material properties.

Although the value of E_c in this study represents the initial tangent modulus, the secant value evaluated at about $0.4f'_c$ and proposed in design codes can be used as a good estimate. For a stress-strain relationship like Eq. 3.7, the value of the secant modulus at $0.4f'_c$ is about 4% smaller than the initial modulus. The Canadian Code (CSA, 1984) equation for E_c takes the following form for normal weight concrete (in MPa):

$$E_c = 5000\,\sqrt{f'_c} \tag{3.32}$$

This equation was derived from best fit secant modulus at 0.4 to 0.5 f'_c for compressive strength varying from 3 to 40 MPa. For high strength

concrete, this equation tends to overestimate E_c and ACI Committee 363 (1984) proposed a new equation for compressive strengths ranging from 21 to 83 MPa

$$E_c = 3320 \sqrt{f'_c} + 6900 \tag{3.33}$$

This expression is adopted in this report to evaluate E_c when it is not provided.

The tensile strength f'_t is almost never evaluated in practical cases. Several methods are available to estimate f'_t, and different values of f'_t are obtained depending upon the method used. Raphael (1984) compared those methods and concluded that the split cylinder test gives the best estimate of f'_t since a large area of concrete is under relatively uniform tensile stress and also because cylinders are almost unaffected by shrinkage effects. He also proposed the following equation for f'_t when only f'_c is available (expressed in MPa) :

$$f'_t = 0.324 \sqrt[2/3]{f'_c} \tag{3.34}$$

The value of f'_t obtained from this equation can be considered to be close to the "true" tensile strength. However, since the concrete in a split cylinder test is in a biaxial state of stress (tension-compression), the tensile strength measured would be slightly smaller than the actual value if one refers to Fig. 3.3b . Shrinkage and creep tensile stresses build up in concrete before any external load is applied, especially for thin members such as slabs and walls. In these cases, a lower value for f'_t should be used and Collins and Mitchell (1987) proposed the following relationship:

$$f'_t = 0.33 \sqrt{f'_c} \tag{3.35}$$

The initial value for the Poisson's ratio ν_o varies usually from 0.15 to 0.25 but can be as high as 0.32 (ACI Committee 363, 1984). In this study a uniform value of 0.2 is adopted for ν_o as recommended by Kupfer *et al* (1969).

In the literature, the value for ε_{co}, the strain at f'_c in uniaxial compression tests, is seldom reported and, to the author's knowledge, no relationships relate ε_{co} to any other material properties. In this study a simple equation is proposed based on approximate measurements made from the ACI Committee 363 (1984) report on high strength concrete. The relationship takes the following form , with f'_c expressed in MPa:

$$\varepsilon_{co} = \frac{f'_c + 60}{40000} \geq 0.002 \qquad (3.36)$$

This equation gives ε_{co} values of 0.002 and 0.003 for f'_c equal to 20 and 60 MPa respectively.

Finally, in the tension stiffening model presented in Chapter 2, effective reinforcement ratios are required. The CEB Model Code (1978) definition, as described earlier in section 2.3.7 of this study, is adopted. In the case of slabs or panels, CEB (1985) proposes a limiting value for the effective depth used in the calculation of ρ_{eff} equal to half the depth of the portion of the slab in tension. The evaluation of this value can be difficult and in this study the limiting value for the effective depth is taken as h/2 .

The ratio of w_c to S_m is needed to define the point on the tension stiffening curve associated with the stabilized cracking (Fig. 2.14b). A constant value for this ratio equal to 0.1 is adopted since there is no evidence of a significant influence of this ratio on the response of a concrete member in

tension. In the comparison of the model to experimental results performed in section 2.4, a value of 0.1 was also used.

3.5 Implementation in the plate-shell element

As mentioned in Chapter 1 , the 3D degenerated plate-shell element was selected to perform the analysis and the material model describe above in this chapter was implemented in the plate-shell element. In the case of reinforced concrete, both materials are treated separately, the element is made of concrete to which the reinforcement is added. The calculations in the element are performed at the integration points, defined in the volume of the element (e.g a 4x4 Gaussian integration rule in the plane of the element and 7 Simpson's integration points over the thickness, for a total of 112 integration points in one element). For a given element the material properties are constant. However, in the evaluation of the stiffness matrix and the stresses in the element, each integration point has its own history and therefore the current tangent moduli and the orientation of the axes of orthotropy can differ from one point to the next one (either in the plane of the element or through the thickness). Each point behaves independently and plane stress conditions are assumed at each point.

In the material model introduced in this chapter, two cracks can form at each integration point and cracks do not need to have the same orientation when going from one layer to the next one through the thickness. In the tension stiffening model presented in Chapter 2 and used in the concrete model, the tension stiffening curve for concrete is a function of the reinforcement ratio and of the angle of the cracks to the reinforcement. As an input to the concrete model, the area of the reinforcement which is expected to be in tension and its orientation in the plane of the element are also required. For members subjected

to flexure, only the reinforcement located on the bottom side of a panel is used to evaluate the effective reinforcement ratio. This is used in the concrete model after a crack as formed to evaluate the equivalent reinforcement ratio in the direction normal to the crack (see Section 2.3.6). Hence for each of the two cracks that can form at one integration point, the tension stiffening curves associated with these cracks are different.

The actual reinforcement present in an element is treated separately as an additional smeared layer having only unidirectional properties. For each layer, its position over the thickness, its orientation in the element plane r-s and its thickness are required. In NISA, up to eight layers of reinforcement can be used in each element.

3.6 Plate problems

The plane stress incremental concrete model presented in this chapter possesses all the features required to model adequately the behavior of concrete in any plane stress situation. The stress-strain relationships adopted describe the behavior of concrete before and after peak stresses are reached , either in tension or in compression. The tension stiffening effect is modelled correctly and strain softening is allowed after the peak stress level in compression. Fixed and rotating crack models are available as options to the user. The model is suitable for nonproportional loading and unloading is allowed at any stage along the stress-strain curve.

However, some aspects of what should include a complete material model for plate type elements have not been included in the current model. This is because these features are not essential to carry out the type of analysis planned

but they should be included if a more general description of reinforced concrete plate elements is required. These points are described briefly hereafter.

Rheological effects such as creep and shrinkage need to be considered in any realistic concrete model. Creep increases long term deflections and highly stressed members could fail in compression under sustained stresses above 0.85 f'_c (Rüsch, 1960). Shrinkage affects the serviceability of structures and in case of plates, cracking occurs at a lower load level since tensile stresses are already present in the member before any external load has been applied to the member (Jokinen and Scanlon, 1987).

In plate type structures, plane stress conditions are assumed. However punching shear failure cannot be predicted using usual plate theory. To model punching shear failures and shear reinforcement in slabs requires real 3D constitutive models (Kotsovos, 1984) which would be more complicated and more time consuming to use. An interesting feature in such cases would be the ability to identify within the concrete model when a plane stress model is satisfactory or when a 3D model should be considered.

However these possible improvements will not affect the performance of the model in the type of analysis planned in this study. In the following chapter, the proposed concrete model, implemented in program NISA, will be used in various plate types problems where its reliability will be checked to experimental results in a series of validation tests.

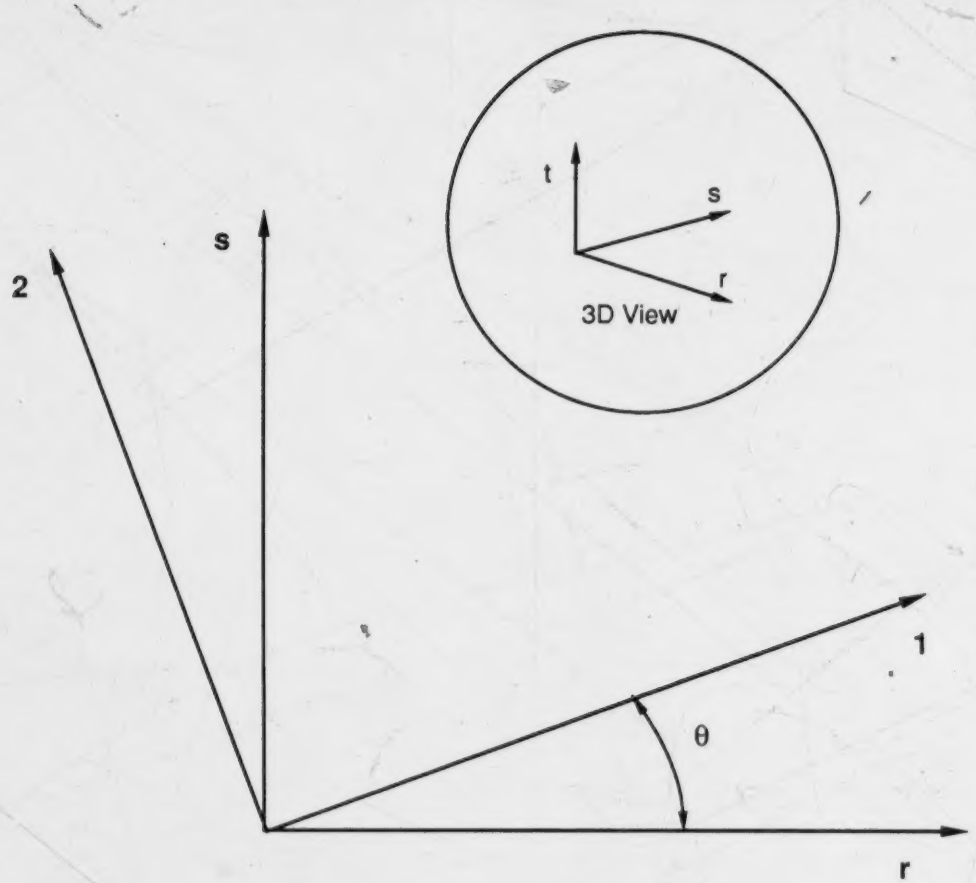

Figure 3.1 - Coordinate system

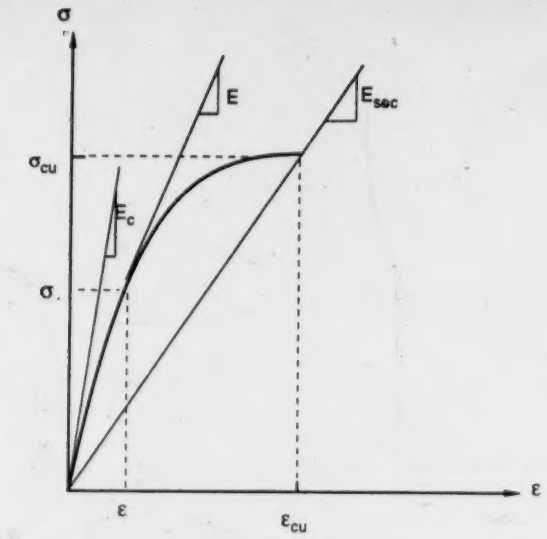

a) Normal stress-strain curve

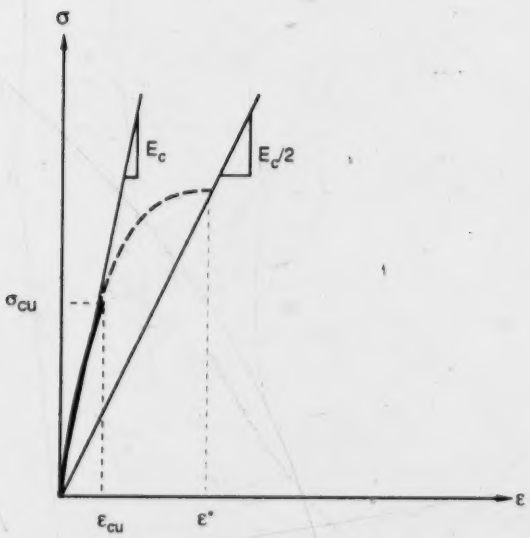

b) Steep stress-strain curve

Figure 3.2 - Uniaxial stress-strain curve

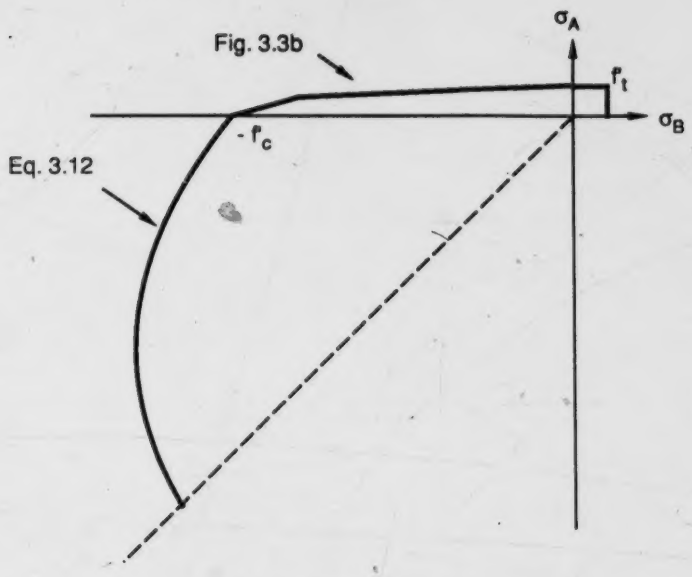

a) Failure envelope

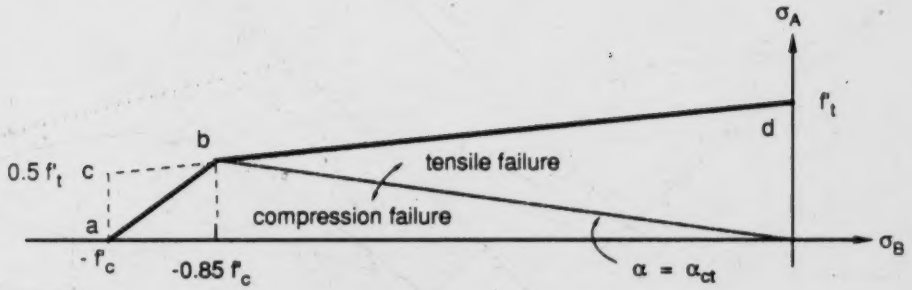

b) Tension - compression

Figure 3.3 - Biaxial failure envelope

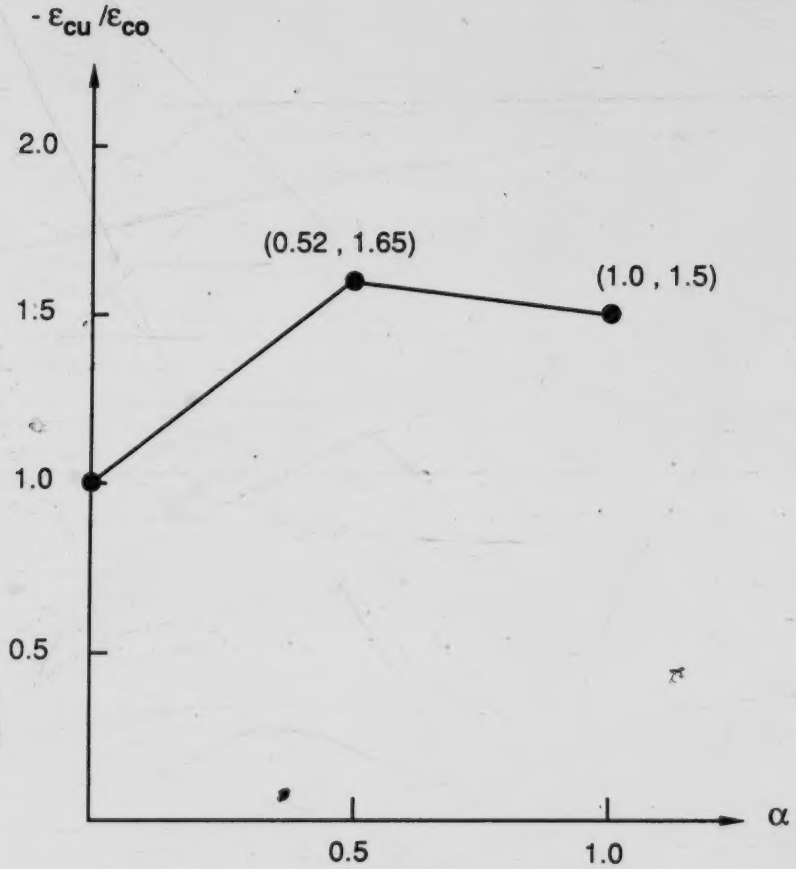

Figure 3.4 - Interpolation function for the uniaxial ultimate strains

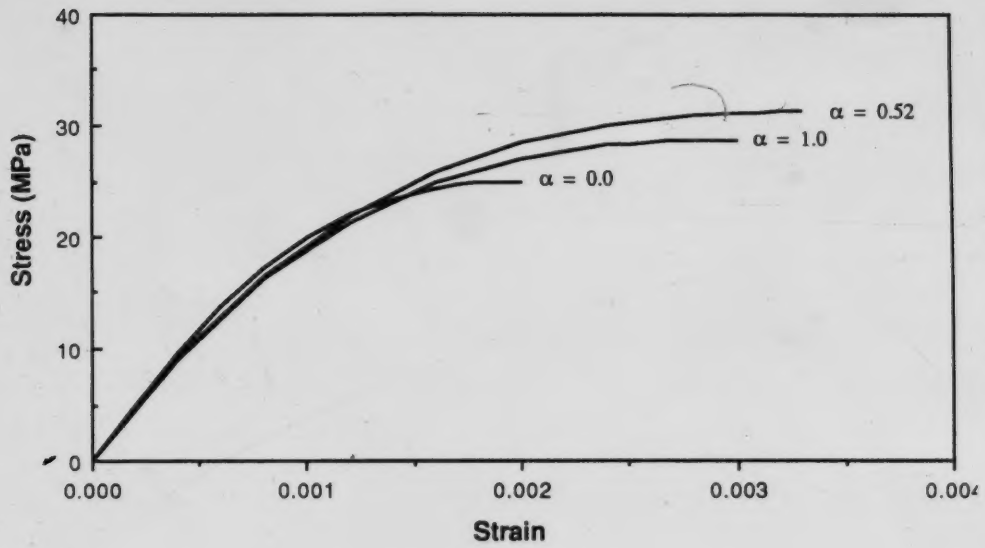

Figure 3.5 - Reference stress-strain curve

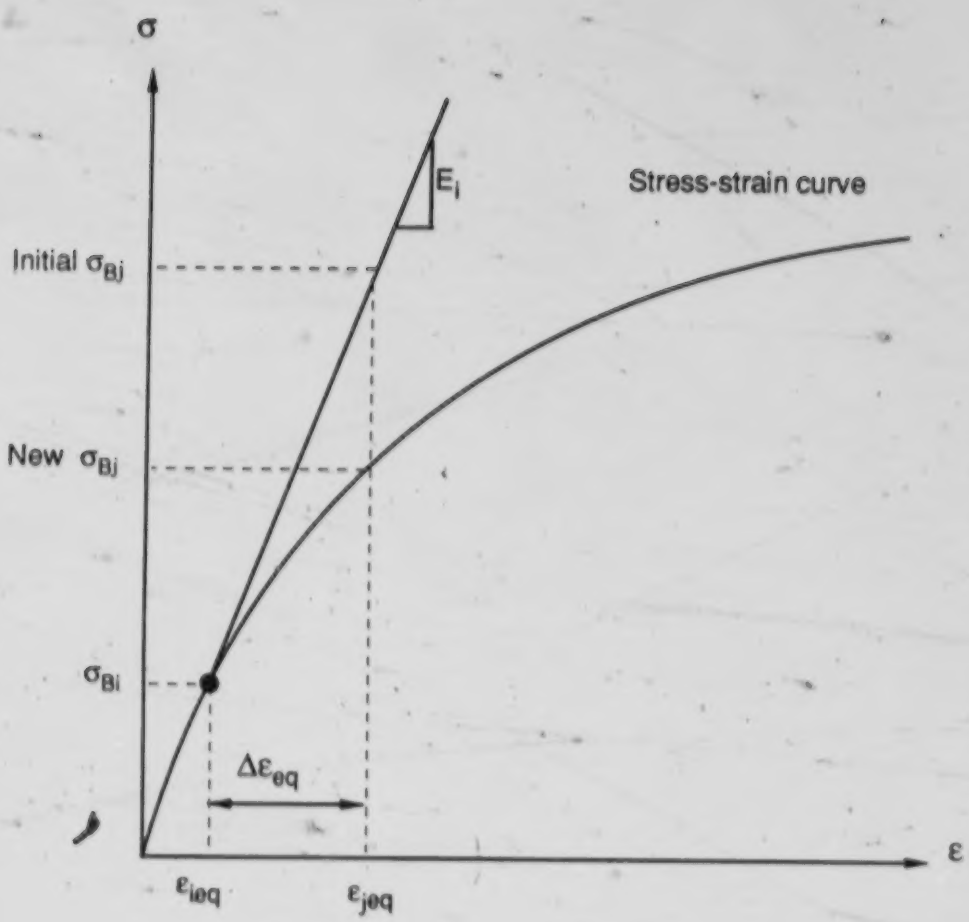

a) Proportional loading

Figure 3.6 - Equivalent uniaxial strain

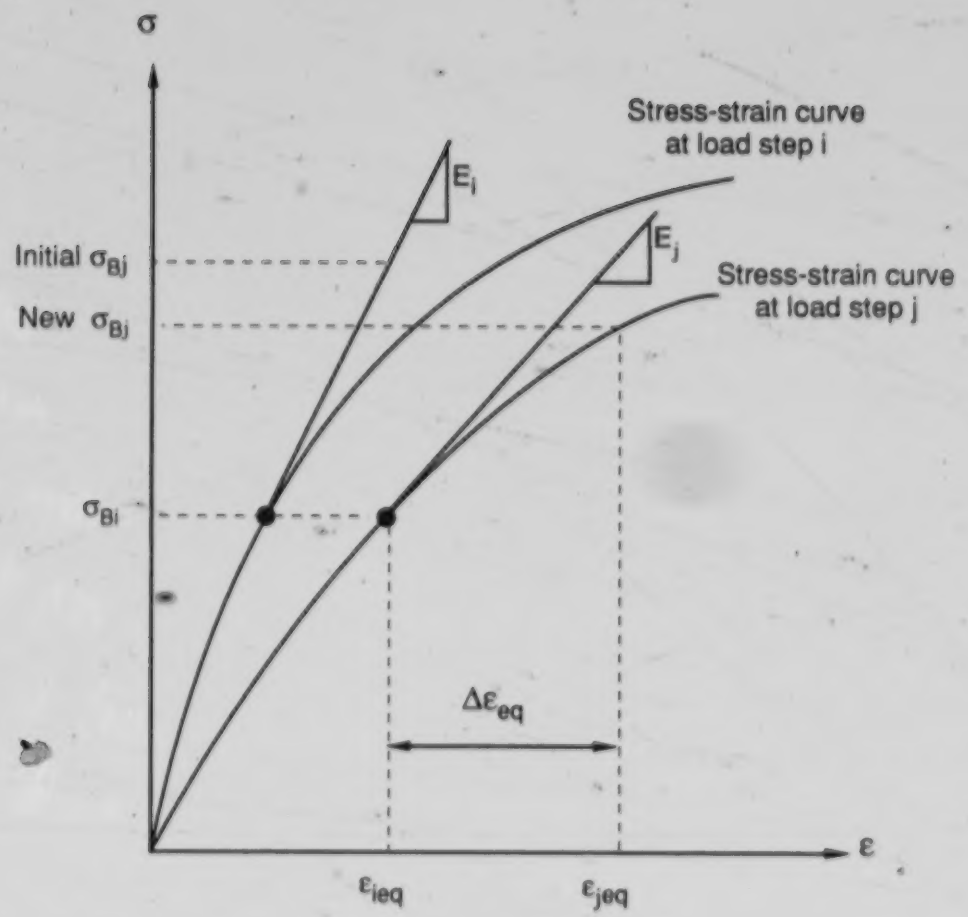

b) Nonproportional loading

Figure 3.6 (Continued) - Equivalent uniaxial strain

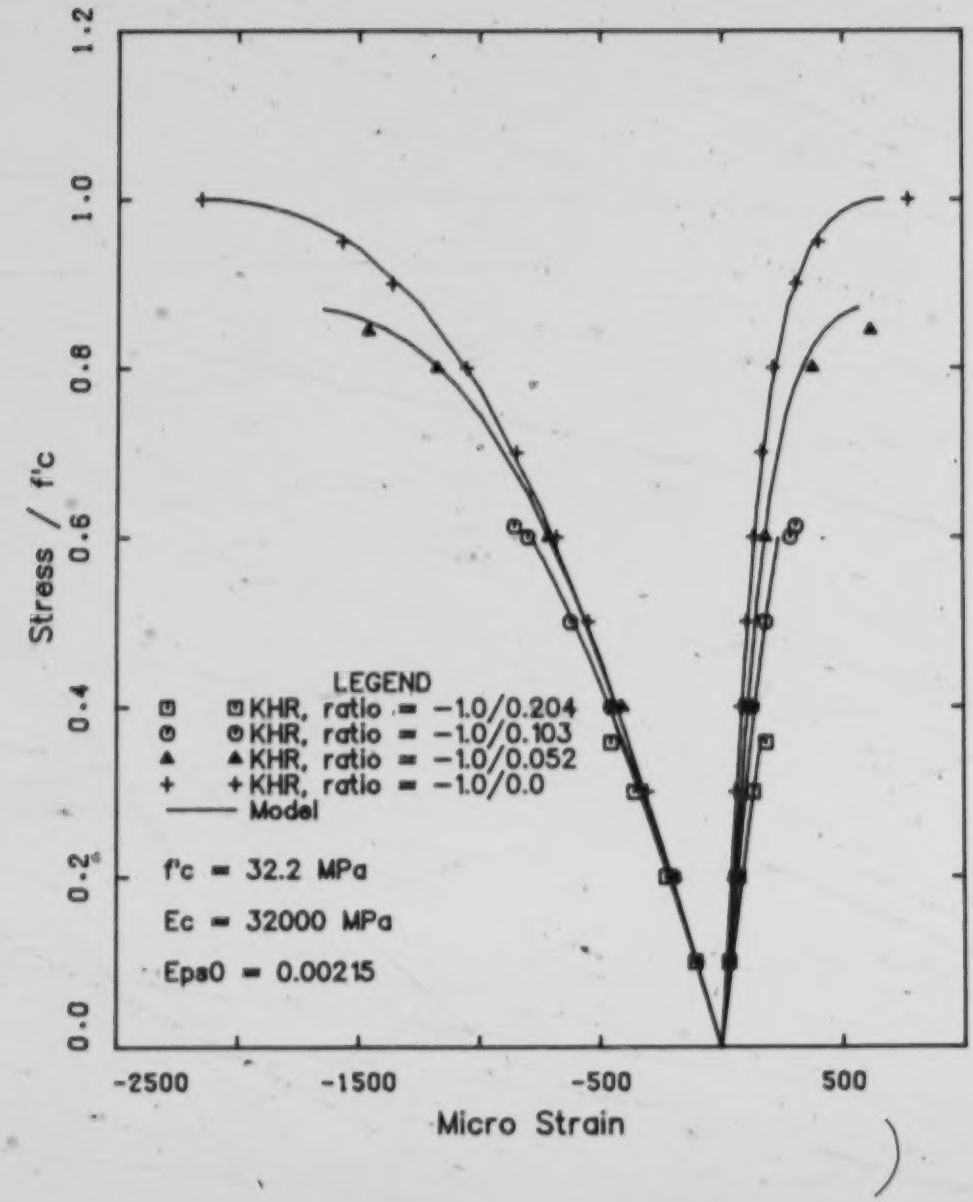

Figure 3.7 - Comparison of model and Kupfer *et al* (1969) in tension-compression

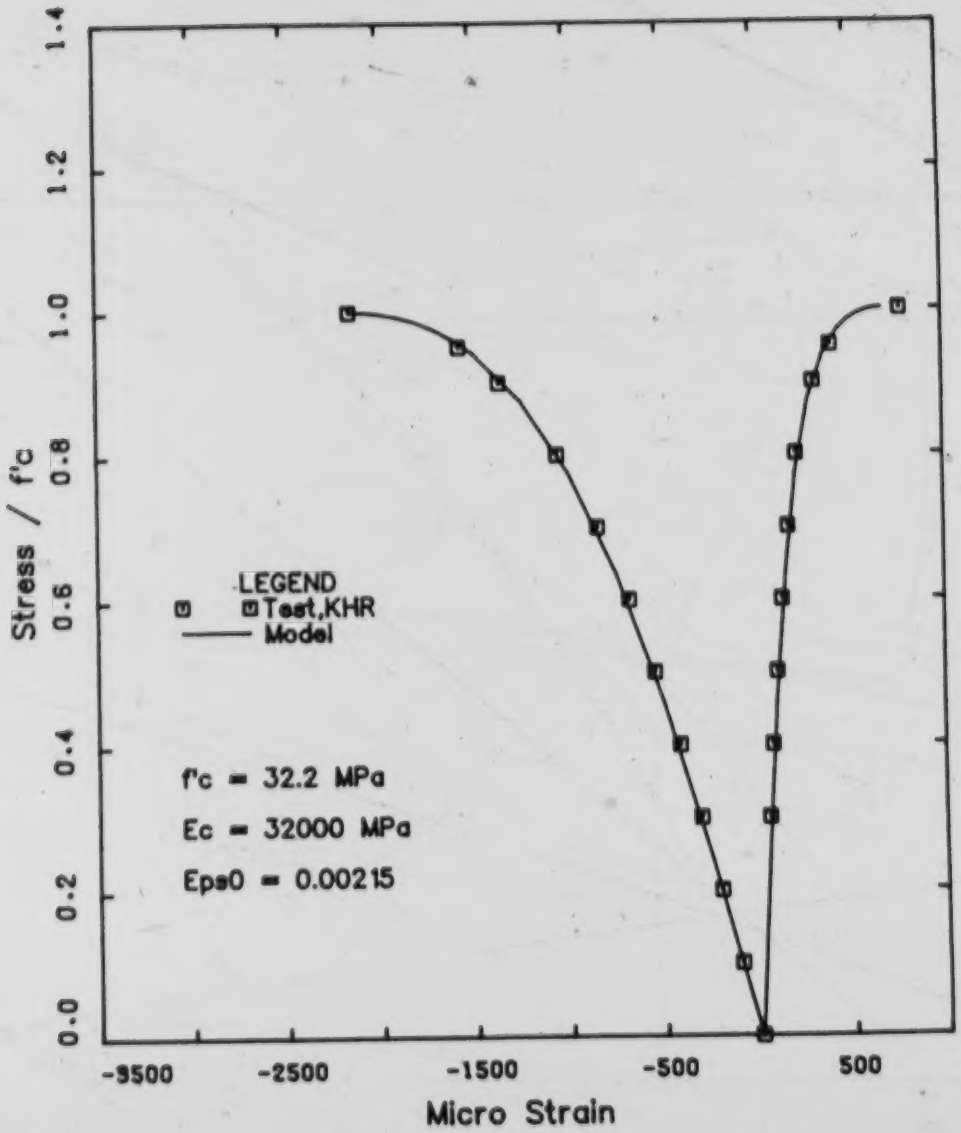

Figure 3.8 - Comparison of model and Kupfer *et al* (1969) in compression, ratio = -1.0/0.0

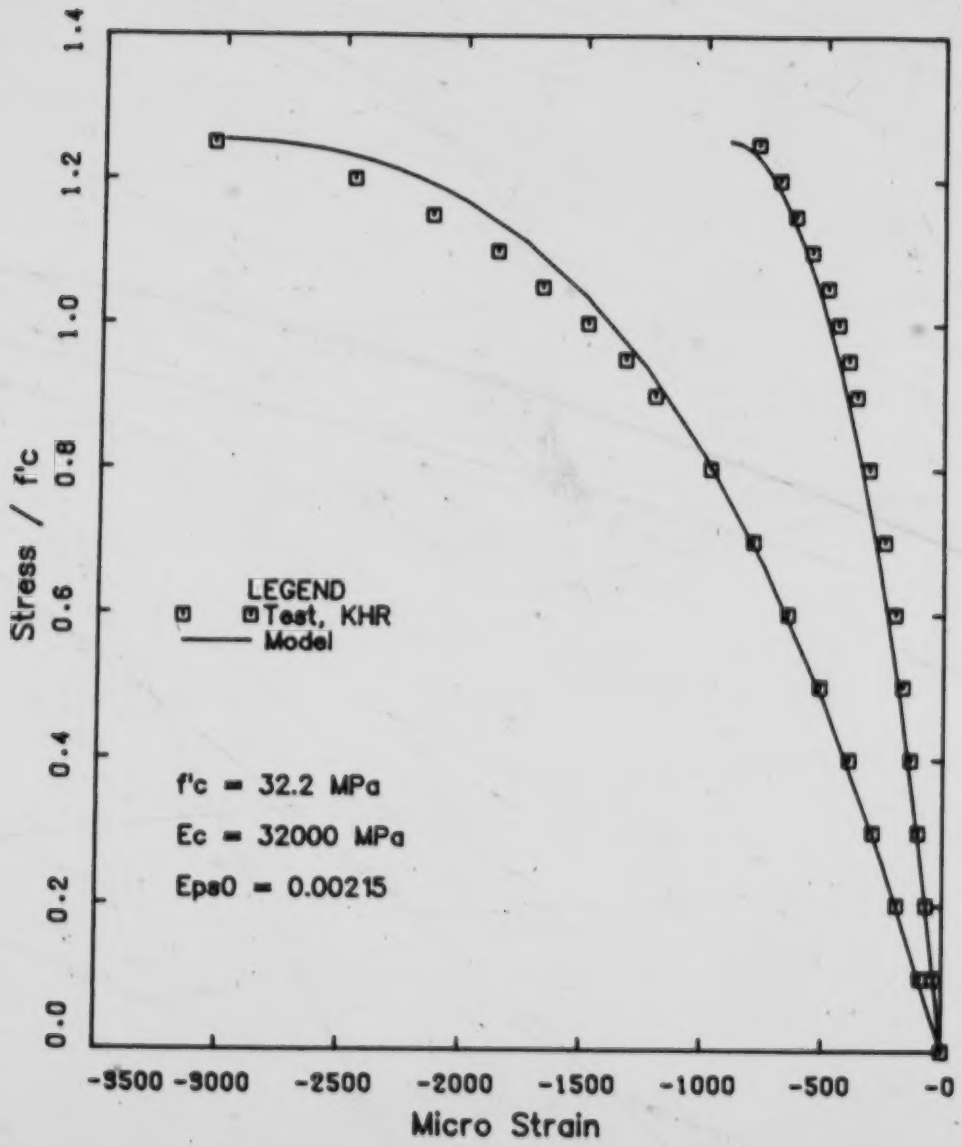

Figure 3.9 - Comparison of model and Kupfer *et al* (1969) in compression, ratio = -1.0/-0.52

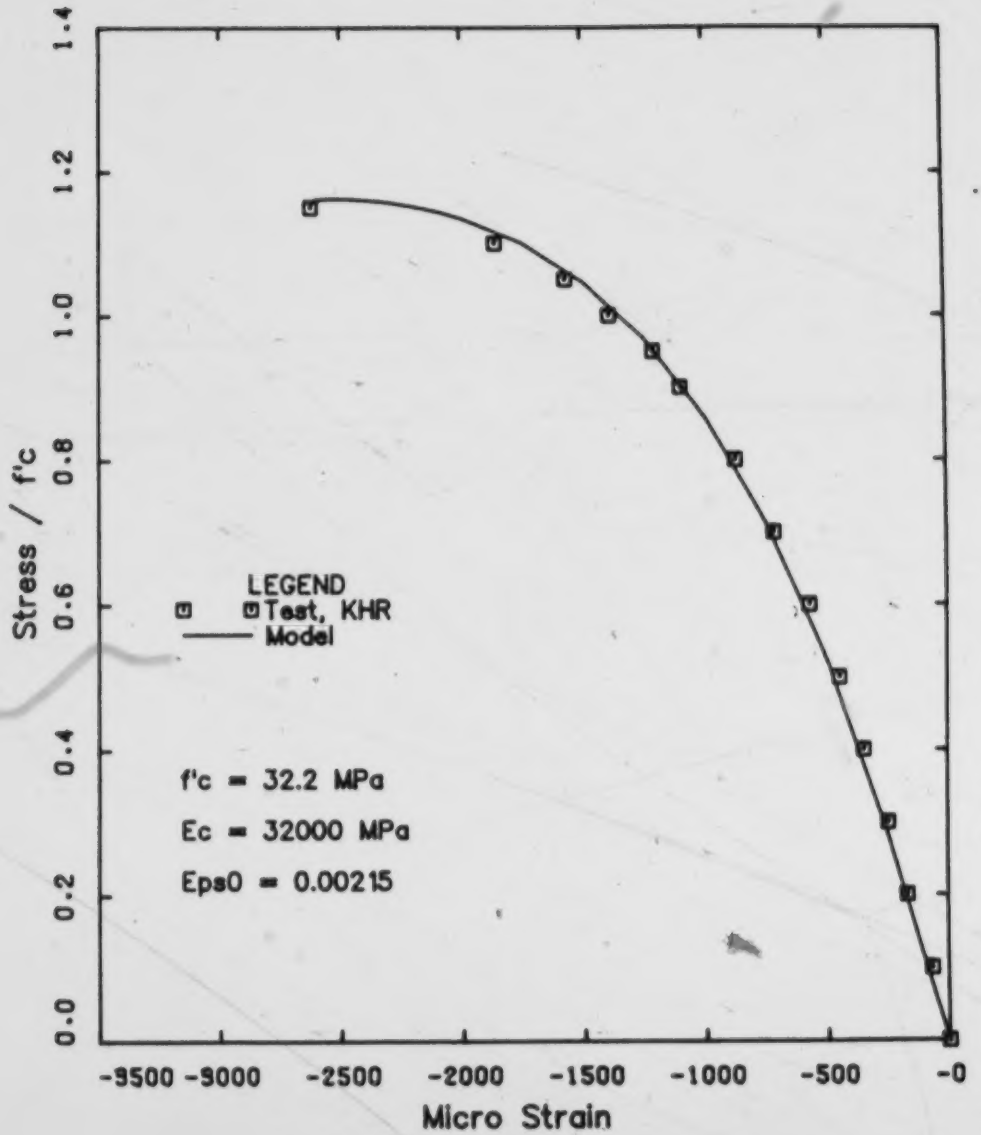

Figure 3.10 - Comparison of model and Kupfer *et al* (1969) in compression, ratio = -1.0/-1.0

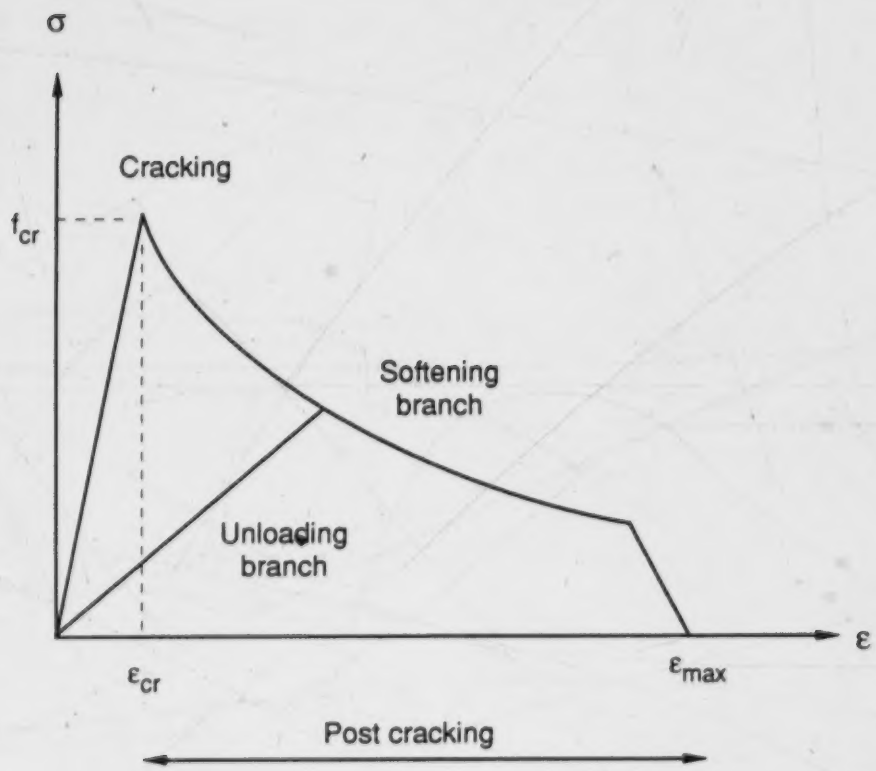

Figure 3.11 - Postcracking stress-strain curve

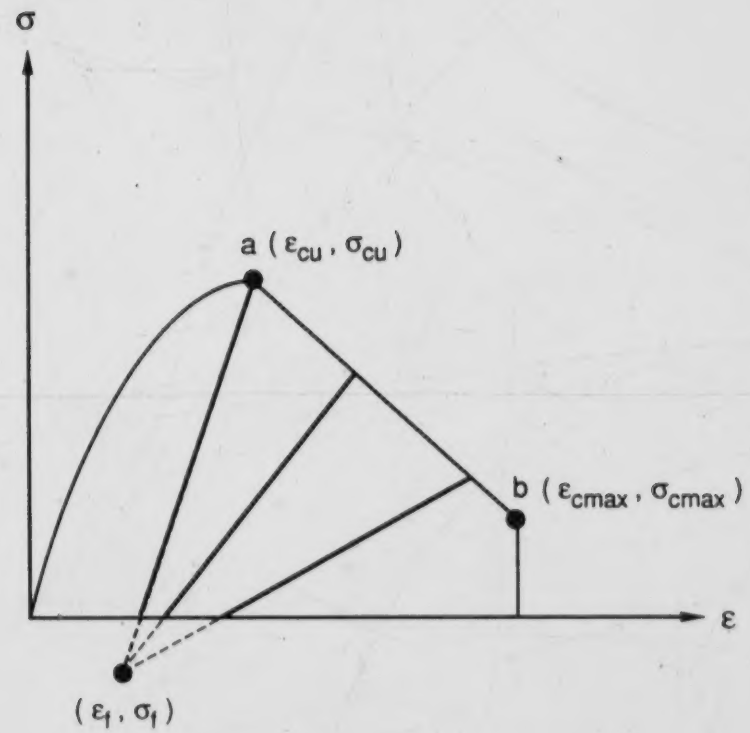

Figure 3.12 - Postcrushing stress-strain curve

CHAPTER IV

VALIDATION OF THE FINITE ELEMENT MODEL

The concrete model described in Chapter 3 and the element described in Chapter 1 contain simplifications and assumptions. Although the concrete model is based on well established knowledge of concrete behavior, one must ensure that the model performs adequately in situations where the behavior is known experimentally before one can proceed with an extensive parametric study or use it to predict the response of actual reinforced concrete panels.

Thus, a series of validation tests, involving various types of structural elements and loading conditions, was performed to measure the reliability of the model. The selection of the test series was based on two criterion: first, the test series selected must allow the verification of the model in various but well defined conditions, and secondly, some of the tests must be similar to the type of structural elements analyzed in this study. The selected test series involve panels subjected to various stress conditions, prestressed concrete panels loaded in biaxial tension, a laterally loaded slab and, finally, a series of thin reinforced concrete panels subjected to inplane and transverse loads.

4.1 Orthotropically reinforced concrete panels

4.1.1 Experimental program

A series of orthotropically reinforced square concrete panels was tested at the University of Toronto by Vecchio and Collins (1982, 1986). Most of the

panels were loaded in monotonic pure shear but some specimens were subjected to uniaxial compression, combined biaxial compression and shear, combined tension and shear, reversed cyclic shear, and changing load ratios. Reinforcement ratios in both directions were also varied.

The test specimens were 890 mm square and 70 mm thick. They were reinforced with two layers of 50 mm grid welded wire mesh, parallel to the specimen edges. Except for one test (PV3), the reinforcement was heat treated and exhibited ductile behavior. The minimum clear cover to the outermost layer of reinforcement was 6 mm whereas the maximum aggregate size was 6 mm.

4.1.2 Modelling with NISA

Among the thirty panels tested by Vecchio and Collins, six were selected based on the variety of the loading conditions (pure shear, shear and biaxial compression, nonproportional loading) and on the range of the reinforcement ratios and the amount of reinforcement in each direction. Of the six panels, four were part of an international competition reported in Collins *et al* (1985). The properties and the type of loading are summarized in Table 4.1. Experimental values of E_c and f'_t were not reported in the reference and were evaluated from Eqs. 3.33 and 3.34 respectively. A four node element, with a 2 by 2 integration rule, was used to discretize the panels since they were subjected to uniform states of stresses. The degrees-of-freedom associated with bending and with the out-of-plane displacement were restrained. The reinforcement was modelled by two smeared reinforcement layers, one in each direction located at the panel mid depth, with a Young's modulus equal to 200 000 MPa. The strain hardening modulus was taken as 400 MPa, based on a typical stress-strain curve presented

by Vecchio and Collins (1982). In Table 4.2, experimental failure loads and failure modes are compared to the model predictions.

In panels PV3, PV4 and PV27, subjected to pure shear, the amount of reinforcement was the same in both directions. Hence no crack rotations are expected and strains in the directions parallel to the edges (called here longitudinal and transverse strains) are the same. In Figs. 4.1 to 4.3 the response of tests PV3, PV4 and PV27 is presented for the longitudinal and the shear strains. Panel PV3 was analyzed with two tensile strength values. In the analysis with an f'_t value of 2.89 MPa, obtained with Eq. 3.34, the reinforcement yielded at onset of cracking whereas a value for f'_t equal to 1.72 MPa, obtained with Eq. 3.35, produced a better agreement with test results. For panel PV4, the value of f'_t was selected so that the cracking load corresponded to the value measured in the test. The value used was between those given by Eq. 3.34 and 3.35. For low reinforcement ratios, the cracking load is important if one wants to follow the postcracking specimen response before onset of yielding in the reinforcement. However, the ultimate load is not affected by the selection of f'_t, except for specimens with very low reinforcement ratios where the tension stiffening in the concrete governs the behavior rather than the reinforcement. It is worth mentioning that the value selected for f'_t is evaluated in terms of f'_c. In the case of Vecchio and Collins panels, the specimens were cured only a few days before testing (between 7 and 10 days for the six panels selected) while Eqs. 3.34 and 3.35 were derived for mature concrete, and hence might not be appropriate for early aged concrete. In the Vecchio and Collins (1982) report, there is no mention of measured values of f'_t.

For the three tests, the model and the experimental results agree satisfactorily. Failure by yielding of the reinforcement layers was adequately predicted by the finite element model for panels PV3 and PV4. In the case of panel PV3 the experimental ultimate strain is smaller than the predicted one because the rebars in the panel broke at the cracks, where the local strain is larger than the average strain over the panel used in the finite element analysis. This premature failure occurred due to the lack of ductility of the unannealed wire reinforcing steel used in this test. The reinforcement stress strain curve used in the analysis was based on a typical curve presented in Vecchio and Collins (1982) which might not represent perfectly the actual stress strain response of the bars in test PV3 .

For panels PV3 (with $f'_t = 1.72$ MPa) and PV4, the failure was caused by yielding of the reinforcement and the stress-strain curves in Figs. 4.1 and 4.2 show a ductile response of the panels after the peak load is reached. Such behavior is due to the low reinforcement ratios in these panels. In panel PV27, which had a higher reinforcement ratio, the failure was caused by the crushing of concrete in compression prior to the yielding of the reinforcement, leading to a brittle failure.

Panel PV19 was also loaded in pure shear but the reinforcement ratios in the longitudinal and transverse directions were different, with a ratio of ρ_l to ρ_t equal to 2.5 . Thus, in this case, cracks are expected to rotate. Before cracking, the reinforcement carries no forces since the longitudinal and the transverse strains are zero and cracks form at an angle equal to 45 degrees with respect to the two reinforcement directions. After cracking, the different stiffnesses of the reinforcement in the two directions causes a rotation of the principal strain field

and the orientation of the subsequent damage tends to rotate, becoming more parallel to the direction of the highest reinforcement ratio. In this case, one can compare the response of the fixed crack and rotating crack models. Since only one crack forms at each point , the two fixed crack models presented in section 3.3 produce the same answer. Stress rotating and strain rotating crack models are both used. Results for test PV19 are illustrated in Figs. 4.4a to 4.4c for the longitudinal, the transverse and the shear strain response. The finite element response for the two rotating crack models is satisfactory but the stress rotating model prediction is slightly closer to the experimental values than the strain rotating model. The stiffness of the plateau and the ultimate strain γ_u are also better in the case of the stress rotating model. The predicted ultimate shear stress and the failure mode were both predicted adequately by the rotating crack models. The fixed crack model overestimated the panel strength and stiffness in the postcracking region. Since panel PV27 had a relatively low reinforcement ratio in one direction, the failure was first initiated by the yielding of the reinforcement in that direction which explains the ductile response illustrated in Fig. 4.4b and 4.4c . However at the ultimate load the failure was due to the crushing of concrete.

Panel PV25 had the same amount of reinforcement in both longitudinal and transverse directions but in addition to the shear stress field, a biaxial compression force equal to 69% of the shear force was applied. In this case there is no crack rotations and the results for only one model are presented in Fig. 4.5, since all models would produce the same answer. The model response is again satisfactory but the test results show postcracking carrying capacity 15% higher than that predicted by the model. No apparent reason which can be related either to the model or to the experiment itself has been found to explain the difference

between the test and the model response. Similar discrepancies in the prediction were obtained by Vecchio and Collins (1982) in their analytical model and also by Balakrishnan and Murray (1986) who analyzed this test with the finite element method. For this panel, the failure was due to the crushing of concrete prior to yielding of the reinforcement, leading to a brittle failure.

Panel PV29, which had a ratio of reinforcement ρ_l to ρ_t equal to 2.0, was initially loaded in pure shear beyond the cracking load, up to a shear stress of 3.8 MPa . Above this point, for each additional shear stress increment an equal biaxial compressive stress increment was applied, causing a nonproportional loading situation. Here again fixed and rotating crack models were used and comparisons between experimental and finite element results are presented in Fig. 4.6a to Fig. 4.6c for longitudinal, transverse and shear strains respectively.

Within the range where only a shear force was applied, all three models used in the analysis (fixed, stress rotating, strain rotating) exhibited the same response and were close to the test measurements. At the point where the loading ratio was changed, the three models differed noticeably. The fixed crack model showed a net increase in the stiffness and the failure load was larger than in the test, occurring at a smaller ultimate shear strain (Table 4.2).

The two rotating crack models predicted adequately the ultimate strength and its associated shear strain. However, the path after the change in the load ratio up to the failure point were somewhat different. The model prediction was very sensitive to the postcracking modelling of concrete. In the case of the stress rotating model, the ultimate strain γ_u was sensitive to the rule adopted for the equivalent uniaxial strain ε_{cu}. The value for ε_{cu} equal to $-1.5\,\varepsilon_{co}$, mentioned in section 3.3.1 was selected based on this Vecchio and Collins test. However the

ultimate strength was not affected noticeably by ε_{cu} or G_{cr}, the cracked shear modulus. In the case of the strain rotating model, the model response was extremely sensitive to the postcracking definition adopted for G_{cr} and both the ultimate strain γ_u and the failure stress τ_u were affected. The rule adopted for G_{cr} in Eq. 3.25 was based on the response of panel PV29 with the strain rotating crack model. The failure modes predicted by the three cracking models was by the crushing of concrete.

Based on the model response illustrated in Fig. 4.1 to 4.6 (summarized in Table 4.2), one can conclude that the concrete model introduced in Chapter 3 performs adequately, especially when rotating cracks are used rather than fixed crack orientations. It should be mentioned that the actual cracks do not rotate in the same way as modelled in the analysis. In cases with unequal reinforcement ratios in the two directions, Vecchio and Collins observed that at stages after initial cracking, other cracks formed at a different angle than the initial crack orientation. This was not a continuous process as it is in the model however. Finally, it should be mentioned also that the failure modes predicted by the model corresponded to those observed in the tests.

As mentioned earlier, four panels (PV19, PV25, PV27 and PV29) were part of an international competition (Collins *et al*, 1985). For these panels, the model prediction of the ultimate strength, with the stress rotating crack model, ranges from 0.99 to 1.12 of the test values, with an average error of 2.8% . The ultimate shear strain obtained with the model ranges from 0.77 to 1.29 of the measured values, with an average error of 3.5% .

4.2 Prestressed concrete wall segments

4.2.1 Experimental investigation

A series of fourteen prestressed concrete wall segments was tested at the University of Alberta by MacGregor *et al* (1979), on which various numerical studies were carried out by Koziak and Murray (1979) and Chitnuyanondh *et al* (1979). In this study, segments #1 and #3 were selected for comparison with the current model predictions.

The wall segment specimens #1 and #3 were 800 mm (31.5 in.) square and 254 mm (10 in.) thick. Reinforcing consisted of two orthogonal meshes of 9.5 mm diameter (#3) bars at 76 mm (3 in.) on center placed at 13 mm (1/2 in.) from each face. The prestressing tendons consisted of four 7 wire tendons in one direction and three 6 wire tendons in the other direction, called directions 1 and 2 respectively. The prestressing tendons had a cross sectional area of 39 mm^2 (0.06 in^2) per tendon, for total prestress areas of 1081 mm^2 (1.676 in^2) and 695 mm^2 (1.077 in^2) in directions 1 and 2 respectively. The total rebar area was equal to 1419 mm^2 (2.2 in^2) in both directions.

Segments #1 and #3 were biaxially prestressed with a 598.7 kN (134.6 kips) force in direction 1 and a 551.6 kN (124.0 kips) force in direction 2 . Loading was applied through two independent perpendicular systems attached to both the reinforcement and the prestressing tendons. Segments #1 was tested under biaxial tension with a 2:1 loading ratio. Segment #3 was also tested under biaxial tension but the loading ratio was 1:1 up to 1668 kN (375 kips) at which point the load in direction 2 was kept constant while the load in direction 1 was increased.

4.2.2 Modelling with NISA

Segments #1 and #3 were modelled using the 3D degenerated plate-shell element, without the degrees-of-freedoms associated with bending and the out-of-plane displacement, using only a four node element and a 2x2 integration rule in the same manner as the orthotropically reinforced concrete panels reported in section 4.1 . Reinforcement was modelled with two smeared layers located at mid depth, one in each direction. The prestressing steel was also modelled with two smeared layers at mid depth. To model the prestressing effects, initial strains equal to -4.73×10^{-3} and -4.28×10^{-3} in directions 1 and 2 respectively were applied to the prestressing tendons so that equilibrium between reinforced concrete and tendons produced the desired prestressing force in both directions. Material properties used to model segments #1 and #3 are given in Table 4.3 where E_c, f'_t, and ε_{co} were evaluated with Eqs. 3.33, 3.35 and 3.36 respectively. The Young's modulus for the rebars was taken as 200 000 MPa (29 000 ksi) whereas the elastic modulus for the tendons was 203 000 MPa (29 400 ksi) with an ultimate tensile strength of 1 174 MPa (264 ksi).

Results for segments #1 and #3 are illustrated in Figs. 4.7 and 4.8, and agreement between experimental and numerical results are adequate. The initial stiffness, the cracking load, and the postcracking response were correctly predicted by the finite element model for both directions. The specimens were not taken to failure and the comparison was stopped at the last load level reported in the reference.

4.3 Reinforced concrete panels loaded axially and transversely

In the last two sections, the reinforced concrete model has been compared to the Vecchio and Collins (1982) shear panels and to the MacGregor *et al* (1979) wall segments. These tests had well defined stress conditions and were selected as two sets of preliminary validation tests. One can conclude that the plane stress material model developed in Chapter 3 and used with NISA can predict correctly the behavior of reinforced concrete structural elements, within the limits of accuracy one would expect in reinforced concrete structures. Now the analysis of more complex situations can be undertaken and the case of panel subjected to inplane and lateral loads is examined in the following section.

4.3.1 Experimental program

An experimental program was carried out at the University of Alberta by Aghayere and MacGregor (1988), to study slender reinforced concrete plates subjected to inplane and transverse loads. As mentioned in Chapter 1, this test series is the only published test series where both types of loadings are applied simultaneously and independently.

The experimental program consisted of nine reinforced concrete plates simply supported on four edges. Seven of the specimens had an aspect ratio of 1.0 , while two had an aspect ratio of 1.50 . Various width to thickness ratios and reinforcement ratios were considered. A total of eight plates were tested under combined in plane and lateral loads. One plate was tested under lateral load only to give an indication of the reduction in lateral load capacity for the plates loaded within the same series. The maximum applied inplane load magnitude (I_m) was 0.47, where I_m is expressed as

$$I_m = \frac{P}{a\ h\ f'_c} \qquad (4.1)$$

In this equation P is the total inplane load, "a" and h are the panel width and thickness respectively whereas f'_c is the uniaxial concrete strength. The test program was divided into four series: series A consisted of three square specimens with side dimensions of 1829 mm. Two of these specimens were tested under combined loads whereas one was tested under lateral load only. Series B consisted of two rectangular specimens 1829 mm by 2745 mm tested under combined loads with the inplane loads applied along the shorter edge. Series C consisted of two square specimens with same side dimensions as series A but with different reinforcement ratios in the two directions. Both specimens were tested under combined loads. Series D consisted of two square specimens having the same side dimensions as series A but with a different width to thickness ratio. Both specimens were also tested under combined loads. The actual plates tested overlapped the side dimensions given above by 152.4 mm all around as shown in Fig. 4.9a. This was necessary for supporting the plates and in order to achieve a near uniform compressive inplane load at the support line.

The specimens were tested in a horizontal position supported above the laboratory floor on steel beams spanning between columns. The testing frame was designed to accommodate a maximum compressive inplane load of 1000 kN/m and a uniform lateral load equivalent to 115 kPa. The inplane load was applied using four hydraulic jacks at one end of the specimen, reacting against four closed frames used to transfer the load to the opposite end of the specimen as illustrated on Fig. 4.9b . At both ends, the inplane load was applied to the panel by mean of 125 mm diameter, 125 mm long, high strength steel half cylinders, four along each edge, bearing on four 381 mm long clamps attached to the edge

of the specimen. A series of separate clamps were used to allow the edge of the specimen to twist to accommodate the slab deflections. Only uniaxial inplane loads were applied in the y direction, along the short edges.

The lateral load was applied by means of hydraulic jacks located underneath the laboratory strong floor, pulling on steel bars passing through 44.5 mm diameter holes in the specimen and attached to 125 mm square steel plates, 12.7 mm thick on the top of the specimen . The load points, nine for the square specimens and twelve for the rectangular ones, were aligned on a 610 mm square grid.

The lateral load reaction along the four edges of the specimen was provided by discrete roller-rocker supports spaced at 458 mm center to center, with a clear gap of 333 mm between adjacent supports, for a total of 16 and 20 support points for square and rectangular specimens respectively. The supports were designed to allow free horizontal movement in any direction and free rotation about an axis parallel to each edge. At the specimen four corners, the supports were located above the panel, instead of underneath, to restrain upward movement at the corners when the plates were loaded transversely. These supports were attached to the testing frame by mean of independent frames at each corner as shown in Fig. 4.9c .

Four layers of reinforcement were provided; two on each side in each direction. Reinforcement parallel to the inplane load direction was placed outermost on each side (Fig. 4.9a). The reinforcement consisted of 6.35 mm diameter deformed bars with an ultimate strength of 670 MPa. Test results of a tension coupon are given in Fig. 4.10 along with the idealized stress-strain

response adopted in this study. Concrete was poured in two phases which gave cylinder compressive strength of about 32.3 MPa and 40.2 MPa.

For seven of the specimens tested with both inplane and lateral loads, the inplane load was applied first and was then kept constant while the lateral load was being applied. For specimen C1, both types of loads were applied simultaneously, whereas specimen A3 was subjected to transverse loads only. All the pertinent information about specimen geometry and properties is given in Tables 4.4 to 4.7. A summary of the loading and behavior of the nine specimens tested is presented in Table 4.8.

4.3.2 Modelling with NISA

The Aghayere and MacGregor (1988) panels were modelled using the 16 node 3D degenerated plate shell element with 5 degrees of freedom per node described in Chapter 1. As shown in Fig. 4.11, the mesh described one quarter of the specimens and the panel region within the center line of the supports was discretized with 2 x 2 elements for the square specimens whereas a 2 x 3 element mesh was used in the case of the rectangular series. The 152 mm portion overhanging the supports was modelled with an additional row of elements, giving final meshes of 3 x 3 and 3 x 4 elements for the square and rectangular series, respectively. The A series panels and the two specimens of the B series were selected for comparison with the numerical predictions. The geometries of the two series are illustrated in Figs. 4.12 and 4.13 .

The supports were located at nodes 34, 37, 40, 64 and 94 for the square series while, for the rectangular series, the supports were located at nodes 34, 37, 40, 64, 94 and 124. At each support the out-of-plane displacement was

restrained. The rotation about an axis parallel to the panel edge was allowed but the rotation in the other direction was restrained to model the actual support conditions and to account for the fact that the supports in the tests were 125 mm long. The inplane load was modelled using a uniformly distributed load between nodes 4 and 10. The transverse loading points were located at nodes 56, 60, 96 and 100 for the square series and at nodes 66, 70, 106 and 110 for the rectangular series B. This corresponds closely to the actual loading points in the test.

A 4 x 4 Gaussian integration rule was used over the plane of each element, while 9 layers were used to discretized the element over its thickness in order to perform the Simpson's type integration. The selection of the number of elements and the number of layers for the integration rule adopted over the thickness were based on a study presented in Appendix B in which the response of different meshes and number of layers are compared.

Reinforcing steel response was described using the idealized stress strain curve of Fig. 4.10 and the four layers of smeared reinforcement were located at the actual positions mentioned in Table 4.6 . In the outside strip, which was not fully reinforced in the tests, only a quarter of the reinforcement amount present in the region located within the center line of the supports was provided to represent the actual specimen reinforcement. A reduced compressive strength f''_c equal to 90% of f'_c was also used to reflect the actual uniaxial compressive strength compared to the compressive strength measured in cylinder test were some confinement exists (Kotsovos, 1983). The value of $0.9\ f'_c$ was chosen based on judgement since, to the author's knowledge, no extensive study is available on the ratio of the compressive strengths measured with different techniques. If the brush system developed by Kupfer *et al* (1969) used on

cylinders is assumed to represent the actual uniaxial compressive strength, the ratio of this strength to the usual cylinder test would probably be around 90 %. One should mention that Todeschini *et al* (1964) and Hognestad (1951) used similar values for f'_c. The material properties for concrete used in the analysis are given in Table 4.9 where f_t was evaluated with Eq. 3.35 and ε_{co} with Eq. 3.36. Initial Poisson's ratio ν_o was set to 0.2 in all cases.

Of the nine specimens tested by Aghayere and MacGregor, five were selected. The three specimens of the A series were chosen because one panel had only lateral loads and the two other were subjected to combined inplane and lateral loads, with a different inplane load level in the two cases. The B series was also selected since the panels were rectangular. The comparison of the model response and the test measurements for specimen A3 is presented in Fig. 4.14, in Fig. 4.15 for specimens A1 and A2 and in Fig. 4.16 for the B series. The modelling of laterally and axially loaded panels includes the corner support effects and the relative edge rotation at inplane load application points, as described in Appendix B. Aghayere and MacGregor (1988) did not measure the out-of-straightness of their specimens before any load was applied but they recorded the out-of-plane displacements produced when the inplane loads were applied. To model those initial displacements, edge moments were applied together with the inplane loads in the first load step. The value of these moments was adjusted in a trial-and-error process until the central out-of-plane displacement corresponded to the value measured experimentally. It is assumed that these edge moments account for the secondary effects and errors that take place in any test but which cannot be evaluated or isolated precisely. In the case analyzed, the ratio of the edge moment to the inplane load, or the eccentricity of

the inplane load measured from the panel midplane, ranged from -0.4 mm in the case of specimen A1 to 6.3 mm in the case of specimen B1, as given in Table 4.9 .

For the five specimens analyzed with program NISA, the model performed satisfactorily, within what one would expect for reinforced concrete structures. In the case of specimen A3, the cracking load predicted by the model was higher than the value measured experimentally. This may be due to tensile stresses in the specimen due to shrinkage. These stresses were not considered in the analysis. This problem appeared only in the case of the laterally loaded panel A3. For the five panels analyzed, the ultimate load and the corresponding deflection at the center of the specimen agreed satisfactorily. The rectangular panels (B series) were affected by the stiffness of the [illegible] holding down the corners. This is discussed more fully in Appendix B. If more tests are performed on a similar test set up, care should be devoted to the stiffness of the corner supports and their relative displacements with respect to the specimens should be monitored and reported.

4.3.3 Analysis of the model results

Nonlinear finite element analyses generate a large amount of information and some of the data obtained in the analysis of specimens A2 and B1 are presented hereafter.

Principal moment orientations and magnitudes are illustrated in Fig. 4.17 for the specimen A2 at the maximum load (Q_u= 119.5 kN). The moments are about the axes shown in the individual rosettes. It can be observed that in a large portion of the plate, the axes of the major principal bending moment are perpendicular to the direction of the inplane loads. The bending moment m_y ,

acting about an axis parallel to the x axis, is equal to 16.89 kN•m/m at the center of the plate with the P-Δ effects included. However it reduces to a value of 2.10 kN•m/m when the bending moment equal to the product of the inplane load times the deflection at the center of the plate is subtracted. The value of m_x at the same location, acting about an axis parallel to the panel y axis, is equal to 3.19 kN•m/m, for a ratio of m_x to m_y equal to 1.52 . This indicates that the a larger portion of the lateral load is carried by reinforcement parallel to the x direction than by the reinforcement parallel to the inplane load direction. This aspect is discussed in more detail in the following chapter.

Figures 4.18 and 4.19 show the material damage on the bottom and top sides respectively, at the maximum load level. As observed in the test, the bottom side is heavily cracked whereas the extent of damage is more reduced on the top side of the specimen. The reduction in the carrying capacity, observed after the maximum load is reached (Fig. 4.15), is due to the progression of crushing on the top side near the corners of the slab which initiated at the maximum load level as shown in Fig . 4.19 and spread along the diagonal as illustrated in Fig. 4.20 . The wide cracks observed along the panel edge (in element #7) were probably due to the anchorage of the membrane forces in the reinforcement oriented in the x direction.

Figure 4.21 shows the reinforcement strains measured in the transverse (x) direction at the center of specimen A2. Both the top and bottom bars undergo tension and the test results are in good agreement with the model prediction. It is interesting to note that both top and bottom strains increase with the increase of the lateral load. This could be explained by the restraining effect exerted by concrete located on the panel periphery on the center region of the specimen

which is subjected to a net tensile force throughout the test. However it is not known at this stage of the study if this restraining action would be observed to the same extent for a specimen without the overhanging strip.

Principal membrane forces in concrete for the last load step just prior to collapse are shown in Fig. 4.22 for the specimen B1. It can be observed that the membrane force trajectories are slightly inclined, principal stress directions fanning toward the longitudinal edges. The membrane forces at the center line are smaller at the center of the plate than on the outside which indicates a significant redistribution of the inplane loads from the edges where they are applied to the center of the plate. On the other hand, forces in the reinforcement are mainly oriented perpendicularly to the direction of the inplane load, as illustrated in Fig. 4.23. Principal bending moments are plotted in Fig. 4.24, showing the same tendency as observed for the specimen A2, with the major principal bending moments about axes in the direction perpendicular to the inplane load action due to the P-Δ effects. One should notice the relative magnitude of the bending moments near the corner support. In the test specimens the region outside the supports was not heavily reinforced which could indicate why the specimen behavior was sensitive to the restraint at this point. The lack of reinforcement at the corners reduces the stiffness of this region, increasing the flexibility of the specimen. This can explain why the specimen behavior was close to the unrestrained corner case presented in Fig. B.10 .

4.3.4 Summary

Five of the nine reinforced concrete panels tested by Aghayere and MacGregor (1988) were used to verify the concrete model and the finite element program. Four of these panels were subjected simultaneously to inplane and

lateral loads and one carried only lateral loads. Three panels were square and two were rectangular, with aspect ratios b/a of 1.0 and 1.5 , respectively. The modelling with the finite element program was performed based on a study on the optimal mesh and number of layers to provide an adequate accuracy. The interactions of the specimens with the test set up were considered in the analysis in the cases where their effects could affect the specimen behavior.

In the five cases analyzed, the finite element model reproduced satisfactorily the experimental measurements. The peak loads and the associated deflections at the center of the specimen are given and compared in Table 4.10 for the tests results and the model predictions. The ultimate load predicted by finite element ranged from 0.99 to 1.07 , with an average value of 1.02 compared to the tests results while the average error for the center deflections is equal to 1.04 , the predicted values varying between 0.91 and 1.32 of the experimental results.

The behavior and the failure modes predicted by the model agree with the experimental observations. The ascending and descending branches of the load-deflection diagrams obtained with the model followed the tests measurements. The cracking and crushing patterns in the model predictions were close to the observations made in the tests.

Based on the validation tests performed with this test series, plus those on the series on reinforced concrete panels and the wall segment series, one can conclude that the reinforced concrete model implemented in the finite element program can model satisfactorily plate type reinforced concrete structures and can be used with confidence to predict the behavior and the ultimate carrying capacity of these elements.

Table 4.1 - Data of the Vecchio and Collins (1982) test series

Test	Loading	ρ_l (%)	f_{yl} (MPa)	ρ_t (%)	f_{yt} (MPa)	f'_c (MPa)	ε_{co} ($x10^{-3}$)	$E_c^{(1)}$ (MPa)	$f'^{(2)}_t$ (MPa)
PV3	PS	0.483	662	0.483	662	26.6	2.30	24020	2.89
PV4	PS	1.056	242	1.056	242	26.6	2.50	24020	2.89
PV19	PS	1.785	458	0.713	299	19.0	2.15	21370	2.31
PV25	SBC	1.785	466	1.785	466	19.2	1.80	21470	2.33
PV27	PS	1.785	442	1.785	442	20.5	1.90	21930	2.43
PV29	CLR	1.785	441	0.885	342	21.7	1.80	22370	2.52

PS	Pure shear
SBC	Combined shear and biaxial compression
CLR	Changing load ratio
(1)	Evaluated from Eq. 3.33
(2)	Evaluated from Eq. 3.34

Table 4.2 - Failure characteristics of the Vecchio and Collins (1982) test series

Test	Experimental			Model			Test / Model	
	τ_u (MPa)	γ_u ($x10^{-3}$)	Failure Modes	τ_u (MPa)	γ_u ($x10^{-3}$)	Failure Modes	τ_u	γ_u
PV3	3.02	5.62	FR/D	3.41[1]	20.00	YR/D	0.89	0.28
				3.41[2]	4.17	FR/B	0.89	0.72
PV4	2.71	14.31	YR/D	2.84	15.15	YR/D	0.95	0.95
PV19	3.96	10.51	YR;CC/D	4.54[3]	7.92	YR;CC/D	0.87	1.33
				3.97[4]	13.63	YR;CC/D	1.00	0.77
				3.97[5]	8.92	YR;CC/D	1.00	1.18
PV25	9.13	5.51	CC/B	8.17	4.27	CC/B	1.12	1.29
PV27	6.24	4.54	CC/B	6.36	4.71	CC/B	0.99	0.96
PV29	5.57	6.12	CC/B	6.70[3]	3.79	CC/B	0.83	1.62
				5.56[4]	5.45	CC/B	1.00	1.12
				5.79[5]	5.16	CC/B	0.96	1.19

(1) f'_t evaluated from Eq. 3.35
(2) f'_t evaluated from Eq. 3.34
(3) Fixed crack model
(4) Stress rotating crack model
(5) Strain rotating crack model
FR Brittle failure of rebars (no yield plateau)
YR Yielding of rebars (with yield plateau)
CC Crushing of concrete
D Ductile failure
B Brittle failure

Table 4.3 - Concrete properties for prestressed wall segments
MacGregor *et al* (1979)

Segment	f'_c (MPa) [ksi]	f'_t (MPa) [ksi]	E_c (MPa) [ksi]	ε_{co} ($x10^{-3}$)	ρ_1 (%)	ρ_2 (%)
1	35.12 [5.093]	2.00 [0.29]	26550 [3850]	2.38	1.20	0.99
2	39.26 [5.694]	2.07 [0.30]	27720 [4020]	2.48	1.20	0.99

Table 4.4 - Nominal dimensions of Aghayere and MacGregor (1988) test series

Series	b (m)	h (mm)	b/a	b/h	ρ_y (%)	ρ_y/ρ_x
A	1.83	63.5	1.0	28.8	0.41	1.16
B	2.74	63.5	1.5	43.2	0.60	1.18
C	1.83	63.5	1.0	28.8	0.52	2.10
D	1.83	54.0	1.0	33.9	0.48	1.16

Table 4.5 - Reinforcement area(1) in Aghayere and MacGregor (1988) test series

Series	Bar area in x direction		Bar area in y direction	
	Top	Bottom	Top	Bottom
A	225	225	260	260
B	324	324	381	381
C	157	157	329	329
D	225	225	260	260

(1) : in mm^2 / m

Table 4.6 - Actual specimen thicknesses and reinforcement positions(1) in Aghayere and MacGregor (1988) test series

Specimen	Thickness (mm)	Bars in x direction		Bars in y direction	
		Top	Bottom	Top	Bottom
A1	67.0	17.0	51.3	10.6	57.6
A2	64.2	18.1	47.0	11.7	53.3
A3	65.3	18.6	49.8	12.2	56.1
B1	64.5	17.1	49.3	10.7	55.6
B2	64.8	17.1	51.1	10.8	57.4
C1	64.7	16.7	47.4	10.3	53.7
C2	63.7	17.5	46.6	11.1	52.9
D1	55.5	18.5	39.9	12.1	46.2
D2	57.0	18.2	41.7	11.9	48.0

(1) : in mm from the top face to the centroid of the bar

Table 4.7 - Concrete properties in Aghayere and MacGregor (1988) test series

Specimen	Age (days)	E_c (MPa)	f'_c (MPa)	f'_t (MPa)
A1	113	22975	32.25	2.80
A2	111	23010	32.25	2.80
A3	98	23151	32.24	2.80
B1	119	25580	40.27	2.97
B2	118	25553	40.23	2.97
C1	122	22904	32.26	2.80
C2	117	22939	32.25	2.80
D1	126	22833	32.26	2.80
D2	112	25487	40.00	2.97

Table 4.8 - Test results in Aghayere and MacGregor (1988) test series

Specimen	p_u (kN/m)	I_m	Q_u (kN)	q_u (kPa)	Δ_{max} (mm)	Δ_{ult} (mm)
A1	962.0	0.47	153.0	45.7	15.8	34.0
A2	765.0	0.37	126.3	37.7	19.0	40.0
A3	0.0	0.00	196.2	58.6	75.2	---
B1	874.3	0.34	142.2	28.3	48.1	53.0
B2	633.9	0.25	182.8	36.4	44.4	49.0
C1	822.5	0.40	116.5	34.8	15.9	38.0
C2	765.0	0.37	109.8	32.8	16.1	38.0
D1	524.6	0.30	89.8	26.8	15.1	48.0
D2	852.6	0.39	121.9	36.4	14.0	39.0

Table 4.9 - Concrete properties used in analyzing Aghayere and MacGregor (1988) test series A and B

Specimen	f'_c (1) (MPa)	f_t (2) (MPa)	ε_{co} (3) ($x10^{-3}$)	ρ_{effx} (%)	ρ_{effy} (%)	e (4) (mm)
A1	29.03	1.89	2.30	1.05	1.05	-0.4
A2	29.03	1.89	2.30	1.05	1.05	2.5
A3	29.03	1.89	2.30	1.05	1.05	—
B1	36.23	2.11	2.50	1.02	1.17	6.3
B2	36.23	2.11	2.50	1.02	1.17	3.0

(1) : $0.9 f'_c$

(2) : from Eq. 3.35

(3) : from Eq. 3.32

(4) : a positive number indicates an initial deflection in the same direction as produced by the effect of the lateral loads

Table 4.10 - Comparison of the finite element predictions to the test results

Specimen	Experimental		Model		Test / Model	
	Q_u (kN)	Δ_u (mm)	Q_u (kN)	Δ_u (mm)	Q_u	Δ_u
A1	153.1	15.8	153.9	16.4	0.99	0.96
A2	126.3	19.1	119.2	19.8	1.06	0.96
A3	196.1	75.2	198.0	82.4	0.99	0.91
B1	142.3	48.1	133.1	36.4	1.07	1.32
B2	182.6	44.5	182.7	42.9	1.00	1.04
Statistics						
Average					1.02	1.04
Stand. dev.					0.04	0.16
Coeff. of var.					3.9%	15.8%

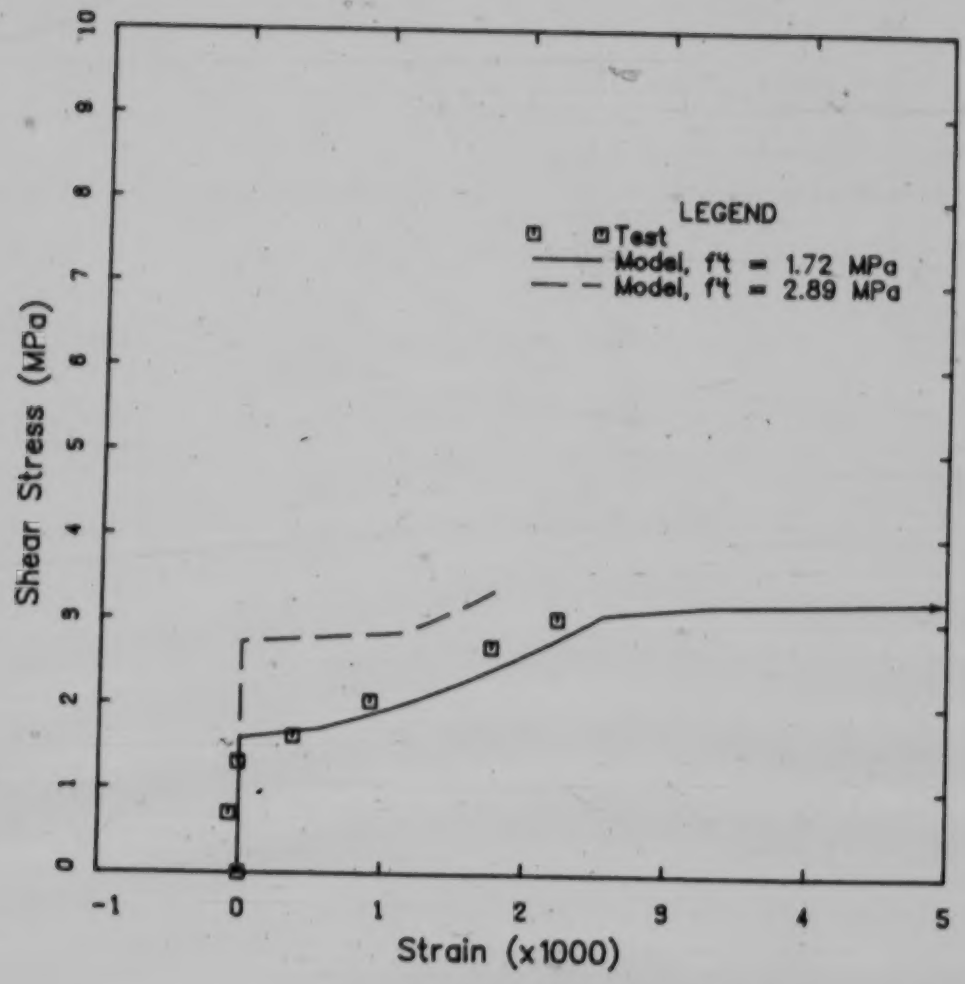

a) Longitudinal strain

Figure 4.1 - Comparison of model and Vecchio and Collins (1982) test PV3

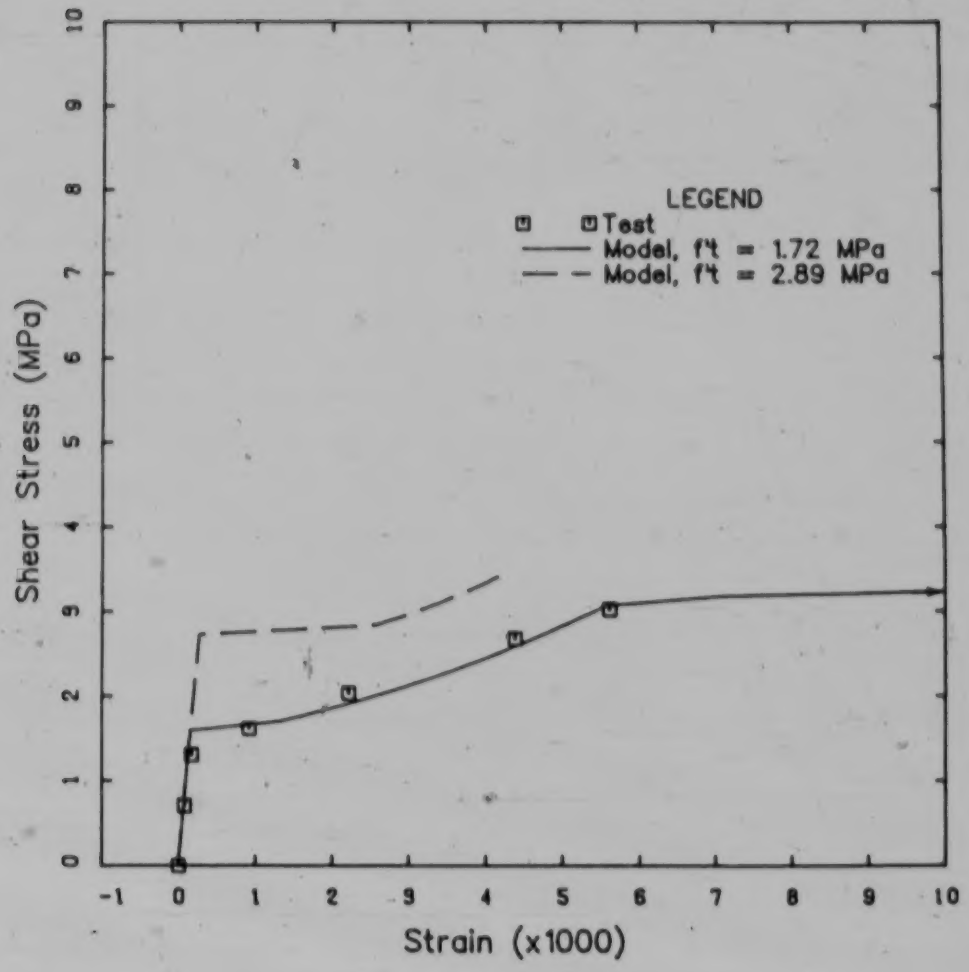

b) Shear strain

Figure 4.1 (continued) - Comparison of model and Vecchio and Collins (1982) test PV3

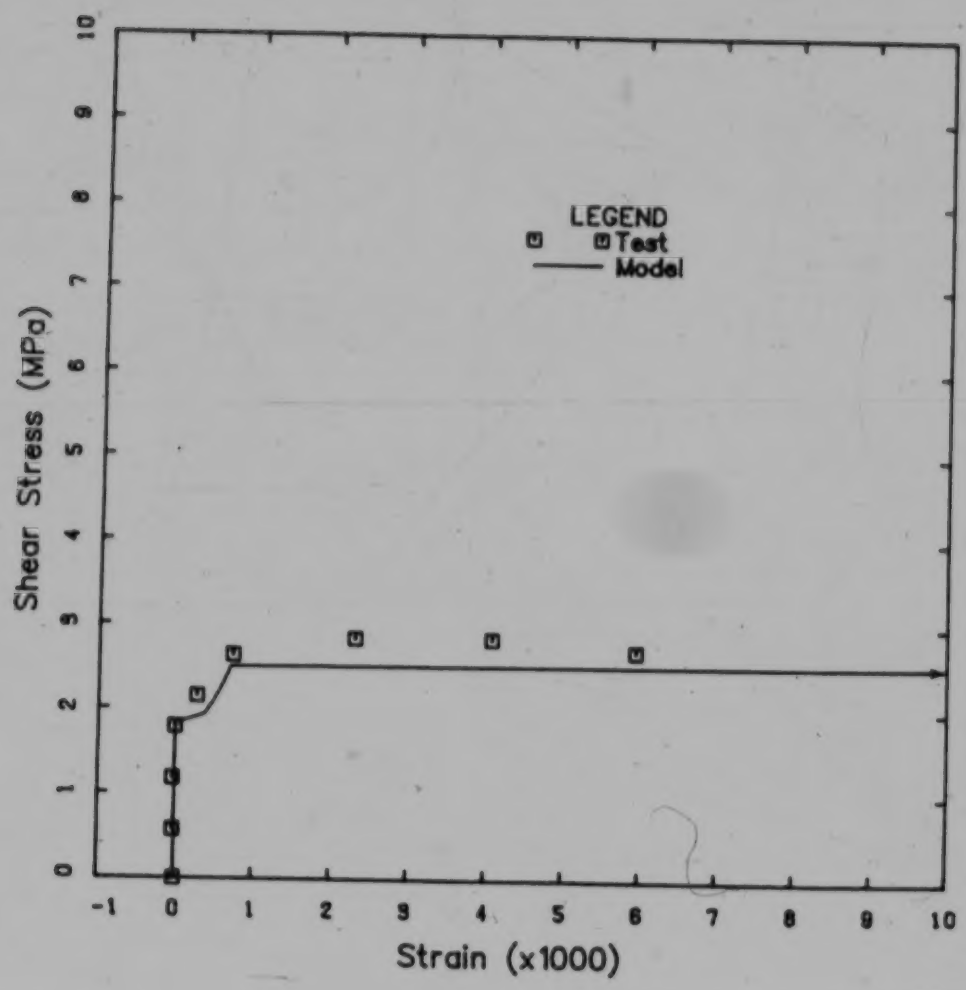

a) Longitudinal strain

Figure 4.2 - Comparison of model and Vecchio and Collins (1982) test PV4

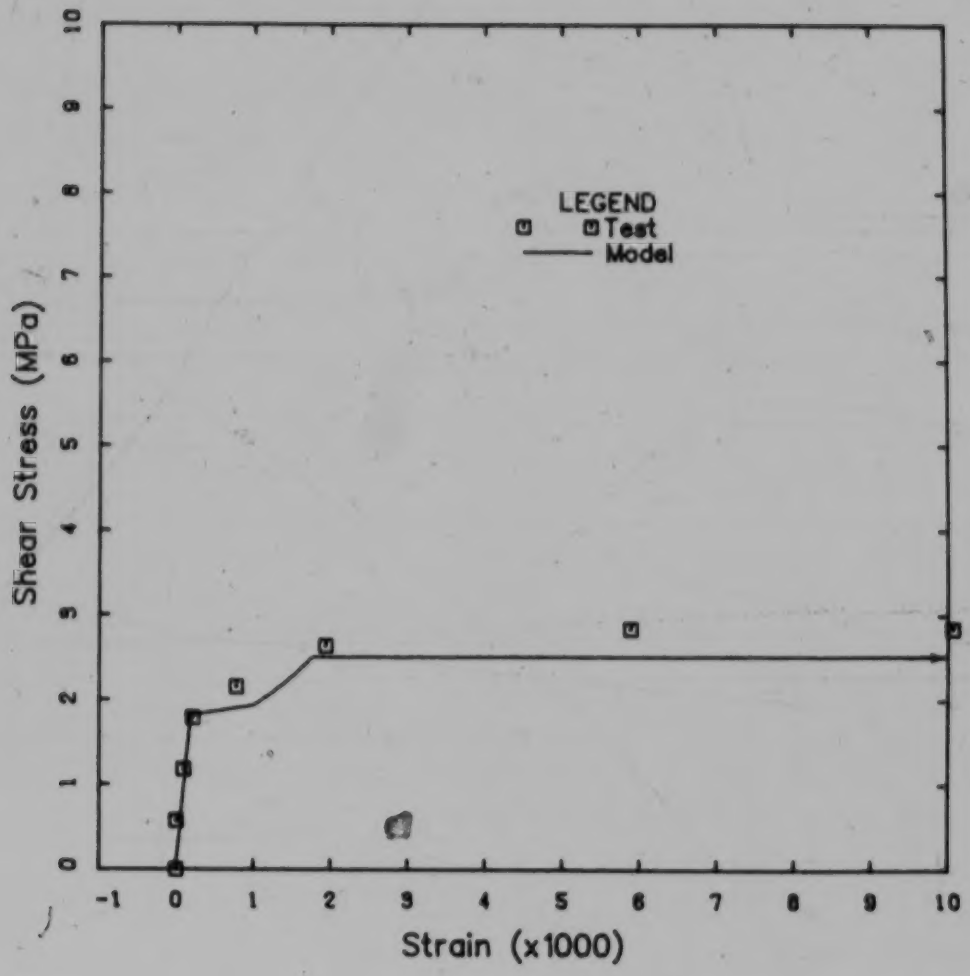

b) Shear strain

Figure 4.2 (continued) - Comparison of model and Vecchio and Collins (1982) test PV4

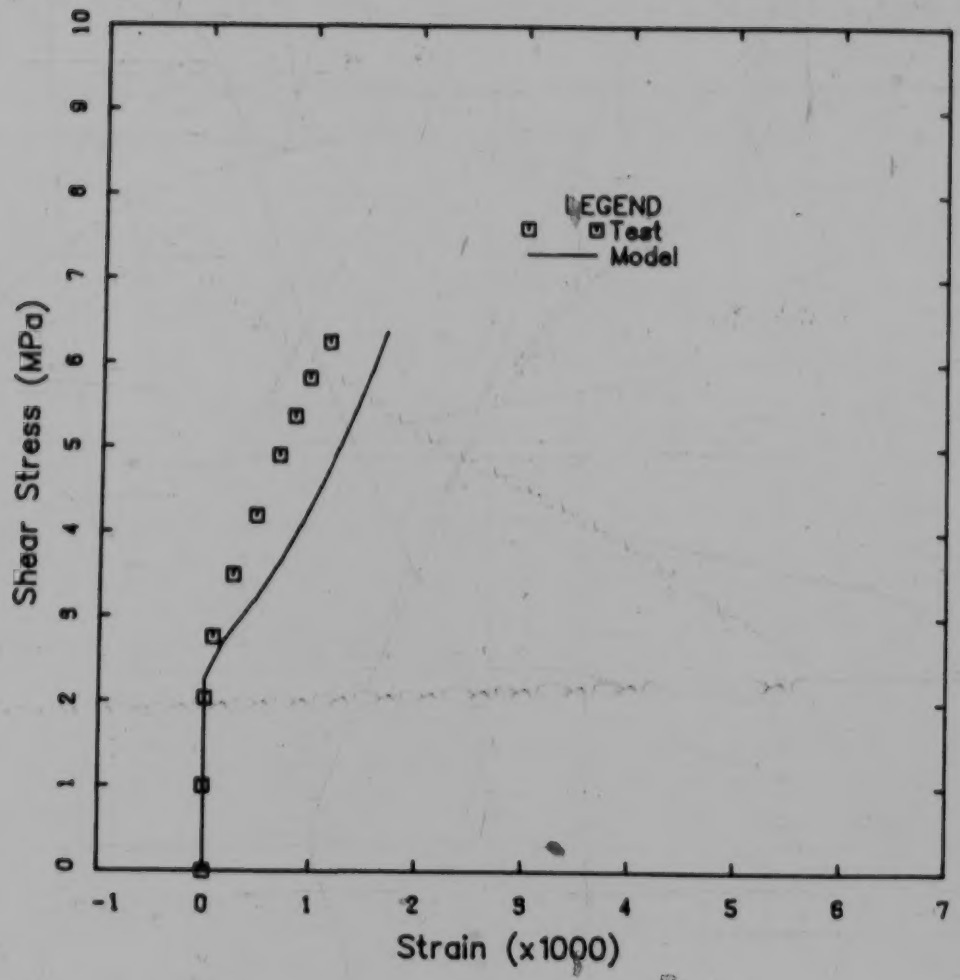

a) Longitudinal strain

Figure 4.3 - Comparison of model and Vecchio and Collins (1982) test PV27

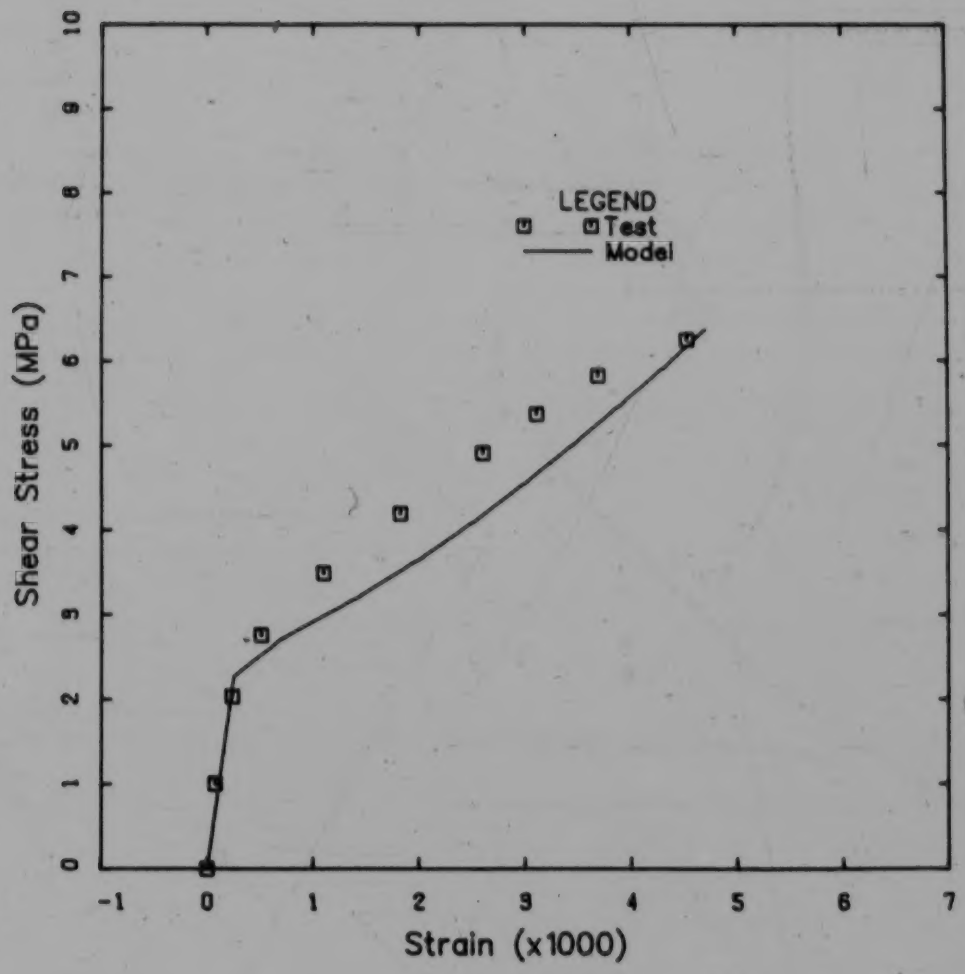

b) Shear strain

Figure 4.3 (continued) - Comparison of model and Vecchio and Collins (1982) test PV27

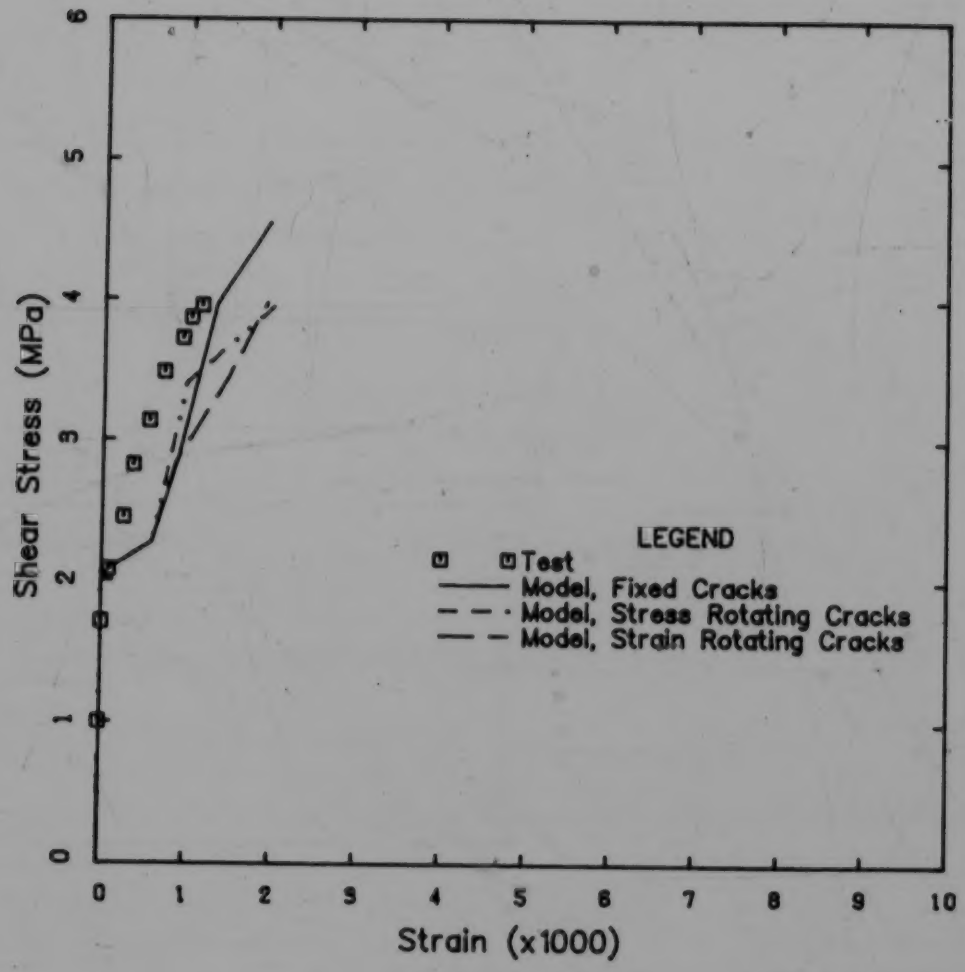

a) Longitudinal strain

Figure 4.4 - Comparison of model and Vecchio and Collins (1982) test PV19

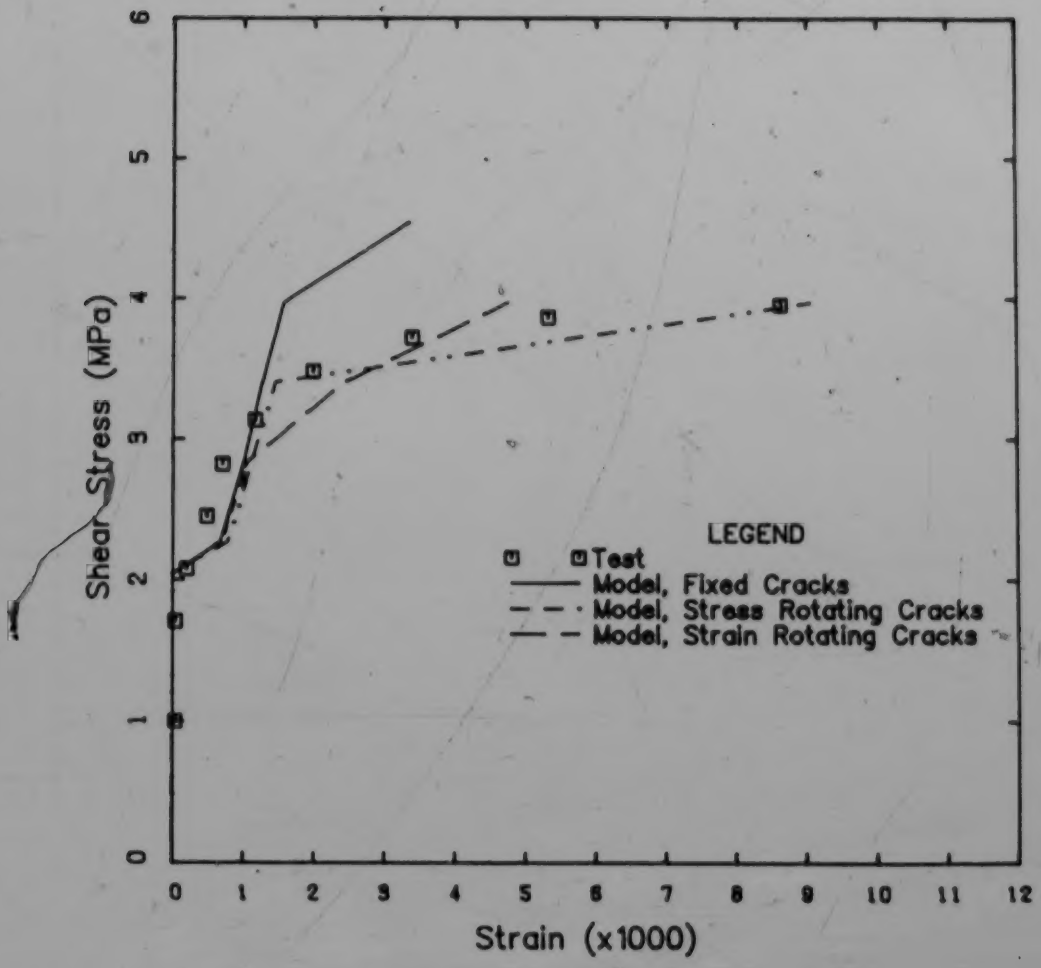

b) Transverse strain

Figure 4.4 (continued) - Comparison of model and Vecchio and Collins (1982) test PV19

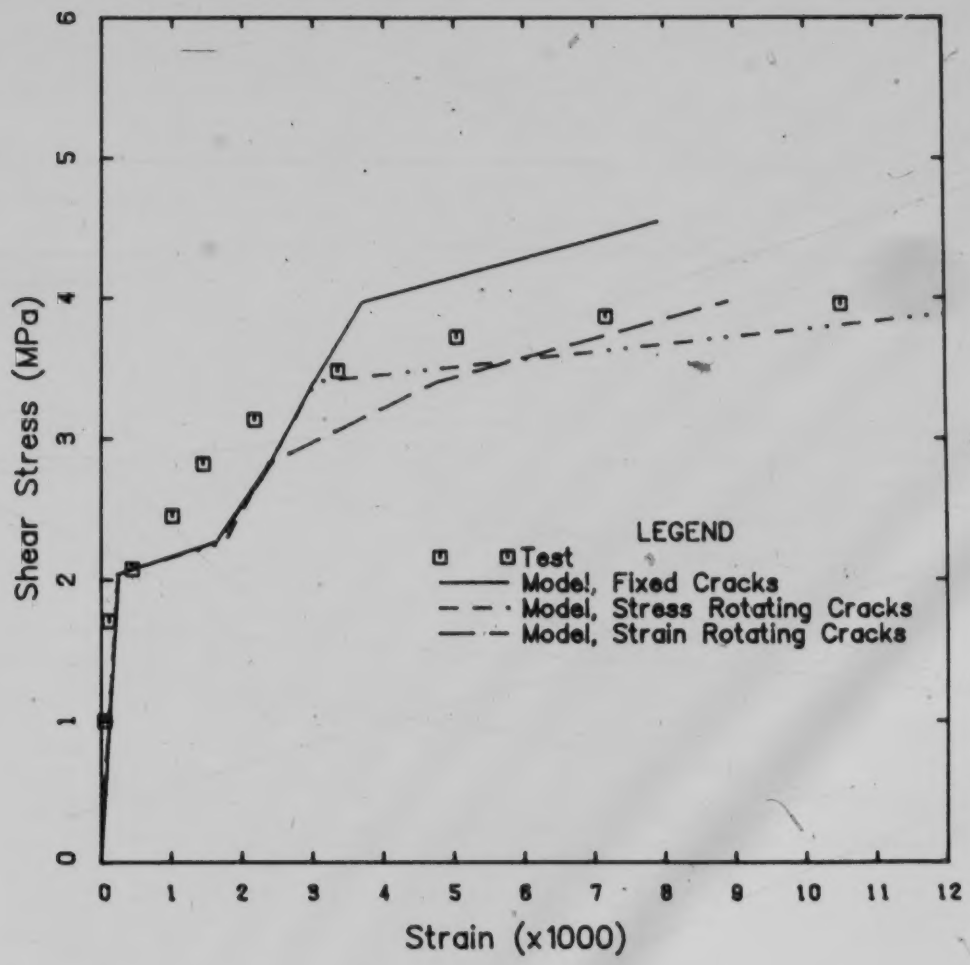

c) Shear strain

Figure 4.4 (continued) - Comparison of model and Vecchio and Collins (1982) test PV19

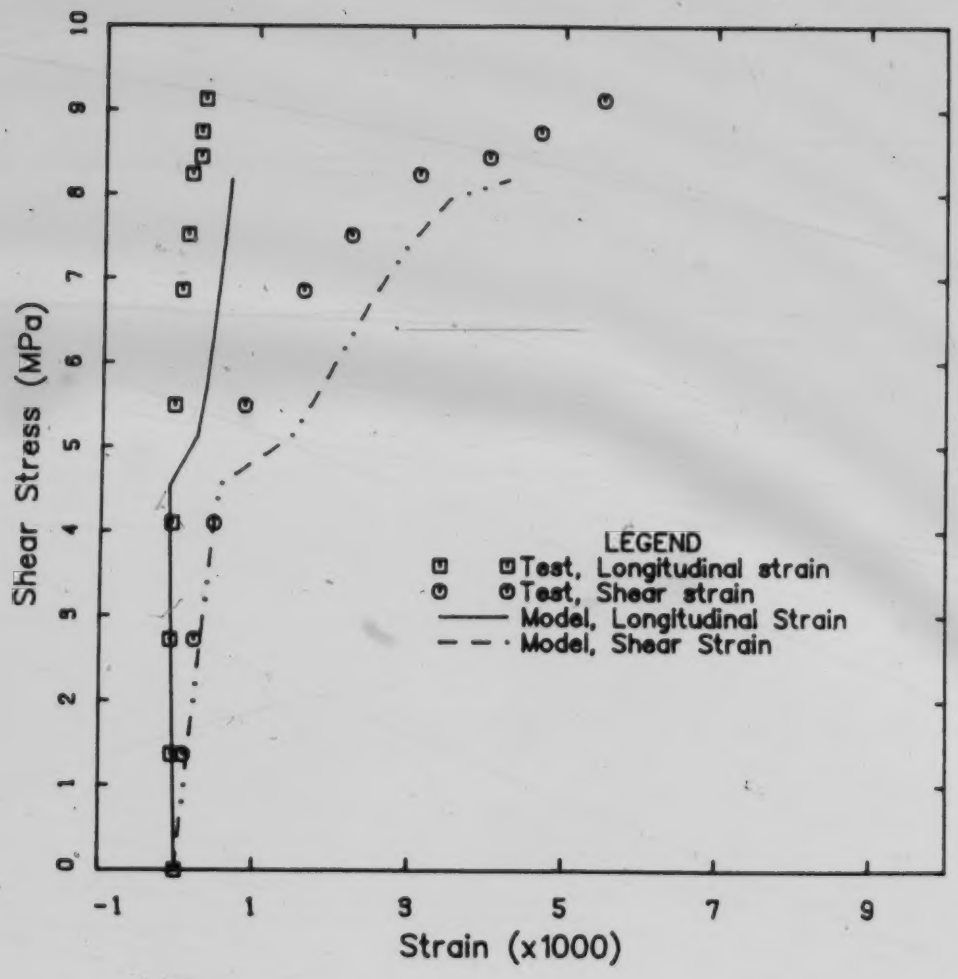

Figure 4.5 - Comparison of model and Vecchio and Collins (1982) test PV25 for longitudinal and shear strains

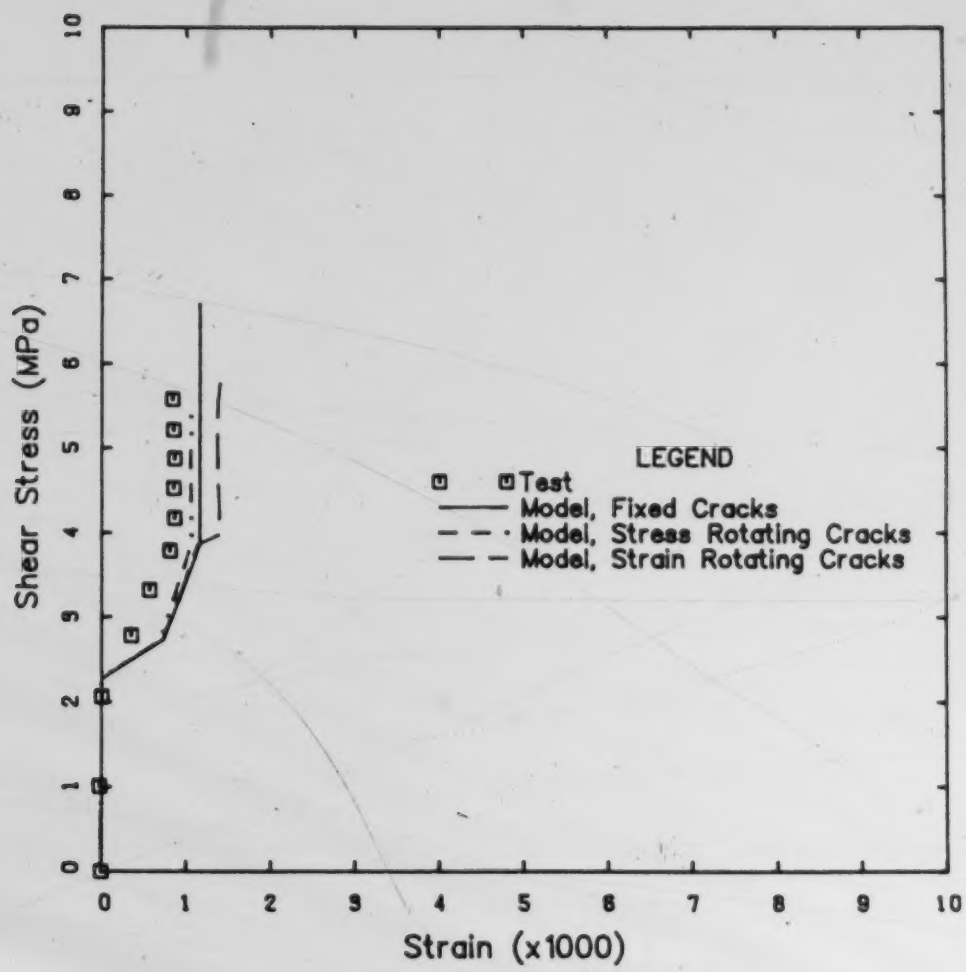

a) Longitudinal strain

Figure 4.6 - Comparison of model and Vecchio and Collins (1982) test PV29

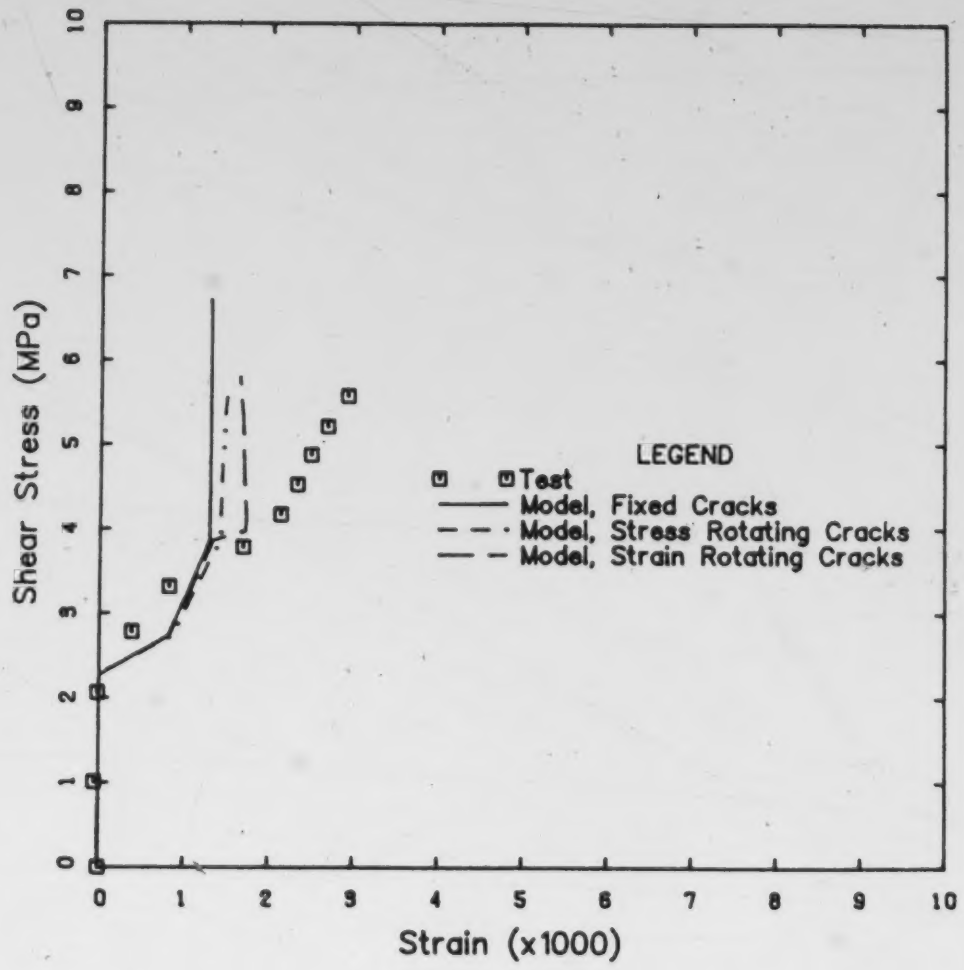

b) Transverse strain

Figure 4.6 (continued) - Comparison of model and Vecchio and Collins (1982) test PV29

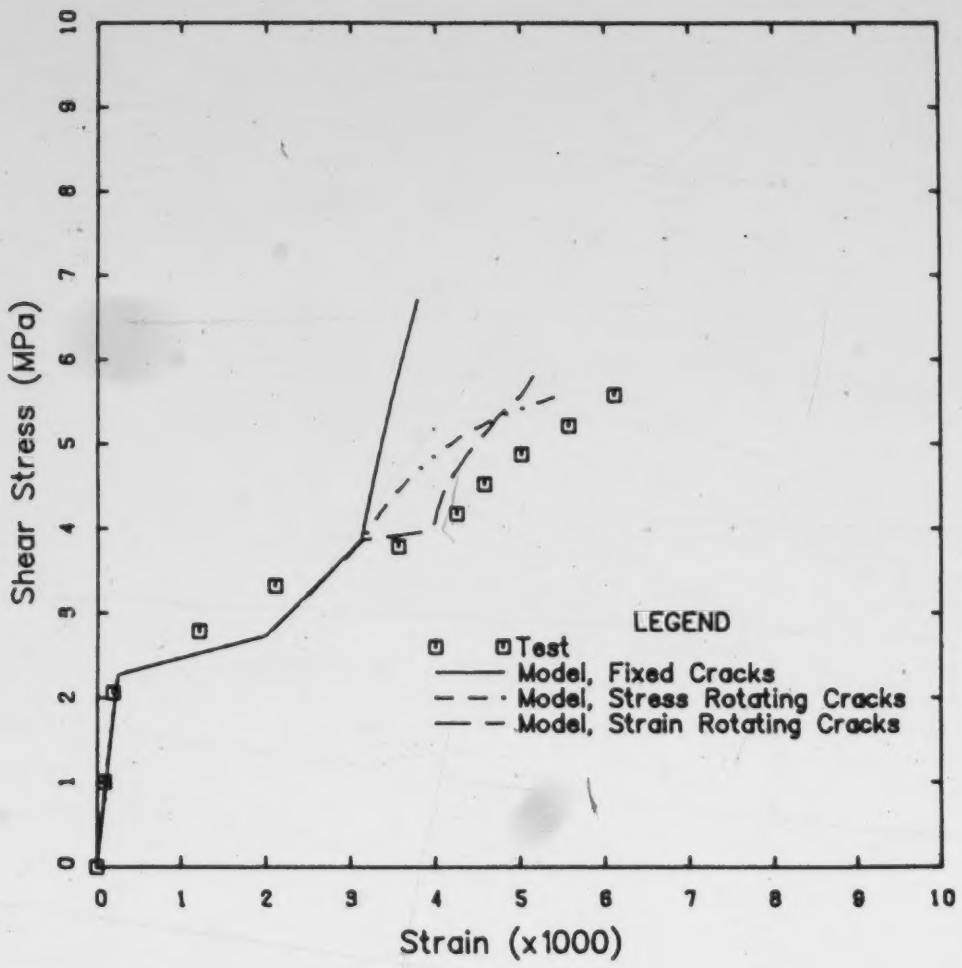

c) Shear strain

Figure 4.6 (continued) - Comparison of model and Vecchio and Collins (1982) test PV29

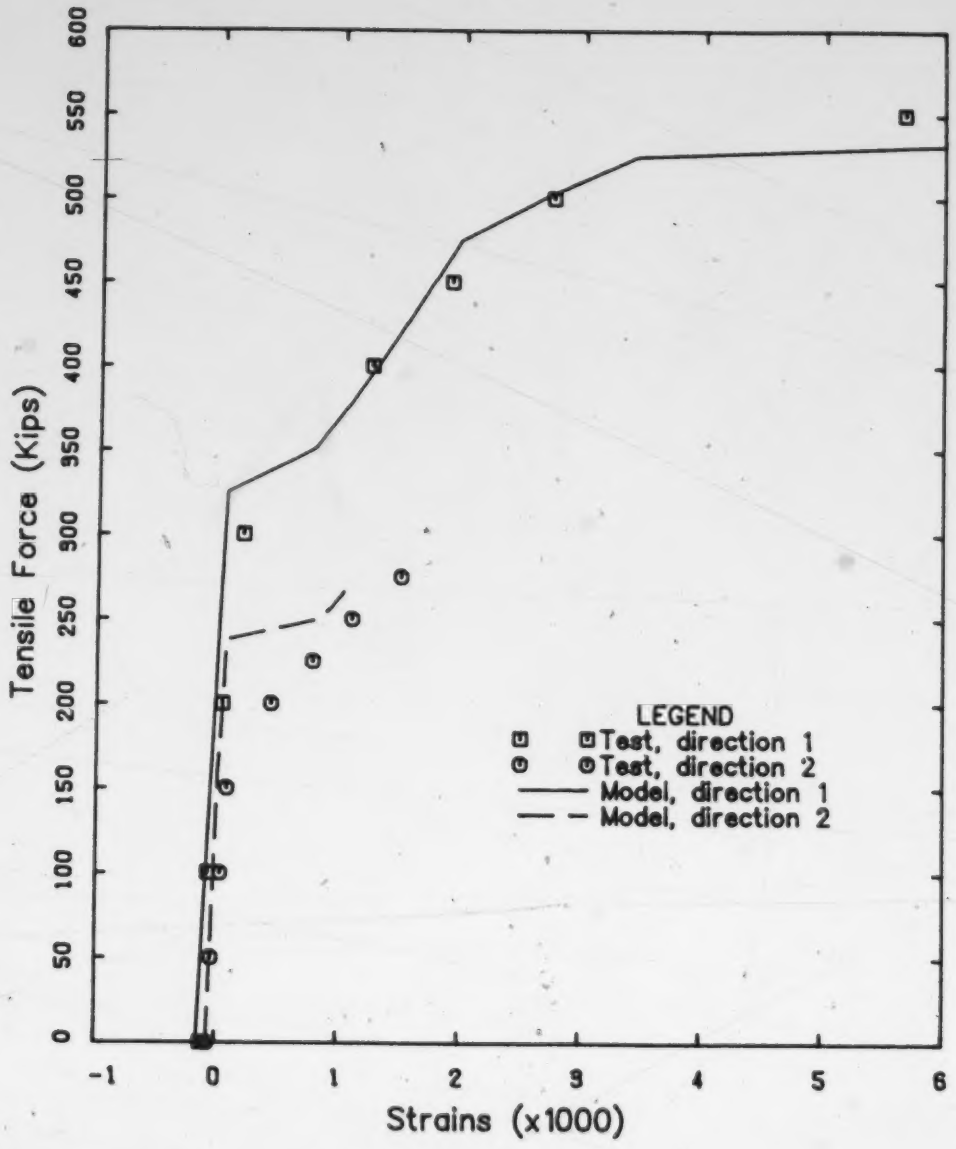

Figure 4.7 - Comparison of model and MacGregor *et al* (1979)
Wall segment #1

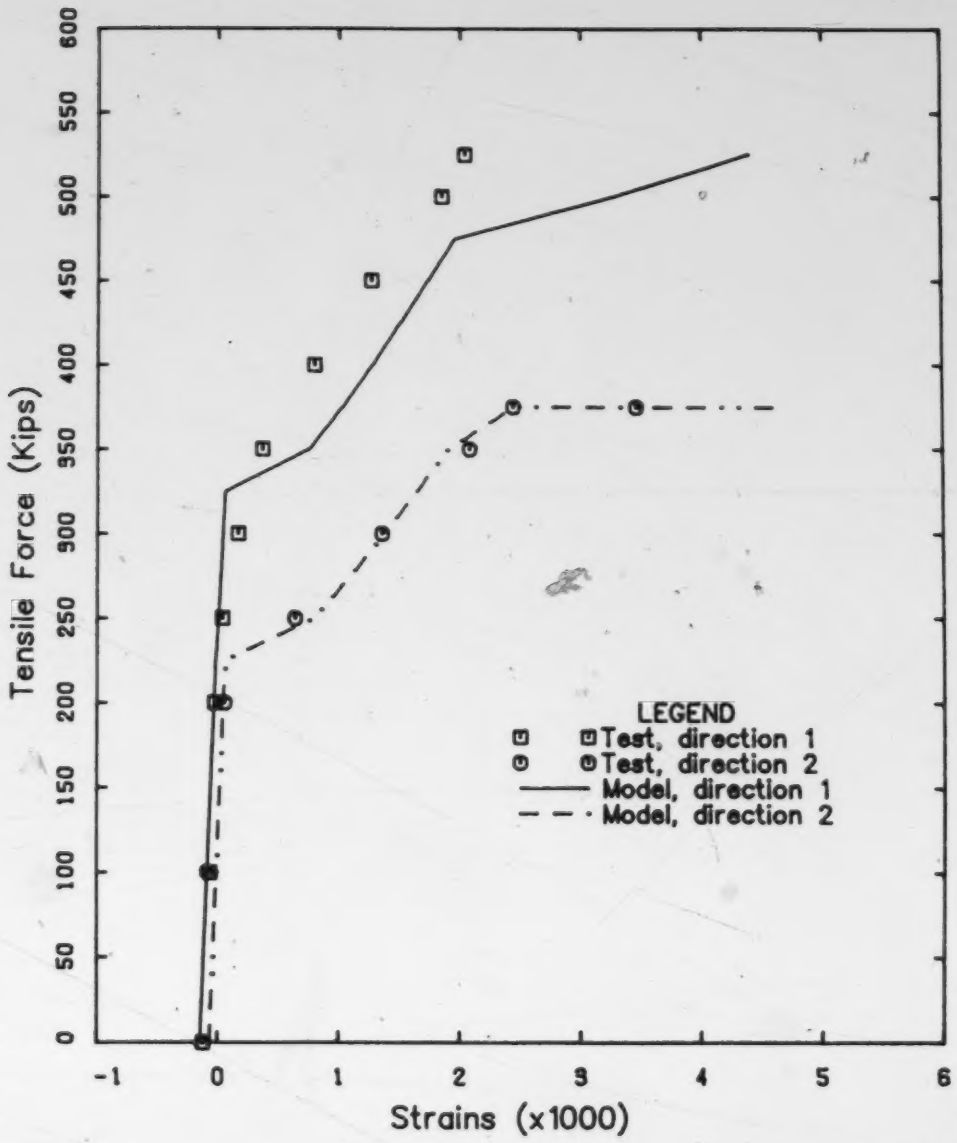

Figure 4.8 - Comparison of model and MacGregor *et al* (1979)
Wall segment #3

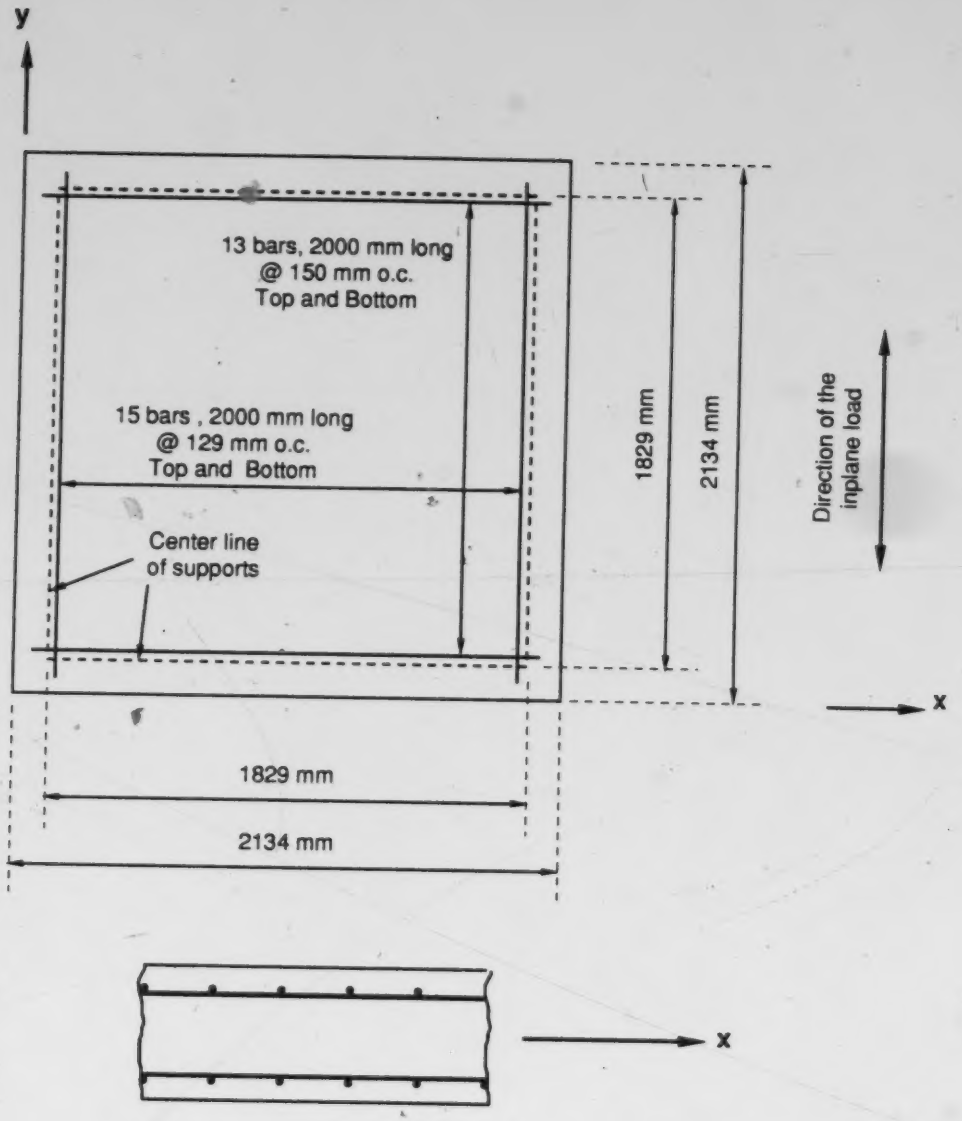

a) Geometry and reinforcement of the A series

Figure 4.9 - Aghayere and MacGregor (1988) test set up

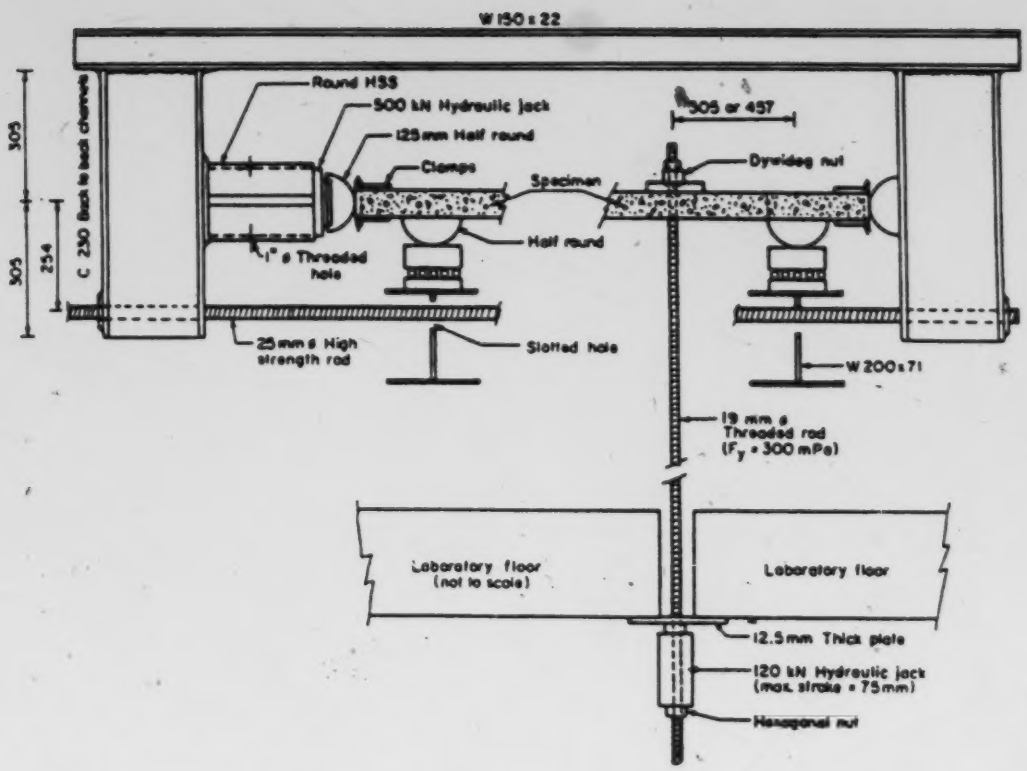

b) Loading apparatus

Figure 4.9 (Contimued) - Aghayere and MacGregor (1988) test set up

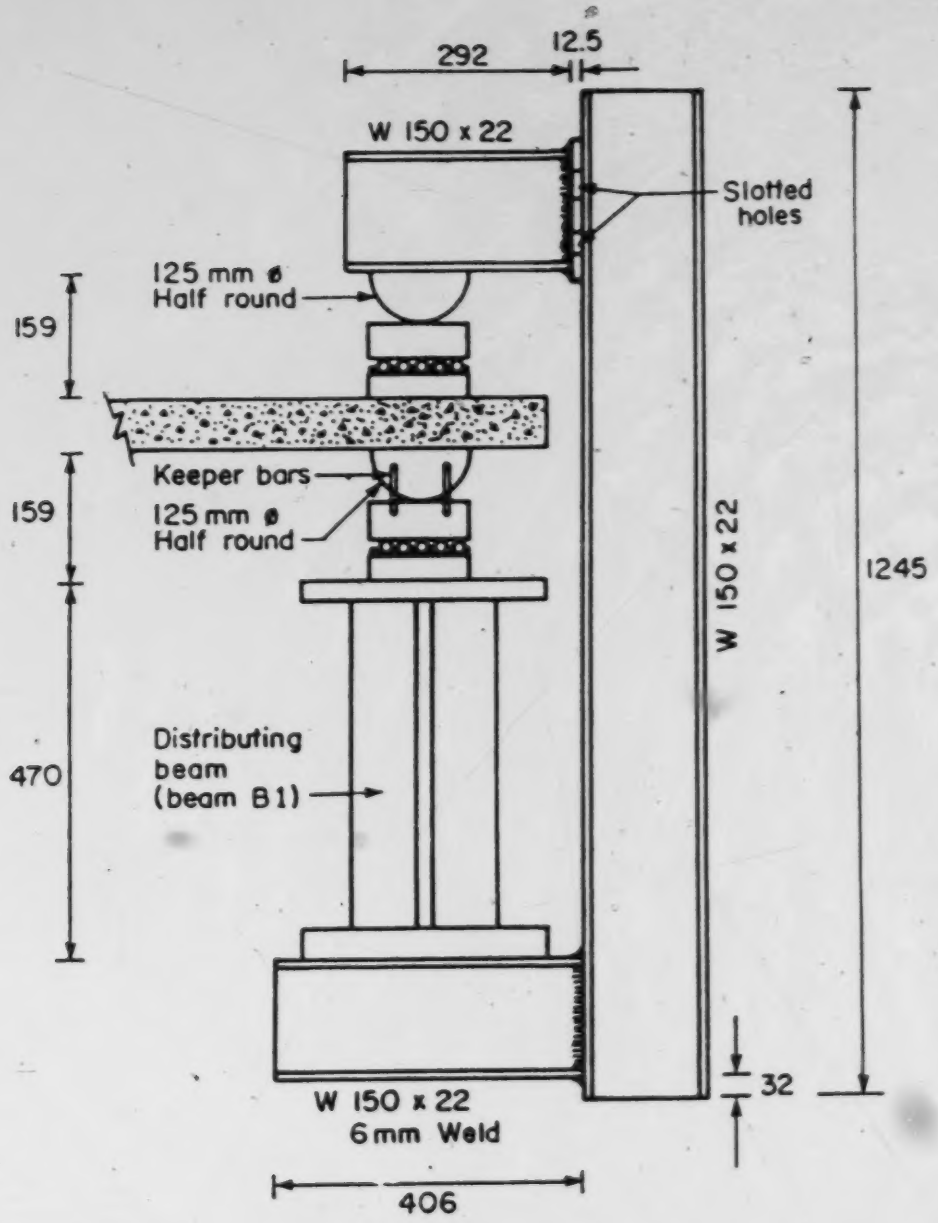

c) Corner support

Figure 4.9 (Continued) - Aghayere and MacGregor (1988) test set up

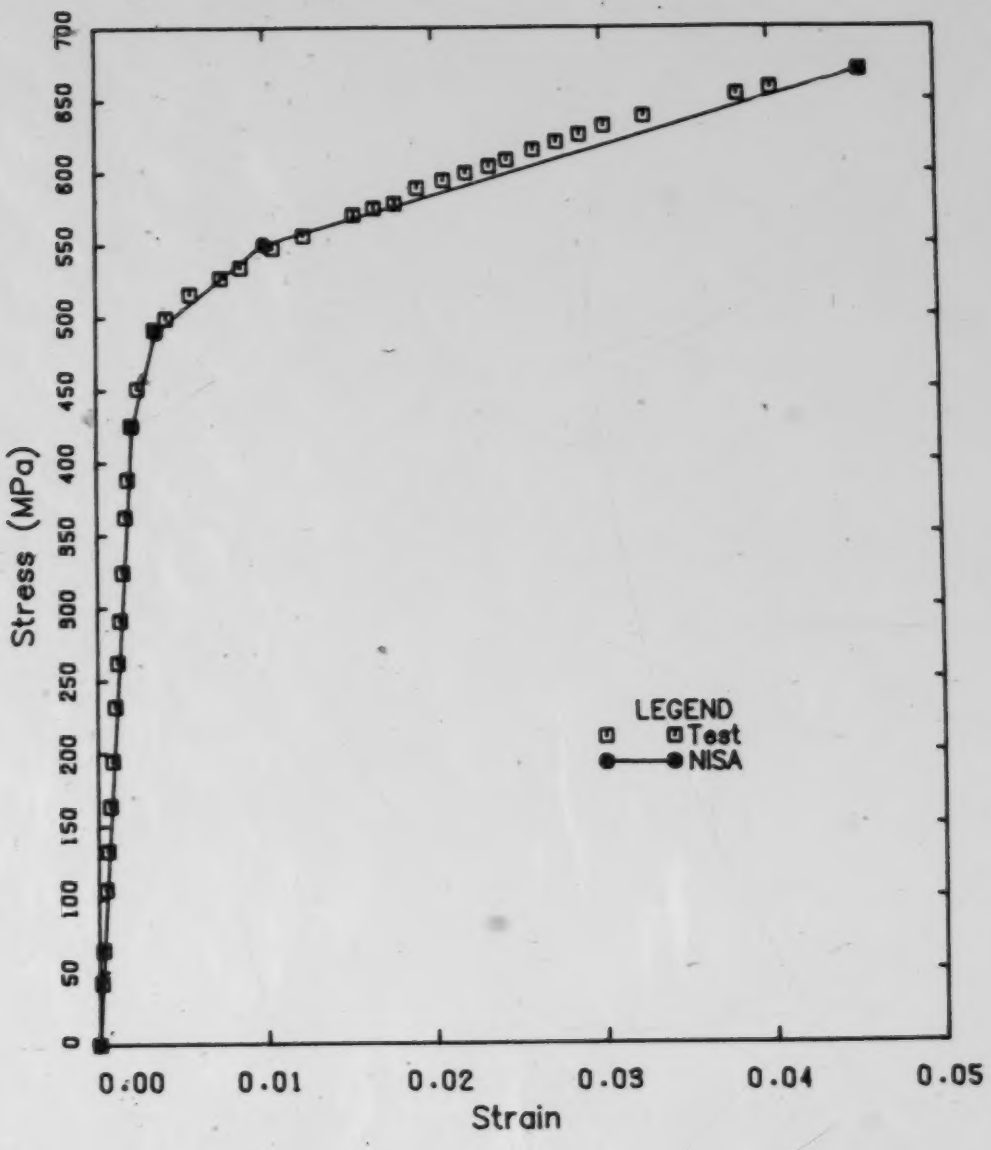

Figure 4.10 - Reinforcing steel tension coupon in Aghayere and MacGregor (1988) test series

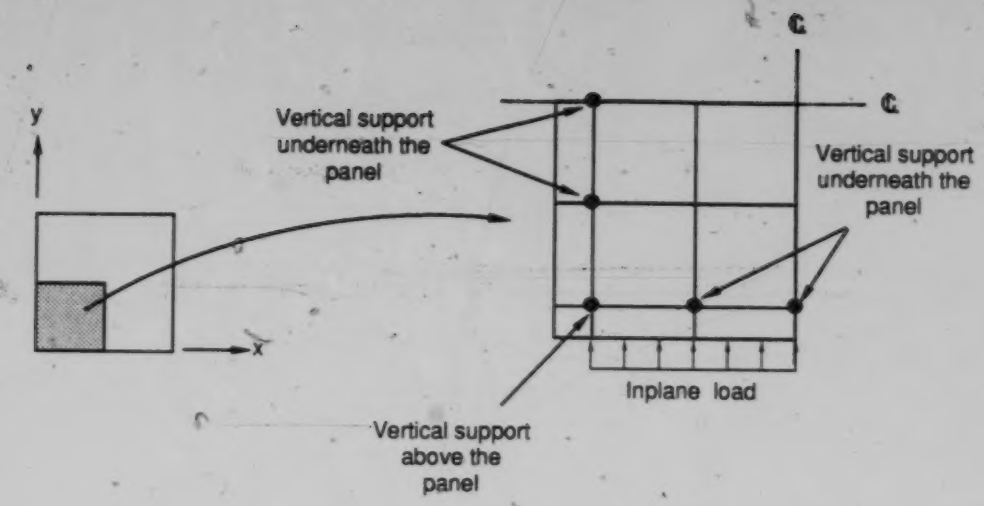

a) Square specimen

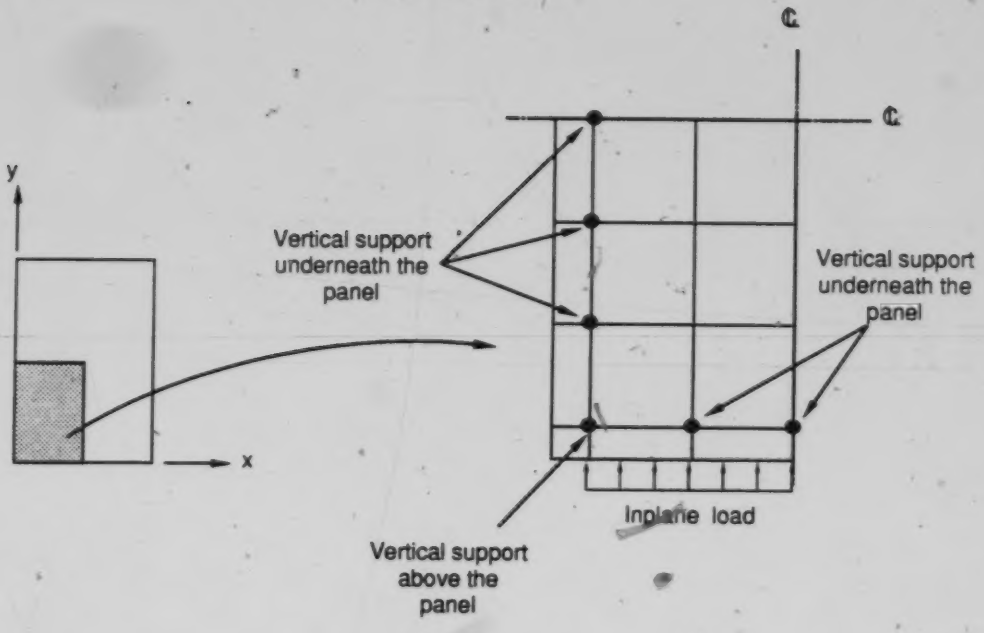

b) Rectangular specimen

Figure 4.11 - Modelling of Aghayere and MacGregor (1988) A and B series

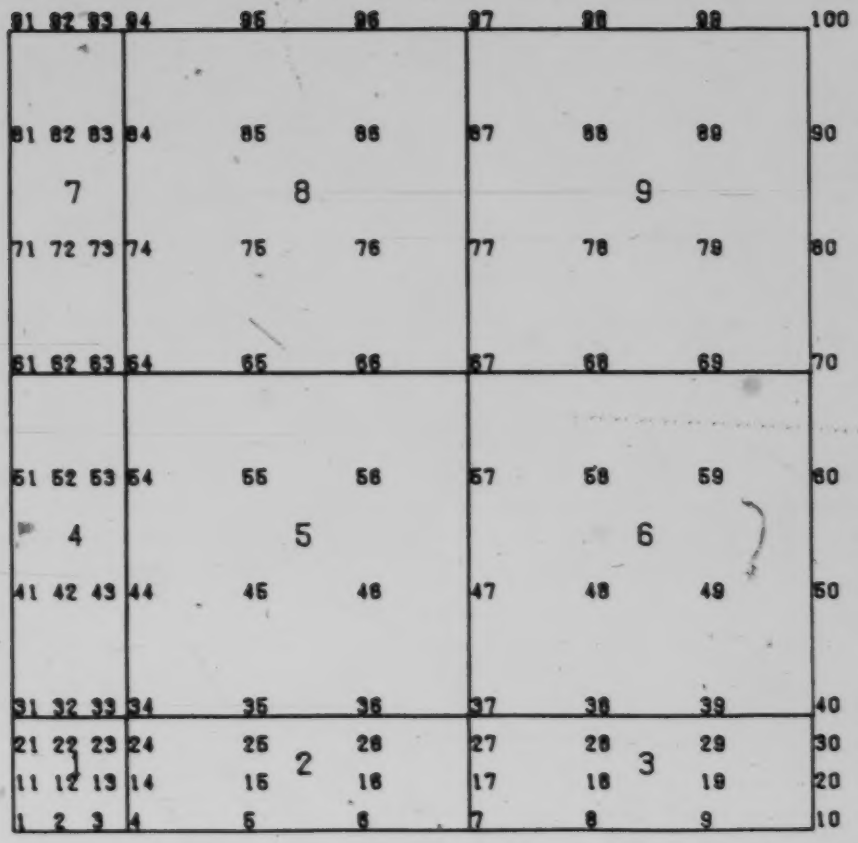

Figure 4.12 - Mesh used for Aghayere and MacGregor (1988) square specimens

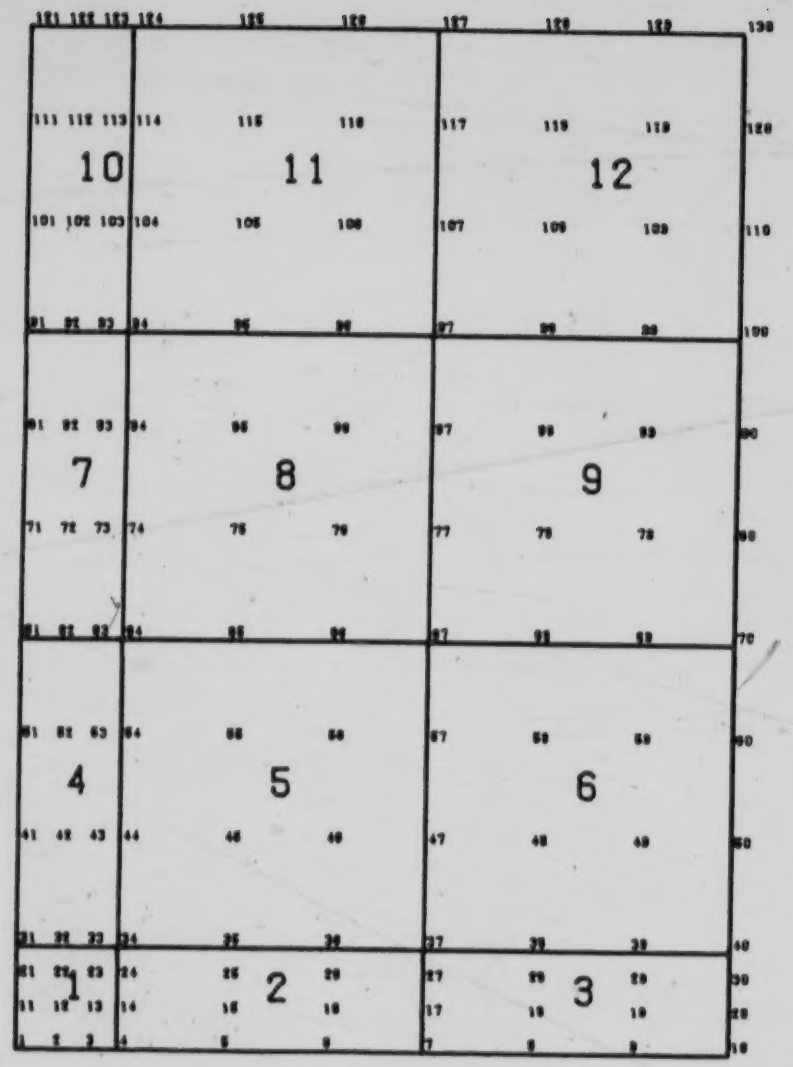

Figure 4.13 - Mesh used for Aghayere and MacGregor (1988) rectangular specimens

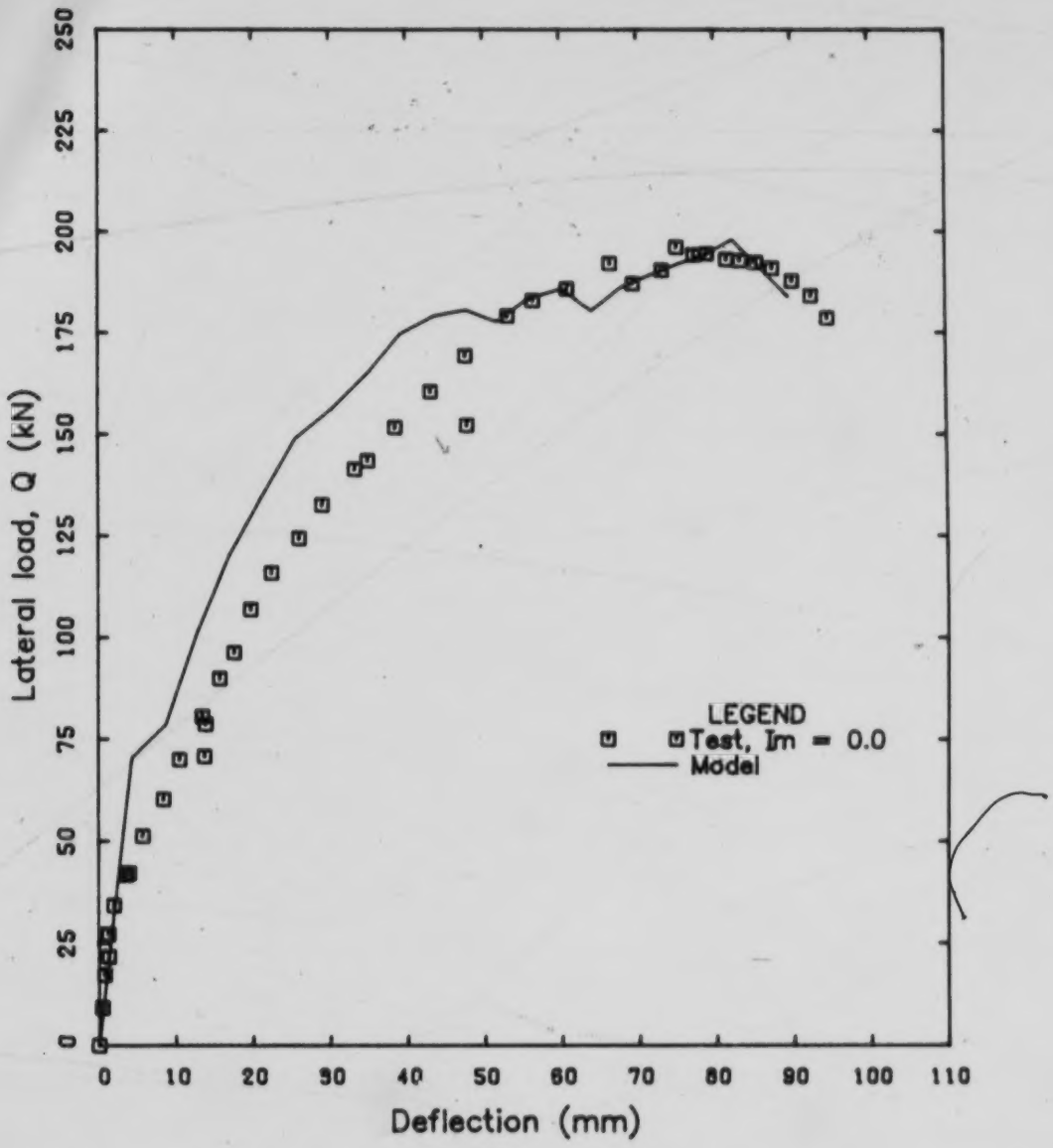

Figure 4.14 - Central deflection in Aghayere and MacGregor (1988) specimen A3

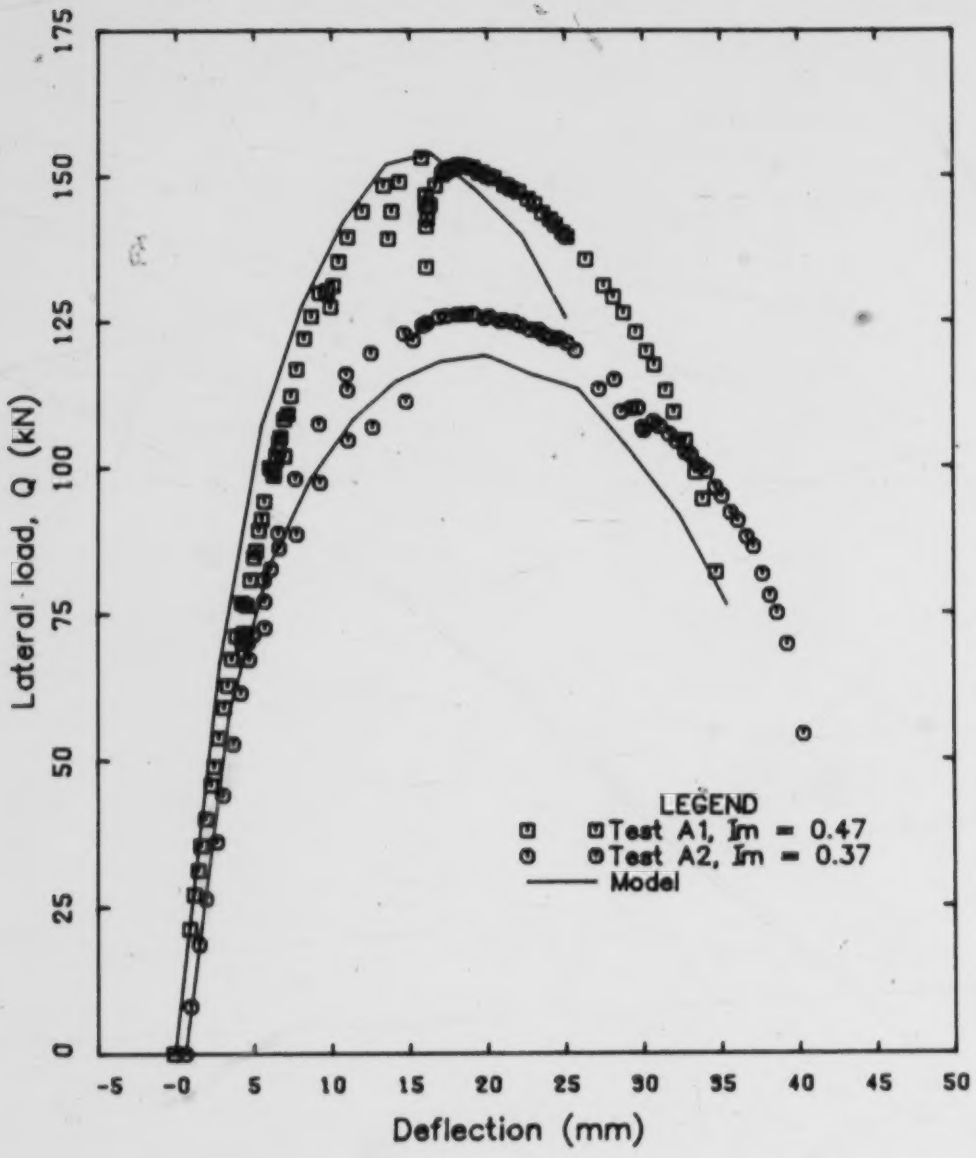

Figure 4.15 - Central deflection in Aghayere and MacGregor (1988) specimens A1 and A2

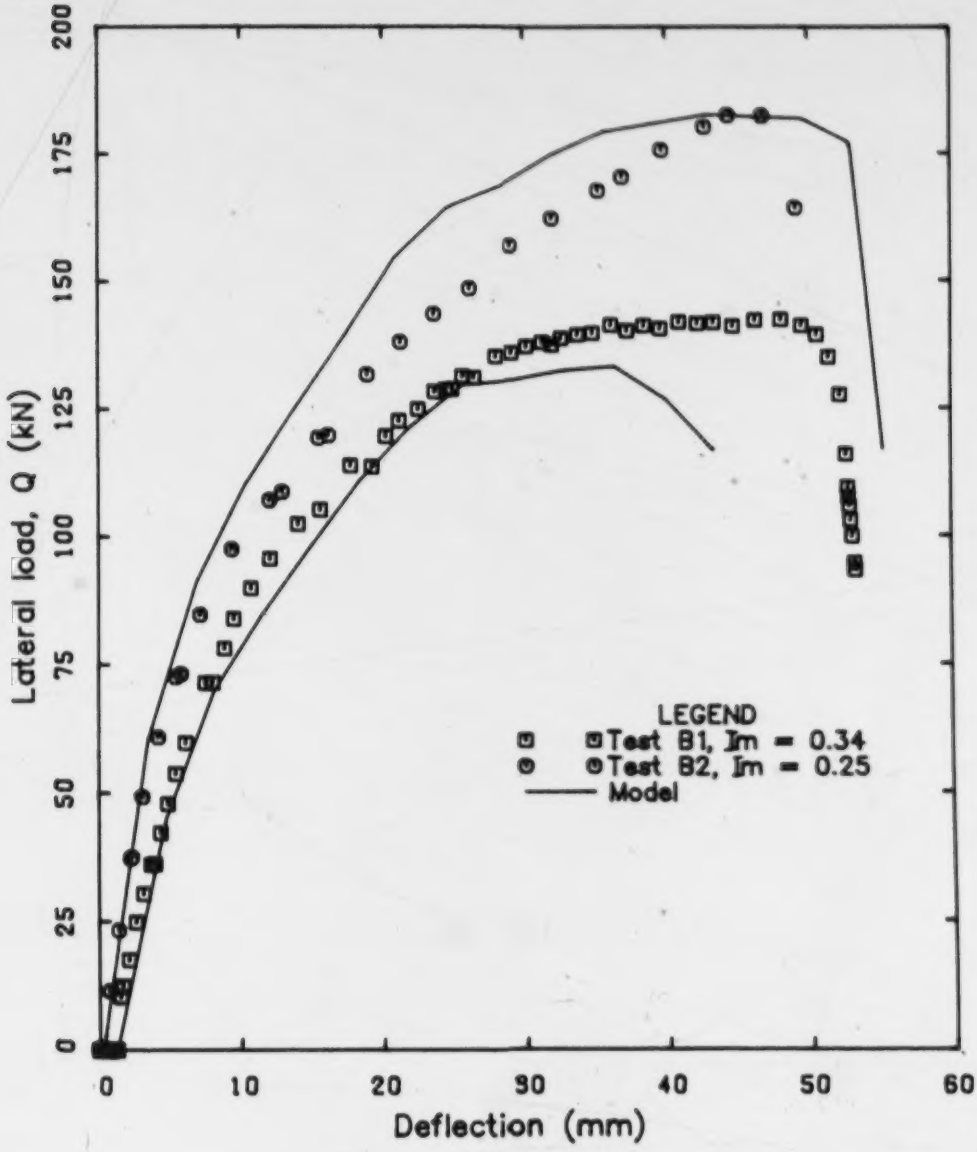

Figure 4.16 - Central deflection in Aghayere and MacGregor (1988) specimens B1 and B2

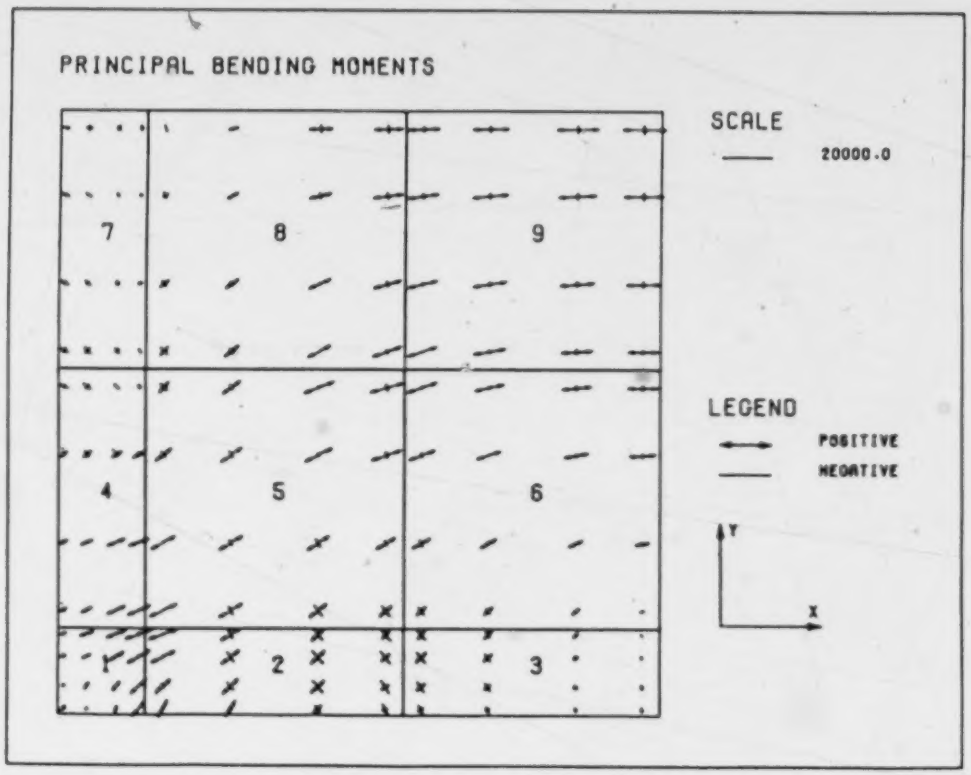

Figure 4.17 - Principal bending moments in Aghayere and MacGregor (1988) specimen A2

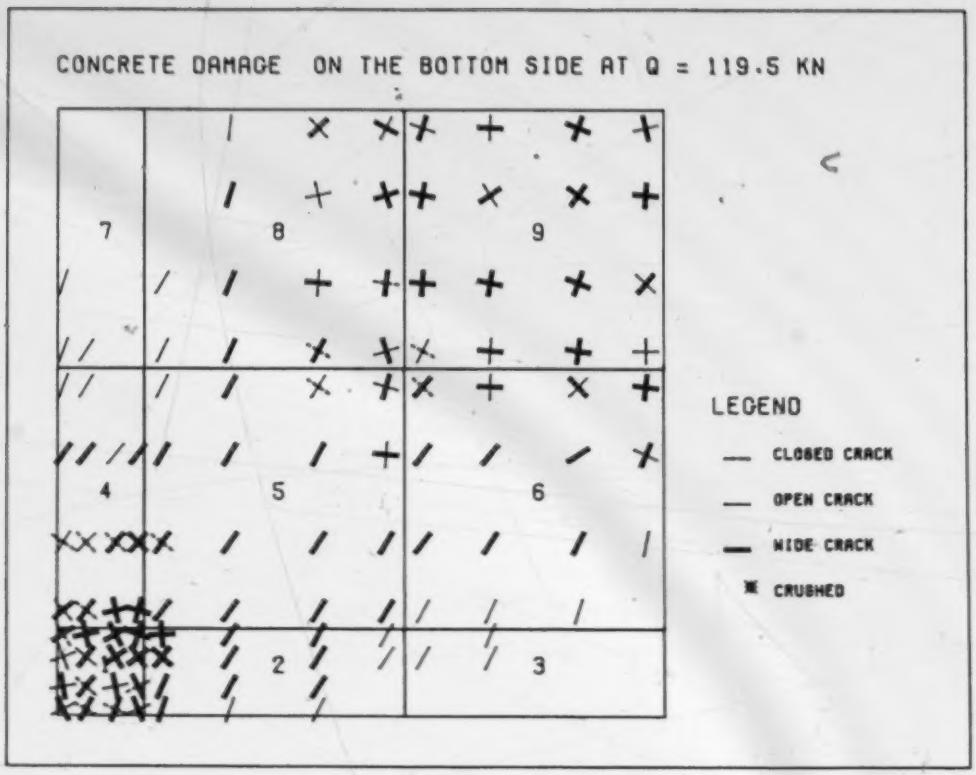

Figure 4.18 - Concrete damage in Aghayere and MacGregor (1988) specimen A2 at peak load

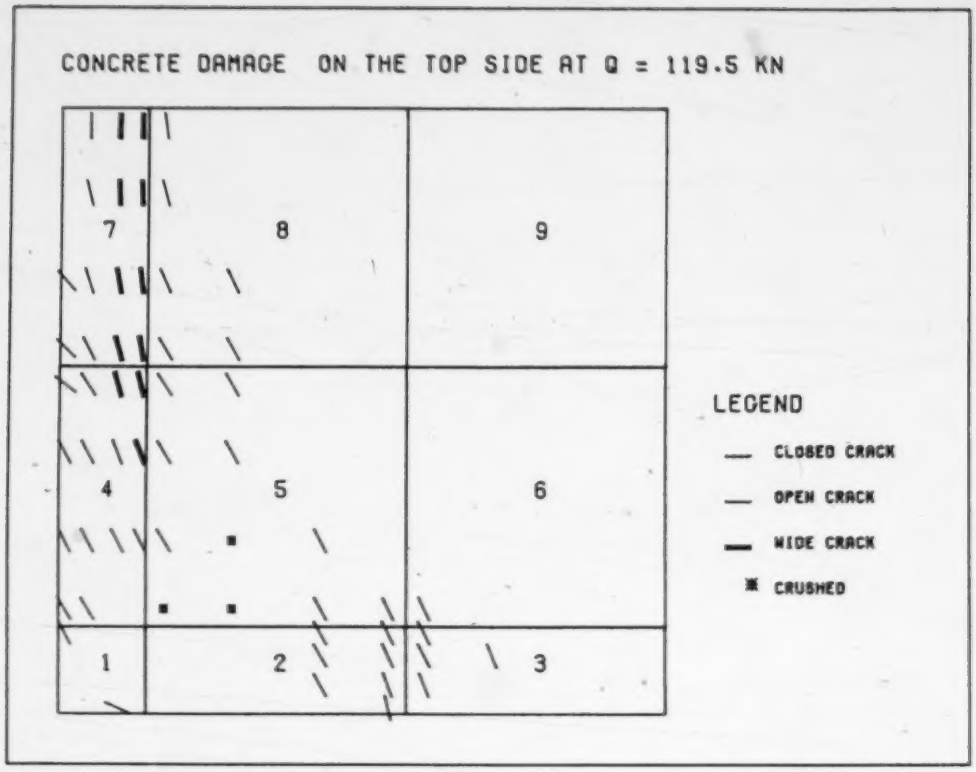

Figure 4.19 - Concrete damage in Aghayere and MacGregor (1988) specimen A2 at peak load

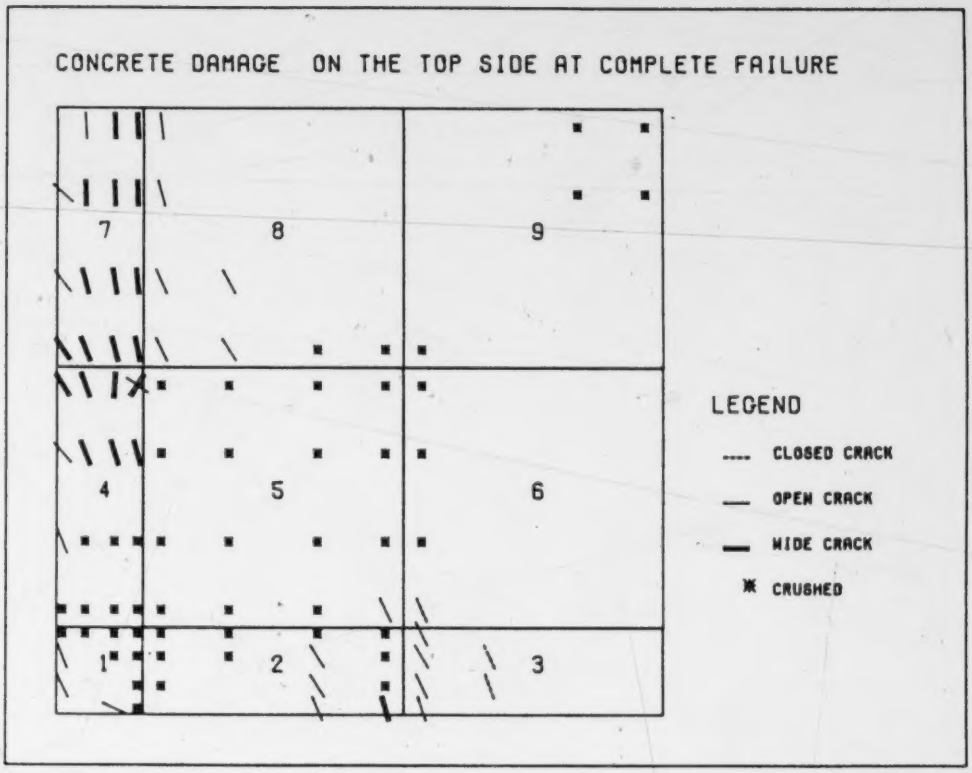

Figure 4.20 - Concrete damage in Aghayere and MacGregor (1988) specimen A2 before collapse

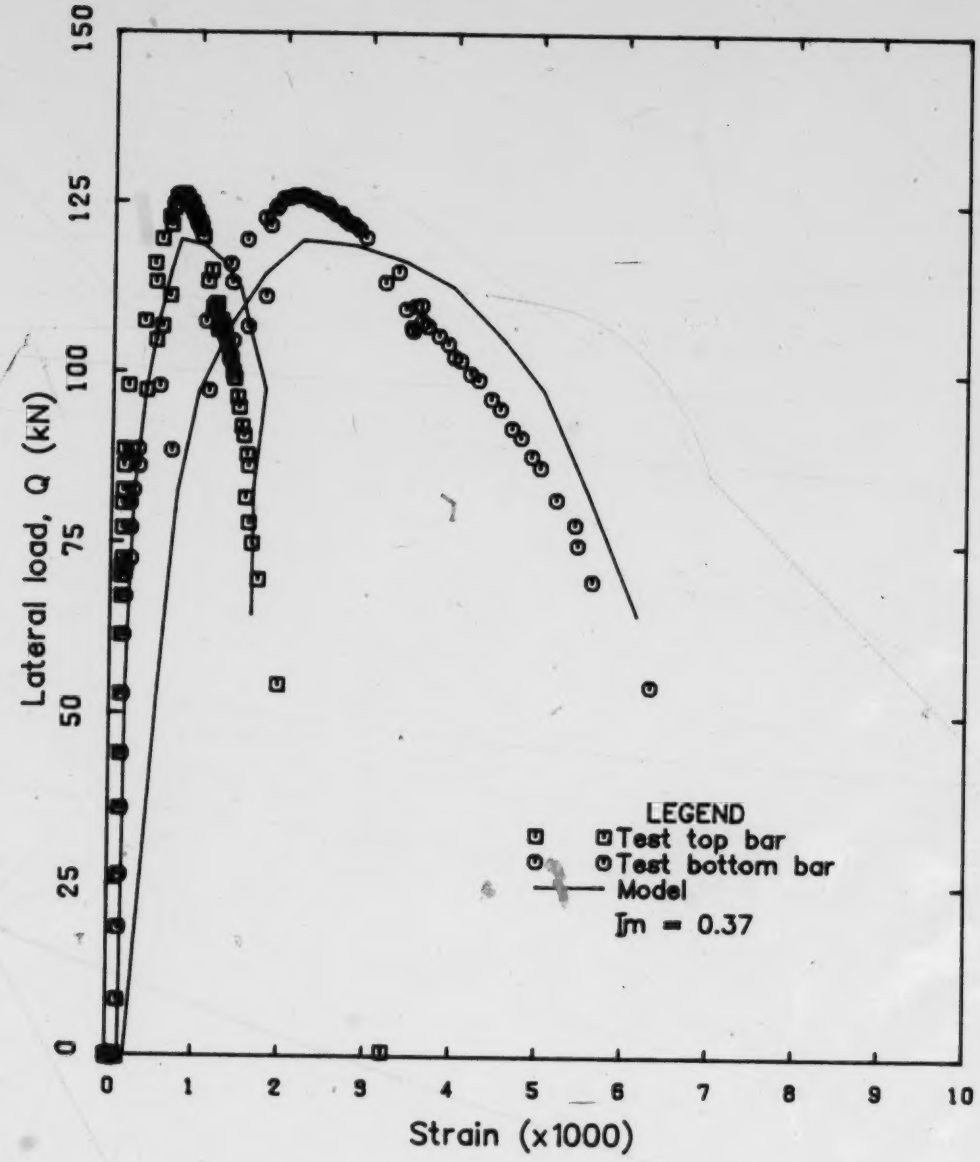

Figure 4.21 - Reinforcement transverse strains in Aghayere and MacGregor (1988) specimen A2

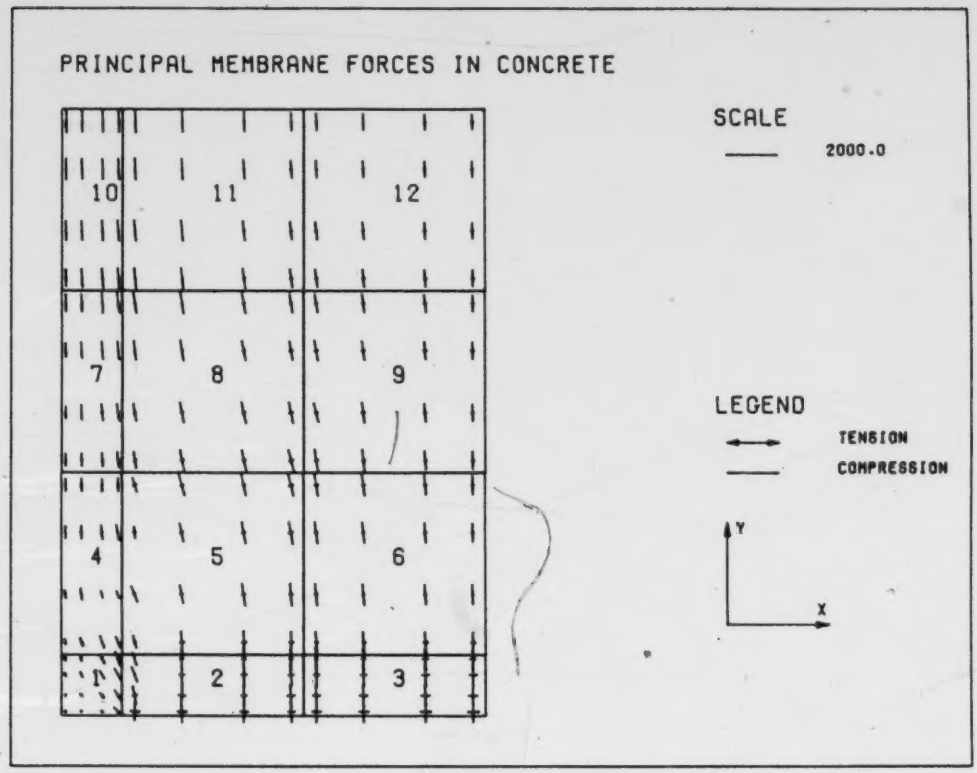

Figure 4.22 - Membrane forces in Aghayere and MacGregor (1988) specimen B1 before collapse

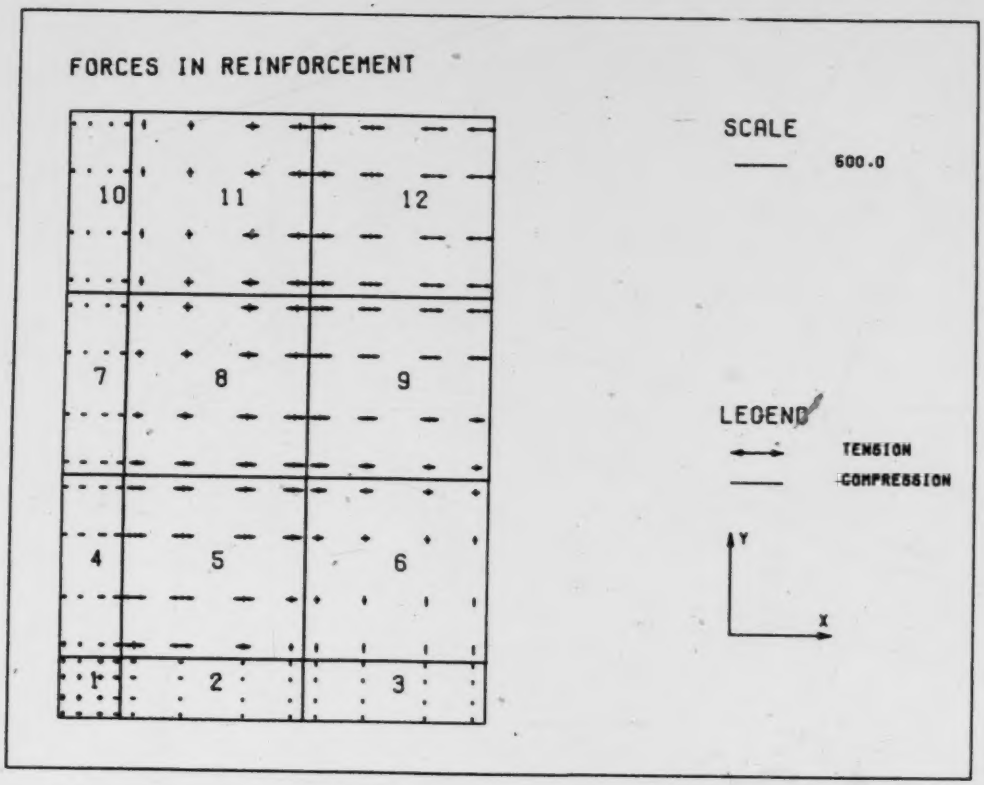

Figure 4.23 - Reinforcement forces in Aghayere and MacGregor (1988) specimen B1 before collapse

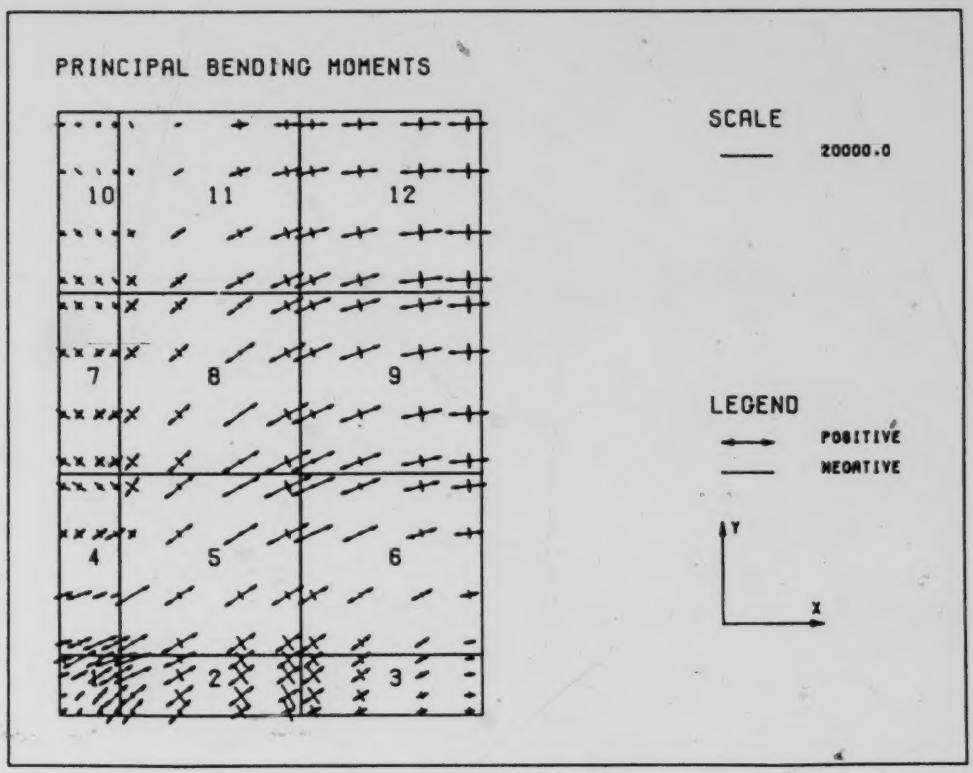

Figure 4.24 - Principal bending moments in Aghayere and MacGregor (1988) specimen B1 before collapse

CHAPTER V

BEHAVIOR OF REINFORCED CONCRETE PANELS

5.1 Solutions available

The behavior of reinforced concrete panels loaded transversely and axially can be examined from various methods. Aghayere and MacGregor (1988) addressed the problem by initiating an experimental program on thin reinforced concrete panels simply supported on four edges. They proposed a crossing beam analogy to predict the panel response and a moment magnifier design procedure to evaluate the ultimate strength of such panels.

The aim of the research initiated by Aghayere and MacGregor and extended herein is to provide a better understanding of the behavior of reinforced concrete panels and ultimately to propose a rational design method. To achieve this objective one must proceed to more analysis and, perhaps, more experiments on panels. However, experimental investigations are more expensive than finite element analysis which, in turn, is more time consuming than calculation methods such as those proposed by Aghayere and MacGregor.

A limited parametric study has been carried out using the finite element program NISA to extend the range of the available test results. This allows the analytical procedure proposed by Aghayere *et al* (1988) to be verified and thus provide a stronger basis for the development of a reliable and rational design method. In the following sections, a parametric study on panels loaded axially and transversely is presented.

5.2 Parametric study

Many parameters affect the behavior of concrete panels supported on four edges and subjected to inplane and transverse loads. The main parameters involved in the panel behavior can be enumerated as follows:

1. the aspect ratio b/a ;
2. the slenderness ratios a/h or b/h;
3. the amount of reinforcement , ρ_y , and the ratio of reinforcement in both directions , ρ_y / ρ_x ;
4. the inplane load magnitude I_m as defined in Eq. 4.1 ;
5. the inplane and rotational edge restraints;
6. the sequence of loading;
7. the ratio of inplane load in each directions.

Aghayere and MacGregor (1988), varied these parameters except the edge restraints, which were simply supported and allowed inplane horizontal motion . In addition to the lateral loads, the panels were subjected to a uniaxial inplane load. A limited parametric study on panels similar to those tested by Aghayere and MacGregor is initiated in this study where the first six parameters mentioned above are varied, but only uniaxial inplane loads are considered.

Twenty six panels divided into eight series (PS1 to PS8) were analyzed; five square series and three rectangular series, with aspect ratios b/a equal to one and two respectively. The width "a" was 1800 mm in all eight series. The thickness h was 60 mm in the first six series, 45 mm for the series PS7 and 90 mm for the series PS8. The reinforcement ratio ρ_y was either 0.4 or 0.8 percent. The ratio of the reinforcement ρ_y to ρ_x ranged from 0.5 to 2.0 .

The panel dimensions selected for the parametric study are summarized in Table 5.1 .

The concrete uniaxial compressive strength f'_c was selected equal to 35 MPa and 90% of this value was used in the analysis for f''_c (see Section 4.3.1). Young's modulus, obtained from Eq. 3.33, was equal to 26 500 MPa, a tensile strength f'_t of 2.0 MPa was evaluated using Eq. 3.35 and ε_{co} was set to 0.0024, based on Eq. 3.36. A constant Poisson's ratio of 0.2 was selected for all series.

The reinforcement was assumed to have a bilinear elastic-strain hardening stress-strain curve. The reinforcement yield stress f_y was set to 400 MPa with an elastic modulus E_s of 200 000 MPa. The ultimate strength of the reinforcement was selected at 500 MPa at a strain of 0.06 , which produces a strain hardening modulus equal to about a hundredth of E_s. The effective reinforcement ratio, based on the relationships given in Section 2.3.7 , was either 1.0% or 1.6%, corresponding to actual reinforcement ratios of 0.4 % and 0.8 % used in this study. For a yield strength of 400 MPa, the minimum reinforcement ratio for beams required by the CSA Code (CSA, 1984) is 0.35 %. The positions of the centroid of the reinforcement in both directions measured from the top surface were set equal to 0.15 h and 0.85 h for the top and bottom layers, respectively.

The inplane load magnitude was also varied, with values for I_m of 0.0 , 0.2 , 0.4 and 0.6 . Four different types of boundary conditions in the first two series were modelled :

1) simply supported with rotation about the edges and inplane movement allowed;

2) inplane movement restrained with edge rotations allowed;

3) free inplane movements and fixed edge rotations;

4) fixed inplane movement and fixed edge rotations.

In series PS3 to PS8 the first type (simply supported edges) was adopted. Finally, for all but two of the panels subjected to both inplane and lateral loads, the inplane load was applied first to its selected value and kept constant while the lateral load was being applied. However the effect of the loading sequence was examined for two panels of the PS1 series. A summary of the variables considered is given in Table 5.2 .

5.3 Results of the parametric study

The failure loads, the deflections and the failure modes are summarized in Table 5.3 . The edge load p_u is given as load per unit length of loaded edge. The transverse load q_u is given as load per unit area. The bending moments acting at the center of the panels are given in Table 5.4 . The results of the analysis performed on the 26 panels selected are presented under five aspects : the load type and the boundary conditions , the magnitude of the inplane load, the ratio of ρ_y to ρ_x , the slenderness effect and the loading sequence.

5.3.1 Load type and boundary conditions

In Figs. 5.1 and 5.2, the response of the first six panels of each of series PS1 and PS2 are presented. It is clear that the panel ductility is significantly reduced by the application of inplane loads, compared to the case with lateral loads only. Compare for example the curves for PS1-1 and PS1-3, or PS2-1 and PS2-3. The addition of edge restraints improves both the carrying capacity and the ductility. Comparison of cases PS1-3 and PS1-5 or PS2-3 and PS2-5 shows

the strong effect of the rotational edge restraint on the ultimate lateral load, as one would expect for clamped panels. The square and the rectangular series exhibited essentially the same trend for all cases analyzed with slightly more ductility for the rectangular specimens. The total lateral load carried by the square panels and the rectangular ones are of the same order of magnitude for identical boundary conditions. However when the lateral loads are evaluated in terms of pressure, the plates with b/a ratios equal to 1.0 carried a larger pressure q at ultimate than the plates with an aspect ratio of 2.0 . For axially loaded plates the maximum pressures on the square plates were 1.95 to 2.4 times those of the rectangular plates.

For the specimens loaded laterally only with the edges free to move horizontally (e.g. PS1-1 , PS2-1 , PS7-1 and PS8-1), the membrane forces at the center of the plates were in tension in the two directions whereas the regions in the periphery of the panels formed a compression ring to equilibrate the tensile forces at the center of the panels. However, for the panels loaded laterally only with restrained horizontal movement at the supports (e.g. PS1-2 and PS2-2), the forces developed at the center of the panels were in compression until the deflection at this location became of the order of the plate thickness, at which point the membrane forces started to be in tension. Thus the panels exhibited what is called compressive membrane action at the early loading stages.

5.3.2 Magnitude of the inplane load

Figures 5.3 and 5.4 illustrate the effect of the magnitude of the inplane load on the panel response. It can be observed that the strength and the ductility decrease with an increase of the inplane load. The reduction is more significant, however, for the rectangular series PS2. The type of failure changed from a

ductile failure initiated by yielding of the reinforcement in the cases without inplane loads to stability failures resulting from crushing of the concrete in the direction of the inplane load for axially loaded plates with a value for I_m of 0.6, where I_m of 0.351 corresponded to the balanced failure. However for the square panels with small and moderate inplane load magnitude, the failure was caused by material failure. All of the rectangular panels with inplane loads failed by instability.

The classification of the type of failure, by material failure or initiated by instability, is based on the ratio of the bending moment m_y, acting at the center of the plate at the maximum load level about an axis perpendicular to the inplane load direction, to the resisting moment for a reinforced concrete section subjected to inplane load, obtained using the ACI stress block and called m_{ACI}. Since the value calculated for m_{ACI} is not based on the same assumptions as those used in the the finite element analysis, one can consider that ratios of m_y to m_{ACI} greater than about 0.9 indicates a material type failure whereas for a ratio of the bending moments smaller than 0.9, the failure is assumed by instability.

5.3.3 Reinforcement ratios ρ_x and ρ_y

The effect of the reinforcement ratios in the two directions is presented in Figs. 5.5 and 5.6 where it is shown clearly that the carrying capacity is affected more by the reinforcement transverse to the inplane load direction than by the amount of steel in the direction of the inplane load. Thus, in Fig. 5.6 slabs PS2-3 and PS4-1 had almost identical behavior. Both slabs had identical values of ρ_x = 0.004 while ρ_y in PS4-1 was twice as big as in PS2-3. In a panel loaded uniaxially there is a gradual transfer of the lateral load carrying mechanism so that at high loads a larger portion of the lateral load applied at the center of the

plate is carried to the supports by strips spanning perpendicular to the direction of the inplane load. This is particularly true for rectangular panels loaded along the short edges.

The change in behavior with a change in ρ_y / ρ_x can be explained by two things: first the inplane load affects the flexural strength more than the reinforcement parallel to the direction of the inplane load does, as can be seen if one refers to an interaction diagram for axial load and bending moment on a column section. On the other hand, in the direction transverse to the inplane load, the strength is directly proportional to the amount of reinforcement, thus an increase in the reinforcement ratio increases the flexural strength . This is particularly noticeable for rectangular slab with ρ_y / ρ_x equal to 2.0 .

5.3.4 Panel slenderness

The effect of slenderness on the behavior of panels is illustrated in Figs. 5.7 , 5.8 and 5.9 . It is interesting to notice that, in the case of the PS7 series which had a slenderness ratio a/h of 40, the lateral load carrying capacity was reduced significantly by the inplane load due to the slenderness effect (Fig. 5.7). However, for the PS8 series, with a slenderness half that of the PS7 case, the carrying capacity is increased by the presence of the inplane load as shown in Fig. 5.8 . The presence of the axial load had three effects: (a) the moment capacity about an axis perpendicular to the inplane load is increased, (b) the occurrence of cracking is delayed and (c) P-Δ effects magnify the bending moment in the direction perpendicular to the inplane load direction. For the case shown in Fig. 5.8, (a) and (b) dominated while for the slender plate (Fig. 5.7), (c) dominated the behavior. Figure 5.9 shows the effect of the panel slenderness ratio a/h on the ratio of the ultimate lateral load q_u , obtained with an inplane load magnitude

of 0.4 , to q_u obtained with lateral load only. The lateral load carrying capacity decreases linearly with a/h in the cases studied. It is interesting to note that for the case of a/h equal to 20 the lateral load carrying capacity increases with the presence of the inplane load in direction y . This is due to the increase in the bending moment capacity in the direction of the inplane load which is 3.37 times higher with an inplane load magnitude of 0.4 than without inplane load.

Figure 5.10, shows the ratios of the ultimate lateral loads obtained by dividing the lateral load at failure for various inplane load magnitudes ($I_m > 0.0$) by the failure load with lateral loads only ($I_m = 0.0$) for the square and rectangular panels with a/h of 30.0 and for the square panels with a/h of 20 and 40 . The ratios of the ultimate capacities obtained with no P-Δ effects included is shown for comparison for the square and rectangular specimens. The ultimate lateral load values on this curve were obtained using a lower bound solution with the Johansen's yield criterion (Park and Gamble, 1980) and the ACI stress block to evaluate the resisting moments. The results in Fig. 5.10 show the effect of the slenderness ratio on the reduction in carrying capacity. For the square and the rectangular series PS1 and PS2 , with a slenderness ratio a/h equal to 30.0 , the two curves are similar showing, however, some dependance of the panel interaction diagram on the ratio of b to "a" . On the other hand, the two curves on the figure associated with slenderness equal to 45 and 90 (drawn for I_m of 0.0 and 0.4 only) illustrate the sensitivity of the ultimate capacity to the slenderness ratio. The buckling load level indicated on the figure was obtained from an analytical solution proposed by Swartz *et al* (1974) for similar panels subjected to uniaxial inplane loads only.

The values given in Table 5.4 provide more insight into the slenderness effect. The bending moments measured at the center of the plates show that for all the square specimens but two, the bending moments m_y at failure, acting about an axis perpendicular to the direction of the inplane loads, were close to the ultimate bending moments evaluated for an axially loaded reinforced concrete cross section using the ACI stress block. This indicates that the panel failure mode in these cases were by material failure or in the vicinity of such a failure mode. The two square panels that did not have bending moments at failure close to the material failure case were panel PS1-8, which was heavily loaded axially, and panel PS7-2 which was moderately loaded axially but with a higher slenderness. On the other hand, all the rectangular panels loaded axially had bending moments m_y noticeably smaller than the material failure values, which indicates clearly that the ultimate carrying capacity was initiated by a stability type failure.

The bending moments m_y in Table 5.4 include the P-Δ moments. If the product of the inplane load acting at the center of the plate by the deflections at this point is subtracted from m_y, the resulting moment m_y^* would give an indication of the portion of the lateral load carried by bending action along the direction of the inplane load. When this is done, it is observed that for all the cases with a stability type failure, the P-Δ moments are larger than the moments at the center of the plate. This shows that, at failure the lateral load is not carried by bending action in the direction of the inplane load at this location, but also that the strips in the direction of the inplane load are supported by strips spanning in the other direction, at least in the central portion of the panels. This can be associated to the strong strips used in the Hillerborg's simple strip method (Park and Gamble, 1980).

Table 5.4 also indicates the value of the internal membrane force N_y taking place at the center of the plate. It is observed that for the square specimens, the reduction in the inplane load magnitude at the center of the plate is smaller than for the rectangular specimens which exhibited a higher redistribution of the inplane load. The amount of redistribution seems to be related to the deflections of the panels compared to the square ones, forcing the inplane load to fan toward the longitudinal edges of the panel, in a similar manner as observed in the post bucking behavior of metallic plates (Chajes, 1984).

5.3.5 Loading sequence

Finally, Fig. 5.11 shows the effect of the loading sequence on the capacity of the panel. In the first case, the inplane load P was applied first and kept constant while the lateral load q was applied, giving an ultimate value for q_u of 30.15 kPa for I_m equal to 0.40 . In the second case, P and q were applied proportionally, based on the ultimate values of the first analysis. This produced a failure at a value for q_u equal to 31.15 kPa and an inplane load magnitude I_m of 0.413, close to the nonproportional loading performed in the first case. In the third case, the lateral load q was applied up to 30.15 kPa and kept constant while P was increased. In this case, the failure load for P corresponded to an inplane load magnitude I_m of only 0.124, compared to the first case value for I_m of 0.4 , producing a reduction of 69% in the inplane load magnitude.

The reason for such behavior is that the lateral deflections were significantly larger after the application of lateral load alone than they were in the first two slabs plotted in Fig. 5.11 due to more extensive cracking of the plate. When the inplane loads were applied the secondary effect increased more rapidly with the application of P . Hence, the panel response can be very

sensitive to the loading sequence when the lateral load is applied first but less sensitive or insensitive to loading history for proportional loadings or for cases where the inplane load is applied first, provided the cracking history is similar. This conclusion is the same as one would obtain for columns.

5.4 Summary of the parametric study

Twenty six panels were analyzed in the parametric study and based on the behavior observed in these cases six conclusions are drawn.

1. The effects of edge restraints are significant and should be investigated more deeply, together with the effects of partial restraints.

2. The ductility of panels is severely affected by the inplane load magnitude. The carrying capacity drops rapidly beyond the peak load level, ending with a brittle failure.

3. An increase of the carrying capacity is achieved more efficiently by increasing the reinforcement ratio in the direction perpendicular to the inplane load than it is by increasing the reinforcement parallel to the inplane load.

4. The slenderness of the panels affects significantly the value of the bending moments acting at the center of the plates and the failure mode is strongly affected by the aspect ratio of the panels.

5. With the increase of the aspect ratio beyond one, the portion of the lateral load applied at the center of the plate carried by bending action in strips spanning the direction of the inplane load reduces rapidly and strips

spanning in the transverse direction carry a larger portion of the lateral load and also support the strips in the direction of the inplane load.

6. In the cases studied, proportional loading or prior application of the inplane load did not affect the ultimate load of the panel. However, prior application of the lateral load changes the cracking history significantly and causes a severe reduction in the inplane load capacity.

The aim of this parametric study was to provide more insight into the behavior of panels subjected combined uniaxial inplane loads and lateral loads. The analysis of the results obtained with the finite element program can be used to verify the assumptions used in the analytical method proposed by Aghayere and MacGregor (1988) which should allow to perform more analysis in the future to extend the knowledge of the behavior of these panels and also improve the design procedures.

Table 5.1 - Panel specifications in the parametric study

Series	b (mm)	h (mm)	b/a	a/h	ρ_y (%)	ρ_y/ρ_x	Number of panels
PS1	1800	60	1.0	30.0	0.40	1.0	10
PS2	3600	60	2.0	30.0	0.40	1.0	8
PS3	1800	60	1.0	30.0	0.80	2.0	1
PS4	3600	60	2.0	30.0	0.80	2.0	1
PS5	1800	60	1.0	30.0	0.40	0.5	1
PS6	3600	60	2.0	30.0	0.40	0.5	1
PS7	1800	45	1.0	40.0	0.40	1.0	2
PS8	1800	90	1.0	20.0	0.40	1.0	2

Note : a = 1800 mm for all series Total : 26 panels

Table 5.2 - Loading and boundary conditions used in the parametric study

Series	Panel number	Load type	Edge restraint Inplane/Rotational	I_m
PS1 and PS2	1	L	F / F	0.0
	2	L	R(x;y) / F	0.0
	3	L & I	F / F	0.4
	4	L & I	R(y) / F	0.4
	5	L & I	F / R(x;y)	0.4
	6	L & I	R(y) / R(x;y)	0.4
	7	L & I	F / F	0.2
	8	L & I	F / F	0.6
PS1	9	L & I	F / F	(1)
	10	L & I	F / F	(2)
PS3 to PS6	1	L & I	F / F	0.4
PS7 and PS8	1	L	F / F	0.0
	2	L & I	F / F	0.4

(1) : Lateral and inplane loads applied proportionally

(2) : Lateral load applied first and kept constant while the inplane load applied

L : Lateral load

I : Inplane load

F : Free

R : Restrained

x : along axes parallel to the x direction

y : along axes parallel to the y direction

Table 5.3 - Results of the parametric study

Series	Panel	p_u (kN/m)	q_u (kPa)	Δ_u [1] (mm)	Failure [2] mode
PS1	1	0.0	32.47	39.1	D
	2	0.0	40.38	23.2	D
	3	840.0	30.15	17.1	M
	4	840.0	38.50	16.0	M
	5	840.0	89.26	14.8	M
	6	840.0	128.80	18.6	M
	7	420.0	32.18	28.8	S
	8	1260.0	21.72	9.8	M
	9	867.3	31.15	14.1	M
	10	260.4	30.15	65.1	M
PS2	1	0.0	20.72	86.1	D
	2	0.0	17.85	26.7	D
	3	840.0	13.23	30.3	S
	4	840.0	16.81	20.3	S
	5	840.0	37.19	27.4	S
	6	840.0	66.20	23.7	S
	7	420.0	16.95	52.6	S
	8	1260.0	9.35	20.0	S
PS3	1	840.0	33.27	17.1	M
PS4	1	840.0	27.08	31.8	S
PS5	1	840.0	37.60	17.2	M
PS6	1	840.0	21.64	40.9	S

(see next page for the remaining part of the table)

Table 5.3 - Results of the parametric study (continued)

Series	Panel	p_u (kN/m)	q_u (kPa)	Δ_u[(1)] (mm)	Failure[(2)] mode
PS7	1	0.0	21.40	51.0	D
	2	630.0	10.52	12.7	S
PS8	1	0.0	67.14	30.8	D
	2	1260.0	93.19	12.9	M

(1) : Deflection at the panel center corresponding to q_u and p_u

(2) : D Ductile failure; no well defined ultimate point; some carrying capacity left

M Material type failure; well defined ultimate point; no carrying capacity left after peak load

S Stability type failure; well defined ultimate point; no carrying capacity left after peak load

Table 5.4 - Bending moments at the center of the panels analyzed in the parametric study

Panel	p_u (kN/m)	Δ_u (mm)	N_y (kN/m)	m_x (kN•m/m)	m_y (kN•m/m)	m_y^* (kN•m/m)	m_y/m_{ACI}
PS1-3	840	15.6	814.2	4.75	16.05	3.35	0.95
PS1-4	840	16.0	767.0	9.24	16.34	4.07	0.97
PS1-5	840	14.8	804.8	5.64	18.57	6.66	1.10
PS1-6	840	18.6	737.8	11.96	17.30	3.58	1.03
PS1-7	420	28.8	348.9	2.85	12.56	2.51	0.93
PS1-8	1260	9.8	1287.0	3.67	11.61	-1.01	0.78
PS2-3	840	27.4	719.2	4.11	8.96	-10.74	0.53
PS2-4	840	20.3	768.4	10.10	7.63	-7.97	0.45
PS2-5	840	27.4	757.9	4.52	11.56	-9.24	0.65
PS2-6	840	23.7	667.6	17.07	10.82	-5.00	0.64
PS2-7	420	52.6	118.8	3.35	5.51	-0.74	0.41
PS2-8	1260	20.0	1210.4	4.65	5.49	-18.72	0.37
PS3-1	840	17.1	807.7	4.28	19.05	5.23	0.93
PS4-1	840	31.8	685.2	4.26	9.99	11.80	0.49
PS5-1	840	17.2	787.6	7.81	16.50	2.95	0.98
PS6-1	840	36.3	645.1	8.48	9.97	13.45	0.59
PS7-2	630	12.7	619.5	1.91	6.86	-1.01	0.68
PS8-2	1260	12.9	1290.0	11.02	40.23	23.59	1.06

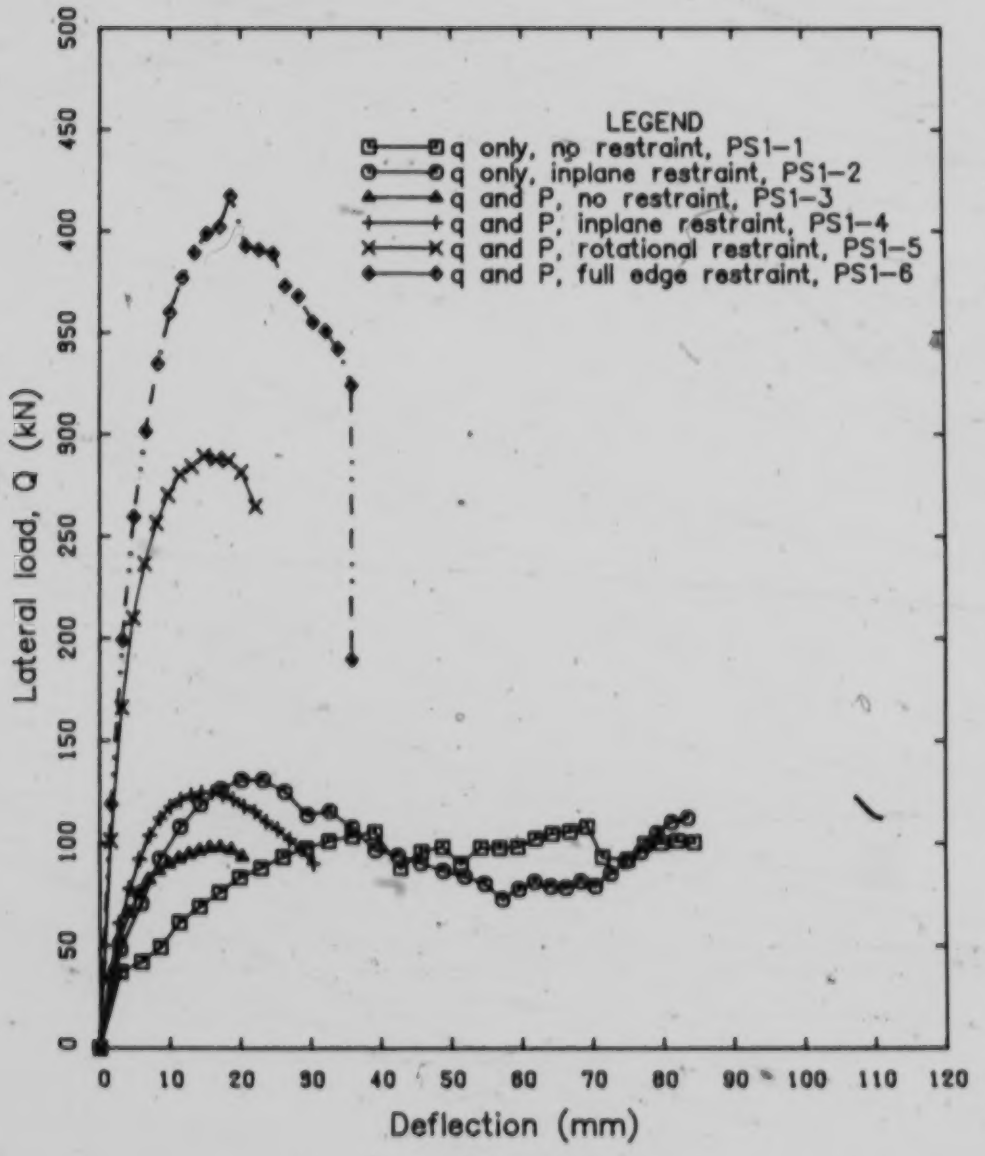

Figure 5.1 - Response of the first six panels of the PS1 series, b/a = 1.0

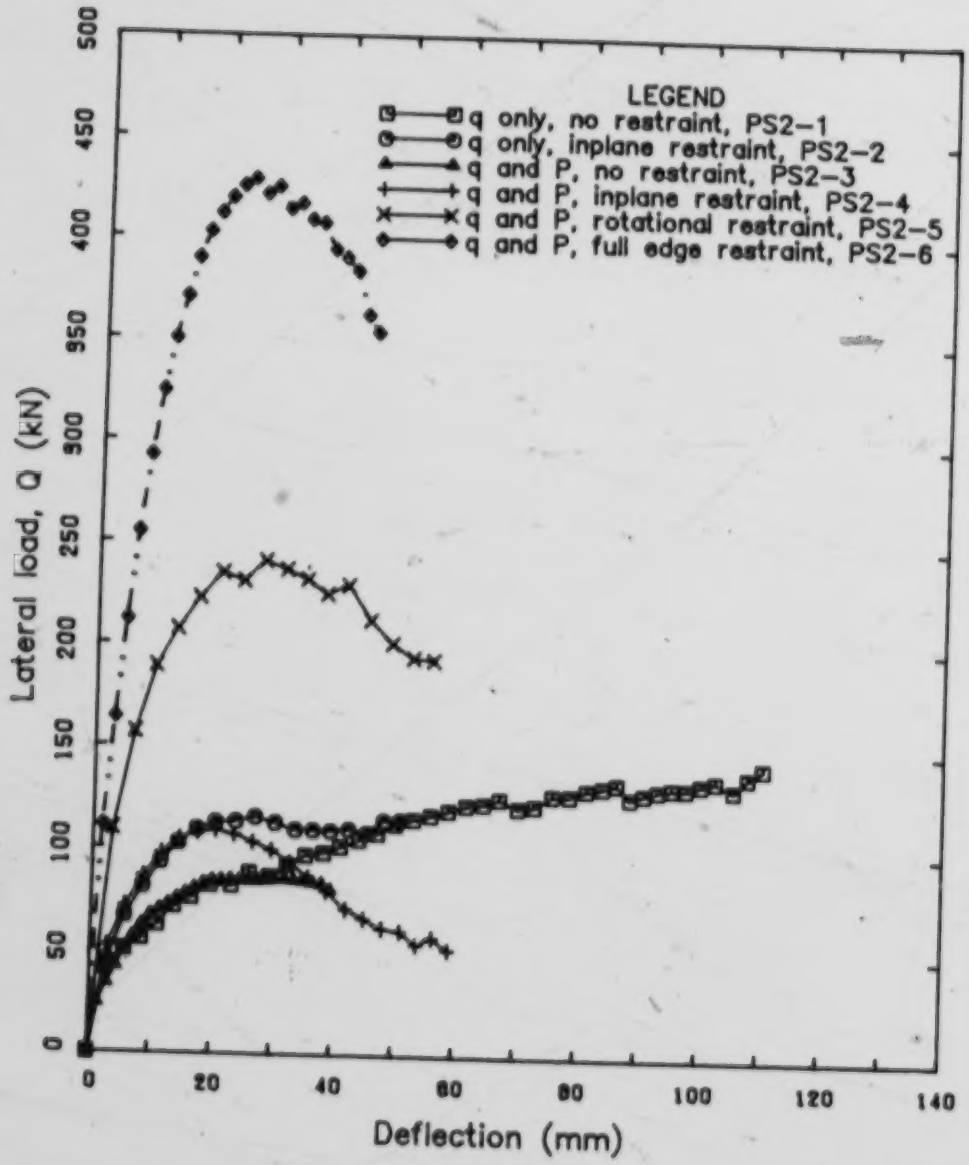

Figure 5.2 - Response of the first six panels of the PS2 series, b/a = 2.0

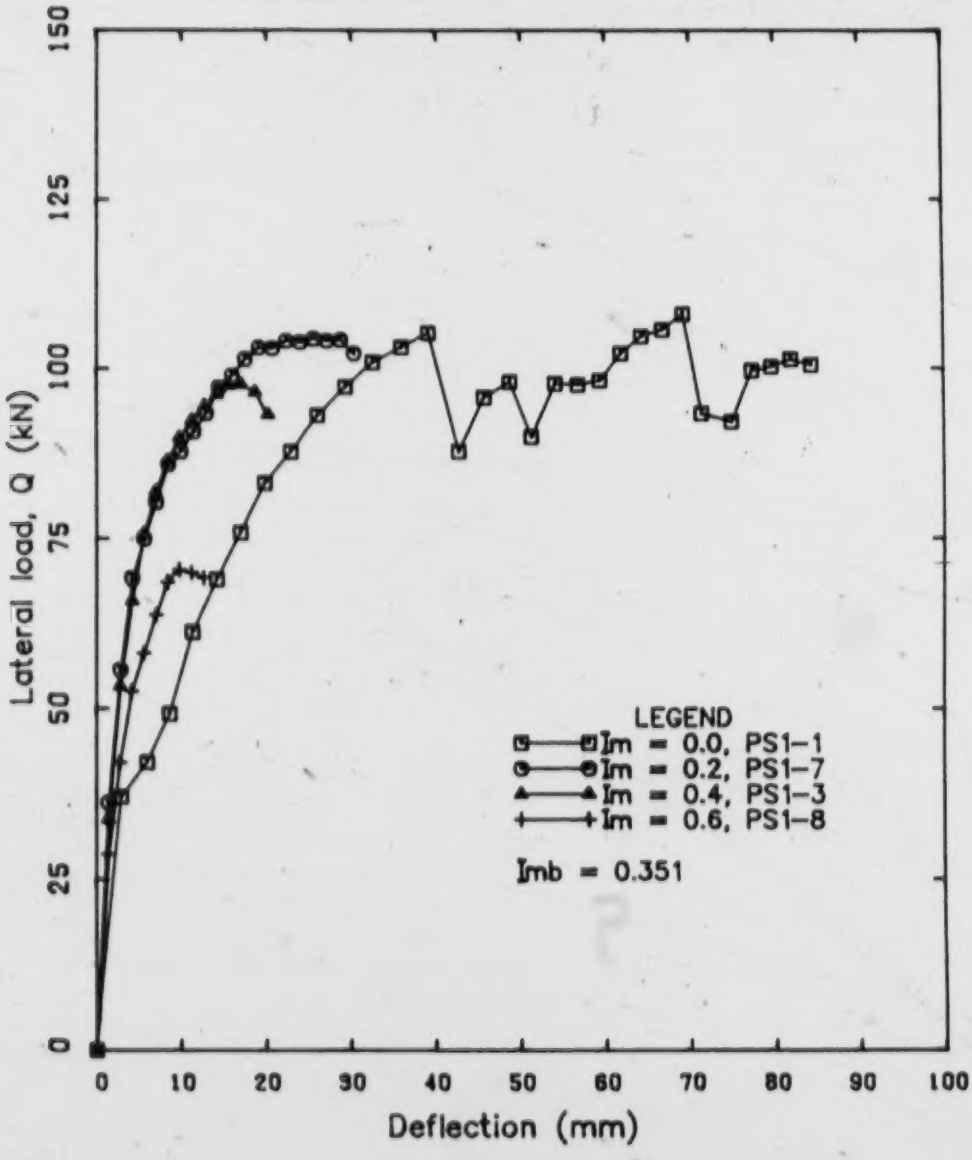

Figure 5.3 - Effect of the inplane load magnitude for the PS1 series

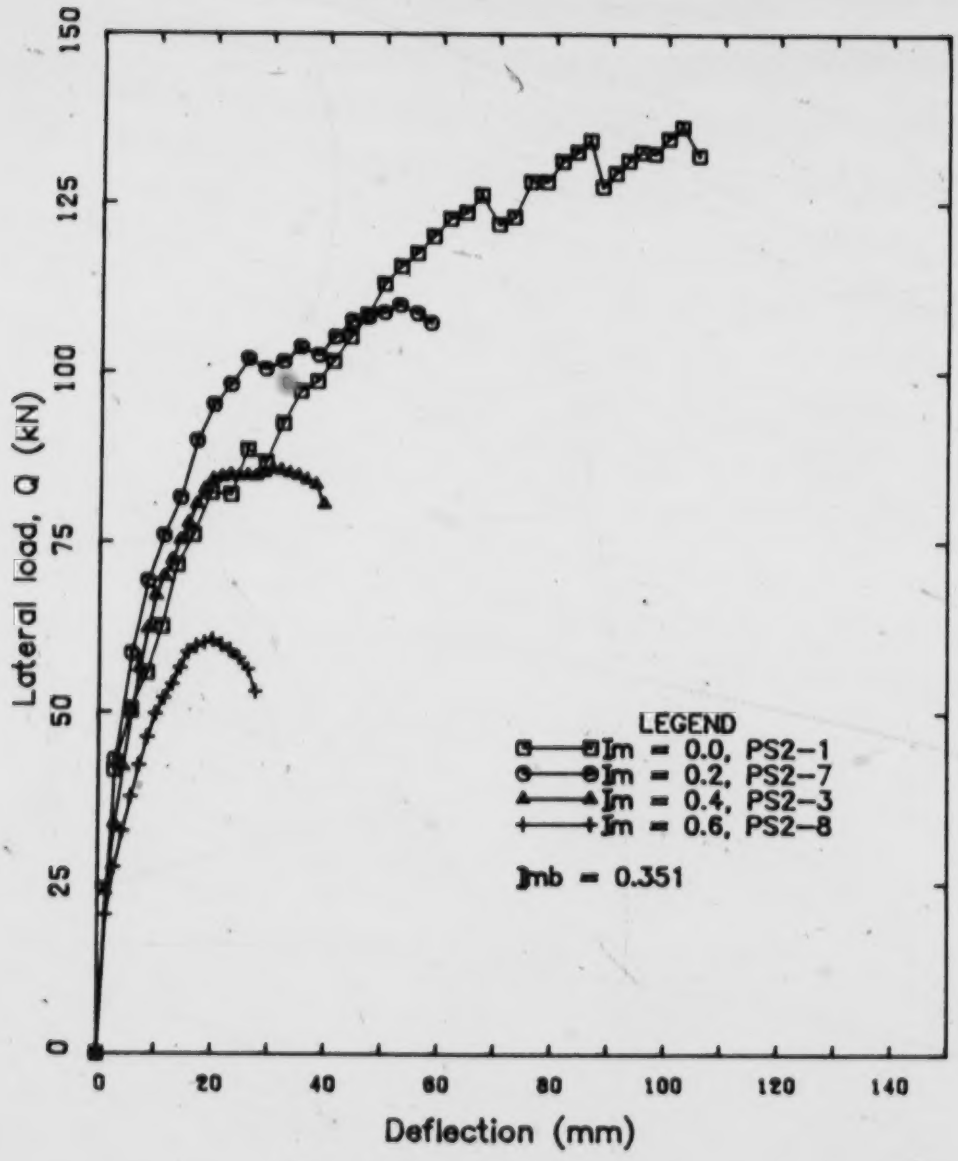

Figure 5.4 - Effect of the inplane load magnitude for the PS2 series

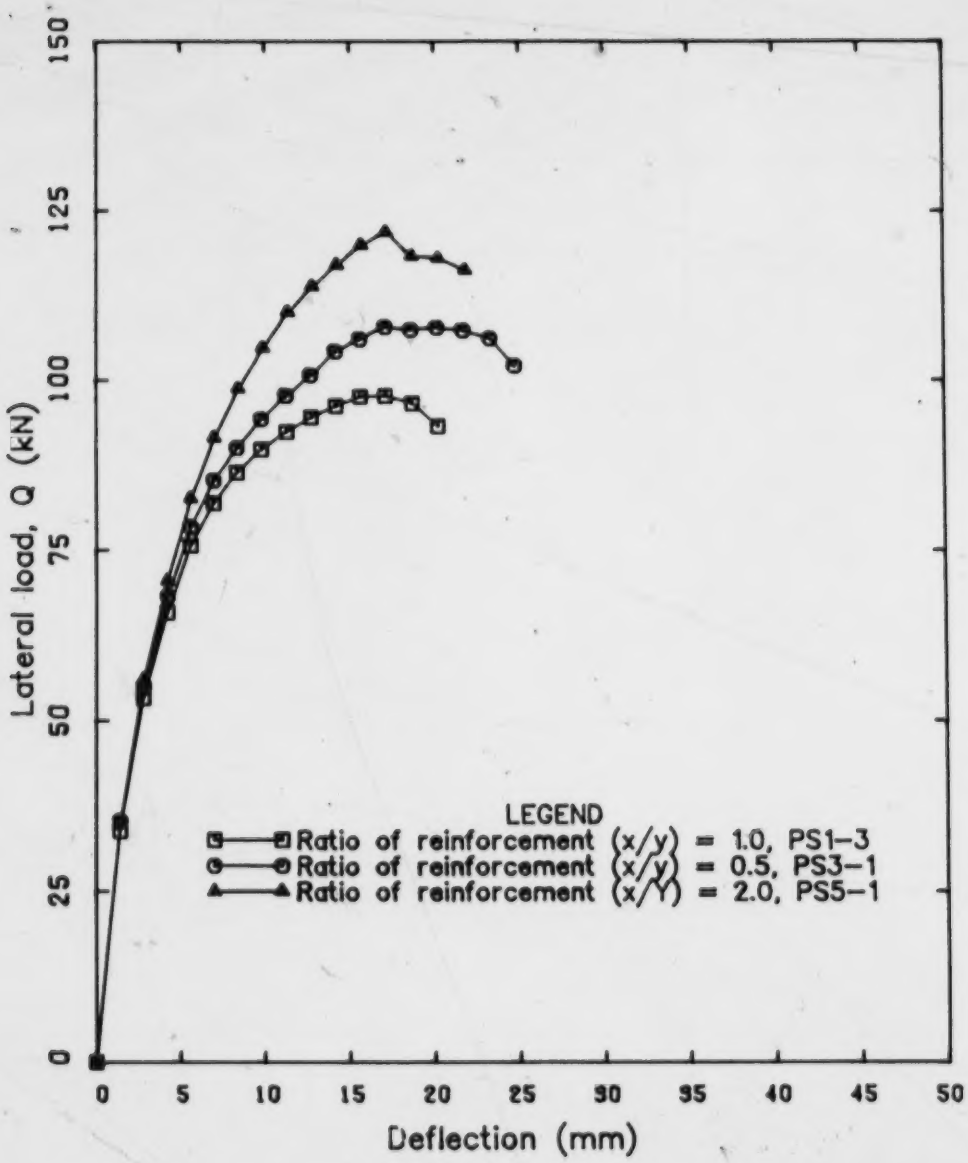

Figure 5.5 - Effect of the reinforcement ratios in the two directions for the square panels

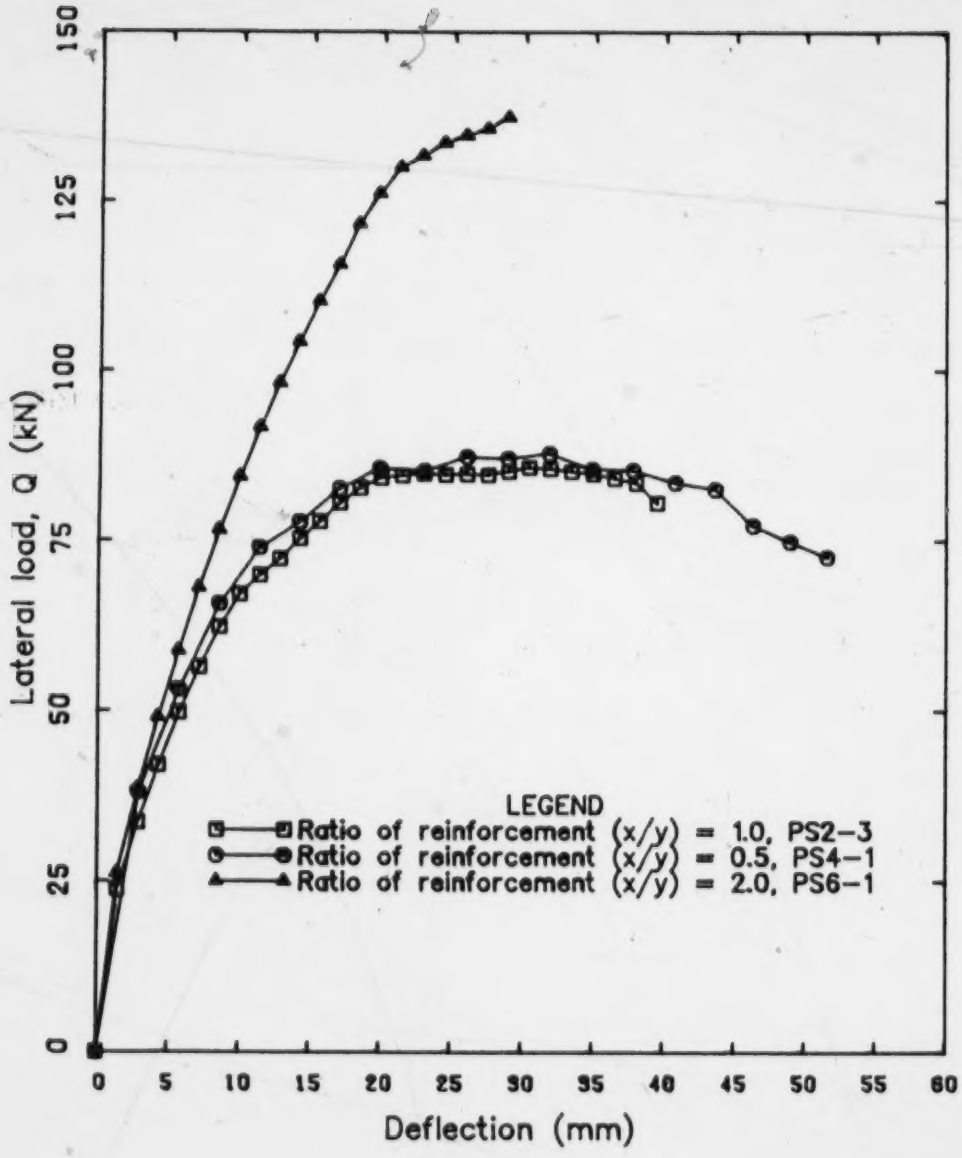

Figure 5.6 - Effect of the reinforcement ratios in the two directions for the rectangular panels

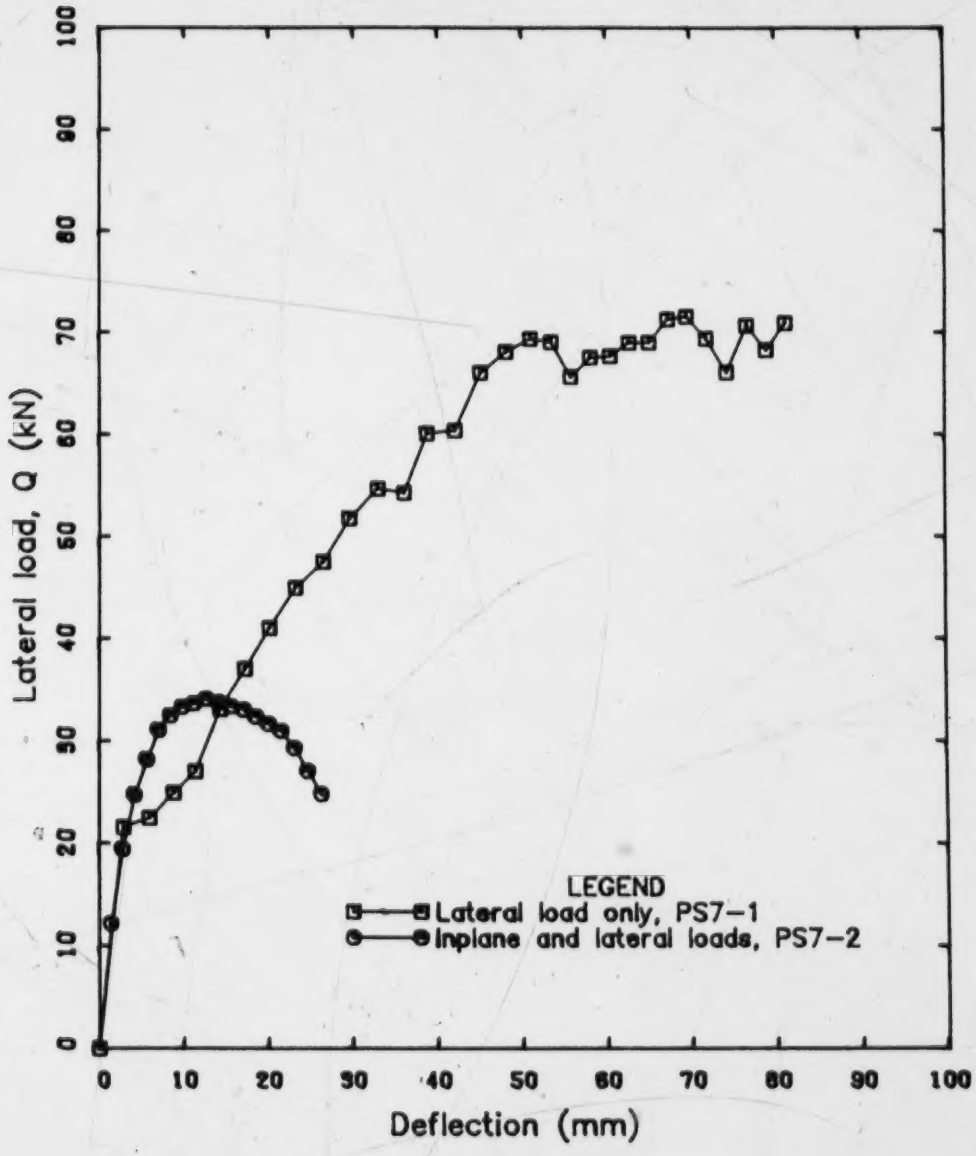

Figure 5.7 - Effect of the inplane load in slender panels, a/h = 40.0, b/a = 1.0

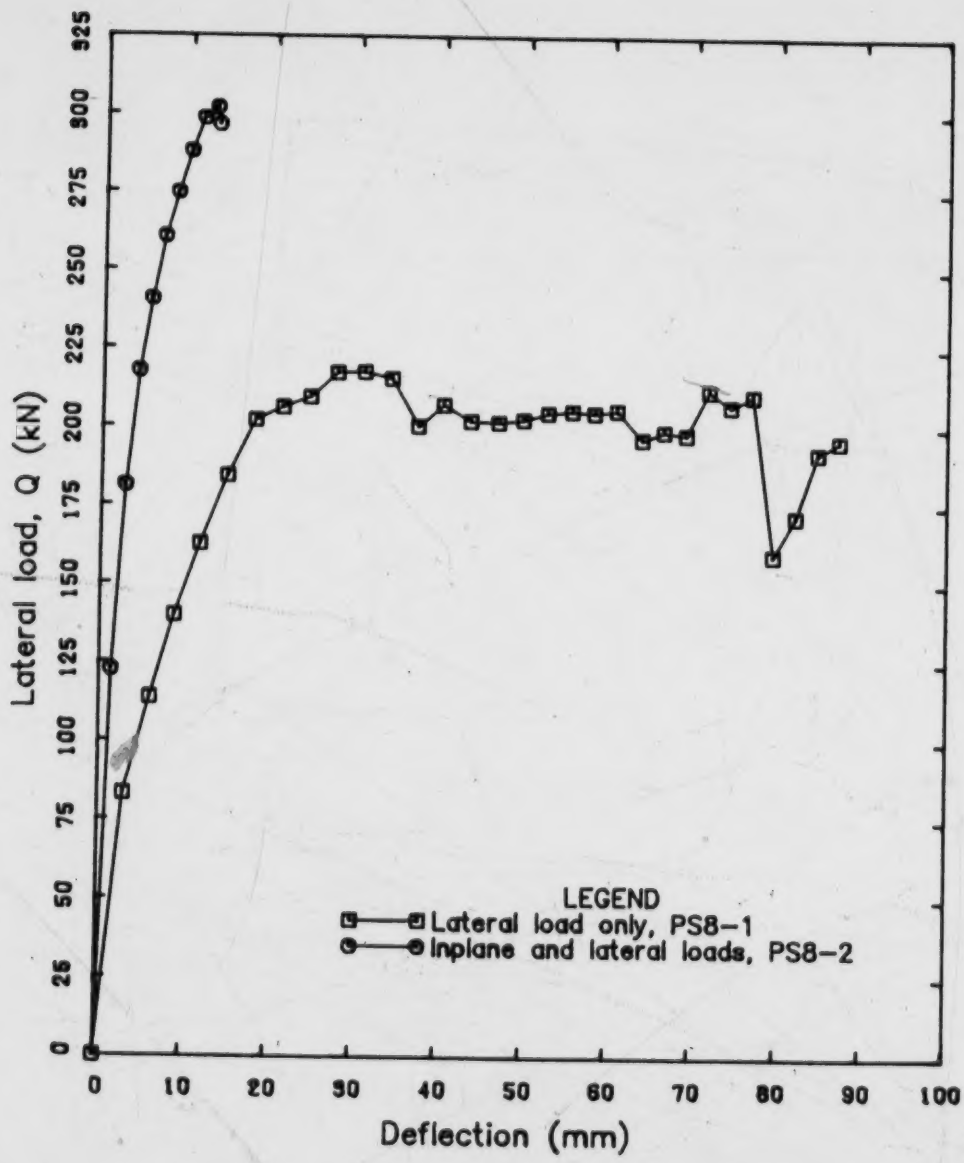

Figure 5.8 - Effect of the inplane load for stocky panels, a/h = 20.0 , b/a = 1.0

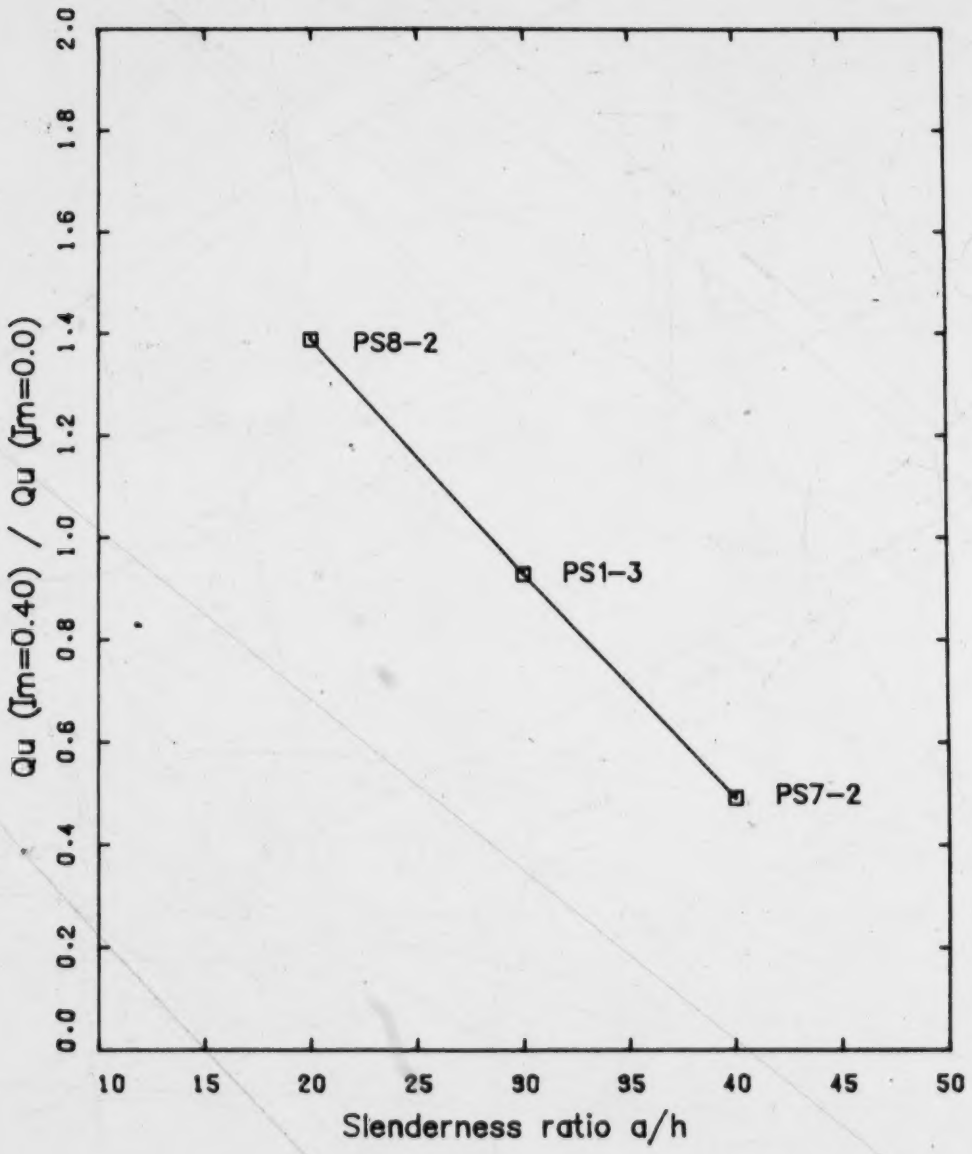

Figure 5.9 - Effect of the slenderness on the failure load

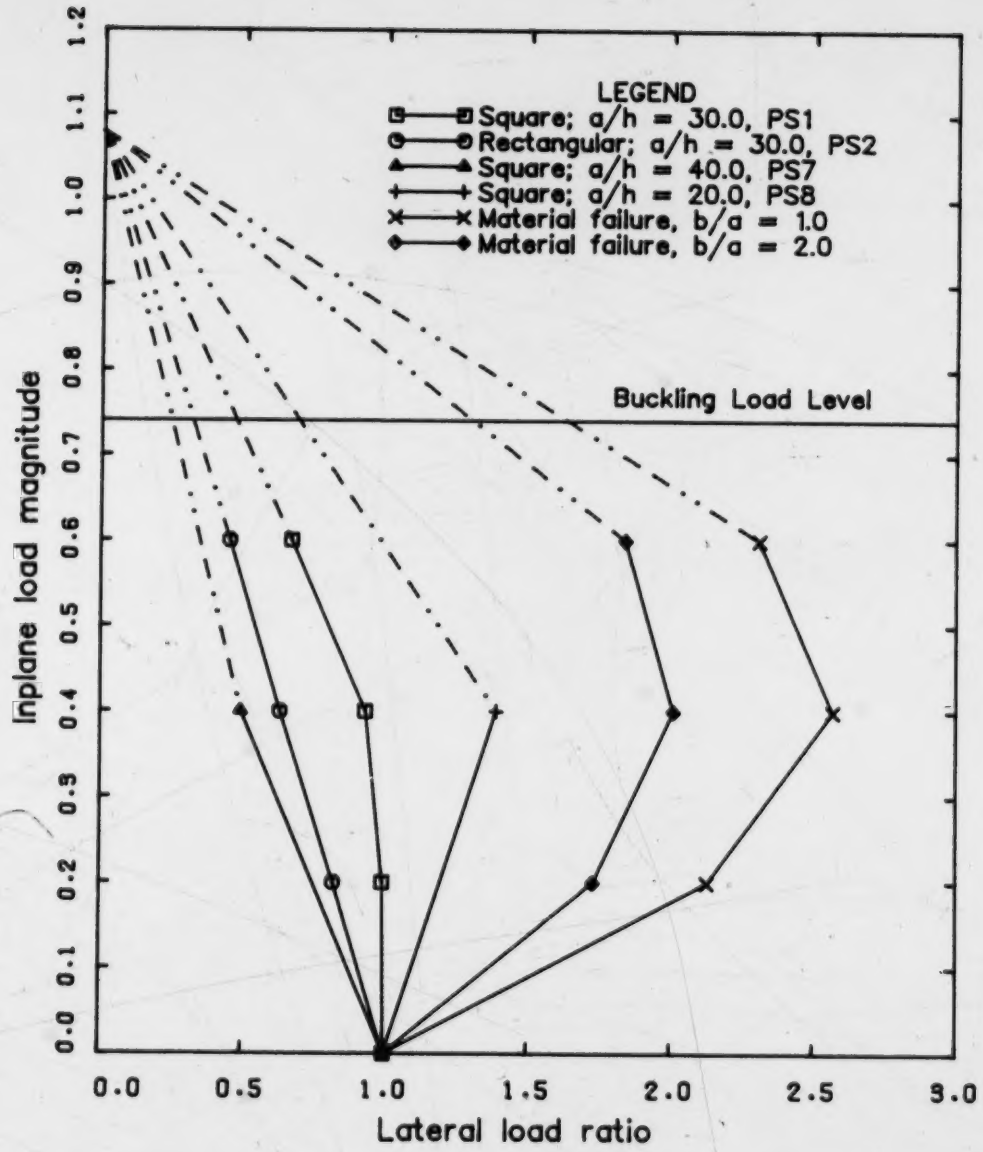

Figure 5.10 - Effect of the slenderness on the ultimate capacity

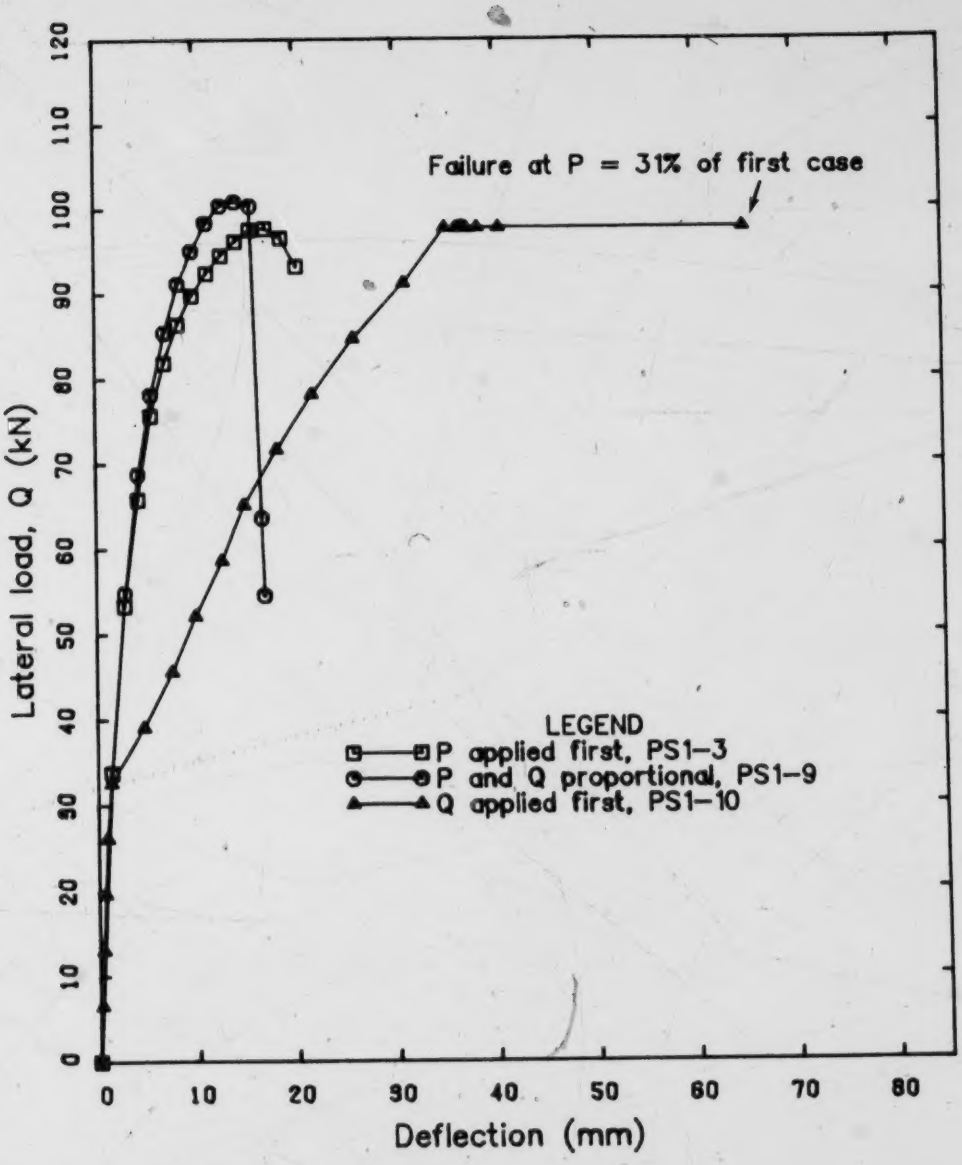

Figure 5.11 - Effect of the loading sequence, a/h = 30.0 , b/a = 1.0

CHAPTER VI

SUMMARY , CONCLUSIONS AND RECOMMENDATIONS

6.1 Summary

A research program has been initiated at the University of Alberta to study the behavior of reinforced concrete panels loaded axially and transversely. Both experimental and numerical approaches were used to investigate the problem. The present work describes the numerical aspect, where the finite element method was used to predict the response of reinforced concrete panels.

In this study, an incremental hypoelastic plane stress concrete model has been developed and implemented in a three dimensional degenerated plate shell element to model the response of reinforced or prestressed concrete structures. The formulation of the material model includes the most recent developments in the modelling of reinforced concrete. After both cracking and crushing, strain softening is allowed. A rational tension stiffening model is developed where the tension softening of plain concrete is incorporated into the CEB description of the tension stiffening phenomenon for reinforced concrete members. Based on the material properties and the amount of reinforcement, this new approach eliminates the necessity for the user to make a decision on the shape of the postcracking stress strain curve for concrete. Stress strain relationships modelling the postcracking behavior of reinforced concrete are then obtained based on the reinforcement ratio and the crack orientation to the reinforcement.

Fixed crack models and rotating crack models were also implemented in the program.

To validate the model, the finite element predictions were compared to results of various experimental investigations: reinforced concrete panels loaded axially in tension, prestressed concrete wall segments loaded biaxially in tension, reinforced concrete panels subjected to pure shear or combined shear and biaxial compression and, finally, reinforced concrete panels loaded axially and transversely. In all the cases studied, the model performed satisfactorily.

Finally, a limited parametric study where 26 problems were considered, was carried out to examine the behavior of reinforced concrete panels subjected simultaneously to uniaxial inplane loads and uniformly distributed lateral loads.

6.2 Conclusions

Based on the results obtained with the finite element method using the element and the material model described previously, it can be concluded that the behavior of planar reinforced structures can be predicted adequately with the finite element method, with respect to the load deflection response, the ultimate strength, the failure mode and also, when applicable, the post ultimate response.

Based on the analysis performed on reinforced concrete panels subjected to inplane and lateral loads, in the comparison with the experimental results of Aghayere and MacGregor (1988) and in the parametric study performed later, two points appeared to have a striking effect on the panel behavior. First, the boundary conditions of the slabs significantly affect the panel response. This is true both when the edges are restrained and when they are simply supported. It

was observed that the vertical stiffness of the hold down points at the corners of the simply supported test specimens affected their response. As a result special attention must be devoted in the modelling of the actual boundary conditions for verification purposes. On the other hand interpretation of the experimental results must also account for interference from the boundary conditions.

The second significant factor is the loading sequence for panels subjected to relatively large lateral loads. The carrying capacity of slab subjected to an inplane load depends largely on deflection and degree of cracking when the axial loads are applied. Various possible loading histories should be investigated in design situations.

6.3 Recommendations for future study

Several recommendations can be made for the future development of the modelling of reinforced concrete structures with the finite element method.

In future improvements of the material model, some attention must be devoted to the prediction of shear type failure through the slab (punching shear). Modelling of shear reinforcement (e.g. prestressed stirrups) can be a significant improvement. Also, rheological effects, such as creep and shrinkage, should be implemented in the model to follow the time dependency of the panel response in various conditions. The modelling of reinforcement in the plate shell element is limited to smeared layers of uniform thickness in each element. Variable thickness and relative position over the element thickness should be added, together with an option for discrete reinforcement.

For the analysis of reinforced concrete panels, other types of loading conditions would be interesting to investigate. Cases with biaxial inplane loads,

inplane shear, concentrated lateral loads or trapezoidal loads (variable hydrostatic pressure) could also be considered. Analyses of panels with aspect ratios b/a smaller than one or larger than two, with various thicknesses, reinforcement ratios and with varying edge restraints would certainly be of great interest as would further tests of such slabs.

REFERENCES

AGHAYERE, A. O. and MACGREGOR, J. G. 1988. "Stability of concrete plates". Structural Engineering Report No. 157, Department of Civil Engineering, University of Alberta, Edmonton, 178 p.

AHMAD, S., IRONS, B. S. and ZIENKIEWICZ, O. C. 1968. "Curved thick shell and membrane elements with particular reference to axisymmetric problems". Proc. 2nd conference on Matrix Methods in Structural Mechanics, Wright-Patterson A.F. Base, Ohio.

AMERICAN CONCRETE INSTITUTE COMMITTEE 224 1986. "Cracking of concrete members in direct tension". American Concrete Institute Journal, Vol. 83, No.1, pp. 3-13.

AMERICAN CONCRETE INSTITUTE COMMITTEE 363 1984. "State of the art report on high strength concrete". American Concrete Institute Journal, Vol. 81, No. 4, pp 364-411.

BAHLIS, J. B. and MIRZA, M. S. 1987. "Nonlinear analysis of planar reinforced concrete structures". Canadian Journal of Civil Engineering, Vol. 14, No. 6, pp 771-779.

BALAKRISHNAN, S. and MURRAY, D. W. 1986. "Finite element prediction of reinforced concrete behavior". Structural Engineering Report No. 138, Department of Civil Engineering , University of Alberta, Edmonton, 487 p.

BATHE, K.-J. 1982. "Finite element procedures in engineering analysis". Prentice-Hall, 735 p.

BAZANT, Z. P. and OH, B. H. 1983. "Crack band theory for fracture of concrete". Materials and Structures, (Matériaux et Constructions), Vol. 16, No. 93, pp 155-177.

BELL, J. C. and ELMS, D. 1971. "Partially cracked finite elements". Journal of the Structural Division, ASCE, Vol. 97, No. ST 7, pp. 2041-2045.

CANADIAN STANDARDS ASSOCIATION (CSA) 1984. "Design of concrete structures for buildings". CAN3-A23.3-M84, Canadian Standards Association, Rexdale, Ontario.

CEB (Comité Euro-International du Béton) 1985. "Cracking and deformations". Bulletin d'information No. 158, Paris.

CEB MODEL CODE FOR CONCRETE STRUCTURES 1978. "International Recommendation", 3rd ed. Cement and Concrete Association, London, England, 348 p.

CHAJES, A. 1984. "Principles of structural stability theory". Prentice-Hall, Englewood Cliffs, New Jersey, 336 p.

CHITNUYANONDH, L., RIZKALLA, S. MURRAY, D. W. and MACGREGOR, J. G. 1979. "An effective uniaxial stress-strain relationship for prestressed concrete". Structural Engineering Report No. 74, Department of Civil Engineering, University of Alberta, Edmonton, 91 p.

COLLINS, M. P., VECCHIO, F. J. and MEHLHORN, G. 1985. "An international competition to predict the response of reinforced concrete panels". Canadian Journal of Civil Engineering, Vol. 12, No. 3, pp 624-644.

COLLINS, M. P., and MITCHELL, D., 1987. "Prestressed concrete basics". Canadian Prestressed Concrete Institute, Ottawa. 614 p.

CONWAY, H. O. 1949. "Bending of rectangular plates subjected to a uniform distributed lateral load and to tensile or compressive forces in the plane of the plate". Journal of Applied Mechanics, ASME, pp. 301-309.

CRISFIELD, M.A. 1982. 'Accelerated solution techniques and concrete cracking". Computer Methods in Applied Mechanics and Engineering, Vol. 33, North-Holland Publ. Company, pp. 585-606.

DARWIN,D. and PECKNOLD,D.A. 1974. "Inelastic model for cyclic biaxial loading of reinforced concrete". Structural Research Series No. 409, University of Illinois, Urbana, Ill.

DARWIN, D. and PECKNOLD, D. A. 1977. "Nonlinear biaxial stress-strain law for concrete". Journal of the Engineering Mechanical Division, ASCE, Vol. 103, No. EM2, pp 229-241.

ELWI, A. A. and MURRAY, D. W. 1979. "A 3D hypoelastic concrete constitutive relationship". Journal of the Mechanical Engineering Division, ASCE, Vol. 105, No. EM4, pp 623-641.

GERSTLE, W., INGRAFFEA, A. R. and GERGELY, P. 1982. "Tension stiffening: a fracture mechanics approach", in BARTOS. P. ed., 1982. "Bond in concrete". Applied Science Publishers, London, pp 97-106.

GOPALARATNAM, V. S. and SHAH, S. P. 1985. "Softening response of plain concrete in direct tension". American Concrete Institute Journal, Vol.82, No.3, pp. 310-323.

GUO, Z.-H. and ZHANG, X.-Q. 1987. "Investigation of complete stress deformation curves for concrete in tension". American Concrete Institute Material Journal, Vol. 84, No.4, pp 278-285.

HAND, F. R., PECKNOLD, D. A. and SCHNOBRICH, W. C. 1973. "Nonlinear layered analysis of reinforced concrete plates and shells". Journal of the Structural Division, ASCE, Vol. 99, No. ST 7, pp. 1491 - 1505.

HILLERBORG, A. 1985. "Numerical methods to simulate softening and fracture of concrete". in SIH, G. C. and DITOMMASO, A. 1985." Fracture mechanics of concrete". Martinus Nijhoff Publ, Dordrecht, The Netherlands., pp 141-170.

HOGNESTAD, E. 1951. "A study of combined bending and axial load in reinforced concrete members". Bulletin 399, University of Illinois Engineering Experiment Station, Urbana, Ill., 128 p.

HSU, T. T. C., SLATE, P. O., STURMAN, G. M. and WINTER, G. 1963. "Micro-cracking of plain concrete and the shape of the stress-strain Curve". American Concrete Institute Journal, Proceedings, Vol. 60, No. 2, pp. 209-224.

JOFRIET, J. C. and MCNEICE, G. M. 1971. "Finite element analysis of reinforced concrete slabs". Journal of the Structural Division, ASCE, Vol. 97, No. ST 3, pp. 785 - 806.

JOKINEN, E. P. and SCANLON, A. 1987. "Field measured two-way slab deflections". Canadian Journal of Civil Engineering, Vol. 14, No. 6, pp. 807-819.

KABIR, A. F. 1976. "Nonlinear analysis of reinforced concrete panels, slabs and shells for time dependent effects", PH. D. Dissertation, Division of Structural Engineering and Structural Mechanics, University of California, Berkely, UC - SESM Report No. 76-6.

KOMPFNER, T. A. 1983. "Ein finites Elementmodell für die geometrisch und physikalisch nichtlineare Berechnung von Stahlbeton-schalen". Dissertation, Institut für Baustatik, Universitat Stuttgart.

KORDINA, K. and STORKEBAUM, K. H. 1973. "Unersuchungen über die Traglasten ausmitting beanspruchter Stahlbetonwande". Institute Für Baustoffkunde Und Stahlbetonbau, Technischen Universitat Braunschweig, 87 p.

KORDINA, K. and TIMM, R. 1979. "Stabilität mehrseitig gelagerter Betonwande, 1. Stufe". Institute Fur Baustoffkunde Und Stahlbetonbau, Technischen Universitat Braunschweig, 115 p.

KORDINA, K. and KIEL, M. 1982. "Stabilitat mehrseitig gelagerter Betonwände, 2. Stufe". Institute Fur Baustoffkunde Und Stahlbetonbau, Technischen Universitat Braunschweig, 116 p.

KOTSOVOS, M. D. 1983. "Effect of testing techniques on the post-ultimate behaviour of concrete in compression". Materials and Structures (Materiaux et Constructions), Vol. 16, No. 91, pp. 3-12.

KOTSOVOS, M.D. 1984. "Concrete. A brittle fracturing material". Materials and Structures (Matériaux et Construction), Vol. 27, No. 98, pp 107-115.

KOZIAK, B. D. P. and MURRAY, D. W. 1979. "Analysis of prestressed concrete wall segments". Structural Engineering Report No. 78, Department of Civil Engineering, University of Alberta, Edmonton, 195 p.

KUPFER, H. B. and GERSTLE, K. H. 1973. "Behavior of concrete under biaxial stresses". Journal of the Engineering Mechanics Division, ASCE, Vol. 99, No. EM4, pp 853-866.

KUPFER, H., HILSDORF, H. K. and RUSCH, H. 1969. "Behavior of concrete under biaxial stresses". American Concrete Institute Journal, Vol. 66, No. 8, pp 656-666.

LIN, C. S. and SCORDELIS, A. C. 1975. "Nonlinear analysis of reinforced concrete shells of general form". Journal of the Structural Division, ASCE, Vol. 101, No. ST3, pp 523.

LINK, R. A., ELWI, A. E. and SCANLON, A. 1988. "Tension stiffening in concrete panels". Proceeding of the Annual Conference of the Canadian Society for Civil Engineering, Calgary.

MACGREGOR, J. G., RIZKALLA, S. H. and SIMMONDS, S. H. 1979. "Cracking of reinforced and prestressed concrete wall segments". Structural Engineering Report No. 82, Dept. of Civil Engineering, University of Alberta, Edmonton.

MILFORD, R. V. and SCHNOBRICH, W. C. 1984. "Numerical model for cracked reinforced concrete", presented at the International Conference on Computer Aided Analysis and Design of Concrete Structures, Split, Yugoslavia, Damjanic, F. *et al.*, Eds., Pineridge Press, Swansea, U.K.

MURRAY, D. W. and WILSON, E. L. 1969. "Finite element large deflection analysis of plates". Journal of the Engineering Mechanics Division, ASCE, Vol. 95, No. EM1, pp. 143-165.

NGO, D. and SCORDELIS, A. C., 1967. "Finite element analysis of reinforced concrete beams". Journal of the American Concrete Institute, Vol. 64, No. 3, pp. 152-163.

PARK, R. and GAMBLE, W. L. 1980. "Reinforced concrete slabs", John Wiley & Sons, 618 p.

PAWSEY, S. F. and CLOUGH, R. W. 1970. "Improved numerical integration of thick slab finite elements". Int. Journal of Mechanical Engineering, Vol. 3, pp.575-586.

RAMM, E. 1976. "Geometrisch nichtlineare elastostatik und finite elemente". Bericht No. 76-2, Institut für Baustatik der Universität Stuttgart, Germany.

RAMM, E. 1977. "A plate/shell element for large deflections and rotations". in: BATHE, K.-J., ODEN, J.T. and WUNDERLICH, W., eds., 1977. "Formulation and computational algorithms", U.S.-Germany symposium, M.I.T., pp 264-293.

RAMM, E. 1980. "Strategies for tracing the nonlinear response near limit points". in WUNDERLICH, W., STEIN, E. and BATHE, K.-J., eds. "Nonlinear Finite Element Analysis in Structural Mechanics". Proceedings of the Europe - U.S. Workshop, Ruhr Universitat, Bochum, West Germany, pp 63-89.

RAMM, E. and KOMPFNER, T. A. 1984. "Reinforced concrete shell analysis using an inelastic large deformation finite element formulation". Proceeding of the International Conference on Computer Aided Analysis and Design of Concrete Structures, Split, Yugoslavia, Pineridge Press, Swansea, U.K. pp 581-597.

RAO, S. 1966. "Umlagerung der Schnittkrafte in Stahlbetonkonstruktionen". Grumdlagen der Berechung bei statisch unbestimmten Tragwerken unter

Berucksichtigung der plastischen Verformunger. Deutscher Ausschuss für Stahlbeton, H. No. 177

RAPHAEL, J. M. 1984. "Tensile strength of concrete". American Concrete Institute Journal, Vol. 81, No. 2, pp 158-165.

RIZKALLA, S. H., HWANG, L. S. and EL SHAHAWI, M. 1983. "Transverse reinforcement effect on cracking behaviour of R.C. members". Canadian Journal of Civil Engineering, Vol. 10, No. 4, pp 566-581.

ROSTASY, F. S., KOCH, R. and LEONHART, F. 1976, "Zur mindestbewehrung für Zwang von auBenwänden aus Stahlleichbeton". Deutscher Ausschuss für Stahlbeton, No 267, pp 1-83.

ROTS, J. G. and DE BORST, R. 1 987. "Analysis of mixed-mode fracture in concrete". Journal of the Engineering Mechanics, ASCE, Vol. 113, No. 11, pp. 1739-1758.

RUSCH, H. 1960. "Research toward a general flexural theory for structural concrete". American Concrete Institute Journal Proceedings, Vol. 57, No. 1, pp. 1-28.

SAENZ, L. P. 1964, discussion of "Equation for the stress-strain curve of concrete" by DESAYI and KRISHNAN, American Concrete Institute Journal, Vol. 61, No. 9, pp 1229-1235.

SCANLON, A. and MURRAY, D. W. 1974. "Time dependent reinforced concrete slab deflections". Journal of the Structural Division, ASCE, Vol. 100, No. ST9, pp. 1911 - 1924.

SCHNOBRICH, W. C. 1985. "The role of finite element analysis of reinforced concrete structures". in Proceedings of the Seminar on "Finite Element Analysis of Reinforced Concrete Structures", Tokyo, Japan. Published by the Structural Division, ASCE, pp. 1-24.

STEGMULLER, H., HAFNER, L., RAMM, E. and SATTELE, J. M. 1983. "Theoretische grundlagen zum FE-programm system NISA 80".

Mitteilung Nr. 1, Institut für Baustatik der Universität Stuttgart, Germany.

STURMAN, G. M., SHAH, S. P. and WINTER, G. 1965. "Microcracking and inelastic behavior of concrete". in Flexural Mechanics of Reinforced Concrete, American Concrete Institute Publication SP-12, pp. 473-500.

SWARTZ, S. E. and ROSEBRAUGH, V. H. 1974. "Buckling of reinforced concrete plates". Journal of the Structural Division, ASCE, Vol. 100, No. ST1, pp. 195-208.

SWARTZ, S. E., ROSEBRAUGH, V. H. and BERMAN, M. Y. 1974. "Buckling tests on rectangular concrete panels". American Concrete Institute Journal, Vol. 71, No. 1, pp 33-39.

TASUJI, M. E. , SLATE, F. O. and NILSON, A. H. 1978. "Stress-strain response and fracture of concrete in biaxial loading". American Concrete Institute Journal, Vol. 75, No. 7, pp. 306-312.

TIMOSHENKO, S. P. and WOINOWSKY-KRIEGER, S. 1959. "Theory of plates and shells", MacGraw-Hill, New-York.

TODESCHINI, C. E., BIANCHINI, A. C. and KESLER, C. E. 1964. "Behavior of concrete columns reinforced with high strength steels". American Concrete Institute Journal, Proceedings, Vol. 61, No. 6, pp. 701 -716.

VAN GREUNEN, J. 1979. "Nonlinear geometric, material and time dependent analysis of reinforced and prestressed concrete slabs and panels". Report No. UC SESM 79-3, Structures and Materials Research, Dept. of Civil Engineering of University of California, Berkeley.

VECCHIO, F. J. and COLLINS, M. P. 1982. "The response of reinforced concrete to in-plane shear and normal stresses". Publication No. 82-03, Dept. of Civil Engineering, University of Toronto, 332 p.

VECCHIO,F. J. and COLLINS, M. P. 1986. "The modified compression field theory for reinforced concrete elements subjected to shear". American Concrete Institute Journal, Vol. 83, No. 2, pp 219-231.

YANKELEVSKY, D. Z. and REINHARDT, H. W. 1987. "Focal points model for uniaxial cyclic behavior of concrete". Proceeding of the IABSE Colloquium, Delft, pp 99-106.

YANKELEVSKY, D. Z., and REINHARDT, H. W. 1987. "Response of plain concrete to cyclic tension". American Concrete Institute Materials Journal, Vol. 84, No.5, pp 365-373.

APPENDIX A

PARAMETRIC DESCRIPTION OF NOTCHED TENSION SPECIMENS

In this appendix, the behavior of specimens similar to those tested by Gopalaratnam and Shah (1985) is described in a parametric form. Using the relationships derived, conclusions on the modelling of tension softening are drawn.

A.1 Parametric description

The type of specimen used is illustrated in Fig. 2.8a where δ is the elongation measured over the gage length L_o and where w_c is the width of the fracture process zone.

The fracture process zone is called region A, while the unaffected concrete outside the fracture zone is assumed to be in region B. The average stress, σ, calculated at the notched section is equal to:

$$\sigma = \frac{T}{h\ b} \tag{A.1}$$

in which T is the tensile force pulling on the specimen, h the specimen thickness and b the distance between the notches. The average stress in region B is expressed as

$$\sigma_o = \frac{T}{h\ b_o} \tag{A.2}$$

where b_o is the specimen width in region B.

The fracture process zone dimensions, b and w_c, are assumed to remain constant, w_c being an unknown value at this stage. However, before cracking, one can assume that the length of region A is equal to the notch depth, c_n, and the length of region B is then equal to L_o less c_n. This is based on the assumption that the stress trajectories in region A expand at a 45 degree angle into region B and that the notch width is negligible compared to its depth.

Based on these assumptions, the stress-elongation relationship $(\sigma - \delta)$ of the specimen in Fig. 2.8a can be derived. Since the stress-strain curve is defined by three segments, three stages in the elongation are considered, δ_{uncr}, δ_1, and δ_2, corresponding to the tangent moduli in region A: E_c, E_1 and E_2 respectively. Let the following geometric parameters be defined

$$\psi_d = \frac{b}{b_o} \leq 1.0 \qquad \text{(A.3)}$$

$$\psi_{Lo} = \frac{c_n}{L_o} \qquad \text{(A.4)}$$

$$\psi_L = \frac{w_c}{L} \qquad \text{(A.5)}$$

To these parameters, one can add the material parameters

$$\psi_1 = \frac{E_c}{E_1} \qquad \text{(A.6)}$$

$$\psi_2 = \frac{E_c}{E_2} \qquad \text{(A.7)}$$

Using the geometric and material parameters defined in Eqs. A.3 to A.7, together with the stress definitions given in Eqs. A.1 and A.2, the elongation δ of the specimen is described by the three following equations:

$$\delta_{uncr} = \frac{\sigma}{E_c} L_o [\, \psi_d + \psi_{Lo}(1 - \psi_d)] \tag{A.8}$$

$$\delta_1 = \frac{f_t}{E_c} L_o [\, \psi_{Lo} + \psi_d(\psi_L - \psi_{Lo}) - \psi_1 \psi_L] + \frac{\sigma}{E_c} L_o [\, \psi_d + \psi_L(\psi_1 - \psi_d)] \tag{A.9}$$

$$\delta_2 = \frac{f'_t}{E_c} L_o [\, \psi_{Lo} + \psi_d(\psi_L - \psi_{Lo}) - \psi_1 \psi_L + \mu \psi_L(\psi_1 - \psi_2)\,] + \frac{\sigma}{E_c} L_o [\, \psi_d + \psi_L(\psi_2 - \psi_d)] \tag{A.10}$$

The average strain ε_m over the gage length L_o is defined as

$$\varepsilon_m = \frac{\delta}{L_o} \tag{A.11}$$

where δ can be replaced by either δ_{uncr}, δ_1, or δ_2. Similarly, the average tangent modulus in each case can be evaluated as

$$E_m = \frac{d\sigma}{d\varepsilon_m} \tag{A.12}$$

From equations A.8 to A.10 the average tangent moduli corresponding to the three phases are expressed as follow:

$$E_{uncr} = \frac{E_c}{\psi_{Lo}(1 - \psi_d) + \psi_d} \tag{A.13}$$

$$E_1 = \frac{E_c}{\psi_L(\psi_1 - \psi_d) + \psi_d} \tag{A.14}$$

$$E_2 = \frac{E_c}{\psi_L(\psi_2 - \psi_d) + \psi_d} \qquad (A.15)$$

These equations represent the slopes of a stress-strain curve for a tension specimen with strains measured over the gage length L_o and based on a material law as illustrated in Fig. 2.7. Also, these equations assume that the length of region A is constant before and after cracking and equal to c_n and w_c respectively.

An example is presented here to illustrate the effect of selecting w_c and L_o on elongation measurements. The assumed values for the numerical calculations are shown in Table A.1 while other parameters needed were taken from Gopalaratnam and Shah (1985) and are summarized in Table A.2 . For the example, the maximum value for δ_{uncr} , δ_1 and δ_2 were calculated and the slopes E_{1m} and E_{2m} were evaluated. Also the crack width measured at one third of f'_t after cracking is given. Results are presented in Table A.3 and illustrated in Fig. A.1 . As can be seen, the width of the fracture process zone, w_c , has a strong influence on the specimen elongation while, as assumed initially, the choice of the gage length affects only the slopes of the $\sigma - \delta$ curve, has little effect on w , and hence no significant effect on G_f. It should be mentioned that in a test δ is measured and w_c is unknown.

A.2 Observation from experimental investigation

The test series by Gopalaratnam and Shah (1985) contains many experimental results which can be used to evaluate parameters needed in the analysis. They tested 12 in. long by 3 in. wide and 3/4 in. or $1^1/_2$ in. thick notched tension specimens made of concrete, mortar and cement paste with maximum aggregate sizes equal to 3/8 in. and 3/16 in. for concrete and mortar respectively.

At mid-length of the specimens, 0.5 in. long and 0.1 in. wide notches were made on both sides. Strains were measured over gage lengths of 3.25 in. and 0.5 in. and also by means of electric strain gages.

One experimental curve (see Fig. 7a in Gopalaratnam and Shah, 1985) shows the stress-strain behavior of a concrete specimen where strains are measured over the 3.25 in. gage length (L_o) and also by an electric strain gages at the crack. Table A.2 contains parameters measured form this curve. Based on those approximate measurements, it is possible to estimate the following parameters:

- from Eq. A.13, $E_c = 4080 \left[0.5 / 3.25 (1 - 2/3) + 2/3 \right] = 2930$ ksi
- from Eq. A.6, $\psi_1 = 2930 / -500 = -5.86$
- from Eq. A.14,

$$\psi_L = \frac{\left[\frac{2930}{-4080} - \frac{2}{3}\right]}{\left[-5.86 - \frac{2}{3}\right]} = 0.21$$

- from Eq. A.5, $w_c = 0.21 \times 3.25 = 0.7$ in.
- finally from Eq. A.15,

$$\psi_2 = \frac{\left[\frac{2930}{-300} - \frac{2}{3}\right]}{0.21} + \frac{2}{3} = -.49$$

Since the values used in this derivation come from coarse measurements on a plot, the values of E_c and the ψ's are only an indication of the order of magnitude of the parameters.

Table A.1 - Parameters assumed for the example

Parameter	Value
ψ_1	- 6
ψ_2	- 33
ψ_d	2/3
μ	1/3
E_c	2930 ksi

Table A.2 - Parameters measured in Gopalaratnam and Shah (1985)

Parameter	Value
f'_t	530 ksi
ε_{mcr}	130 με
c_n	0.5 in.
E_{mcr}	4080 ksi
E_{1cr}	-4080 ksi
E_{2m}	-300 ksi
E_1	-500 ksi

Table A.3 - Specimen response in the example

Case	w_c (in)	L_o (in)	δ_{uncr} (μ in)	δ_{1max} (μ in)	δ_{2max} (μ in)	E_{1m} (ksi)	E_{2m} (ksi)	w [1] (μ in)
1	0.5	3.25	422	563	1449	-8139	-649	422
2	2.0	3.25	422	1768	5694	-853	-149	1627
3	2.0	6.50	814	1901	5704	-2113	-302	1630

(1) crack width for σ equal to $f_t / 3$

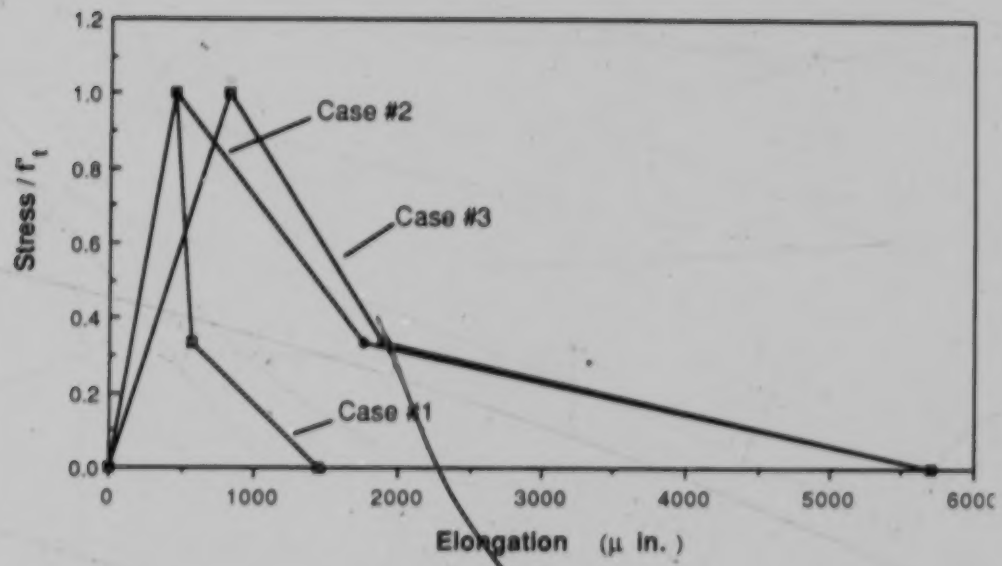

Figure A.1 - Results for the example

APPENDIX B

MODELLING OF REINFORCED CONCRETE PANELS SUBJECTED TO AXIAL LOAD AND LATERAL LOADING

The Aghayere and MacGregor (1988) specimens used in the validation tests of Chapter 4 are analyzed in this appendix. The effect of the mesh refinement, the influence of the number of layers over the thickness and the modelling of the test set up (and its interaction with the specimen) are discussed. The results obtained with the finite element program treat the various refinements mentioned above separately whereas the comparison with the experimental results presented in Chapter 4 , incorporates all these aspects.

B.1 Finite element modelling

In modelling panels with the 3D degenerated 16 node plate shell element of NISA, one must assess how many elements are required to discretize correctly the specimen, or one quarter of the specimen when symmetry can be used, such as the present case. Also, another important parameter is the number of layers used to perform the numerical integration over the thickness. As an indication, Ramm (1976) modelled successfully one quarter of a thin square plate undergoing large displacements with a 2 x 2 mesh. These two parameters were varied for the Aghayere and MacGregor (1988) specimens A3 , modelled up to the maximum load level using a load control scheme with either 5 or 9 layers and either a 2 x 2 or a 3 x 3 mesh. As illustrated in Fig. B1, the number of layers used for the

numerical integration over the thickness affects the solution more significantly than the mesh refinement. The nine layer elements modelled the measured load deflection more closely. The ultimate load and the associated displacement are similar for a four element mesh or a nine element mesh. Thus, a 2 x 2 element mesh (for a quarter of the specimen) with nine integration layers describes adequately panels bent in single curvature. This rule is adopted in this study and used in the subsequent analyses presented in this appendix.

As mentioned in chapter 1, there are two types of solution strategies available in NISA: the load control method and the modified constant arc-length method (CALM). Specimen A3 is modelled again using the CALM (Fig. 1.8) with two different arc-lengths ΔS , equal to 5.0 or 20.0 , and using the load control method. With the small arc-length equal to 5.0 , four times more load steps are necessary to trace the specimen response than with the longer arc-length of 20.0 . The results obtained with the three schemes are shown in Fig. B.2 . As illustrated, the three solution strategies give approximately the same solution up to the first peak load. The post peak behavior can be followed by the CALM whereas it is more difficult when the load control method is used, a large amount of iterations being required to reach the second ascending branch of the curve. Therefore the CALM can be used to model the type of panels analyzed in this research and the selected arc-length ΔS does not affect significantly the results up to the failure load. The difference in the second ascending branch with the two CALM analyses can be related to the norm used to measure the convergence. The finite element response compare adequately to the experimental results, except near the ultimate. However the boundary conditions in the analysis do not correspond to those in the test, the horizontal movement in the analyzed panel

being restrained and the overhanging portion of the slab present in the experiment was not included in the analysis. This was done to avoid any confusion in the interpretation of the response obtained with the two meshes and the two number of layers. The post peak response modelled in the numerical analysis were not recorded in the test which had to be stopped due to lack of travel in the loading mechanism.

Four cracking models are available in NISA: the fixed orthogonal, the fixed non orthogonal, the stress rotating and the strain rotating crack models. Solutions obtained using these four models for the specimen A3 are presented in Fig. B.3 and compared to the test results. In these cases, the test boundary conditions were modelled, using discrete supports and with the overhanging portion of the slab. It is shown clearly that the two rotating crack models give approximately the same results while the fixed orthogonal crack model overestimates the failure load by about 10% compared to the predictions obtained by the two rotating crack models. The fixed non orthogonal crack model does not behave like the three other models and should be avoided. In this study the stress rotating model is selected but the strain rotating crack model could have been selected also. The choice was based on the sensitivity observed with the strain rotating model in the postcracking prediction of shear panel behavior with respect to the description of the cracked shear modulus G_{cr}, especially for the specimen PV29 in the Vecchio and Collins (1982) series (see discussion in section 4.1.2).

In these analyses performed with NISA, the convergence of the solution was based on a displacement norm with a tolerance of 0.01 on the ratio of the norm of the increment of displacement at a given iteration to the norm of the total

increment of displacement in the load step. No load norm was used in the analysis. The same rule is applied in all analysis performed on panels subjected to inplane and lateral loads.

B.2 Test set up effects

This section treats the effects of test set up used by Aghayere and MacGregor (1988) in their experimental investigation. The effects of the overhanging strip, the type of supports and the inplane load application system are examined.

B.2.1 Overhanging strip and discrete supports

In order to support the slab adequately, the specimens had a 152 mm wide overhanging strip all around. Also, 125 mm long by 125 mm wide discrete supports spaced at 457 mm apart were used instead of a continuous support system. These two effects are compared in Fig. B.4 where the actual slab modelling includes the overhanging strip and the discrete supports. In the analysis the supports were modelled by restraining the out-of-plane movement at the node corresponding the the actual support. The rotation about an axis parallel to the panel edge was allowed but the rotation about an axis perpendicular to the edge was restrained, as do the actual supports in the tests. The overhanging region was modelled using an additional row of element in each direction and only one quarter of the reinforcement of the central part of the slab was used to provide an amount of reinforcement comparable to the quantity present in the actual specimens.

It can be observed that the overhanging strip increases the panel carrying capacity by about 15% if the actual modelling is compared with the discrete

support case. On the other hand, continuous supports all around the specimen increase the ultimate load by about 10% when compared to the same specimen with discrete point supports. The actual support conditions were between those assumptions. Thus the actual slab with the overhanging strip and the discrete supports behaves closely to what one wanted to model, a slab supported all along the edges without a surrounding strip, the effect of the overhanging strip cancelling those caused by the discrete support system.

B.2.2 Inplane load application

As mentioned in Chapter 4, the inplane load was applied through four jacks, at one end, enclosed in a self contained frame which carried the reaction at the other end (Fig. 4.9). Half round cylinders where also provided allowing for the edge rotation while panels deflect. However, when the edge rotations become important, the point of application of the in plane load moves. As illustrated in Fig. B.5, the downward movement (in this case) is function of the edge rotation θ_e and the radius r of the cylinder. The eccentricity is expressed as

$$e = r\,\theta_e \qquad (B.1)$$

where θ_e is expressed in radiants. Thus this eccentricity induces a moment along the edge equal to Pe . To model this effect with NISA, a rotational spring element was used, with the spring stiffness derived with the following equation:

$$K_\theta = P\,r \qquad (B.2)$$

where r was equal to 62.5 mm. This produces a bending moment along the edges equal to $K_\theta\,\theta_e$, equal to Pe .

The effect of this edge rotation is illustrated in Figs. B.6 and B.7 for Aghayere and MacGregor specimens A1 and B1 , respectively. The increase in strength is about 10% in the case of specimen A1 whereas it is only 5% for specimen B.1 This phenomenon is less important for rectangular specimens than for square ones since the effect of the edge moments are damped out rapidly in rectangular specimens. Timoshenko and Woinowsky-Krieger (1959) indicate a bending moment at the center of the plate equal to 0.256 M_o for square plates and only 0.046 M_o for rectangular plates with an aspect ratio b/a of 1.5, where M_o is the bending moment applied along the edges.

In Fig. B.8 Aghayere specimen B1 is modelled again with and without edge moments. In this case, constant eccentricity values of -5.0, 0.0 and +5.0 mm where used. Compared to the case without eccentricity, the effect of a 5 mm eccentricity changed the strength by 20% , either side, for the case studied.

B.2.3 Corner support

Another peculiar aspect of the test set up used by Aghayere and MacGregor was the corner supports. Since the corners of a uniformly loaded panel loaded laterally want to lift up, the corner support was placed on the top side of the specimen rather than underneath the panel. So far, all analyses presented in this Appendix assumed an infinitely stiff corner support, the degree of freedom associated with the vertical movement at each corner (in the center line of supports) being suppressed. However, if the actual stiffness of the frame holding the corners is evaluated, one obtains an equivalent spring stiffness in the direction of the vertical corner movement (w) of 25000 N/mm. This value is a maximum value since only one displacement at the corner (w) was assumed. The effect of the corner support, replaced by a spring at the associated degree-of-

freedom, give the results presented in Figs. B.9, B.10 and B.11 for specimens A2, B1 and B2 respectively.

The effect of that detail on the panel behavior is not significant for square panels since deflections (and thus the upward movement at the corner) are not as important as for rectangular specimens where a striking effect of the corner support on the ultimate load and on the panel behavior can be observed. In Fig. B.10 the progression from the stiff support case to the case without any restraint illustrates the importance of this detail. The corner support displacements were not monitored in Aghayere's test series but this aspect should be examined more closely in future test series.

B.3 Summary

Based on the effect of the discretization by finite element and the interaction of the tested panels with the test set up, the modelling of the Aghayere and MacGregor (1988) panels include the following features:

1. a 2 x 2 or a 3 x 3 mesh (for the square or the rectangular specimens respectively) models the interior portion of the panels within the support center line;
2. 9 concrete layers are used through the thickness;
3. the panels are supported at discrete points;
4. the overhanging slab is modelled with one quarter of the interior slab reinforcement;
5. the location of the inplane loads on the edges of the specimen is modelled with rotational springs;

6. the finite stiffness of the corner supports is included for the panels with inplane and lateral loads.

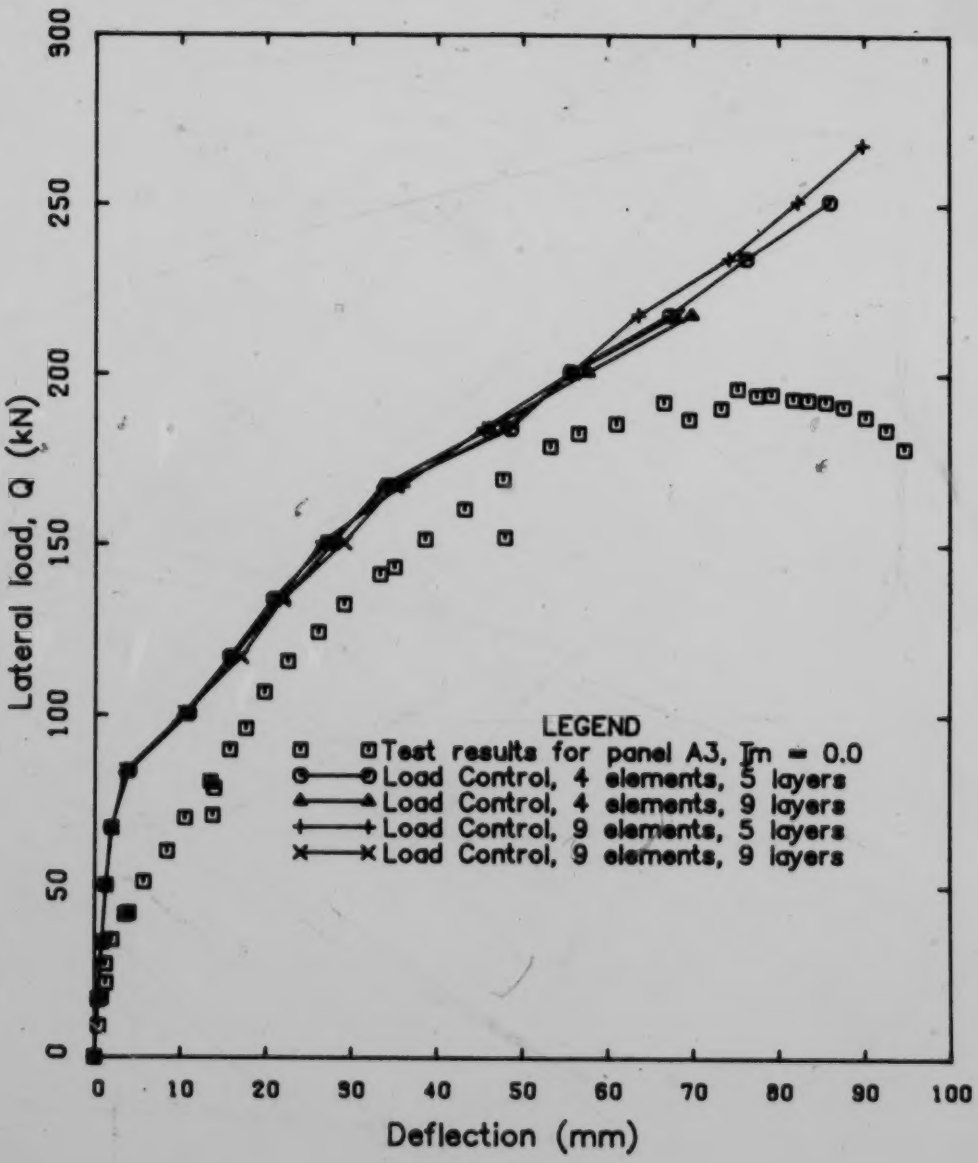

Figure B.1 - Effect of the number of elements and the number of layers

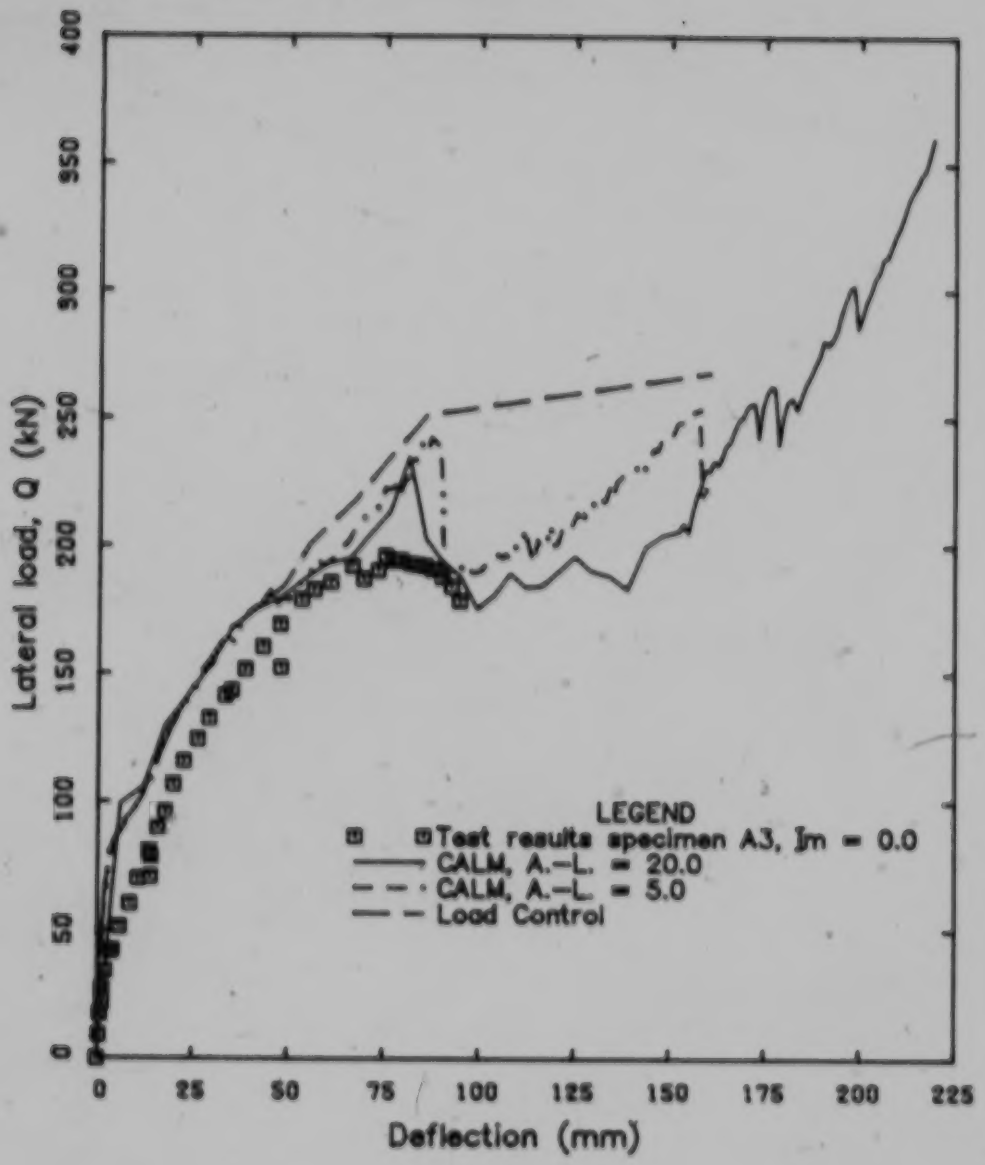

Figure B.2 - Effect of the solution strategies

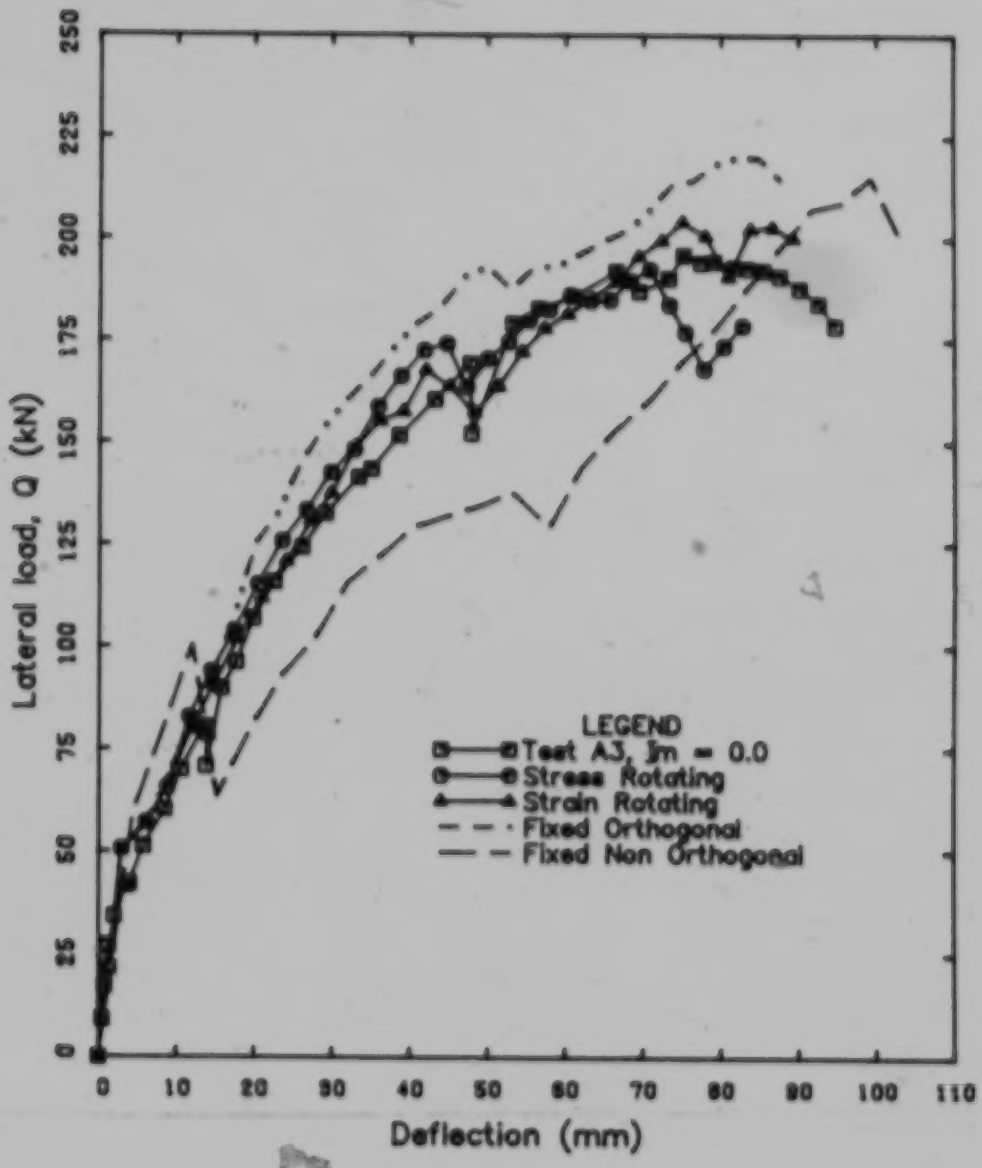

Figure B.3 - Effect of the cracking model

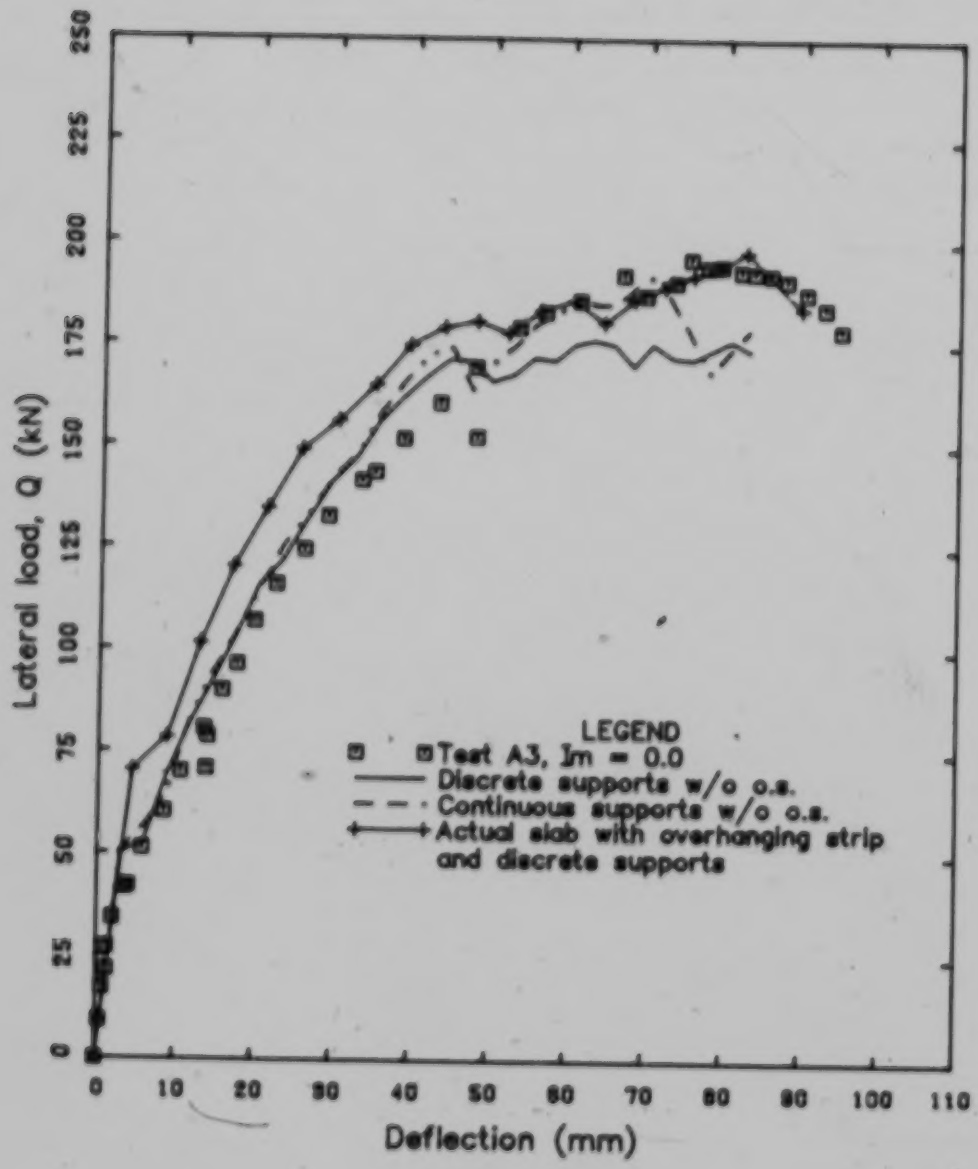

Figure B.4 - Effect of the supports

Inplane load application system

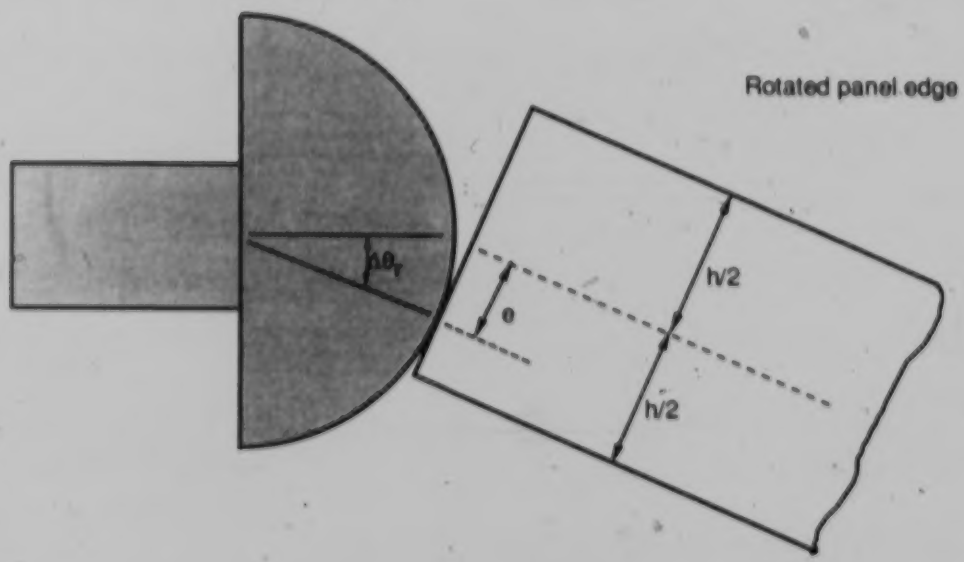

Figure B.5 - Effect of the edge rotation

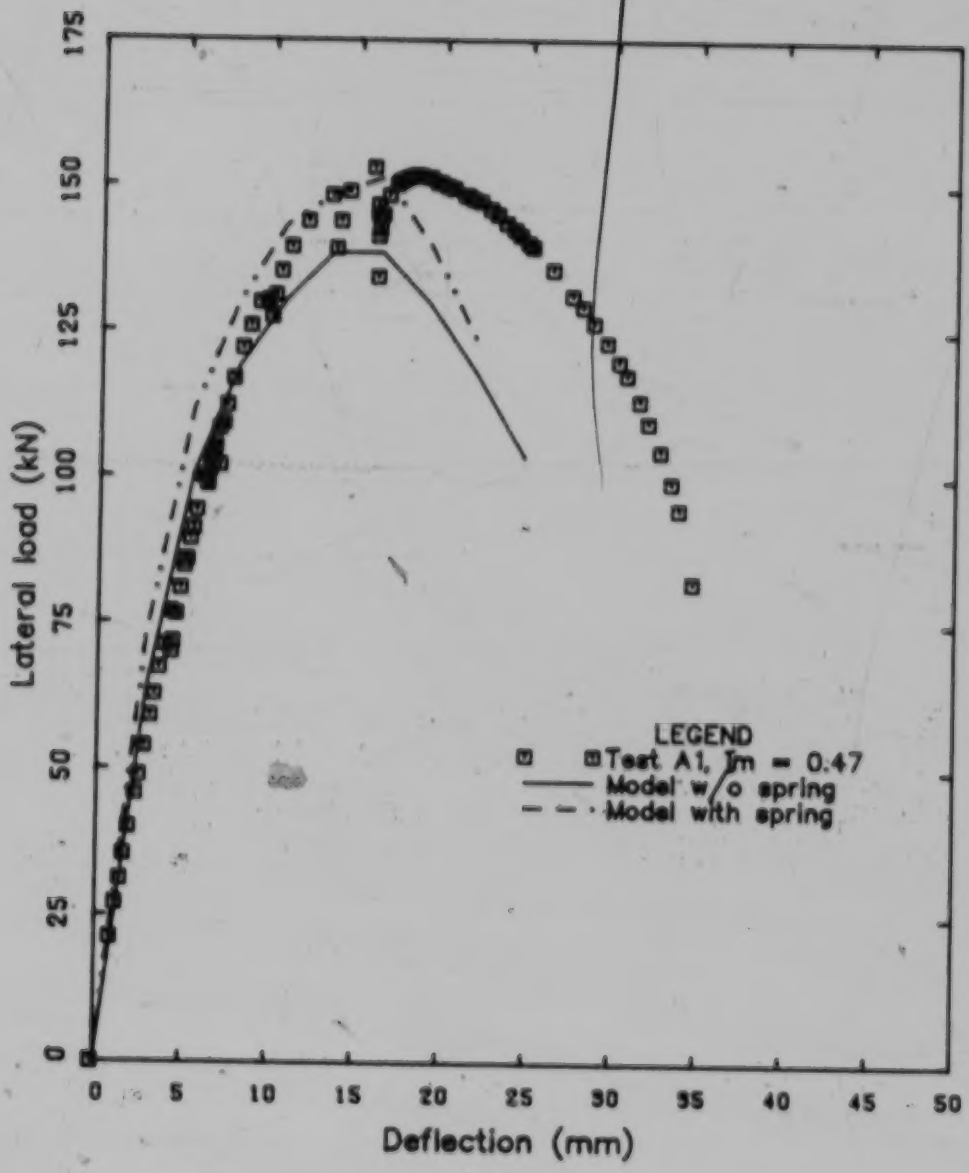

Figure B.6 - Effect of the edge rotation for specimen A1

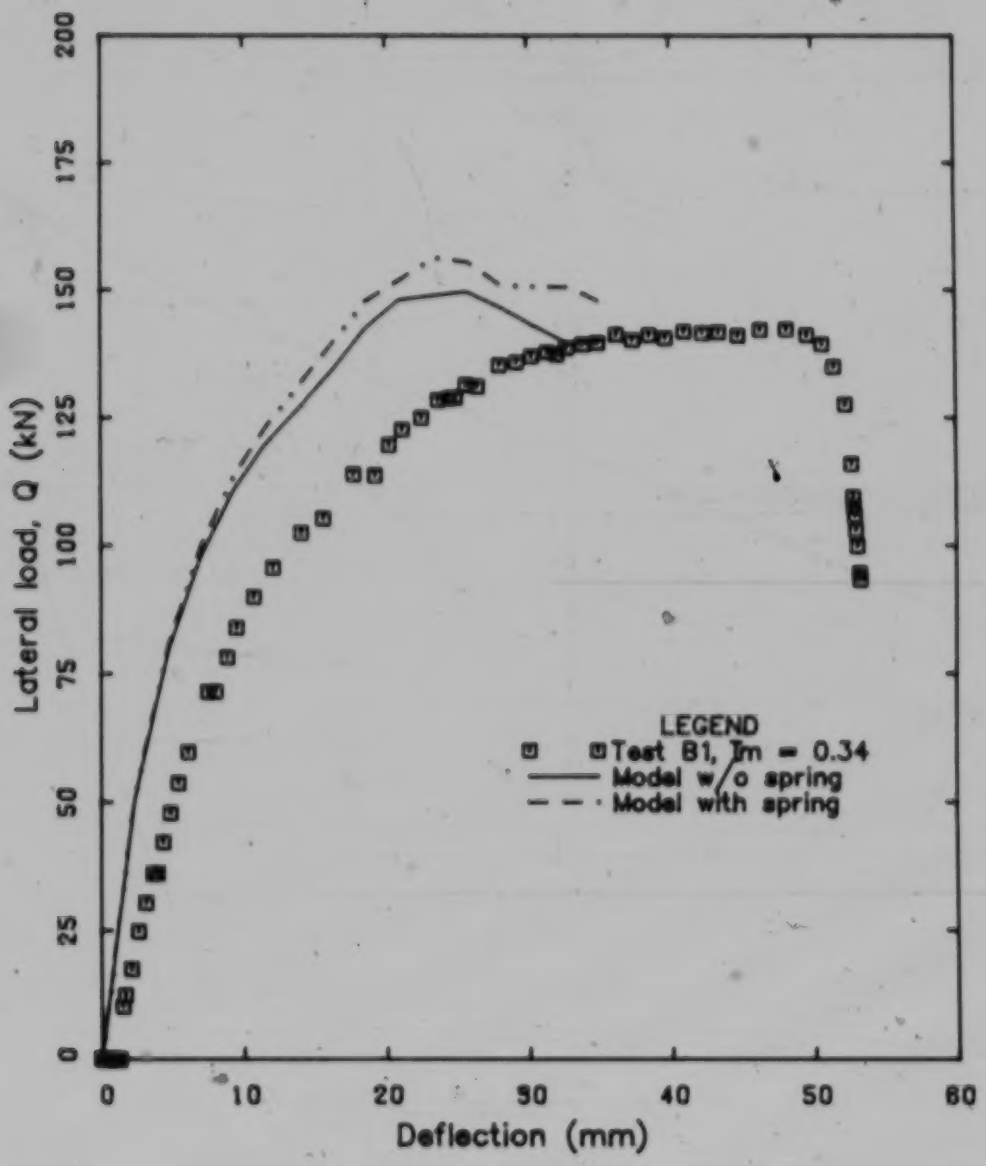

Figure B.7 - Effect of the edge rotation for specimen B1

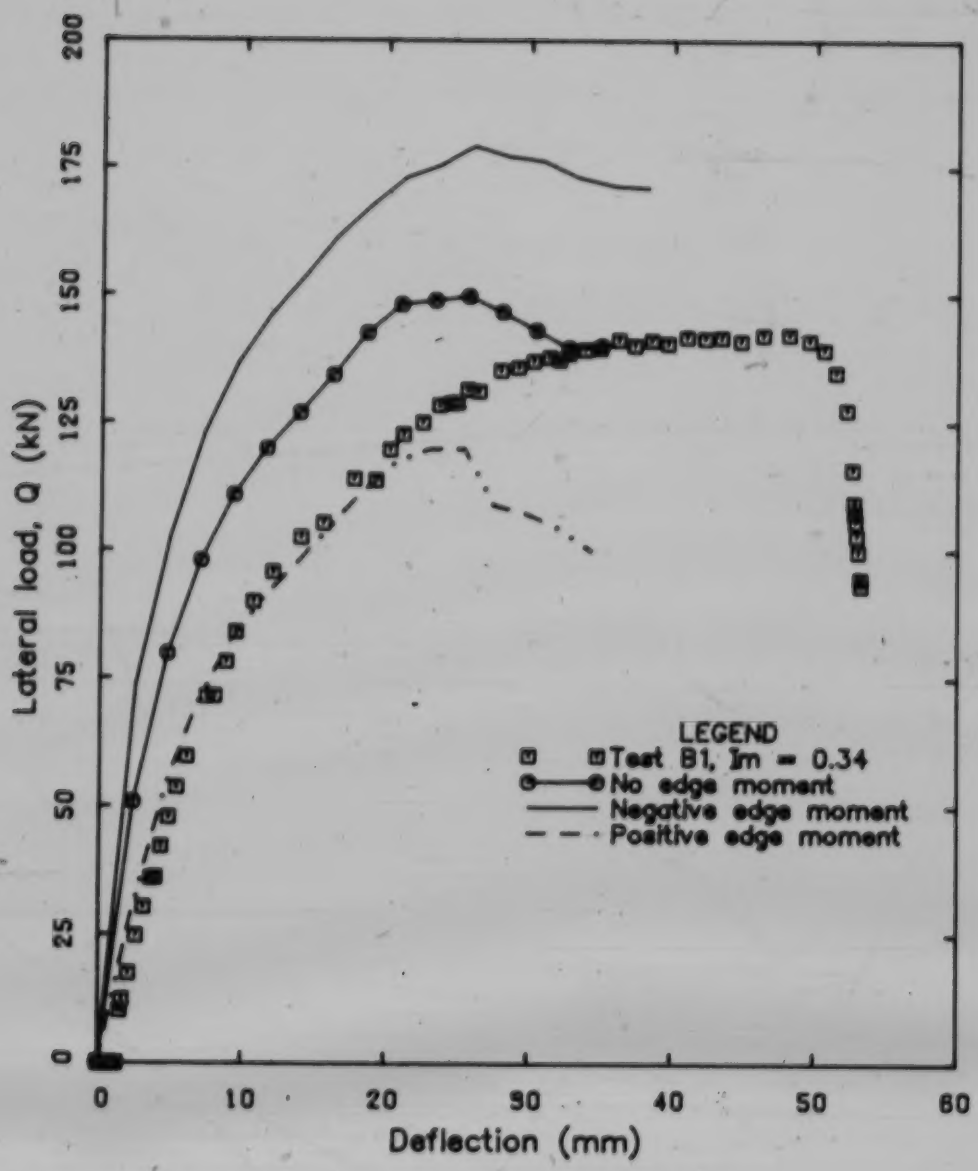

Figure B.8 - Effect of the inplane load eccentricity for specimen B1

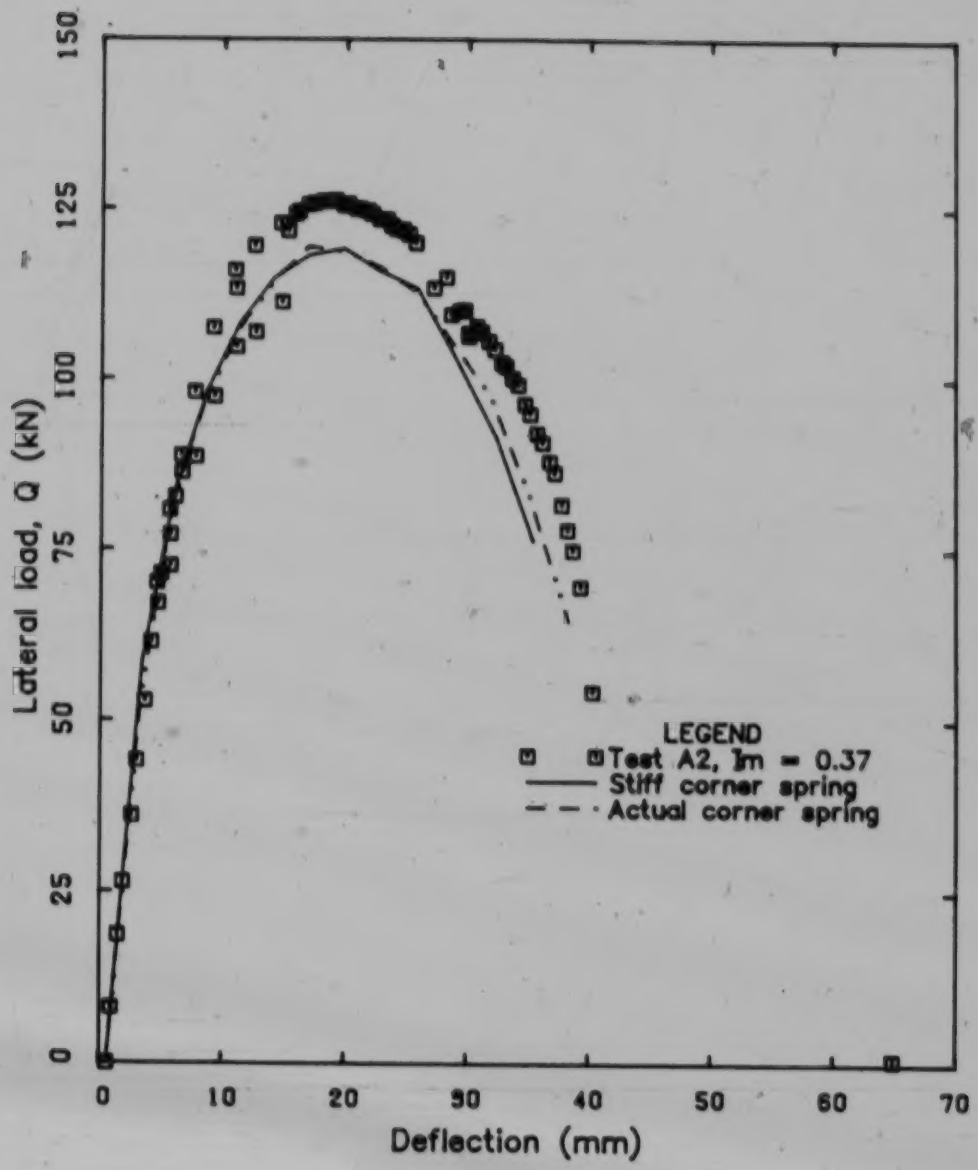

Figure B.9 - Effect of the corner supports for specimen A2

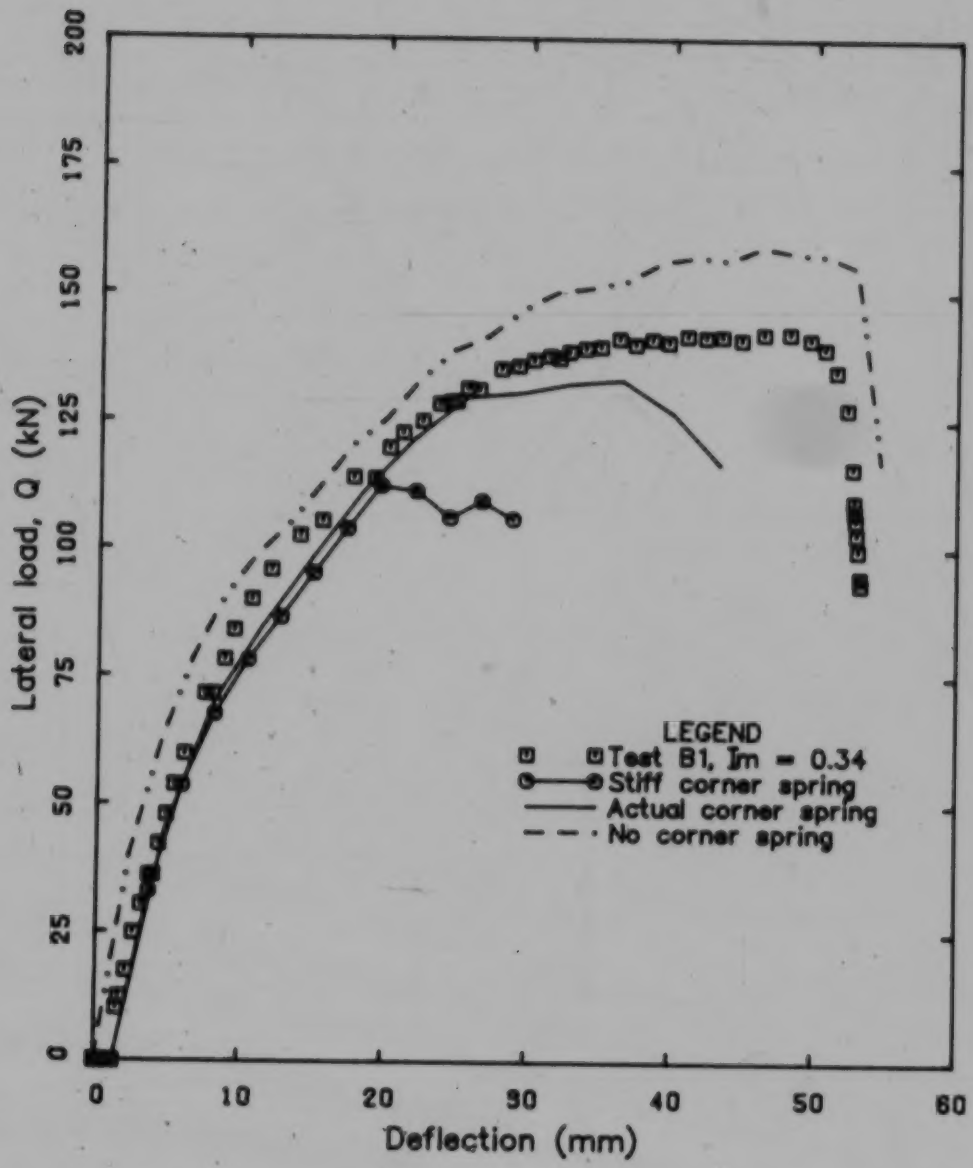

Figure B.10 - Effect of the corner supports for specimen B1

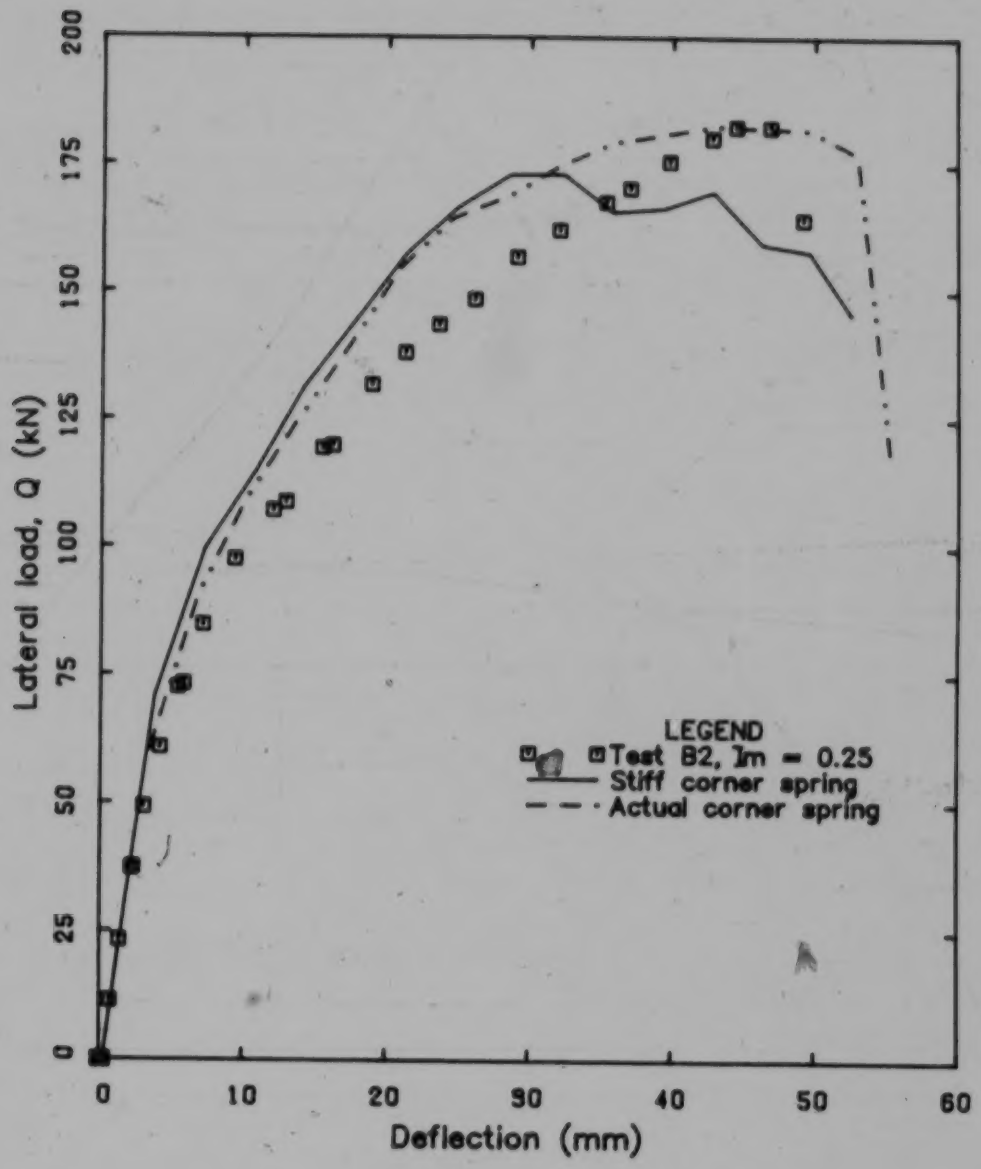

Figure B.11 - Effect of the corner supports for specimen B2